# Biomarkers in paleoenvironmental reconstructions: novel applications and data-driven evaluation

**Dissertation**

**(kumulativ)**

zur Erlangung des akademischen Grades doctor rerum naturalium

(Dr. rer. nat.)

vorgelegt dem Rat der Chemisch-Geowissenschaftlichen Fakultät der

Friedrich-Schiller-Universität Jena

von M.Sc. Natalie Schroeter

geboren am 31.12.1989 in Mosbach

Gutachter:

1. apl. Prof. Dr. Gerd Gleixner, Max Planck Institute for Biogeochemistry Jena.
2. Prof. Dr. Roland Mäusbacher, Institut für Geographie, Friedrich-Schiller-Universität Jena.
3. Prof. Dr. Jaime Toney, School of Geographical & Earth Sciences, University of Glasgow.

Tag der Verteidigung: 23.03.2022.

**Table of Contents**

Table of Contents ..... 1

List of Papers ..... 3

List of Figures ..... 4

Abbreviations ..... 5

1. Introduction ..... 6

1.1 Earth's Climate Variabilities ..... 6

1.2 Paleoenvironmental Reconstructions from Lake Sediments using Biomarkers ..... 7

1.3 Compound-specific Isotope Analysis of Biomarkers ..... 9

1.4 Limitations and Challenges of Biomarker Analysis ..... 11

1.4.1 Data-driven evaluation of paleoenvironmental datasets ..... 12

1.4.2 Residence times and Chronology ..... 13

1.4.3 Human - Paleoenvironmental Interactions ..... 14

2. Discussion ..... 16

2.1. Aquatic and Terrestrial Biomarkers in Lake Sediments: Manifold Applications ..... 16

2.2. Data-driven Evaluation of Biomarker Results ..... 18

2.3. Holocene Human- Paleoenvironmental Interaction in Western Central Asia ..... 19

2.4. Conclusion and Outlook ..... 22

3. Summary ..... 24

4. Zusammenfassung ..... 28

5. Bibliography ..... 32

6. Acknowledgments ..... 44

7. Selbstständigkeitserklärung ..... 45

8. Erklärung zu den Eigenanteilen ..... 46

9. Erklärung der Betreuer ..... 46

10. Angabe der Publikationsäquivalente ..... 47

## List of Papers

Manuscript 1

Status: published in Frontiers in Earth Science - Quartenary Science, Geomorphology and Paleoenvironment

Citation: **Schroeter N**, Toney JL, Lauterbach S, Kalanke J, Schwarz A, Schouten S and Gleixner G (2020) How to deal with multi-proxy data for paleoenvironmental reconstructions: Applications to a Holocene lake sediment record from the Tian Shan, Central Asia. Front. Earth Sci. 8:353. doi: 10.3389/feart.2020.00353

Manuscript 2

Status: submitted to Frontiers in Earth Science – Biogeoscience

Title: The lake reservoir effect varies with the mobilization of pre-aged organic carbon in a high-altitude Central Asian catchment.

Authors: **Schroeter N**, Mingram J, Kalanke J, Lauterbach S, Tjallingii R, Schwab VF and Gleixner, G

Manuscript 3

Status: published in Frontiers in Earth Science – Quartenary Science, Geomorphology and Paleoenvironment

Citation: **Schroeter N**, Lauterbach S, Stebich M, Kalanke J, Mingram J, Yildiz C, Schouten S and Gleixner G (2020) Biomolecular Evidence of Early Human Occupation of a High-Altitude Site in Western Central Asia During the Holocene. Front. Earth Sci. 8:20. doi: 10.3389/feart.2020.00020

## List of Figures

**Figure 1** Changes in the monthly global mean surface temperature (grey line) since instrumental observations, depicted as deviation relative to 1850–1900, and projected temperature trends (light green plume). Yellow and orange line represent human-induced and total externally-forced temperature changes, respectively. Blue lines show modelled global mean surface air temperature (dashed) and combined surface air and sea surface temperature (solid) from the CMIP5 (Coupled Model Intercomparison Project - Phase 5). Pink shading reflects temperature ranges over the Holocene. Figure adapted from Allen et al., 2018. ..... 7

**Figure 2** Schematic representation of the characterization of organic matter in terms of source specificity (left arrow) and the respective fraction of bulk organic matter (right arrow). Redrawn and modified after Bianchi and Canuel, 2011..... 8

**Figure 3** Principal Component Analysis (PCA) visualization of lipid biomarker distribution over the course of the Holocene. Correspondingly, concentrations for human- and herbivore- specific sterols and stanols are likely controlled by the Evaporation-to-Inflow ratio E/I, indicating a relationship between aridity and human presence. ..... 20

**Figure 4** Concentrations for coprostanol as a representative indicator for human presence (blue line) and Evaporation-to-Inflow (E/I) ratio (red line). Yellow shading indicates time period of enhanced human occupancy, which coincides with dry environmental conditions..... 21

## Abbreviations

ACL – Average Chain Length

CSIA – Compound-Specific Isotope Analysis

CSRA – Compound-Specific Radiocarbon Analysis

E/I – Evaporation-to-Inflow Index

IPCC – Intergovernmental Panel on Climate Change

LCA – Long-Chain Alkenone

LCD – Long-Chain Alkyl Diol

LRE – Lake Reservoir Effect

OM – Organic Matter

PCA – Principal Component Analysis

TOC – Total Organic Carbon

UMAP – Uniform Manifold Approximation and Projection

# 1. Introduction

"The paleoclimate record shouts to us that, far from being self-stabilizing, the Earth's climate system is an ornery beast which overreacts even to small nudges."

— Wallace Smith Broecker

This thesis investigates versatile applications of biomarkers in paleoenvironmental research and their subsequent evaluation in an innovative, statistical manner. Its aim is to get closer to understanding Earth's climate and environmental changes. The work presented in this dissertation is guided by the central hypothesis that an integrated, *data-driven* evaluation of diverse molecular and environmental data will lead to more holistic representations of past climate variability and remove subjective biases from their interpretation. Furthermore, the statistical analysis of variations in past climate will provide valuable analogues for predictions of future climatic changes. In addition to the joint evaluation of climate and environmental change, special attention must be paid to processes that affect the life of humans. The assessment of modern, human-specific biomolecular markers together with reconstructions of the environmental changes that occurred in their habitats reveals detailed human-environmental interactions. Especially, information on human adaptation to climate change in the past is vital to understanding the potential impact of future climate change on population movement, lifestyle and evolution.

## 1.1 Earth's Climate Variabilities

Earth's climate is a highly dynamic and nonlinear system with changes occurring frequently abrupt and episodic as a result of instabilities, external factors, anthropogenic forcing and crossing thresholds (Alley et al., 2003; Rial et al., 2004). According to the Intergovernmental Panel on Climate Change (IPCC), the observed global mean surface temperature has risen approximately 1.0°C compared to pre-industrial levels, reflecting a contemporary warming trend (Fig. 1, IPCC 2019, http://www.ipcc.ch). For the future, global warming is projected to reach 1.5°C between 2030 and 2052 at current rate (Allen et al., 2018; IPCC, 2018), inevitably entailing environmental and climatic changes, such as changes in precipitation patterns (Dore, 2005) and an intensification of extreme weather events (Meehl et al., 2000). These climate extremes may have negative effects on the carbon balance of terrestrial ecosystems, which potentially could inhibit an expected increase in global terrestrial carbon uptake (Reichstein et al., 2013). Despite the fact that the details of climate change are still controversial and contested (Anderson, 2014), undeniably earth's climate is complex and ever evolving under manifold forcings. Establishing reliable predictions about future climate trends requires a profound understanding how earth's climate naturally developed in the past. In search for this understanding, paleoclimate records have been extensively investigated since modern instrumental records largely encompass only the past ~170 years (Guillot et al., 2015). Paleoclimate records revealed episodes of large, globally occurring, abrupt climatic changes occurring repeatedly over geological time scales (Alley et al., 2003; Rial et al., 2004). Due to its close analogue to modern day climate, it is of special interest to reconstruct

climate and environmental conditions of the Holocene and their impacts on earth's diverse ecosystems. The Holocene covers the last 11,700 years (Walker et al., 2012) and encompasses both extended human societal development and major technological progress. Conventionally, the climate of the Holocene was regarded as relatively stable compared to preceding geological epochs (Dansgaard et al., 1993). However, the Holocene was interrupted by several abrupt climatic events, with the Little Ice Age being one of the most recent widespread climate change occurrence (DeMenocal and Bond, 1997).

## 1.2 Paleoenvironmental Reconstructions from Lake Sediments using Biomarkers

Amongst others, information about past climatic and environmental conditions can be inferred by the analysis of chemical fossils, so-called biomarkers (Eglinton and Calvin, 1967). Biomarkers derive from certain biotic sources and even after burial in environmental archives preserve their source information (Meyers, 2003). Accordingly, these compounds offer distinct benefits over measuring bulk organic matter (OM), since they can be utilized to identify specific sources of OM and can therefore provide additional information (Fig. 2). Due to their recalcitrance, biomarkers are stable over geological timescales and therefore enable the reconstruction of paleoclimatic and

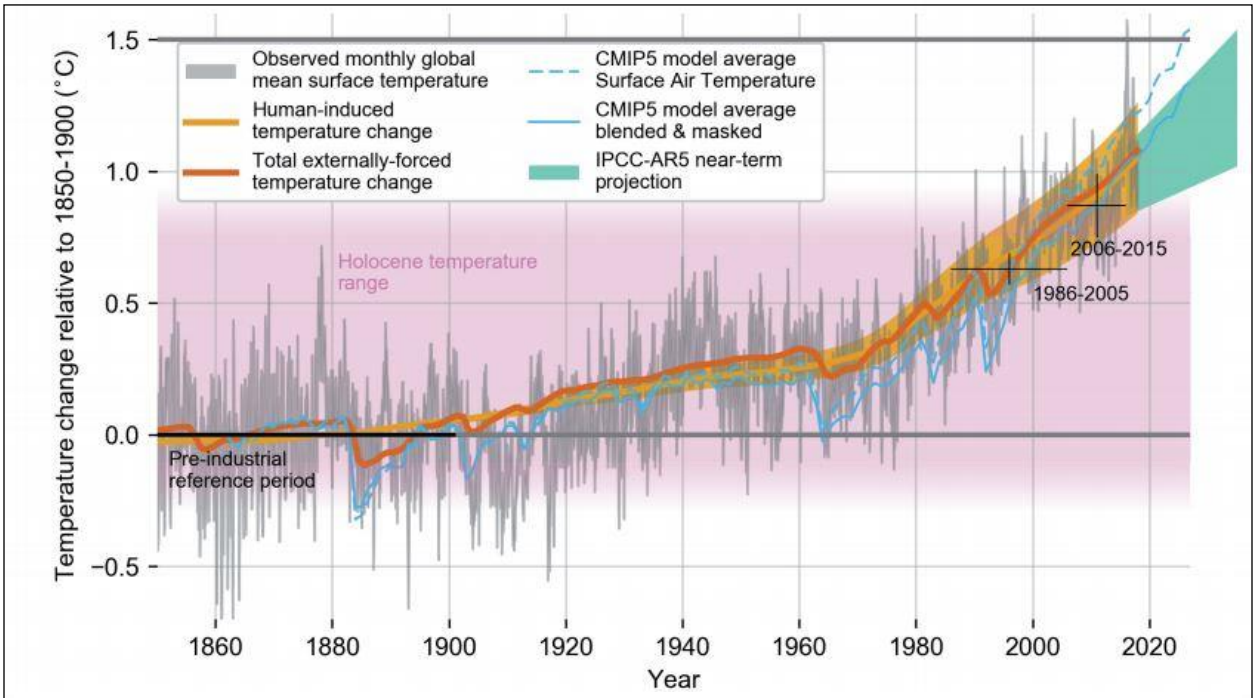


**Figure 1** Changes in the monthly global mean surface temperature (grey line) since instrumental observations, depicted as deviation relative to 1850–1900, and projected temperature trends (light green plume). Yellow and orange line represent human-induced and total externally-forced temperature changes, respectively. Blue lines show modelled global mean surface air temperature (dashed) and combined surface air and sea surface temperature (solid) from the CMIP5 (Coupled Model Intercomparison Project - Phase 5). Pink shading reflects temperature ranges over the Holocene. Figure adapted from Allen et al., 2018.

paleoenvironmental conditions (Simoneit, 2002). Conventionally, biomarkers in organic geochemistry primarily belong to the group of lipids (Brocks and Pearson, 2005), whose definition derived from their physical properties. Lipids are categorically insoluble in water but are extractable by nonpolar organic solvents (e.g., chloroform, toluene, and acetone) (Ohlrogge and Browse, 1995). For example, *n*-alkanes are a commonly analyzed group of biomarkers, which characterize different origins of OM sources by their average chain length (ACL) and their distribution (Meyers, 2003). Generally, short.chain *n*-alkanes, such as $nC_{15}$ to $nC_{19}$, are biologically produced by photosynthetic bacteria and algae (Cranwell et al., 1987; Giger et al., 1980), whereas mid-chain *n*-alkane homologues $nC_{21}$ to $nC_{25}$ are prevalently synthesized by submerged and floating aquatic plants (Ficken et al., 2000). The identification of such molecular patterns, which are associated with distinct OM sources, are crucial for paleoenvironmental reconstruction. This is because, when applied in specific ecosystems, these biomarker patterns can provide information, which goes far beyond mere molecular ratios. One ecosystem, where the application of lipid biomarkers can give very specific and localized information, are lacustrine sediments (i.e. lake sediments) (Castañeda and Schouten, 2011). Compared to marine settings, lakes generally have higher rates of both sedimentation and primary production per volume of water (Castañeda and Schouten, 2011), which enables the detection of shorter-term variations. Moreover, lacustrine sediments with annual laminations (varves) provide continuous, high-resolution climate records (Tylmann et al., 2013). Biomarker studies from lacustrine sediments uniquely record changes in both the lacustrine and terrestrial ecosystem since they can additionally incorporate terrestrial derived biomarkers (Vogts et al., 2009). Therefore, lake sediments offer a unique opportunity, where a combination of short- and mid-chain *n*-alkanes can be utilized to retrace changes in lacustrine productivity levels (Meyers, 2003). In contrast to the aquatic source of short- and mid-chain *n*-alkanes, long-chain *n*-alkanes ($nC_{27}$ to $nC_{31}$) are common constituents of vascular epicuticular leaf waxes of terrestrial higher plants (Eglinton and Hamilton, 1967). These leaf wax lipids can be transported over long distances by rivers and wind and may end up deposited in lacustrine sediments, too (Conte and Weber, 2002). Consequently, long-chain *n*-alkanes reflect integrated signals of terrestrial organic productivity within the catchment area (Meyers, 2003). Together, short-, mid- and long-chain *n*-alkanes can reveal the dynamics of autochthonous and allochthonous OM in lake ecosystems, giving information about in-lake primary production, the vegetation in the catchment, and the transport

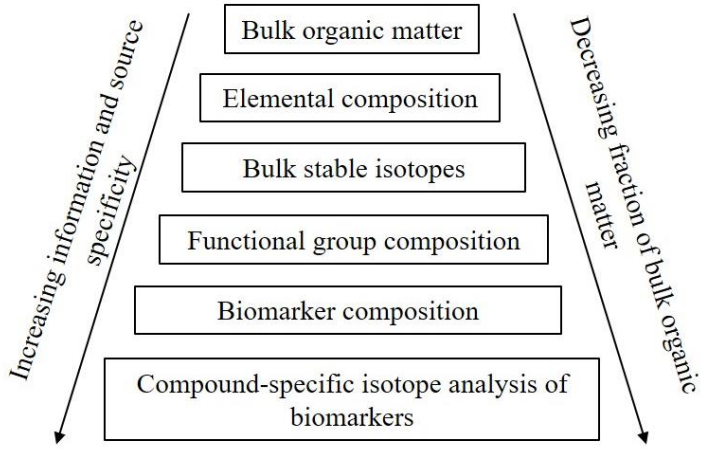


**Figure 2** Schematic representation of the characterization of organic matter in terms of source specificity (left arrow) and the respective fraction of bulk organic matter (right arrow). Redrawn and modified after Bianchi and Canuel, 2011.

dynamics from the catchment into the lake.

### 1.3 Compound-specific Isotope Analysis of Biomarkers

In addition to the information about the composition of biomarkers and thus about their respective sources, compound-specific isotope analysis (CSIA) in paleoenvironmental research can be used to disclose biochemical, environmental, hydrological, and atmospheric processes affecting the fate of OM. Moreover, CSIA can additionally provide age information of specific sources embedded in OM. With this progress in analytical methods to measure isotope ratios on specific organic compounds (e.g. Eglinton et al., 1996; Hayes et al., 1990; Hilkert et al., 1999), this technique provides promising benefits over measuring bulk organic fractions (Fig. 2). The isotopic signature of biomarkers is altered by isotopic fractionation by both kinetic and equilibrium effects occurring during physical, chemical and biological processes. Briefly, kinetic fractionation describes irreversible and unidirectional processes largely affecting the rate constant of a reaction (Tiwari et al., 2015). Generally, lighter isotopes tend to react faster and become concentrated in the products. An example for kinetic fractionation includes the carbon fixation during photosynthesis, in which the lighter isotope of carbon $^{12}C$ is preferentially taken up leaving OM depleted in the heavier carbon isotope $^{13}C$. On the other hand, equilibrium fractionation occurs due to an exchange of isotopes (i.e. change of the isotopic distribution) with no net reaction at equilibrium (Tiwari et al., 2015). An example for equilibrium fractionation is the isotope distribution when water vapor condenses at equilibrium. Here, the heavier isotopes of water molecules ($H_2{}^{18}O$ and $^2H_2O$) tend to remain in the liquid phases, while the lighter isotopes ($H_2{}^{16}O$ and $^1H_2O$) tend to become enriched in the vapor phase. Thus, by CSIA, one can draw conclusions about what drove these fractionations and deduce process changes in the paleoenvironment. For instance, compound-specific hydrogen isotopes of biomarkers from lacustrine sediments have shown to be ideal for the investigation of

**Infobox**: Reporting Stable Isotope Values.

Isotopes are atoms of the same element only differing in their number of neutrons and therefore in their masses. The name "isotope" derives from the Greek words ísos (equal) and tópos (place) and means at the same place (meaning in the periodic system). Isotopes are categorized into stable (e.g. $^2H$) and radioactive (e.g. $^{14}C$) isotopes. As opposed to radioactive isotopes, stable isotopes do not radioactively decay. Generally, isotopic ratios for stable isotopes are reported with the δ-notation in per mil (‰) as a relative deviation from a reference material or a standard:

$$\delta = \frac{R_{Sample} - R_{Standard}}{R_{Standard}} \times 1000 = \left(\frac{R_{Sample}}{R_{Standard}} - 1\right) \times 1000$$

where "R" is the ratio of the heavy to the light stable isotope in a sample or standard. Examples for common international standards are VSMOW (Vienna Standard Mean Ocean Water) and PDB (Pee Dee Belemnite). More positive δ- values reflect an isotopic composition of a sample being enriched in the heavy isotopes relative to the standard. Conversely, a sample with more negative δ- values is depleted in the heavy isotopes relative to the standard.

variabilities within the paleohydrological cycle (Huang et al., 2002; Sachse et al., 2012; Sauer et al., 2001). This is enabled through the integration of the δD ($\delta^2$H, deuterium) of the source water by biomarkers. Thereby, the δD of terrigenous biomarkers reflect the δD signature of the meteoric water (precipitation), which can be affected by evapotranspiration (Mügler et al., 2008). Whereas the δD signature of a studied lake (including modifications by evaporation) can be inferred by the δD of aquatic-derived biomarkers (Guenther et al., 2013; Sachse et al., 2012). Additionally, based on the isotopic differences, the Evaporation-to-Inflow index (E/I) can provide further information about a lake's hydroclimatic balance (Mügler et al., 2008). Higher E/I values reflect semi-arid of arid environmental conditions as evaporation amounts exceed amounts supplied by input water, therefore leading to an evaporative enrichment of a lake's water δD (Mügler et al., 2008). In contrast, lower E/I values indicate humid climate conditions as inflow water amounts exceed evaporation amounts (Mügler et al., 2008).

Paleoenvironmental reconstructions hinge on a correct age-model of the analyzed material, yet individual biomarkers oftentimes vary distinctly in their source. As these source differences could imply that individual biomarkers differ in their age-model as well, compound-specific radiocarbon analysis (CSRA) has been implemented in paleoenvironmental studies. CSRA provides a complementary, powerful tool for studying the cycling of OM by unraveling its sources together with their respective ages across a range of environmental settings (Bianchi and Canuel, 2011; Sun et al., 2020). Thereby, CSRA can additionally elucidate transport mechanisms of biomarkers (Sun et al., 2020). Especially within the last two decades, CSRA has become more feasible due to analytical progress, which significantly decreased sample size requirements to <100 µgC (Eglinton et al., 1996; Pearson et al., 1998; Santos et al., 2007). Nevertheless, only relatively few paleolimnological studies so far employed CSRA. Therefore, uncertainty remains about the mechanisms, that lead to age offsets between individual biomarkers and bulk OM ages (Makou et al., 2018). This is further complicated by the results of several CSRA studies of lake sediments, which indicated that the age offsets of the same biomarkers can vary based on the specific environmental setting in which they are studied For example, Uchikawa et al. (2008) ascertained a fairly good accordance of $^{14}$C ages derived from long-chain *n*-alkanes ($n$C$_{27}$ – $n$C$_{33}$) with the ages of terrestrial higher plant macrofossils from Ordy Pond sediments, Hawaii. By contrast, Douglas et al. (2014), for instance, found a substantial age offset when analyzing long-chain *n*-alkanoic acid plant waxes ($n$C$_{26}$ – $n$C$_{32}$) from sediments of a mexican lake. $^{14}$C ages of these compounds were a hundred to a thousand years older than $^{14}$C ages of terrigenous macrofossils, indicating a source of a millennial-age soil carbon pool (Douglas et al., 2014). Thus, site-specific environmental parameters likely control the magnitude of time lags introduced between biomarker biosynthesis and biomarker deposition in sediments.

**Infobox**: Reporting Radiocarbon Values

In contrast to stable isotopes, radioactive isotopes are unstable and decay. A commonly utilized radioactive isotope in biogeochemical studies (and also this dissertation) is radiocarbon ($^{14}C$). However, there are several ways to report the $^{14}C$ data. One frequent way is known as the Fraction Modern ($F_m$):

$$F_m = \frac{R_{Sample}\left(\frac{0.975}{1+{}^{\delta}/_{1000}}\right)^2}{= 0.95 R_{OXI,-19}}$$

Where: $R_{Sample}$ = Ratio $^{14}C$ to $^{12}C$ in sample.

$\left(\frac{0.975}{1+{}^{\delta}/_{1000}}\right)^2$ = Correction for isotopic fractionation using sample's $\delta^{13}C$. Sample is normalized to a $\delta^{13}C$ of -25‰.

0.95 = Normalization of $^{14}C$ of oxalic acid I standard to preindustrial levels.

$R_{OXI}$ = Ratio $^{14}C$ to $^{12}C$ in oxalic acid stand I.

-19 = $\delta^{13}C$ of oxalic acid standard I, -19‰

Another common way to report 14C data is the $\Delta^{14}C$ notation, which integrates correction for the standard's radioactive decay between the year 1950 and the year a sample was collected:

$$\Delta^{14}C = \left[F_m * e^{\lambda(1950-\gamma)} - 1\right] * 1000$$

Where "λ" is 1/(true mean-life of $^{14}C$) = 1/8267 and "γ" = year of sample's collection.

### 1.4 Limitations and Challenges of Biomarker Analysis

Even though biomarker analyses provide numerous advantages in paleoenvironmental research, there are some limitations and challenges, which complicate their application. One limitation is simultaneously closely linked to the convenient source-specific nature of biomarkers. Typically, biomarkers occur at trace levels and only account for less than 5% of bulk OM (Feng et al., 2015).

Therefore, these compounds may not represent bulk OM but rather reflect environmental conditions affecting their characteristic sources (Fig. 2). Another limitation of biomarker analysis is that biomarkers are generally taxonomically specific, meaning that they can be assigned to a designated group of organisms (Brocks and Pearson, 2005) instead of having a well-defined single organism-specific source. Consequently, most biomarkers recovered from natural archives are semi-specific, such as *n*-alkanes. According to their ACL, *n*-alkanes can be assigned to aquatic and terrestrial sources (see chapter 1.2). However, noteworthily, there are examples of fairly specific biomarkers, such as botryococcenes (Metzger et al., 1985; Metzger and Largeau, 2005). These are triterpenoids comprising acyclic and cyclic compounds, which are specific to the microalga *Botryococcus braunii* (Metzger et al., 1985; Metzger and Largeau, 2005). Ideally, every biomarker studied would encompass a biochemical structure representative of one specific species (Dubois and Jacob, 2016). As this, however, is rather the exception than the norm, single biomarker analyses encounter some challenges when trying to reconstruct large-scale environmental parameters shaping a complex ecosystem.

### 1.4.1 Data-driven evaluation of paleoenvironmental datasets

To overcome the challenges that come with single biomarker investigations, the combined analysis of multiple biomarkers (multi-proxy) has proven to provide more robust results and strengthens subsequent interpretations by simultaneously examining different aspects of an ecosystem (Birks and Birks, 2006; Mann, 2002). As a result, larger and more complex datasets are being generated, which require detailed, joint evaluation and interpretation. However, oftentimes the results of multi-proxy biomarker studies are still published in a descriptive or narrative way (Birks and Birks, 2006) and biomarker evaluation is frequently carried out subjectively with little usage of statistical or computational techniques. In many cases, interpretation is based on visually aligning several proxy records. This subjectiveness, however, will inevitably lead to deceptive results and does not reflect the full complexity of the dataset. Clearly, as the number of larger datasets increases and the temporal resolution concurrently becomes finer, there is a growing need for statistical techniques to decipher and summarize intricate multi-proxy patterns and their potential interrelations.

Common aims of studies in the field of paleoenvironmental reconstructions are the identification of drivers of past environmental changes and the dating of their occurrences. Furthermore, there is a need to identify which combinations of changes together may lead to an environmental or climatic phase transition and their potential to influence and shape human societies. As introduced, a variety of proxies exist which target parts of these questions. However, distilling the multitude of proxy information into distinct predictions about environmental change requires a multivariate evaluation, which is close to impossible to perform well ‘by eye’. Multi-proxy datasets frequently encompass a high dimensionality. In order to exploit their full informational content adequately, it is essential to reduce their dimensionality. Dimensionality reduction describes the transformation of data from a high-dimensionality into a lower-dimensionality, which facilitates, for example, better understanding and visualization (van der Maaten et al., 2009). As it is challenging to visualize high-dimensional data, reducing it into a low-dimensional space allows to create two-

dimensional and three-dimensional plots and therefore enables to detect trends and variability more clearly. In the ideal case, the dimensionality should comply with the intrinsic dimensionality of the data, i.e., the minimum number of variables necessary in a minimal representation of a data, while minimizing significant information loss (Bennett, 1969; van der Maaten et al., 2009). Commonly, methods for dimensionality reduction are categorized into linear and nonlinear techniques. Particularly in the early application of dimensionality reduction, linear techniques were traditionally performed, with Principal Component Analysis (PCA) being the most popular one (van der Maaten et al., 2009). PCA is a multivariate statistical analysis technique, which generates new variables, so-called principal components, as linear combinations of the initial variables (Abdi and Williams, 2010; Ringnér, 2008). Doing so, PCA aims to preserve as much of the variability present in the original variables and therefore discloses hidden patterns of similarity and interdependencies between variables (Abdi and Williams, 2010). However, PCA and other linear dimensionality reduction techniques are incapable of adequately processing complex nonlinear data (van der Maaten et al., 2009), which is often the case for paleoenvironmental data. Therefore, nonlinear dimensionality reduction methods may be more suitable for handling paleoenvironmental and paleoclimatic datasets, since they are able to visualize nonlinear relations. Yet, although various nonlinear techniques already exist, that could reduce the dimensionality of a multi-proxy dataset and may be applicable, there is still hesitancy in their applications. One approach of utilizing modern analysis tools (ordination techniques, machine learning tools and packages in the statistical programming language R) for paleoenvironmental studies is thoroughly outlined in manuscript one.

### 1.4.2 Residence times and Chronology

In spite of the advantages provided by the analysis of lake sediments and their integrated biomarkers, there are still limitations regarding the chronology and residence times of individual biomarkers. Radiocarbon dating is the most commonly applied method to establish chronologies for paleolimnological studies. Yet, dating lacustrine sediments has proven to be a challenging task, since OM from lakes commonly shows anomalously old $^{14}C$ ages owing to a lake reservoir effect (LRE, also ‘old carbon’ or ‘dead carbon’ effect) (Hou et al., 2012; Mischke et al., 2013). The LRE refers to the introduction of pre-aged carbon (organic or inorganic) into the lake OM pool inevitably resulting in large chronological uncertainties. Factors influencing the magnitude and temporal variability of the LRE include the dissolution of inorganic carbon in the lake water and the catchment geology (Hou et al., 2012; Mischke et al., 2013; Philippsen, 2013). One potential remedy to overcome the LRE is the independent dating of lake sediments through the counting of fine seasonal laminated layers, so-called varves (Brauer et al., 2014; Zolitschka et al., 2015). Unfortunately, oftentimes, lake sediments are not varved. Instead, terrestrial plant macrofossils are typically most suited for reliable $^{14}C$ dating as they absorb carbon directly from the atmosphere during photosynthesis and are therefore independent of the in-lake OM pool (Bertrand et al., 2012). However, in some regions, vegetation cover is extremely scarce, and terrestrial plant macrofossils are consequently absent in sediments. Therefore, one often resorts to dating the total organic carbon (TOC) in the sediment layers. Yet, TOC comprises a mixture of allochthonous and

autochthonous carbon, which means that aquatic and terrestrial biomarkers, even though they are deposited in the same sedimentary layer, might have very different spatial and temporal origins. Still, transport and residence times of individual biomarkers are subject to debate and can accordingly be an additional source of chronological uncertainties. As a consequence, both aquatic and terrestrial factors have to be taken into consideration when considering the amplitude of the LRE. One workaround may be to employ of biomarker-specific $^{14}C$ dating, which will allow for comparisons of residence and transport times of aquatic and terrestrial derived biomarkers with independent chronologies. The development and implementation of an isolation method of both aquatic and terrestrial derived biomarkers for subsequent $^{14}C$ analysis, providing temporal details on the residence times, is elaborated in manuscript two.

### 1.4.3 Human - Paleoenvironmental Interactions

An emerging and promising field in paleoclimatic and paleoenvironmental studies is the investigation and integration of human – environmental interactions. Understanding the long-term evolution of socio-environmental dynamics and how humans both responded and adapted to past environmental variability may help with the current global climate problems and the prospective adaptability (Yang et al., 2019b). Generally, tracing of prehistoric human presence depends on the excavation of archaeological sites and their respective artifacts. However, as sample sizes and prehistoric human settlements are oftentimes limited, the development and applicability of human indicative biomarkers is of growing interest. Tracing human activity in paleolimnological studies can be achieved either by directly identifying molecular remains of human presence or by evaluating proxies that indirectly include information resulting from human settlement or activity in the area. Both the direct and indirect way of tracing human-environment interactions are highly active fields of research. The direct molecular way of identifying human presence near lakes is employed by analyzing lacustrine sediments for fecal biomarkers, such as sterols and stanols. These are organic compounds, which based on their recalcitrance, can persist in sediments for thousands of years (Bull et al., 2003; Bull et al., 2002). In the intestinal tract of mammals, sterols, i.e. cholesterol (Cholest-5-en-3β-ol), are being microbially reduced to 5β-stanols (Eyssen et al., 1973; Macdonald et al., 1983), particularly coprostanol (5β-cholestan-3β-ol) and 5β-stigmastanol (24β-ethyl-5β-cholestan-3β-ol). Based on their differing diet, humans and herbivores can be differentiated from each other as herbivorous feces comprise predominantly 5β-stigmastanol, whereas human feces largely consist of coprostanol.

The indirect way of detecting human presence near lakes includes pollen analysis, which enables the reconstruction of terrestrial vegetation changes of the past that may be related to human disturbance. For instance, the appearance of cereal pollen is usually associated with agricultural practices and also vegetation shifts as a result of land clearance can be ascertained by pollen analysis (Dubois and Jacob, 2016). However, the results of this indirect approach for the human-environment interaction can contain substantial ambiguity. Several pollen grains are transported over great distances by wind movement and therefore do not necessarily reflect environmental conditions of their repository (Dawson and Mayes, 2015). Furthermore, the presence of early humans is not always interlinked with sedentary agricultural practice as a nomadic pastoral culture

may not induce vegetation shifts linked to pollen changes. Therefore, the development of lipid biomarkers indicative of prehistoric humans is becoming increasingly progressive (Dubois and Jacob, 2016). In order to bridge the gap between archaeology and paleoenvironmental reconstructions, more diverse, geographically spread and better resolved data is fundamental. Hence, the information about human – environmental dynamics can primarily be obtained by interdisciplinary investigations combined with multi-proxy analyses (Bell and Blais, 2020). Interdisciplinary approaches combining both archaeology and molecular paleoenvironmental reconstructions can enable the reconstruction of not only the presence of early humans, but also the consequences and interactions with environmental conditions. The detection of prehistoric human presence by a lipid biomarker approach, its relation to paleoenvironmental conditions, and its complementarity to local and regional archaeological findings, is discussed in detail in manuscript three.

## 2. Discussion

Uncertainties in predicting future climatic and environmental change fuel the search for adequate analogues in the past. Even though modern biomolecular studies can provide highly detailed information on past events, the statistical analysis and interpretation of biomarker data has remained challenging. The attached manuscripts address three of the currently most critical issues: the need for unbiased and data-driven multi-proxy biomarker evaluation, process-specific age models and the implications of environmental shifts for the life of humans. In the following, the results of the individual studies are jointly discussed. Special emphasis is given to human – environmental interactions during the Holocene as these present valuable insight into how human populations adapt to and migrate around environmental changes in their homeland. Since ongoing climate change threatens the environmental stability of many human-populated areas, millions of people will face widespread landscape degradation (IPCC, 2019). In this respect, this dissertation presents highly valuable perspectives from the past on one of the most pressing global issues in the near future.

### 2.1. Aquatic and Terrestrial Biomarkers in Lake Sediments: Manifold Applications

The manuscripts included in this thesis clearly demonstrate the potential and versatile application possibilities of lipid biomarkers in paleolimnological studies. Fields of application encompassed (1) the reconstruction of environmental conditions both in and around a lake setting over the course of the Holocene, (2) the detection of prehistoric humans and herbivores in a remote high-altitude terrain, and (3) the temporal influence of the terrestrial and aquatic component on a lake's chronology. In detail, in order to achieve the reconstructon of Holocene lacustrine environmental variability, a multi-proxy approach was utilized. This included the analysis of long-chain alkenones (LCAs) as a paleotemperature proxy and long-chain alkyl diol (LCD) distribution as an indicator for relative changes of algal input. Moreover, the compound-specific stable hydrogen isotope compositions of both long-chain *n*-alkanes, $n\mathrm{C}_{29}$, and mid-chain *n*-alkanes, $n\mathrm{C}_{23}$, were ascribed to reflect changes in the δD of the meteoric water and changes in the δD of the lake water, respectively. LCAs comprise a group of aliphatic unsaturated ketones biosynthesized by haptophyte algae from the Isochrysidales order (Theroux et al., 2010). Based on the strong interrelationship between the LCA unsaturation and lake surface temperature, the respective alkenones unsaturation index $\mathrm{U}_{37}^{\mathrm{K}}$ is progressively utilized in paleolimnological studies to reconstruct lake surface temperatures (Sun et al., 2012; Theroux et al., 2010; Toney et al., 2010). Similar to LCAs, LCD distributions are reported to correlate with sea surface temperatures (Rampen et al., 2012), however in the lacustrine setting, sources of LCDs and controlling environmental parameters on their distribution are still not sufficiently known (Rampen et al., 2014). Presumably, the Eustigmatophyceae class of algae is a central biological producer of LCDs in freshwater environments (Lattaud et al., 2018; Rampen et al., 2014; Shimokawara et al., 2010), therefore changes in their concentration are likely to reflect variations in the biological productivity of microorganisms. Merged together, our multi-proxy analysis enabled a profound and detailed insight into various facets of the lake's ecosystem over the course of the Holocene, therefore

providing substantial advantages over the analysis of single proxies. By investigating both aquatic and terrestrial derived biomarkers, this allowed the reconstruction of environmental changes effecting the lake ecosystem as well as environmental variability in the catchment area of the lake, respectively.

For the aim of the detection of prehistoric human signals, manuscript three reviews the fairly recent and emergent application of fecal biomarkers preserved in lake sediments. In this respect, sterols and stanols were analyzed to provide evidence for the presence of both humans and associated livestock in a low-human-impact area. On account of their diet and resulting sterol and stanol distribution, herbivores and humans can be distinguished. A herbivorous diet generates an excess of predominantly 5β- stigmastanol and epi-5β-stigmastanol (24β-ethyl-5β-cholestan-3α-ol) originating from β-sitosterol (3β-stigmast-5-en-3-ol) and stigmasterol (Stigmasta-5,22-dien-3β-ol), which are the most common and the third most common phytosterol (plant sterol), respectively (Bull et al., 2002; Rogge et al., 2006). By contrast, human feces comprise the highest amount of coprostanol, a cholesterol derivative, which accounts for more than 60% of the total sterols (Bull et al., 2002; Leeming et al., 1996). However, as 5β-stanol background concentrations can also occur naturally in soils not exposed to fecal deposition, diagnostic ratios of specific sterols and stanols are oftentimes applied, therefore providing results independent of total concentrations (Bull et al., 2001; Bull et al., 1999; Grimalt et al., 1990). For example, a ratio proposed by Bull et al. (1999) (R1) allows to take microbial degradation into account as it comprises 5α-cholestanol, which is produced by the degradation of cholesterol by soil microorganisms (Bull et al., 2001; Wakeham, 1989):

$$R1 = \frac{coprostanol + epicoprostanol}{coprostanol + epicoprostanol + 5\alpha - cholestanol}$$

High R1 values imply increased human fecal deposition, whereas lower R1 values reflect less human fecal input. Additionally, a ratio established by Evershed and Bethell (1996) (R2) attemps to distinguish between human and higher mammal fecal input by considering the ratio of coprostanol and 5β- stigmastanol:

$$R2 = \frac{coprostanol}{5\beta - \ stigmastanol}$$

Based on the work reported in manuscript three, considerably enhanced R1 values for the investigated lake sediments between ~5900 a BP and 4400 a BP, especially at ~4,800 a BP (R1=0.6), indicate the early human occupancy of the lake's catchment area during the mid-Holocene. Coincidently, elevated R2 values at ~5,700 and particularly at ~4800 a BP reinforce a potential human origin of the stanols and consequently an early human occupation. Archeological findings in proximity to the investigated lake further support the assumption of human occupancy during the mid-Holocene and affirm the potential of sterols and stanols in paleolimnological studies as an emergent valuable analytical tool (e.g. D'Anjou et al., 2012; Engels et al., 2018; White et al., 2018).

Lastly, manuscript two comprises the use of long-chain ($C_{24}$, $C_{26}$, and $C_{28}$) and short-chain ($C_{16}$ and $C_{18}$) saturated fatty acids to decipher the temporal influence of the terrestrial and aquatic component on the LRE. Similar to *n*-alkanes, the chain length and distribution is characteristic for different origins of OM sources. Generally speaking, long-chain saturated fatty acids (> $C_{24}$) are considered to originate from terrestrial plant leaf waxes (Meyers, 1997; Parkes and Taylor, 1983). Conversely, short-chain saturated fatty acids ($C_{16}$ & $C_{18}$) occur more ubiquitously, though being largely ascribed to autotrophic and heterotrophic microbes (Cranwell et al., 1987; Meyers, 1997). By developing a relatively easy to adapt method to isolate both long-chain and short-chain saturated fatty acids for subsequent CSRA, manuscript two discloses the remobilization of pre-aged terrestrial OC integrated in lake sediments as $^{14}C$ ages of long-chain saturated fatty acids were predominantly older than corresponding dates determined by varve counting. Therefore, the inclusion of CSRA to conventional biomarker analysis, provided a temporal dimension to understand time lags and residence times and consequently the temporal influences of the terrestrial and aquatic component to the LRE.

### 2.2. Data-driven Evaluation of Biomarker Results

As introduced in chapter 1.4.1 and reported in manuscript one, multi-proxy analysis offers considerable advantages over measuring one single proxy as it provides a broader perspective. However, even though it is beneficial to investigate a wide variety of biomarkers, this inevitably leads to creating greater and simultaneously more complex datasets. Consequently, there is a growing interest in adapting appropriate methodological techniques to summarize patterns in these eclectic multi-proxy datasets. Still, in spite of all the comprehensive analysis capabilities publicly available, the results of biomarker analyses are oftentimes assessed rather subjectively ("by eye") with virtually no or little usage of statistical or computational techniques. Due to its subjective nature, this approach is neither free of bias nor does it discloses the full extent of the underlying information. Nonetheless, dimensionality reduction techniques suitable for the evaluation of paleoenvironmental datasets already exist (see chapter 1.4.1). In addition to more conventionally applied dimension reduction techniques, such as PCA, methodological advances in recent years made it feasible to represent one hundred percent of the variability within a deliberate number of dimensions. Such a tool, for instance, is uniform manifold approximation and projection (UMAP), which was just recently introduced by McInnes et al. (2018). Briefly, UMAP is a neighbor-embedding method that uses Riemannian geometry and algebraic topology to construct a weighted graph in high dimensions. The novelty of UMAP lies in its capability of constructing optimized representation of both the local (small-scale) and global (large-scale) variability within high-dimensional data sets (McInnes et al., 2018). In the context of paleoenvironmental studies, UMAP may offer significant advantages over the application of PCA. Firstly, as discussed above, PCA preserves as much variability as possible within the first few principal components (Jolliffe and Cadima, 2016), which, however, practically never amounts to one hundred percent. Inevitably, small-scale variance may be neglected although potentially containing important information. Secondly, PCA is an orthogonal linear transformation, yet, in many cases, paleoenvironmental data are nonlinear. This is particularly the case around phase transitions. Indeed, many

paleoenvironmental studies aim at identifying distinct phases, whose respective boundaries may be insufficiently represented by PCA. By contrast, since UMAP is a nonlinear dimension reduction technique, it may present a distinct advantage for the detection of phase transitions. We demonstrated its feasibility in both manuscript one and two, where distinct lake phases were clearly separated in a data-driven manner. Accordingly, in manuscript one, UMAP separated the sediment core into five temporally distinct phases (I–V), with Phase I: ~11,000 – 10,200 a BP, Phase II: ~10,200 – 8050 a BP, Phase III: ~8050 – 2600 a BP, Phase IV: ~2600 – 780 a BP, and Phase V: ~780 a BP – present. Convincingly, apart from only one data point between Phase I and II, all data points could be attributed to distinct phases. Although temporally separated, Phase I and Phase V were allocated in the same cluster and therefore likely reflect similar prevalent environmental conditions at ~11,000 – 10,200 a BP and ~780 a BP – present, respectively. Even though UMAP has been successfully applied in various research fields (Becht et al., 2018; Diaz-Papkovich et al., 2019; Smets et al., 2019), in the scientific community of paleoenvironmentalists, UMAP or comparable methods have not yet received full attention. Moreover, additional tools are necessary to characterize the transition from one phase to the other. Naturally, phase transitions can hold two substantial properties. First, a true abrupt shift, oftentimes classified as a tipping point (Lenton, 2011; Lenton et al., 2008), and secondly, a temporally gradual phase transition. Just recently, a statistical method for detecting abrupt shifts in time series, called *asdetect*, was introduced (Boulton and Lenton, 2019). *Asdetect* is a statistics package implemented in the programming language R, whose algorithm focuses more on significant changes of gradients within a series compared to other methods, which detect significant changes in mean values (Boulton and Lenton, 2019). When deploying *asdetect* to the dataset generated in manuscript one, phase boundaries assigned by UMAP at ~10,200 and ~8050 a BP are likely event-based phase transitions as respective maxima/minima of multiple proxies are coincidently overlapping during these specific time points. Potentially, these phase transitions could be classified as tipping points since most of the biomarker signals show a simultaneous and rather abrupt trend at ~10,200 and ~8050 a BP. On the other hand, phase boundaries in the mid- and late Holocene at ~2600 and 780 a BP are marked by a consecutive temporal succession of biomarker shifts, which points to more gradual phase transitions during these time periods.

However, *asdetect* is originally intended as a tool to analyze single-proxy data, which underlines the need for novel and/or expanded statistical methods to facilitate the data-driven evaluation of multi-proxy datasets. Both manuscripts one and two demonstrate the implementability and potential of modern general purpose bioinformatical tools for the handling of paleoclimate data. Still, they also showcase the partial disregard of accessible statistical methods in paleoenvironmental investigations and the necessity of their future enhancements to provide a viable alternative to common visual inspection.

### 2.3. Holocene Human- Paleoenvironmental Interaction in Western Central Asia

In the context of global climate change, the Tian Shan (Chinese for 'Celestial Mountains') in Central Asia is projected to be highly affected by increasing temperatures and altered precipitation patterns. The Tian Shan is one of the largest mountain ranges in the world and modulates the

hydrology and climate regime of northern Central Asia. Therefore, as the Tian Shan is also known as the "water tower of Central Asia" (Sorg et al., 2012), it is particularly vital to comprehend past climatic variability in this region in order to cope with prospective water resources and management predicaments as glaciers in the Tian Shan have been constantly retreating since the end of the Little Ice Age (Sorg et al., 2012; Yang et al., 2017). For this reason, the lacustrine sediments utilized for the interpretation and discussion in this dissertation primarily derived from Lake Chatyr Kol (~3,500 m above sea level), a mountainous lake located in the southern Tian Shan of Kyrgyzstan. However, the Tian Shan is not only an ideal location to study the climatic and hydrological fluctuations affecting Central Asia. Being part of the ancient Silk Road territory, it is complementarily a key region to understand early human high-altitude occupation and migration patterns. As biomarkers applied in manuscript one enabled the reconstruction of the climatic and environmental conditions in Western Central Asia, and the analysis of sterols and stanols in manuscript three allowed for the identification of human occupancy, when merged together, these results provide details about the human and paleoenvironmental interaction during the Holocene.

Firstly, based on the sterol and stanol concentrations, UMAP facilitated the separation of the sediment core into three temporally distinctive phases (Phase I–III), with Phase I: ~11,400–8300 a BP, Phase II: ~7600–2400 a BP and Phase III: 2300 a BP–present.

Secondly, a PCA of the biomarker dataset revealed interdependencies between various biomarkers indicative of paleoenvironmental conditions and fecal biomarkers indicative of humans and herbivores (Fig. 3). Evidently, the E/I parameter was likely a controlling factor of both the human-specific and higher mammal-specific biomarkers. Higher E/I values pointing to more arid conditions would therefore potentially promote the presence of humans within the lake's catchment area. As a matter of fact, E/I values and coprostanol concentrations are significantly correlated (Pearson correlation coefficient $r = 0.35$, $p < 0.02$), hence indicating a strong relationship. The earliest biomolecular evidence of human occupancy in the sediment core occurs

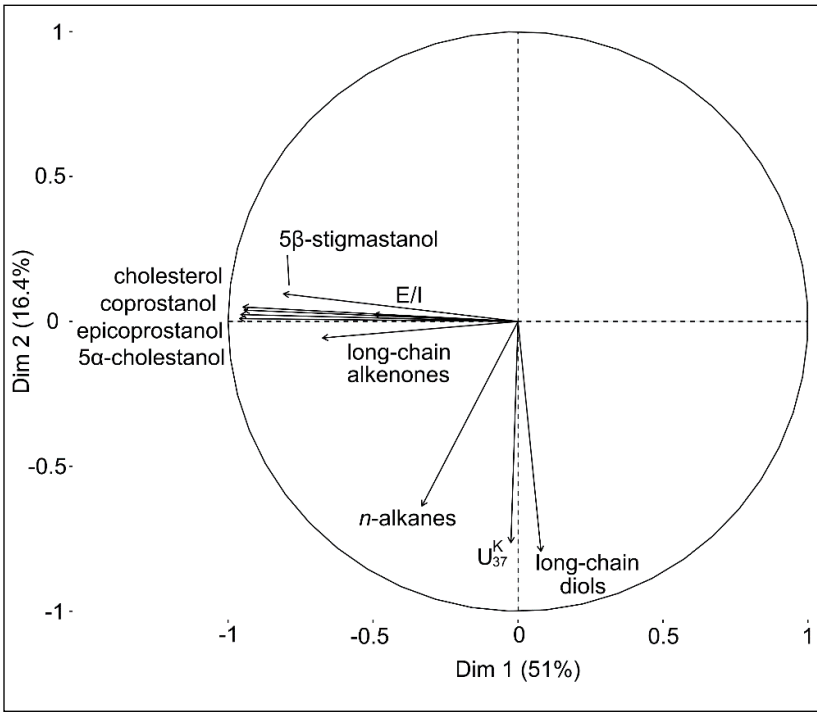


**Figure 3** Principal Component Analysis (PCA) visualization of lipid biomarker distribution over the course of the Holocene. Correspondingly, concentrations for human- and herbivore-specific sterols and stanols are likely controlled by the Evaporation-to-Inflow ratio E/I, indicating a relationship between aridity and human presence.

at ~5900 a BP and particularly at ~4800 a BP as concentrations of coprostanol, epicoprostanol, and cholesterol strongly increased. Increases are accompanied by a simultaneous concentration maximum of 5β-stigmastanol, presumably indicating the presence of domesticated livestock. Concurrently, E/I values are enhanced, indicating dry periods, particularly at ~4800 a BP (Fig. 4). Therefore, dry environmental conditions at that time likely influenced the presence of humans by increasing the accessibility of high-altitude regions and/or the necessity of exploiting new herding grounds. Indeed, dryness is reported to be an essential environmental factor threatening great parts of the Silk Road areas (Yang et al., 2019a). Consequently, the migration from one area to another due to a demographic pressure on resources, is widely observed along the Silk Road (Yang et al., 2019a). However, this certainly does not imply the collapse of a population, but rather showcases the resilience of humans and their ability to adapt.

Our findings emphasize climatic and environmental changes as a plausible driver for human migration flows. However, this is not to say that dry environmental conditions constantly provoke human migration as strongly increased E/I values at ~2300 and ~1500 a BP do not coincide with high sterol and stanol concentrations. Nevertheless, the significant interrelation underlines that prehistoric human populations were able to adapt to changing environmental conditions and reiterates that prehistoric societies have widely been exposed to climatic variability, which in turn influenced migration patterns. As the findings presented here reflect highly local information, more research in diverse geographic regions is still needed before a holistic picture of human and paleoenvironmental interaction during the Holocene can be obtained (Bell and Blais, 2020). The combined results of all three attached manuscripts suggest that even though multi-proxy biomarker analysis is a rapidly growing field of research, data interpretation must be based on objective statistical measures in order for the results to be unbiased and globally comparable.

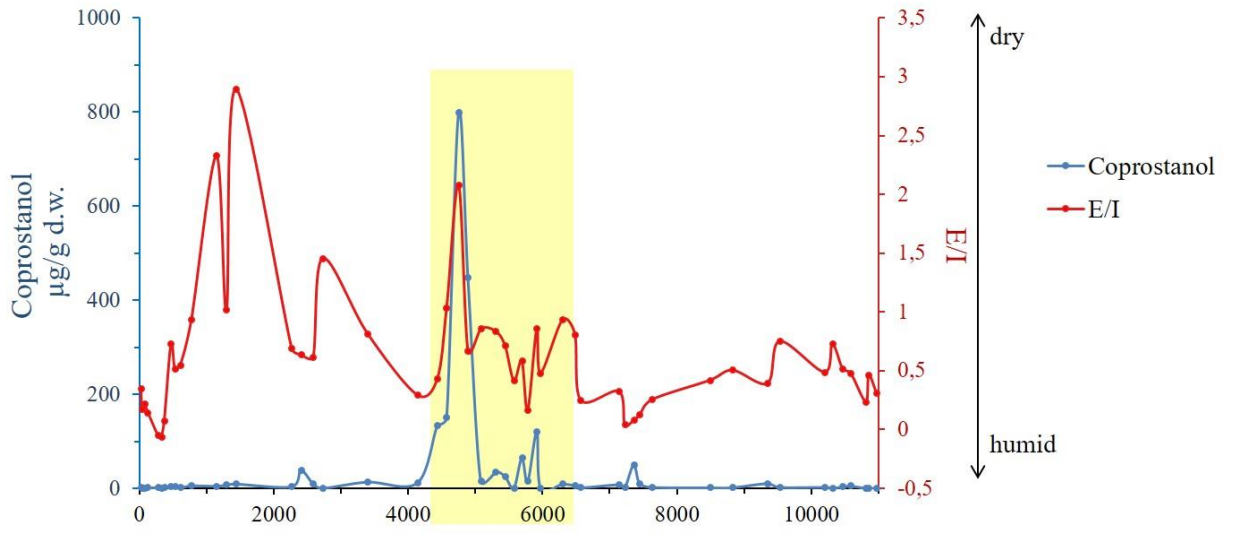


**Figure 4** Concentrations for coprostanol as a representative indicator for human presence (blue line) and Evaporation-to-Inflow (E/I) ratio (red line). Yellow shading indicates time period of enhanced human occupancy, which coincides with dry environmental conditions.

## 2.4. Conclusion and Outlook

The studies outlined in this dissertation highlight the manifold applications of lipid biomarkers, extracted from lake sediments, in paleoenvironmental research questions. Questions encompassed the reconstruction of Holocene environmental variability applying statistical and computational techniques, the biomolecular identification of human occupancy and finally, the utilization of CSRA to ascertain the aquatic and terrestrial influence on a lake's chronology. Nonetheless, the afore-going discussion inevitably entails various interesting scientific follow-up topics. Firstly, as this thesis primarily focuses on one study area, comparable studies from other regions influenced by different parameters, would enable the discrimination between local and regional environmental signals. This applies to both paleoenvironmental and paleoanthropological research.

In order to obtain a broad and enhanced picture about the world's environmental dynamics during the Holocene, it is essential to have widespread comparable studies to provide insights into temporal and spatial discrepancies and similarities. Only then will we be able to constitute reliable climate predictions for the future by reducing certain sources of uncertainty through our better understanding of interactions between different systems. However, for the future, as this thesis emphasizes, forthcoming multi-proxy paleoenvironmental studies should integrate more statistical techniques as this will eliminate subjective data evaluation. Consequently, this will allow for a straightforward comparison of statistically analysed time benchmarks between various studies. This is best facilitated through the public access of proxy data stored at digital data repositories. Regardless of the benefits proposed by data libraries, data is oftentimes only available upon request. Examples for big databases in Earth & Environmental Science are PANGAEA (Diepenbroek et al., 2002) and NOAA's National Centers for Environmental Information (https://www.ncei.noaa.gov/). They archive environmental data with related metainformation and make them freely available for further utilization and direct comparisons. As one of the main outcome of this thesis was the computational identification of potential tipping points, it would be interesting to establish a database encompassing statistically ascertained tipping points from diverse regions in order to discriminate global from regional effects.

CSRA on aquatic and terrestrial biomarkers clearly showcased compound-specific chronologies indicative of processes affecting biomarkers differently. Therefore, the discrepancy between biomarker-specific ages and those of the surrounding sediments, reveals important information on the residence time of biomarkers in the soil carbon stock (Douglas et al., 2014). As the degree of disparity is also site-specific, it is indispensable to integrate CSRA in prospective paleoenvironmental studies. This is, however, faced with the analytical challenges of small sample sizes and time-consuming laboratory preparations (Mollenhauer and Rethemeyer, 2009). Although recent technical advancements in accelerator mass spectrometry decreased sample size requirements to <25 µg of carbon (Mollenhauer and Rethemeyer, 2009; Shah and Pearson, 2007), analytes oftentimes do not exceed 10 µg of carbon (Walker and Xu, 2019). Therefore, studies,

including the one outlined in this thesis, frequently resort to pooling resembling homologues, which undisputedly leads to ambiguous results. Consequently, there is a growing demand to measure ultra-small samples reliably.

Furthermore, even though past investigations comprising CSRA on various biomarkers, demonstrated it's implementability in paleoenvironmental studies (e.g. Douglas et al., 2014; Makou et al., 2018; Ohkouchi and Eglinton, 2008; Smittenberg et al., 2004; Uchikawa et al., 2008), the ages of these biomarkers only represent a small fraction of TOC and do not reflect ages of other biomarkers. Hence, there is still a large number of biomarkers to analyze, which have not been subject to CSRA and thus require the development of protocols for their processing and handling. Nevertheless, in light of lacking dating materials, such as macrofossils and tephra layers, CSRA on biomarkers facilitates the narrowing of a lake's chronology as $^{14}C$ ages of the aquatic biomarker in manuscript two were in fairly good agreement with the independent varve chronology compared to $^{14}C$ ages of TOC. Ultimately, CSRA in future paleoenvironmental studies will be more feasible as technical progress in accelerator mass spectrometry will likely reduce the sample quantities of biomarkers required for their $^{14}C$ measurement.

The investigation of human and paleoenvironmental interactions is by nature an interdisciplinary task, which requires the integration of classical archaeology and biogeochemistry. Cross-collaborations are fruitful in bringing paleoenvironmentalists and archaeologists together to overcome their field's current challenges and broadening their respective views. The work reported in this dissertation gives a promising example of how biomolecular and archaeological information can be combined to reveal patterns of human migration in the past. Considering the high number of long sediment cores stored in archives as well as ongoing continental deep drilling projects, biomolecular studies of sediments older than the Holocene could provide valuable tests of long-held archaeological theories. Seeing as central theories of human origin and migration, such as the 'out-of-africa' theory, are continuously being challenged (Begun, 2016; Böhme et al., 2019), the additional tests that biomolecular studies can provide have global relevance.

In addition to its perspective on the past, the study of biomolecules targeting interactions between humans and their environment can yield critical information for predictions of human migration in response to future climate change. The effects of drought, desertification and land degradation are predicted to increase the migration of people (IPCC, 2014). The biomolecular results presented in this dissertation exemplify drought-induced human migration to a local high-altitude lake area. Even though such regions are currently only scarcely populated due to their harsh nature, they could potentially come into focus again as the conditions in some lowland areas will worsen. This highlights the relevance and urgency for the data-driven biomolecular approaches, which are outlined in this dissertation, to be adapted and scaled up. Their widespread implementation could close essential knowledge gaps on human migration and its drivers in the past and contribute substantially to our understanding of human responses to environmental change in the present and near future. Through this dissertation, our perspectives on the past have come a great step closer to becoming an objective analogue for our future.

## 3. Summary

As the world is contemporarily facing various aspects of global climate change, more than ever is it essential to unravel past climatic and environmental fluctuations and dynamics of the Earth system. This ensures a better understanding of different forcing mechanisms and interconnections, which will ultimately improve predictions of future climate trends and their consequences. Particularly the Holocene, that is the last 11,700 years, has been the subject of numerous paleoenvironmental studies due to its modern day climate resemblance and its significance for the development of human societies. Knowledge about past climatic and environmental variability can be inferred by the analysis of lipid biomarkers, which reflect various environmental conditions based on their specific source. After burial, biomarkers may be deposited and preserved in sediments stemming from a multitude of natural settings, such as lakes, oceans and estuaries. Here we focus on lipid biomarkers from lake sediments as these provide continuous, high-resolution archives to study local environmental factors affecting both terrestrial and hydrological processes. Geographical focus is placed on Lake Chatyr Kol, southern Kyrgyzstan, Central Asia. Lake Chatyr Kol holds favourable features, which makes it a key site to study past environmental conditions and their impacts on early humans, which are still insufficiently known. Firstly, the lake's location at the intersection of the reach of three major atmospheric systems (mid-latitude Westerlies, the Siberian High and partially the Asian monsoon system), enables the investigation of their interplay at high resolution. And secondly, as part of a prehistoric Silk Road network, the area holds valuable information about the cultural development and migration flow patterns.

In particular, we focus on long-chain alkenones (LCAs) and the respective alkenones unsaturation index $U_{37}^{K}$ utilized as a paleotemperature proxy and long-chain alkyl diols (LCDs) were investigated to indicate relative variations in the algal bioproductivity. Moreover, the compound-specific stable hydrogen isotope compositions (δD) of long-chain *n*-alkanes and mid-chain *n*-alkanes were analyzed to reflect changes in the δD of the meteoric water and n the δD of the lake water, respectively. Although the combined analysis of numerous biomarkers (multi-proxy analysis) provides multiple benefits over the analysis of a single biomarker, there is still no uniform solution how to evaluate the results in a statistical manner. Despite already existing and available techniques suitable for data processing, interpretation is still oftentimes carried out subjectively by visually aligning similarities and disparities of different biomarker records. Addressing this issue, this thesis examines the potential of novel statistical and computational techniques applied in the context of paleoenvironmental studies. We merge the outputs of Principal Component Analysis (PCA), Uniform Manifold Approximation and Projection (UMAP) and results of the time series analysis R package *asdetect* aiming (1) to disclose interdependencies of the investigated biomarkers and parameters and (2) to locate and specify lake phases and respective phase boundaries over the course of the Holocene in a valid and reproducible manner. According to the PCA result, lake water evaporation was highly dependent on winter solar insolation. Coherently, higher lake evaporation likely enhanced water salinity, which was a potential controlling parameter for the concentration of LCAs. On the other hand, occurences and concentrations of LCDs and *n*-alkanes were likely regulated by the $U_{37}^{K}$ index, with higher $U_{37}^{K}$ values pointing to higher temperatures. As the *n*-alkane distribution is predominantly represented by their long-chain homologues, an increase in their concentrations at higher temperatures would imply an

allochthonous origin, either by higher erosion and/or a growth stimulation of the terrestrial vegetation. Potentially, this led to enhanced discharge of nutrients into the lake promoting algae growth, which may have induced higher occurences of LCDs.

Based on the biomarker distribution, UMAP and *asdetect* partitioned the sediment core into five distinct phases (I–V) and characterized the responding phase transitions, respectively. The combination of multiple statistical techniques therefore enabled the reconstruction of Holocene environmental conditions of Western Central Asia carried out in a statistical manner. Accordingly, Phase I (~11,000 – 10,200 a BP) during the early Holocene encompassed low levels of concentration in all biomarker records under a cold and arid climate as observed by low $U_{37}^{K}$ index values and less negative δD values of the terrestrial derived *n*-alkane $nC_{29}$. However, an increase in the concentrations of long-chain *n*-alkanes and LCDs starting from ~10,900 a BP, indicated amplified terrigenous input and biological productivity, respectively. An abrupt and likely event-based transition from Phase I to Phase II occurred at 10,200 a BP, since the biomarker records simultaneously showed coinciding shifts at this time point. Potentially, this phase transition was temperature-dependent and related to the Holocene Climate Optimum, as $U_{37}^{K}$ index values sharply increased, which in turn likely provoked both enhanced input from the catchment area and enhanced algal bioproductivity. The shift towards Phase II might have been associated with the crossing of a lake-internal system threshold, which caused a rapid and abrupt reorganization of the ecosystem. Advantageous lake conditions persisted till ~8050 a BP as temperatures dropped substantially, which marks the transition and onset of Phase III. Similarly to the previous phase shift, the transition to Phase III was facilitated by a potential abrupt event-based tipping point triggered by changes in temperature, potentially linked to the North Atlantic 8.2 ka BP event. Over the course of Phase III, microorganisms strongly decreased, whereas LCA concentrations increased due to a likely stress response to colder conditions. Generally speaking, isotope ratios indicate dry environmental conditions and lower lake levels. In contrast to the preceding phase transitions, the shift towards Phase IV at ~2600 a BP was likely a gradual shift as it is characterized by a continuous temporal succession of biomarker variabilities. Following a short-term humid phase, warm and dry environmental conditions prevailed, particularly at ~2300 and ~1500 – 1000 a BP, coincing with the Roman Warm Period and the Medieval Climate Anomaly, respectively. Subsequently, isotope ratios and values for the $U_{37}^{K}$ index reflected cold and humid conditions between ~1030 and ~780 a BP, which potentially coincided with the Little Ice Age. Similar to Phase IV, the transition to Phase V at ~780 a BP was also gradually, provoking a response in a singular biomarker and entailing a lagged temporal shift succession of the remaining biomarkers. Phase V encompassed the youngest part of the sediment core and although being temporally separated, was assigned to the same cluster as Phase I (~11,000 – 10,200 a BP), reflecting alike prevailing environmental conditions. Isotope ratios pointed towards wetter conditions and more rainfall under warmer temperatures.

However, although located along a prehistoric Silk Road, human occupation and its interdependency with climate and the environment, is still scarcely known. As this is generally related to limited archeological evidences, we explored the potential of fecal biomarkers (sterols and stanols) as an emergent alternative approach to detect human activity. Fecal stanols derive from mammals by the microbial reduction of sterols and which, based on their diet, can be assigned

to herbivorous (primarily 5β-stigmastanol) or human (primarily coprostanol) fecal input. Here, UMAP separated the sediment core into three dinstict phases (Phases 1–3). Phase 1 (∼11,400–8300 a BP) disclosed conditions of prehuman occupancy as human-specific fecal biomarker were at low background levels. Nevertheless, elevated 5β-stigmastanol concentrations during Phase 1, indicated the presence of indigenous higher mammals, possibly coupled to the aforementioned favourable conditions inferred by the multi-proxy approach for Lake Phase II. Earliest considerable concentrations of human-specific stanols occurred over the course of Phase 2 (∼7600–2400 a BP) at ∼5900 a BP and particularly at ∼4800 a BP. Since these concentrations were accompanied by simultaneous rises of 5β-stigmastanol concentrations, human activity was potentially linked to pastoralism with domesticated livestock. Our findings were further affirmed by archaeological evidence in the surrounding area. The occurences of humans in our sediment core were significantly correlated to parameters indicative of Lake Evaporation and thus likely facilitated by dry environmental conditions. Dry periods either enabled a better accessibility of remote regions and/or exerted pressure on locating new herding grounds, which consequently influenced corresponding migration flows. However, human-specific biomarkers diminished again during Phase 3 (∼2300 a BP – Present) towards background concentrations. Similarly, herbivorous-specific biomarker concentrations decreased some time later after ∼1300 a BP. These findings reflect current conditions at the Lake's catchment area as it is presently little used and the majority of usage taking place in the summer months from June to mid- September. Summarising, fecal biomarkers enabled the high-resolution reconstruction of early human presences independent of archaeological excavation sites as promising approach. Furthermore, in an innovative statistical approach, our results highlight climatic and environmental change, inter alia, as underlying controlling parameters for human presence in the past.

However, despite their advantages, lacustrine multi-proxy reconstructions frequently suffer from insufficient accuracies of the chronology since lakes are sensitive to the Lake Reservoir Effect (LRE). This effect misleadingly displays anomalously old apparent radiocarbon ages due to the incorporation of preaged carbon into the lake system. Employing a rapid isolation method, we present a compound-specific radiocarbon analysis (CSRA) approach to investigate the temporal dependency of the LRE on the aquatic and terrestrial environment. Long-chain saturated fatty acid methyl ester (FAME) ($C_{24}$, $C_{26}$, $C_{28}$) and short-chain ($C_{16}$, $C_{18}$) homologues were isolated and dated to reflect the terrestrial and aquatic signal, respectively. Generally, long-chain FAMEs were older than short-chain FAMEs and in closer agreement to $^{14}C$ ages of the total organic carbon. We found a strong correlation of the age offset between long-chain and short-chain FAMEs with higher Ti/K values, which are indicative of grain-size increases. Therefore, during time periods of enhanced input of detrital terrigenous material, e.g. erosion, pre-aged terrestrial biomarkers were remobilized and thus influenced the magnitude of the LRE. Accordingly, our results demonstrated the potential of CSRA to delineate process-specific biomarker chronologies from complex organic mixtures in lake sediments.

The research presented in this dissertation reveals a modern and data-driven perspective on biomarker analysis for paleoenvironmental reconstructions. A lack of knowledge on the future development and impact of the present climate crisis necessitated the search for past analogues of climate and environmental evolution during the Holocene. This thesis emphasizes that, for

paleoenvironmental reconstructions to be relevant and useful analogues, the underlying biomarker data should integrate multiple proxies, be jointly analyzed in a statistical and objective manner, and employ biomarker-specific chronologies. It furthermore demonstrates that interdisciplinary research combining archaeological and biomolecular investigations has the potential to disclose the detailed relationship of environmental change, human migration and adaptation.

## 4. Zusammenfassung

Da sich die Welt heute mit verschiedenen Aspekten des globalen Klimawandels konfrontiert sieht, ist es mehr denn je unerlässlich, die vergangenen klimatischen und ökologischen Schwankungen und die Dynamik des Erdsystems zu entschlüsseln. Dies gewährleistet ein besseres Verständnis der verschiedenen Antriebsmechanismen und Wechselbeziehungen, was letztlich die Vorhersagen künftiger Klimatrends und ihrer Folgen verbessert. Insbesondere das Holozän, d.h. die letzten 11.700 Jahre, ist aufgrund der Ähnlichkeit zum heutigen Klima und der Relevanz für die Entwicklung der menschlichen Gesellschaft, Fokus zahlreicher paläoökologischer Studien. Kenntnisse über vergangene Klima- und Umweltveränderungen können durch die Analyse von Lipid-Biomarkern abgeleitet werden, die aufgrund ihrer unterschiedlichen biologischen Ursprünge, verschiedene Umweltbedingungen widerspiegeln können. Nach ihrer Ablagerung können Biomarker in einer Vielzahl von Naturarchiven sedimentiert und konserviert werden, wie beispielsweise Seesedimente, Meeressedimente und Flussmündungssedimente. Hier konzentrieren wir uns auf Lipid-Biomarker, die aus Seesedimenten extrahiert wurden. Seesedimente stellen kontinuierliche, hochauflösende Naturarchive zur Untersuchung lokaler Umwelvariablen dar, die sowohl durch das terrestrische als auch das hydrologische Regime beeinflusst werden. Geografischer Schwerpunkt wurde auf den See Chatyr Kol in Südkirgisistan, Zentralasien, gelegt. Der See besitzt mehrere günstige Eigenschaften, welche ihn zu einer regionalen Schlüsselkomponente für die Untersuchung von früheren Umweltbedingungen und deren gegenwärtig noch unzureichend bekannten Auswirkungen auf vorgeschichtliche Menschen, macht. Zum einen ermöglicht die Lage des Sees am Schnittpunkt dreier großer Windsysteme (Westwinde der mittleren geographischen Breiten, Sibirienhoch und teils Asiatischen Monsun) die hochauflösende Analyse ihres atmosphärischen Zusammenspiels. Zum anderen war die Region um den See Teil eines frühen Seidenstraßen-Netzwerks und birgt daher wertvolle Informationen über die kulturelle Entwicklung und Migrationsmuster von frühgeschichtlichen Menschen.

Im Speziellen konzentrieren wir uns auf langkettige Alkenone (LCA) und dem zugehörigen Alkenon-Sättigungs Index ($U_{37}^{K}$) als einen Index für Paläotemperaturen, und langkettige Alkyldiole (LCD) wurden untersucht, um relative Produktivitätsschwankungen von Algen festzustellen. Darüber hinaus wurden die komponenten-spezifischen stabilen Wasserstoffisotope (δD) von langkettigen und mittelkettigen *n*-Alkanen analysiert, um Veränderungen im meteorischen Wasser beziehungsweise im Seewasser widerzuspiegeln. Obgleich die kombinierte Analyse verschiedener Biomarker (Multi-Proxy Analyse) mehrere Vorteile gegenüber der Analyse eines einzelnen Biomarkers bietet, gibt es immer noch keine einheitliche Lösung, wie die Ergebnisse statistisch ausgewertet werden können. Trotz bereits vorhandener und verfügbarer Techniken, die für die Datenverarbeitung geeignet sein könnten, erfolgt die Interpretation oft noch subjektiv, indem Ähnlichkeiten und Unterschiede verschiedener Biomarker-Datensätze visuell abgeglichen werden. Um sich dieser Problematik anzunehmen, untersucht diese Dissertation das Potenzial neuartiger statistischer und rechnergestützter Techniken im Rahmen von Paläoumweltstudien. Wir führten die Ergebnisse einer Hauptkomponentenanalyse (englisch Principal Component Analysis, kurz: PCA), einer Dimensionsreduktion mittels Uniform Manifold Approximation and Projection (UMAP) und der Zeitreihenanalyse im R-Paket *asdetect*, zusammen mit dem Ziel (1) die Wechselbeziehungen der untersuchten Biomarker und Parameter aufzudecken und (2) spezifische,

holozäne Seephasen und zugehörige Phasengrenzen auf eine statistisch fundierte und reproduzierbare Weise ausfindig zu machen. Den Ergebnissen der PCA zufolge, hing die Verdunstung des Seewassers stark von der winterlichen Sonneneinstrahlung ab. Gleichzeitig erhöhte eine stärkere Verdunstung vermutlich den Salzgehalt des Seewassers, was ein Steuerungsparameter für die Konzentration der LCA zu sein schien. Auf der anderen Seite wurden Vorkommen und Konzentrationen von LCD und *n*-Alkanen wahrscheinlich durch den $U_{37}^{K}$ index reguliert, wobei höhere $U_{37}^{K}$ Werte auf höhere Temperaturen hindeuteten. Da die Verteilung der *n*-Alkane überwiegend durch ihre langkettigen Homologe bestimmt wurde, würde ein Anstieg ihrer Konzentrationen bei höheren Temperaturen einen allochthonen Ursprung implizieren, der entweder durch höhere Erosion und/oder durch eine Wachstumsbelebung der terrestrischen Vegetation gesteuert wurde. Möglicherweise führte dies zu einem erhöhten Nährstoffeintrag in den See, der das Algenwachstum förderte und wiederum zu einem stärkeren Vorkommen von LCD geführt hat.

Basierend auf der Biomarkerverteilung teilten UMAP und *asdetect* den Sedimentkern in fünf verschiedene Phasen (I-V) auf und charakterisierten die jeweils zugehörenden Phasenübergänge. Die Kombination mehrerer statistischer Techniken ermöglichte daher die statistische Rekonstruktion der holozänen Umweltbedingungen im westlichen Zentralasien. Dementsprechend umfasste Phase I (~11.000 - 10.200 a BP) das frühe Holozän, welches durch niedrige Konzentrationen aller Biomarker gekennzeichnet war. Klimatische Bedingungen waren möglicherweise kalt und trocken, wie sie durch niedrige $U_{37}^{K}$ und weniger negative δD des terrestrisch abgeleiteten *n*-Alkans $nC_{29}$ beobachtet wurden. Jedoch deutete ein Anstieg der Konzentrationen von langkettigen *n*-Alkanen und LCD ab ~10.900 a BP auf einen verstärkten terrigenen Input beziehungsweise auf eine erhöhte biologische Produktivität hin. Ein abrupter und wahrscheinlich ereignisbasierter Übergang von Phase I zu Phase II erfolgte bei ~10.200 a BP, da die Biomarker-Aufzeichnungen zu diesem Zeitpunkt gleichzeitig übereinstimmende und starke Veränderungen aufwiesen. Möglicherweise war dieser Phasenübergang temperaturabhängig und hing mit dem Holozänen Optimum zusammen, da $U_{37}^{K}$-Indexwerte stark anstiegen, was wiederum sowohl einen verstärkten Input aus dem Einzugsgebiet als auch eine erhöhte Algenbioproduktivität zur Folge hatte. Der Übergang zu Phase II könnte mit dem Überschreiten der Schwelle eines seeinternen Systems verbunden gewesen sein, was zu einer raschen und abrupten Reorganisation des Ökosystems führte. Vorteilhafte Seebedingungen blieben bis ~8050 a BP bestehen, als die Temperaturen deutlich sanken, was den Übergang und den Beginn von Phase III markierte. Ähnlich wie bei der vorherigen Phasenverschiebung wurde der Übergang zu Phase III möglicherweise durch einen abrupten, ereignisbasierten Kipppunkt hervorgerufen, der eventuell mit dem 8.2 kiloyear Ereignis im Nordatlantik zusammenhing. Im Verlauf von Phase III nahmen Mikroorganismen stark ab, während die LCA-Konzentrationen aufgrund einer wahrscheinlichen Stressreaktion auf kältere Bedingungen, anstiegen. Generell wiesen die Wasserstoff-Isotopenverhältnisse auf trockene Umweltbedingungen und einen niedrigeren Seepegel hin.

Im Gegensatz zu den vorhergehenden Phasenübergängen war der Übergang zu Phase IV um ~2600 a BP, wahrscheinlich ein gradueller Übergang, da dieser durch eine kontinuierliche zeitliche Abfolge der Biomarker-Variabilitäten gekennzeichnet war. Nach einer kurzzeitigen humiden Klimaphase herrschten warme und trockene Umweltbedingungen vor, insbesondere um ~2300

und ~1500 - 1000 a BP, die mit der römischen Warmzeit beziehungsweise mit der mittelalterlichen Klimaanomalie zusammenhingen. Darauf folgend spiegelten sowohl Wasserstoff-Isotopenverhältnisse als auch niedrige $U_{37}^{K}$ Werte, kalte und feuchte Bedingungen zwischen ~1030 und ~780 a BP wider, die möglicherweise mit der Kleinen Eiszeit zusammenfielen.

Ähnlich zu Phase IV, erfolgte der Übergang zu Phase V um ~780 a BP graduell. Der Übergang wurde zunächst durch einen singulären Biomarker signalisiert und hatte eine zeitlich verzögerte Wechselabfolge der restlichen Biomarker zur Folge. Phase V umspannte den jüngsten Teil des Sedimentkerns und wurde, obwohl zeitlich getrennt, dem gleichen Cluster wie Phase I zugeordnet (~11.000 - 10.200 a BP). Dies deutete auf vergleichbare vorherrschende Umweltbedingungen während Phase I und Phase V hin. Wasserstoff-Isotopenverhältnisse reflektierten ein feuchteres und wärmeres Klima unter vermehrten Niederschlag.

Trotz seiner bedeutsamen, geografischen Lage als Teil einer prähistorischen Seidenstraße, ist über die menschliche Besiedlung Zentralasiens und der Wechselbeziehung von Mensch mit der Umwelt, noch unzureichend bekannt. Da dies oft mit begrenzten archäologischen Beweisstücken zusammenhängt, haben wir als zweiten Schwerpunkt dieser Dissertation, das Potenzial von fäkalen Biomarkern (Sterole und Stanole) als alternativen Ansatz zum Nachweis frühmenschlicher Aktivitäten untersucht. Fäkale Stanole entstammen der mikrobiellen Reduktion von Sterolen und können aufgrund der unterschiedlichen Ernährung, pflanzenfressenden Säugetieren (hauptsächlich 5β-Stigmastanol) und Menschen (hauptsächlich Coprostanol) zugeordnet werden. Hier trennte UMAP den Sedimentkern in drei abgegrenzte Phasen (Phasen 1-3). Phase 1 (~11.400 - 8300 a BP) spiegelte Bedingungen vor einer menschlichen Besiedlung wider aufgrund von sehr niedrigen human-spezifischen fäkalen Biomarkerkonzentrationen. Allerdings deuteten höhere 5β-Stigmastanol-Konzentrationen während Phase 1 auf die Präsenz einheimischer, höherer Säugetiere hin. Möglicherweise wurde das Vorhandensein von Säugetieren durch die oben ausgeführten vorteilhaften Umweltbedingungen der Multi-Proxy Rekonstruktion für die See-Phase II, begünstigt.

Die frühesten nennenswerten Konzentrationen der human-spezifischen Stanole traten im Laufe der Phase 2 (~7600-2400 a BP) auf, insbesondere um ~4800 a BP. Da diese Konzentrationen mit einem gleichzeitigen Anstieg der 5β-Stigmastanol-Konzentrationen einhergingen, ist es möglich, dass die menschliche Aktivität von Pastoralismus mit domestiziertem Vieh abhing. Unsere Ergebnisse wurden durch archäologische Funde in der Umgebung weiter bestätigt. Generell war das Vorkommen von Menschen in unserem Sedimentkern mit Parametern indikativ für Seeverdunstung korreliert, und folglich möglicherweise durch trockene Umweltbedingungen ermöglicht. Trockenperioden ermöglichten entweder eine bessere Erreichbarkeit abgelegener Regionen und/oder übten Druck auf die Ansiedlung neuer Weideflächen aus, was folglich entsprechende Migrationsströme beeinflusste. Jedoch nahmen die human-spezifischen Biomarker während Phase 3 (~2300 a BP - Present) wieder ab und zeigten Hintergrundkonzentration. Ebenfalls sanken die Konzentrationen der Herbivoren-spezifischen Biomarker nach ~1300 a BP. Diese Ergebnisse spiegeln die aktuellen Bedingungen im Einzugsgebiet des Sees wider, da es gegenwärtig wenig genutzt wird und der Großteil der Nutzung in den Sommermonaten von Juni bis Mitte September stattfindet.

Zusammenfassend lässt sich sagen, dass fäkale Biomarker die hochauflösende Rekonstruktion früher menschlicher Anwesenheit, unabhängig von archäologischen Ausgrabungsstätten, als vielversprechenden Ansatz ermöglichten. Darüber hinaus konnte die Wechselbeziehung von Klima- und Umweltveränderungen mit frühgeschichtlichen Menschen auf eine innovative und statistisch fundierte Weise untersucht werden.

Trotz ihrer Vorteile leiden lakustrine Multi-Proxy-Rekonstruktionen jedoch häufig unter unzureichender Genauigkeit der Chronologie, da Seen empfindlich auf den Lake Reservoir Effect (LRE) reagieren. Dieser Effekt zeigt irreführenderweise scheinbare, anomal alte Radiokohlenstoffalter an, die auf die Aufnahme von vorgealtetem Kohlenstoff in das Seesystem zurückzuführen sind. Mittels einer schnellen Isolierungsmethode für gesättigte Fettsäuren Methylester (englisch fatty acid methyl ester, kurz: FAME), entwickelten wir einen Ansatz zur komponenten-spezifischen Radiocarbon Analyse (englisch compound-specific radiocarbon analysis, kurz: CSRA), um die zeitliche Abhängigkeit des LRE von der aquatischen und terrestrischen Umwelt zu untersuchen. Langkettige FAME ($C_{24}$, $C_{26}$, $C_{28}$) und kurzkettige ($C_{16}$, $C_{18}$) FAME wurden isoliert und datiert, um das terrestrische beziehungsweise aquatische Signal widerzuspiegeln. Generell waren die langkettigen FAMEs älter als die kurzkettigen FAMEs und in engerer Übereinstimmung mit den $^{14}C$-Altern datiert am organisch gebundenen Gesamtkohlenstoff. Wir fanden eine starke Korrelation der Altersdifferenz zwischen langkettigen und kurzkettigen FAMEs mit höheren Ti/K-Werten, die auf eine Zunahme der Korngröße hindeuteten. Daher wurden in Zeiträumen mit erhöhtem Eintrag von detritalem terrigenem Material, z.B. durch Erosion, vorgealterte terrestrische Biomarker remobilisiert und beeinflussten somit die Magnitude des LRE. Dadurch zeigten unsere Ergebnisse das Potential von CSRA, prozessspezifische Biomarkerchronologien aus komplexen organischen Mischungen in Seesedimenten wiederzugeben.

Die in dieser kumulativen Dissertation vorgestellten Studien zeigen eine moderne und datengestützte Perspektive der Biomarkeranalyse für paläoökologische Rekonstruktionen. Unzureichendes Wissen über die zukünftige Entwicklung und die Auswirkungen der gegenwärtigen Klimakrise machte die Suche nach Analogien der vergangenen Klima- und Umweltentwicklung notwendig.

Diese Dissertation legt grundlegende Kriterien dar, die es ermöglichen aus paläoökologischen Rekonstruktionen nützliche Analoga für zukünftige Umweltszenarien zu entwickeln. Dabei sollten die den Studien zugrunde liegenden Biomarker-Daten auf mehreren Proxies basieren, die einzelnen Proxies gemeinsam mit objektiven statistischen Analysen ausgewertet werden und für ihre Datierung biomarker-spezifische Chronologien verwendet werden. Darüber hinaus wird verdeutlicht, dass interdisziplinäre Forschung, die archäologische und biomolekulare Untersuchungen kombiniert, das Potenzial hat, die detaillierte Beziehung zwischen Umweltveränderungen, menschlicher Migration und Anpassungsstrategien offenzulegen.

## 5. Bibliography

Abdi, H., and Williams, L. J., 2010, Principal component analysis: Wiley Interdisciplinary Reviews: Computational Statistics, v. 2, no. 4, p. 433–459, doi: 10.1002/wics.101

Allen, M. R., Dube, O. P., Solecki, W., Aragón-Durand, F., Cramer, W., Humphreys, S., Kainuma, M., Kala, J., Mahowald, N., Mulugetta, Y., Perez, R., Wairiu, M., and Zickfeld, K., 2018, Framing and Context, in Masson-Delmotte, V., Zhai, P., Pörtner, H.-O., Roberts, D., Skea, J., Shukla, P. R., Pirani, A., Moufouma-Okia, W., Péan, C., Pidcock, R., Connors, S., Matthews, J. B. R., Chen, Y., Zhou, X., Gomis, M. I., Lonnoy, E., Maycock, T., Tignor, M., and Waterfield, T., eds., Global Warming of 1.5°C. An IPCC Special Report on the impacts of global warming of 1.5°C above pre-industrial levels and related global greenhouse gas emission pathways, in the context of strengthening the global response to the threat of climate change, sustainable development, and efforts to eradicate poverty (In Press).

Alley, R. B., Marotzke, J., Nordhaus, W. D., Overpeck, J. T., Peteet, D. M., Pielke, R. A., Pierrehumbert, R. T., Rhines, P. B., Stocker, T. F., Talley, L. D., and Wallace, J. M., 2003, Abrupt Climate Change, v. 299, no. 5615, p. 2005–2010, doi: 10.1126/science.1081056

Anderson, A. G., 2014, Media, Environment and the Network Society, London, Palgrave Macmillan, Palgrave Studies in Media and Environmental Communication, X, 203 p.ISBN: 978-1-349-30399-1. doi: 10.1057/9781137314086

Becht, E., McInnes, L., Healy, J., Dutertre, C. A., Kwok, I. W. H., Ng, L. G., Ginhoux, F., and Newell, E. W., 2018, Dimensionality reduction for visualizing single-cell data using UMAP: Nature Biotechnology, doi: 10.1038/nbt.4314

Begun, D. R., 2016, The Real Planet of the Apes: A New Story of Human Origins, Princeton & Oxford, Princeton University Press.ISBN: 978-0-691-14924-0, doi: 10.2307/j.ctt21c4v71

Bell, M. A., and Blais, J. M., 2020, Paleolimnology in support of archeology: a review of past investigations and a proposed framework for future study design: Journal of Paleolimnology, doi: 10.1007/s10933-020-00156-8

Bennett, R. S., 1969, The intrinsic dimensionality of signal collections: IEEE Transactions on Information Theory, v. 15, no. 5, p. 517–525, doi: 10.1109/TIT.1969.1054365

Bertrand, S., Araneda, A., Vargas, P., Jana, P., Fagel, N., and Urrutia, R., 2012, Using the N/C ratio to correct bulk radiocarbon ages from lake sediments: Insights from Chilean Patagonia: Quaternary Geochronology, v. 12, p. 23–29, doi: 10.1016/j.quageo.2012.06.003

Bianchi, T. S., and Canuel, E. A., 2011, Chemical Biomarkers in Aquatic Ecosystems, Princeton, Oxford, Princeton University Press, 392 p.ISBN: 978-0691134147

Birks, H. H., and Birks, H. J. B., 2006, Multi-proxy studies in palaeolimnology: Vegetation History and Archaeobotany, v. 15, no. 4, p. 235-251, doi: 10.1007/s00334-006-0066-6

Böhme, M., Spassov, N., Fuss, J., Tröscher, A., Deane, A. S., Prieto, J., Kirscher, U., Lechner, T., and Begun, D. R., 2019, A new Miocene ape and locomotion in the ancestor of great apes and humans: Nature, v. 575, p. 489–493, doi: 10.1038/s41586-019-1731-0

Boulton, C. A., and Lenton, T. M., 2019, A new method for detecting abrupt shifts in time series [version 1; peer review: 2 approved with reservations]: F1000 Research, v. 8, no. 746, doi: 10.12688/f1000research.19310.1

Brauer, A., Hajdas, I., Blockley, S. P. E., Bronk Ramsey, C., Christl, M., Ivy-Ochs, S., Moseley, G. E., Nowaczyk, N. N., Rasmussen, S. O., Roberts, H. M., Spötl, C., Staff, R. A., and Svensson, A., 2014, The importance of independent chronology in integrating records of past climate change for the 60–8 ka INTIMATE time interval: Quaternary Science Reviews, v. 106, p. 47–66, doi: 10.1016/j.quascirev.2014.07.006

Brocks, J. J., and Pearson, A., 2005, Building the Biomarker Tree of Life: Reviews in Mineralogy & Geochemistry, v. 59, no. 1, p. 233–258, doi: 10.2138/rmg.2005.59.10

Bull, I. D., Elhmmali, M. M., Roberts, D. J., and Evershed, R. P., 2003, The application of steroidal biomarkers to track the abandonment of a Roman wastewater course at the Agora (Athens, Greece): Archaeometry, v. 45, p. 149–161, doi: 10.1111/1475-4754.00101

Bull, I. D., Evershed, R. P., and Betancourt, P. P., 2001, An organic geochemical investigation of the practice of manuring at a Minoan site on Pseira Island, Crete: Geoarchaeology, v. 16, no. 2, p. 223–242 doi: 10.1002/1520-6548(200102)16:2<223::aid-gea1002>3.0.co;2-7

Bull, I. D., Lockheart, M. J., Elhmmali, M. M., Roberts, D. J., and Evershed, R. P., 2002, The origin of faeces by means of biomarker detection: Environment International, v. 27, p. 647–654, doi: 10.1016/s0160-4120(01)00124-6

Bull, I. D., Simpson, I. A., Van Bergen, P. F., and Evershed, R. P., 1999, Muck ‘n’ molecules: organic geochemical methods for detecting ancient manuring: Antiquity, v. 73, no. 279, p. 86–96, doi: 10.1017/s0003598x0008786x

Castañeda, I. S., and Schouten, S., 2011, A review of molecular organic proxies for examining modern and ancient lacustrine environments: Quaternary Science Reviews, v. 30, no. 21-22, p. 2851–2891, doi: 10.1016/j.quascirev.2011.07.009

Conte, M. H., and Weber, J. C., 2002, Plant biomarkers in aerosols record isotopic discrimination of terrestrial photosynthesis: Nature, v. 417, p. 639–641, doi: 10.1038/nature00777

Cranwell, P. A., Eglinton, G., and Robinson, N., 1987, Lipids of aquatic organisms as potential contributors to lacustrine sediments – ll∗: Organic Geochemistry, v. 11, p. 513–527, doi: 10.1016/0146-6380(87)90007-6

D'Anjou, R. M., Bradley, R. S., Balascio, N. L., and Finkelstein, D. B., 2012, Climate impacts on human settlement and agricultural activities in northern Norway revealed through sediment biogeochemistry: Proceedings of the National Academy of Sciences, v. 109, p. 20332–20337, doi: 10.1073/pnas.1212730109

Dansgaard, W., Johnsen, S. J., Clausen, H. B., Dahl-Jensen, D., Gundestrup, N. S., Hammer, C. U., Hvidberg, C. S., Steffensen, J. P., Sveinbjörnsdottir, A. E., Jouzel, J., and Bond, G., 1993, Evidence for general instability of past climate from a 250-kyr ice-core record: Nature, v. 364, p. 218–220, doi: 10.1038/364218a0

Dawson, L. A., and Mayes, R. W., 2015, Criminal and Environmental Soil Forensics: Soil as Physical Evidence in Forensic Investigations, in Murphy, B. L., and Morrison, R. D., eds., Introduction to Environmental Forensics: Cambridge, Massachusetts, Academic Press, p. 457–486.

DeMenocal, P. B., and Bond, G., 1997, Holocene climate less stable than previously thought: EOS, v. 78, no. 41, p. 447–454, doi: 10.1029/97EO00279

Diaz-Papkovich, A., Anderson-Trocme, L., Ben-Eghan, C., and Gravel, S., 2019, UMAP reveals cryptic population structure and phenotype heterogeneity in large genomic cohorts: PLoS Genet, v. 15, no. 11, p. e1008432, doi: 10.1371/journal.pgen.1008432

Diepenbroek, M., Grobe, H., Reinke, M., Schindler, U., Schlitzer, R., Sieger, R., and Wefer, G., 2002, PANGAEA—an information system for environmental sciences: Computers & Geosciences, v. 28, no. 10, p. 1201–1210, doi: 10.1016/S0098-3004(02)00039-0

Dore, M. H. I., 2005, Climate change and changes in global precipitation patterns: What do we know?: Environmental International, v. 31, no. 8, p. 1167–1181, doi: 10.1016/j.envint.2005.03.004

Douglas, P. M. J., Pagani, M., Eglinton, T. I., Brenner, M., Hodell, D. A., Curtis, J. H., Ma, K. F., and Breckenridge, A., 2014, Pre-aged plant waxes in tropical lake sediments and their influence on the chronology of molecular paleoclimate proxy records: Geochimica et Cosmochimica Acta, v. 141, p. 346–364, doi: 10.1016/j.gca.2014.06.030

Dubois, N., and Jacob, J., 2016, Molecular Biomarkers of Anthropic Impacts in Natural Archives: A Review: Frontiers in Ecology and Evolution, v. 4, no. 92, p. 4–16, doi: 10.3389/fevo.2016.00092

Eglinton, G., and Calvin, M., 1967, Chemical fossils: Scientific American, v. 216, p. 32–43

Eglinton, G., and Hamilton, R., 1967, Leaf Epicuticular Waxes: Science, v. 156, no. 3780, p. 1322–1335, doi: 10.1126/science.156.3780.1322

Eglinton, T., Aluwihare, L. I., Bauer, J. E., Druffel, E. R., and McNichol, A. P., 1996, Gas Chromatographic Isolation of Individual Compounds from Complex Matrices for Radiocarbon Dating: Analytical Chemistry, v. 68, no. 5, p. 904–912

Engels, S., van Oostrom, R., Cherli, C., Dungait, J. A. J., Jansen, B., van Aken, J. M., van Geel, B., and Visser, P. M., 2018, Natural and anthropogenic forcing of Holocene lake ecosystem development at Lake Uddelermeer (The Netherlands): Journal of Paleolimnology, v. 59, no. 3, p. 329–347, doi: 10.1007/s10933-017-0012-x

Evershed, R. P., and Bethell, P. H., 1996, Application of Multimolecular Biomarker Techniques to the Identification of Fecal Material in Archaeological Soils and Sediments: Archaeological Chemistry, v. 625, p. 157–172, doi: 10.1021/bk-1996-0625.ch013

Eyssen, H. J., Parmentier, G. G., Compernolle, F. C., G., d. P., Piessens-Denef, M., and M., M. A., 1973, Biohydrogenation of sterols by Eubacterium ATCC 21,408 — nova species: European Journal of Biochemistry, v. 36, p. 411–421, doi: 10.1111/j.1432-1033.1973.tb02926.x

Feng, X., Gustafsson, Ö., Holmes, R. M., Vonk, J. E., van Dongen, B. E., Semiletov, I. P., Dudarev, O. V., Yunker, M. B., Macdonald, R. W., Wacker, L., Montluçon, D. B., and Eglinton, T. I., 2015, Multimolecular tracers of terrestrial carbon transfer across the pan-Arctic:14C characteristics of sedimentary carbon components and their environmental controls: Global Biogeochemical Cycles, v. 29, no. 11, p. 1855–1873, doi: 10.1002/2015gb005204

Ficken, K. J., Li, B., Swain, D. L., and Eglinton, G., 2000, An n-alkane proxy for the sedimentary input of submerged/floating freshwater aquatic macrophytes: Organic Geochemistry, v. 31, p. 745–749, doi: 10.1016/S0146-6380(00)00081-4

Giger, W., Schaffner, C., and Wakeham, S. G., 1980, Aliphatic and olefinic hydrocarbons in recent sediments of Greifensee, Switzerland: Geochimica et Cosmochimica Acta, v. 44, no. 1, p. 119–129, doi: 10.1016/0016-7037(80)90182-9

Grimalt, J. O., Fernandez, P., Bayona, J. M., and Albaiges, J., 1990, Assessment of fecal sterols and ketones as indicators of urban sewage inputs to coastal waters: Environmental Science & Technology, v. 24, no. 3, p. 357–363, doi: 10.1021/es00073a011

Guenther, F., Aichner, B., Siegwolf, R., Xu, B., Yao, T., and Gleixner, G., 2013, A synthesis of hydrogen isotope variability and its hydrological significance at the Qinghai–Tibetan Plateau: Quaternary International, v. 313-314, p. 3–16, doi: 10.1016/j.quaint.2013.07.013

Guillot, D., Rajaratnam, B., and Emile-Geay, J., 2015, Statistical paleoclimate reconstructions via Markov random fields: The Annals of Applied Statistics, v. 9, no. 1, p. 324-352, doi: 10.1214/14-aoas794

Hayes, J. M., Freeman, K. H., Popp, B. N., and Hoham, C. H., 1990, Compound-specific isotopic analyses: A novel tool for reconstruction of ancient biogeochemical processes: Organic Geochemistry, v. 16, no. 4-6, p. 1115–1128

Hilkert, A. W., Douthitt, C. B., Schlüter, H. J., and Brand, W. A., 1999, Isotope ratio monitoring gas chromatography/mass spectrometry of D/H by high temperature conversion isotope ratio mass spectrometry: Rapid Commun Mass Spectrometry, v. 13, p. 1226–1230

Hou, J., D'Andrea, W. J., and Liu, Z., 2012, The influence of 14C reservoir age on interpretation of paleolimnological records from the Tibetan Plateau: Quaternary Science Reviews, v. 48, p. 67–79, doi: 10.1016/j.quascirev.2012.06.008

Huang, Y., Shuman, B., Wang, Y., and Webb III, T., 2002, Hydrogen isotope ratios of palmitic acid in lacustrine sediments record late Quaternary climate variations: Geology, v. 30, no. 12, p. 1103–1106, doi: 10.1130/0091-7613(2002)030<1103:HIROPA>2.0.CO;2

IPCC, 2014: Climate Change 2014: Impacts, Adaptation, and Vulnerability. Part A: Global and Sectoral Aspects. Contribution of Working Group II to the Fifth Assessment Report of the Intergovernmental Panel on Climate Change [Field, C.B., V.R. Barros, D.J. Dokken, K.J. Mach, M.D. Mastrandrea, T.E. Bilir, M. Chatterjee, K.L. Ebi, Y.O. Estrada, R.C. Genova, B. Girma, E.S. Kissel, A.N. Levy, S. MacCracken, P.R. Mastrandrea, and L.L.White (eds.)]. Cambridge University Press, Cambridge, United Kingdom and New York, NY, USA, 1132 pp.

IPCC, 2018: Global Warming of 1.5°C.An IPCC Special Report on the impacts of global warming of 1.5°C above pre-industrial levels and related global greenhouse gas emission pathways, in the context of strengthening the global response to the threat of climate change, sustainable development, and efforts to eradicate poverty [Masson-Delmotte, V., P. Zhai, H.-O. Pörtner, D. Roberts, J. Skea, P.R. Shukla, A. Pirani, W. Moufouma-Okia, C. Péan, R. Pidcock, S. Connors, J.B.R. Matthews, Y. Chen, X. Zhou, M.I. Gomis, E. Lonnoy, T. Maycock, M. Tignor, and T. Waterfield (eds.)]. In Press.

IPCC, 2019: Summary for Policymakers. In: Climate Change and Land: an IPCC special report on climate change, desertification, land degradation, sustainable land management, food security, and greenhouse gas fluxes in terrestrial ecosystems [P.R. Shukla, J. Skea, E. Calvo Buendia, V. Masson-Delmotte, H.- O. Pörtner, D. C. Roberts, P. Zhai, R. Slade, S. Connors, R. van Diemen, M. Ferrat, E. Haughey, S. Luz, S. Neogi, M. Pathak, J. Petzold, J. Portugal Pereira, P. Vyas, E. Huntley, K. Kissick, M. Belkacemi, J. Malley, (eds.)]. In press.

Jolliffe, I. T., and Cadima, J., 2016, Principal component analysis: a review and recent developments: Philosophical Transactions of the Royal Society A: Mathematical, Physical and Engineering Sciences, v. 374, no. 2065, p. 20150202, doi: 10.1098/rsta.2015.0202

Lattaud, J., Kirkels, F., Peterse, F., Freymond, C. V., Eglinton, T. I., Hefter, J., Mollenhauer, G., Balzano, S., Villanueva, L., van der Meer, M. T. J., Hopmans, E. C., Sinninghe Damsté, J. S., and Schouten, S., 2018, Long-chain diols in rivers: distribution and potential biological sources: Biogeosciences, v. 15, no. 13, p. 4147–4161, doi: 10.5194/bg-15-4147-2018

Leeming, R., Ball, A., Ashbolt, N., and Nichols, P., 1996, Using faecal sterols from humans and animals to distinguish faecal pollution in receiving waters: Water Research, v. 30, no. 12, p. 2893–2900, doi: 10.1016/s0043-1354(96)00011-5

Lenton, T. M., 2011, Early warning of climate tipping points: Nature Climate Change, v. 1, no. 4, p. 201–209, doi: 10.1038/nclimate1143

Lenton, T. M., Held, H., Kriegler, E., Hall, J. W., Lucht, W., Rahmstorf, S., and Schellnhuber, H. J., 2008, Tipping elements in the Earth's climate system: Proceedings of the National Academic of Sciences USA, v. 105, no. 6, p. 1786–1793, doi: 10.1073/pnas.0705414105

Macdonald, I. A., Bokkenheuser, V. D., Winter, J., McLernon, A. M., and Mosbach, E. H., 1983, Degradation of steroids in the human gut: Journal of Lipid Research v. 24, p. 675–700

Makou, M., Eglinton, T., McIntyre, C., Montluçon, D. B., Antheaume, I., and Grossi, V., 2018, Plant Wax n-Alkane and n-Alkanoic Acid Signatures Overprinted by Microbial Contributions and

Old Carbon in Meromictic Lake Sediments: Geophysical Research Letters, v. 45, no. 2, p. 1049–1057, doi: 10.1002/

Mann, M. E., 2002, The Value of Multiple Proxies: Science, v. 297, no. 5586, p. 1481–1482, doi: 10.1126/science.1074318

McInnes, L., Healy, J., Saul, N., and Großberger, L., 2018, UMAP: Uniform Manifold Approximation and Projection: Journal of Open Source Software v. 3, p. 861, doi: 10.21105/joss.00861

Meehl, G. A., Zwiers, F., Evans, J., Knutson, T., Mearns, L., and Whetton, P., 2000, Trends in Extreme Weather and Climate Events: Issues Related to Modeling Extremes in Projections of Future Climate Change: Bulletin of the American Meteorological Society, v. 81, no. 3, p. 427–436, doi: 10.1175/1520-0477(2000)081<0427:TIEWAC>2.3.CO;2

Metzger, P., Berkaloff, C., Casadevall, E., and Coute, A., 1985, Alkadiene- and botryococcene-producing races of wild strains of Botryococcus braunii: Phytochemistry, v. 24, no. 10, p. 2305–2312, doi: 10.1016/S0031-9422(00)83032-0

Metzger, P., and Largeau, C., 2005, Botryococcus braunii: a rich source for hydrocarbons and related ether lipids: Applied Microbiology and Biotechnology, v. 66, p. 486–496, doi: 10.1007/s00253-004-1779-z

Meyers, P. A., 1997, Organic geochemical proxies of paleoceanographic, paleolimnologic, and paleoclimatic processes: Organic Geochemistry, v. 27, no. 5–6, p. 213–250, doi: 10.1016/S0146-6380(97)00049-1

Meyers, P. A., 2003, Applications of organic geochemistry to paleolimnological reconstructions: a summary of examples from the Laurentian Great Lakes: Organic Geochemistry, v. 34, p. 261–289, doi: 10.1016/s0146-6380(02)00168-7

Mischke, S., Weynell, M., Zhang, C., and Wiechert, U., 2013, Spatial variability of 14C reservoir effects in Tibetan Plateau lakes: Quaternary International, v. 313-314, p. 147–155, doi: 10.1016/j.quaint.2013.01.030

Mollenhauer, G., and Rethemeyer, J., 2009, Compound-specific radiocarbon analysis – Analytical challenges and applications: IOP Conference Series: Earth and Environmental Science, v. 5, p. 012006, doi: 10.1088/1755-1307/5/1/012006

Mügler, I., Sachse, D., Werner, M., Xu, B., Wu, G., Yao, T., and Gleixner, G., 2008, Effect of lake evaporation on δD values of lacustrine n-alkanes: A comparison of Nam Co (Tibetan Plateau) and Holzmaar (Germany): Organic Geochemistry, v. 39, no. 6, p. 711–729, doi: 10.1016/j.orggeochem.2008.02.008

Ohkouchi, N., and Eglinton, T. I., 2008, Compound-specific radiocarbon dating of Ross Sea sediments: A prospect for constructing chronologies in high-latitude oceanic sediments: Quaternary Geochronology, v. 3, no. 3, p. 235–243, doi: 10.1016/j.quageo.2007.11.001

Ohlrogge, J., and Browse, J., 1995, Lipid Biosynthesis: The Plant Cell, v. 7, p. 957–970, doi: 10.1105/tpc.7.7.957

Parkes, R. J., and Taylor, J., 1983, The relationship between fatty acid distributions and bacterial respiratory types in contemporary marine sediments: Estuarine, Coastal and Shelf Science, v. 16, no. 2, p. 173–189, doi: 10.1016/0272-7714(83)90139-7

Pearson, A., McNichol, A. P., Schneider, R. J., Von Reden, K. F., and Zheng, Y., 1998, Microscale AMS 14C Measurement at NOSAMS: Radiocarbon, v. 40, no. 01, p. 61–75, doi: 10.1017/s0033822200017902

Philippsen, B., 2013, The freshwater reservoir effect in radiocarbon dating: Heritage Science, v. 1, no. 24, p. 1–19, doi: 10.1186/2050-7445-1-24

Rampen, S. W., Datema, M., Rodrigo-Gámiz, M., Schouten, S., Reichart, G.-J., and Sinninghe Damsté, J. S., 2014, Sources and proxy potential of long chain alkyl diols in lacustrine environments: Geochimica et Cosmochimica Acta, v. 144, p. 59–71, doi: 10.1016/j.gca.2014.08.033

Rampen, S. W., Willmott, V., Kim, J.-H., Uliana, E., Mollenhauer, G., Schefuß, E., Sinninghe Damsté, J. S., and Schouten, S., 2012, Long chain 1,13- and 1,15-diols as a potential proxy for palaeotemperature reconstruction: Geochimica et Cosmochimica Acta, v. 84, p. 204–216, doi: 10.1016/j.gca.2012.01.024

Reichstein, M., Bahn, M., Ciais, P., Frank, D., Mahecha, M. D., Seneviratne, S. I., Zscheischler, J., Beer, C., Buchmann, N., Frank, D. C., Papale, D., Rammig, A., Smith, P., Thonicke, K., van der Velde, M., Vicca, S., Walz, A., and Wattenbach, M., 2013, Climate extremes and the carbon cycle: Nature, v. 500, p. 287–295, doi: 10.1038/nature12350

Rial, J. A., Pielke Sr., R. A., Beniston, M., Claussen, M., Canadell, J., Cox, P., Held, H., de Noblet-Ducoudré, N., Prinn, R., Reynolds, J. F., and Salas, J. D., 2004, Nonlinearities, Feedbacks and

Critical Thresholds within the Earth's Climate System: Climatic Change, v. 65, p. 11–38, doi: 10.1023/B:CLIM.0000037493.89489.3f

Ringnér, M., 2008, What is principal component analysis?: Nat Biotechnol, v. 26, p. 303–304, doi: 10.1038/nbt0308-303

Rogge, W. F., Medeiros, P. M., and Simoneit, B. R. T., 2006, Organic marker compounds for surface soil and fugitive dust from open lot dairies and cattle feedlots: Atmospheric Environment, v. 40, no. 1, p. 27–49, doi: 10.1016/j.atmosenv.2005.07.076

Sachse, D., Billault, I., Bowen, G. J., Chikaraishi, Y., Dawson, T. E., Feakins, S. J., Freeman, K. H., Magill, C. R., McInerney, F. A., van der Meer, M. T. J., Polissar, P., Robins, R. J., Sachs, J. P., Schmidt, H.-L., Sessions, A. L., White, J. W. C., West, J. B., and Kahmen, A., 2012, Molecular Paleohydrology: Interpreting the Hydrogen-Isotopic Composition of Lipid Biomarkers from Photosynthesizing Organisms: Annual Review of Earth and Planetary Sciences, v. 40, no. 1, p. 221–249, doi: 10.1146/annurev-earth-042711-105535

Santos, G. M., Southon, J. R., Griffin, S., Beaupre, S. R., and Druffel, E. R. M., 2007, Ultra small-mass AMS 14C sample preparation and analyses at KCCAMS/UCI Facility: Nuclear Instruments and Methods in Physics Research Section B: Beam Interactions with Materials and Atoms, v. 259, no. 1, p. 293–302, doi: 10.1016/j.nimb.2007.01.172

Sauer, P. E., Eglinton, T. I., Hayes, J. M., Schimmelmann, A., and Sessions, A. L., 2001, Compound-specific D/H ratios of lipid biomarkers from sediments as a proxy for environmental and climatic conditions: Geochimica et Cosmochimica Acta, v. 65, no. 2, p. 213–222

Shah, S. R., and Pearson, A., 2007, Ultra-microscale (5-25 μg C) analysis of individual lipids by 14C AMS: Assessment and correction for sample processing blanks: Radiocarbon, v. 49, no. 1, p. 69–82, doi: 10.2458/azu_js_rc.49.2900

Shimokawara, M., Nishimura, M., Matsuda, T., Akiyama, N., and Kawai, T., 2010, Bound forms, compositional features, major sources and diagenesis of long chain, alkyl mid-chain diols in Lake Baikal sediments over the past 28,000 years: Organic Geochemistry, v. 41, no. 8, p. 753–766, doi: 10.1016/j.orggeochem.2010.05.013

Simoneit, B. R., 2002, Molecular indicators (biomarkers) of past life: The Anatomical Record, v. 268, no. 3, p. 186–195, doi: 10.1002/ar.10153

Smets, T., Verbeeck, N., Claesen, M., Asperger, A., Griffioen, G., Tousseyn, T., Waelput, W., Waelkens, E., and De Moor, B., 2019, Evaluation of Distance Metrics and Spatial Autocorrelation

in Uniform Manifold Approximation and Projection Applied to Mass Spectrometry Imaging Data: Analytical Chemistry, v. 91, no. 9, p. 5706–5714, doi: 10.1021/acs.analchem.8b05827

Smittenberg, R. H., Hopmans, E. C., Schouten, S., Hayes, J. M., Eglinton, T. I., and Sinninghe Damsté, J. S., 2004, Compound-specific radiocarbon dating of the varved Holocene sedimentary record of Saanich Inlet, Canada: Paleoceanography, v. 19, no. 2, doi: 10.1029/2003pa000927

Sorg, A., Bolch, T., Stoffel, M., Solomina, O., and Beniston, M., 2012, Climate change impacts on glaciers and runoff in Tien Shan (Central Asia): Nature Climate Change, v. 2, no. 10, p. 725–731, doi: 10.1038/nclimate1592

Sun, S., Meyer, V. D., Dolman, A. M., Winterfeld, M., Hefter, J., Dummann, W., McIntyre, C., Montluçon, D. B., Haghipour, N., Wacker, L., Gentz, T., van der Voort, T. S., Eglinton, T. I., and Mollenhauer, G., 2020, 14C Blank Assessment in Small-Scale Compound-Specific Radiocarbon Analysis of Lipid Biomarkers and Lignin Phenols: Radiocarbon, v. 62, no. 1, p. 207–218, doi: 10.1017/RDC.2019.108

Sun, Y.-Y., Zhang, K.-X., Liu, J., He, Y.-X., Song, B.-W., Liu, W.-G., and Liu, Z.-H., 2012, Long chain alkenones preserved in Miocene lake sediments: Organic Geochemistry, v. 50, p. 19–25, doi: 10.1016/j.orggeochem.2012.06.007

Theroux, S., D'Andrea, W. J., Toney, J., Amaral-Zettler, L., and Huang, Y., 2010, Phylogenetic diversity and evolutionary relatedness of alkenone-producing haptophyte algae in lakes: Implications for continental paleotemperature reconstructions: Earth and Planetary Science Letters, v. 300, no. 3-4, p. 311–320, doi: 10.1016/j.epsl.2010.10.009

Tiwari, M., Singh, A. K., and Sinha, D. K., 2015, Stable Isotopes: Tools for Understanding Past Climatic Conditions and Their Applications in Chemostratigraphy, in Ramkumar, M., ed., Chemostratigraphy: Concepts, Techniques, and Applications: Amsterdam, Netherlands, Elsevier, p. 65–92.

Toney, J. L., Huang, Y., Fritz, S. C., Baker, P. A., Grimm, E., and Nyren, P., 2010, Climatic and environmental controls on the occurrence and distributions of long chain alkenones in lakes of the interior United States: Geochimica et Cosmochimica Acta, v. 74, no. 5, p. 1563–1578, doi: 10.1016/j.gca.2009.11.021

Tylmann, W., Zolitschka, B., Enters, D., and Ohlendorf, C., 2013, Laminated lake sediments in northeast Poland: distribution, preconditions for formation and potential for paleoenvironmental investigation: Journal of Paleolimnology, v. 50, p. 487–503, doi: 10.1007/s10933-013-9741-7

Uchikawa, J., Popp, B. N., Schoonmaker, J. E., and Xu, L., 2008, Direct application of compound-specific radiocarbon analysis of leaf waxes to establish lacustrine sediment chronology: Journal of Paleolimnology, v. 39, no. 1, p. 43-60, doi: 10.1007/s10933-007-9094-1

van der Maaten, L. J. P., Postma, E. O., and van den Herik, H. J. (2009). "Dimensionality reduction: A comparative review."Technical Report TiCC-TR 2009-005. Tilburg University.

Vogts, A., Moossen, H., Rommerskirchen, F., and Rullkötter, J., 2009, Distribution patterns and stable carbon isotopic composition of alkanes and alkan-1-ols from plant waxes of African rain forest and savanna C3 species: Organic Geochemistry, v. 40, no. 10, p. 1037-1054, doi: 10.1016/j.orggeochem.2009.07.011

Wakeham, S. G., 1989, Reduction of stenols to stanols in particulate matter at oxic–anoxic boundaries in sea water: Nature, v. 342, p. 787–790, doi: 10.1038/342787a0

Walker, B. D., and Xu, X., 2019, An improved method for the sealed-tube zinc graphitization of microgram carbon samples and 14C AMS measurement: Nuclear Instruments and Methods in Physics Research Section B: Beam Interactions with Materials and Atoms, v. 438, p. 58–65, doi: 10.1016/j.nimb.2018.08.004

Walker, M. J. C., Berkelhammer, M., Björck, S., Cwynar, L. C., Fisher, D. A., Long, A. J., Lowe, J. J., Newnham, R. M., Rasmussen, S. O., and Weiss, H., 2012, Formal subdivision of the Holocene Series/Epoch: a Discussion Paper by a Working Group of INTIMATE (Integration of ice-core, marine and terrestrial records) and the Subcommission on Quaternary Stratigraphy (International Commission on Stratigraphy): Journal of Quaternary Science, v. 27, no. 7, p. 649–659, doi: 10.1002/jqs.2565

White, A. J., Stevens, L. R., Lorenzi, V., Munoz, S. E., Lipo, C. P., and Schroeder, S., 2018, An evaluation of fecal stanols as indicators of population change at Cahokia, Illinois: Journal of Archaeological Science, v. 93, p. 129–134, doi: 10.1016/j.jas.2018.03.009

Yang, J., Fang, G., Chen, Y., and De-Maeyer, P., 2017, Climate change in the Tianshan and northern Kunlun Mountains based on GCM simulation ensemble with Bayesian model averaging: Journal of Arid Land, v. 9, p. 622–634, doi: 10.1007/s40333-017-0100-9

Yang, L., Bork, H.-R., Fang, X., Mischke, S., Weinelt, M., and Wiesehöfer, J., 2019a, On the Paleo-climatic/Environmental Impacts and Socio-Cultural System Resilience along the Historical Silk Road, in Yang, L., Bork, H.-R., Fang, X., and Mischke, S., eds., Socio-Environmental Dynamics along the Historical Silk Road: Cham, Springer, p. 3–22.

Yang, L. E., Bork, H.-R., Fang, X., and Mischke, S., 2019b, Socio-Environmental Dynamics along the Historical Silk Road, Cham, Springer, XXVI, 525 p.ISBN: 978-3-030-00728-7

Zolitschka, B., Francus, P., Ojala, A. E. K., and Schimmelmann, A., 2015, Varves in lake sediments – a review: Quaternary Science Reviews, v. 117, p. 1–41, doi: 10.1016/j.quascirev.2015.03.019

## 6. Acknowledgments

I sincerely thank my advisors at the Max-Planck-Institute for Biogeochemistry Jena and the Friedrich Schiller University Jena, Prof. Dr. Gerd Gleixner and Prof. Dr. Roland Mäusbacher, for supervising this work and for their helpful comments.

This PhD project was part of the BMBF-funded research project "CAHOL – Central Asian Holocene Climate".

Special thanks also go to the MPG and the International Max Planck Research School for Global Biogeochemical Cycles (IMPRS-gBGC), Dr. Steffi Rothhardt in particular, for additional project funding and both scientific and organizational support.

I'd like to thank all of my co-authors: Prof. Dr. Jaime L. Toney, Prof. Dr. Stefan Schouten, Dr. Jens Mingram, Julia Kalanke, Caglar Yildiz, Dr. Anja Schwarz, Dr. Stefan Lauterbach, Dr. Rik Tjallingii, Dr. Martina Stebich and Dr. Valérie Schwab-Lavric for their constructive comments and great collaborations.

For technical assistance, Steffen Rühlow, Dr. Julien Plancq and Dr. Axel Steinhof and the $^{14}C$ analytics group, are greatly acknowledged.

Furthermore, I thank my colleagues at the molecular Biogeochemistry working group for a pleasant working atmosphere.

Finally, I'd like to express my sincere gratitude to my family, especially my parents and fiancé Simon, for their constant support and encouragement.

## 7. Selbstständigkeitserklärung

Ich erkläre, dass ich die vorliegende Arbeit selbständig und unter Verwendung der angegebenen Hilfsmittel, persönlichen Mitteilungen und Quellen angefertigt habe.

Jena, 03.03.2021

Natalie Schroeter

## 8. Erklärung zu den Eigenanteilen

Erklärung zu den Eigenanteilen der Promovendin/des Promovenden sowie der weiteren Doktorandinnen/Doktoranden als Co-Autorinnen/-Autoren an den Publikationen und Zweitpublikationsrechten bei einer kumulativen Dissertation.

Für alle in dieser kumulativen Dissertation verwendeten Manuskripte liegen die notwendigen Genehmigungen der Verlage („Reprint permissions“) für die Zweitpublikation vor.

Die Co-Autorinnen/-Autoren der in dieser kumulativen Dissertation verwendeten Manuskripte sind sowohl über die Nutzung, als auch über die oben angegebenen Eigenanteile der weiteren Doktorandinnen/Doktoranden als Co-Autorinnen/-Autoren an den Publikationen und Zweitpublikationsrechten bei einer kumulativen Dissertation informiert und stimmen dem zu (es wird empfohlen, diese grundsätzliche Zustimmung bereits bei Einreichung der Veröffentlichung einzuholen bzw. die Gewichtung der Anteile parallel zur Einreichung zu klären).

Die Anteile der Promovendin/des Promovenden sowie der weiteren Doktorandinnen/Doktoranden als Co-Autorinnen/Co-Autoren an den Publikationen und Zweitpublikationsrechten bei einer kumulativen Dissertation sind in der Anlage aufgeführt.

| | | | |
|---|---|---|---|
| Natalie Schroeter | Datum | Ort | Unterschrift |

## 9. Erklärung der Betreuer

Ich bin mit der Abfassung der Dissertation als publikationsbasierte Dissertation, d.h. kumulativ, einverstanden und bestätige die vorstehenden Angaben.

| | | | |
|---|---|---|---|
| apl. Prof. Dr. Gerd Gleixner | Datum | Ort | Unterschrift |
| Prof. Dr. Roland Mäusbacher | Datum | Ort | Unterschrift |

## 10. Angabe der Publikationsäquivalente

**Erklärung zu den Eigenanteilen der Promovendin/des Promovenden sowie der weiteren Doktorandinnen/Doktoranden als Co-Autorinnen/Co-Autoren an den Publikationen und Zweitpublikationsrechten bei einer kumulativen Dissertation.**

| **Publikation 1:** Schroeter N, Toney JL, Lauterbach S, Kalanke J, Schwarz A, Schouten S and Gleixner G (2020) How to deal with multi-proxy data for paleoenvironmental reconstructions: Applications to a Holocene lake sediment record from the Tian Shan, Central Asia. Front. Earth Sci. 8:353. doi: 10.3389/feart.2020.00353 | | | | | | | |
|---|---|---|---|---|---|---|---|
| **beteiligt an (Zutreffendes ankreuzen)** | | | | | | | |
| | NS | JLT | SL | JK | AS | SS | GG |
| Konzeption des Forschungsansatzes | X | | | | | | X |
| Plannung der Untersuchungen | X | | | | | | X |
| Datenerhebung | X | X | | X | X | X | |
| Datenanalyse und -interpretation | X | X | X | X | X | X | X |
| Schreiben des Manuskripts | X | | | | | | |
| Vorschlag Anrechnung Publikationsäquivalente | 1,0 | | | | | | |

| **Publikation 2:** Schroeter N, Mingram J, Kalanke J, Lauterbach S, Tjallingii R, Schwab V F, Gleixner G (submitted to Frontiers in Earth Science) The lake reservoir effect varies with the mobilization of pre-aged organic carbon in a high-altitude Central Asian catchment. | | | | | | | |
|---|---|---|---|---|---|---|---|
| **beteiligt an (Zutreffendes ankreuzen)** | | | | | | | |
| | NS | JM | JK | SL | RT | VS | GG |
| Konzeption des Forschungsansatzes | X | | | | | | X |
| Plannung der Untersuchungen | X | | | | | X | X |
| Datenerhebung | X | X | X | | X | X | |
| Datenanalyse und -interpretation | X | | | X | | X | X |
| Schreiben des Manuskripts | X | | | | | | |
| Vorschlag Anrechnung Publikationsäquivalente | 1,0 | | | | | | |

| **Publikation 3:** Schroeter N, Lauterbach S, Stebich M, Kalanke J, Mingram J, Yildiz C, Schouten S and Gleixner G (2020) Biomolecular Evidence of Early Human Occupation of a High-Altitude Site in Western Central Asia During the Holocene. Front. Earth Sci. 8:20. doi: 10.3389/feart.2020.00020 | | | | | | | | |
|---|---|---|---|---|---|---|---|---|
| **beteiligt an (Zutreffendes ankreuzen)** | | | | | | | | |
| | NS | SL | MS | JK | JM | CY | SS | GG |
| Konzeption des Forschungsansatzes | X | | | | | | | X |
| Plannung der Untersuchungen | X | | | | | | | X |
| Datenerhebung | X | | X | X | X | X | X | |
| Datenanalyse und -interpretation | X | X | X | X | X | X | X | X |
| Schreiben des Manuskripts | X | | | | | | | |
| Vorschlag Anrechnung Publikationsäquivalente | 1,0 | | | | | | | |

Erläuterung der Namenskürzel:

NS: Natalie Schroeter

AS: Anja Schwarz

CY: Caglar Yildiz

GG: Gerd Gleixner

JLT: Jaime L. Toney

JM: Jens Mingram

JK: Julia Kalanke

MS: Martina Stebich

RT: Rik Tjallingii

SL: Stefan Lauterbach

SS: Stefan Schouten

frontiers in Earth Science

ORIGINAL RESEARCH
published: 03 September 2020
doi: 10.3389/feart.2020.00353

# How to Deal With Multi-Proxy Data for Paleoenvironmental Reconstructions: Applications to a Holocene Lake Sediment Record From the Tian Shan, Central Asia

*Natalie Schroeter[1], Jaime L. Toney[2], Stefan Lauterbach[3,4], Julia Kalanke[5], Anja Schwarz[6], Stefan Schouten[7,8] and Gerd Gleixner[1]**

[1] *Max Planck Institute for Biogeochemistry, Research Group Molecular Biogeochemistry, Jena, Germany,* [2] *School of Geographical and Earth Sciences, University of Glasgow, Glasgow, United Kingdom,* [3] *Kiel University, Leibniz Laboratory for Radiometric Dating and Stable Isotope Research, Kiel, Germany,* [4] *Kiel University, Institute of Geosciences, Kiel, Germany,* [5] *Section 4.3 – Climate Dynamics and Landscape Evolution, GFZ German Research Centre for Geosciences, Potsdam, Germany,* [6] *Technische Universität Braunschweig, Institute of Geosystems and Bioindication, Braunschweig, Germany,* [7] *Department of Marine Microbiology and Biogeochemistry, NIOZ Royal Netherlands Institute for Sea Research, Den Burg, Netherlands,* [8] *Department of Earth Sciences, Faculty of Geosciences, Utrecht University, Utrecht, Netherlands*

OPEN ACCESS

**Edited by:**
*Michaël Hermoso, UMR 8187 Laboratoire d'Océanologie et de Géosciences (LOG), France*

**Reviewed by:**
*Philip Alan Meyers, University of Michigan, United States*
*Nathalie Dubois, Swiss Federal Institute of Aquatic Science and Technology, Switzerland*
*Remo Röthlin, Swiss Federal Institute of Aquatic Science and Technology, Dübendorf, Switzerland, in collaboration with reviewer ND*

***Correspondence:**
*Gerd Gleixner*
*gerd.gleixner@bgc-jena.mpg.de*

**Specialty section:**
*This article was submitted to Quaternary Science, Geomorphology and Paleoenvironment, a section of the journal Frontiers in Earth Science*

**Received:** *07 June 2020*
**Accepted:** *29 July 2020*
**Published:** *03 September 2020*

**Citation:**
*Schroeter N, Toney JL, Lauterbach S, Kalanke J, Schwarz A, Schouten S and Gleixner G (2020) How to Deal With Multi-Proxy Data for Paleoenvironmental Reconstructions: Applications to a Holocene Lake Sediment Record From the Tian Shan, Central Asia. Front. Earth Sci. 8:353. doi: 10.3389/feart.2020.00353*

Multi-proxy investigations on geological archives provide valuable information about environmental variations in the past. As opposed to single-proxy studies, the combination of several proxies can reveal more detailed information and strengthen subsequent paleoenvironmental reconstructions. However, there is still no consensus about how to deal with resulting highly dimensional datasets in a statistical manner. In many cases, the interpretations of multi-proxy datasets rely on visually matching several proxy records, which can lead to incorrect or insufficient interpretations. Here we report an innovative approach that combines the novel dimension reduction technique Uniform Manifold Approximation and Projection (UMAP) and the time series analysis R package *asdetect* to identify and characterize Holocene environmental phases and phase boundaries in a sediment core from Lake Chatyr Kol, southern Kyrgyzstan. Despite the fact that the Holocene climate evolution of Central Asia has been intensively studied during the last decades, knowledge about regional climate development during the Holocene and the underlying mechanisms is still relatively scarce. We particularly focus on phase transitions and differentiate between event-based shifts as opposed to gradual phase transitions. For this study, long-chain alkenones were used as a paleotemperature proxy and variations in long-chain alkyl diol distributions were ascribed to relative changes of algal input. The compound-specific stable hydrogen isotope compositions (δD) of individual *n*-alkanes were utilized as paleohydrological proxies, with the δD of mid-chain *n*-alkanes reflecting changes in the δD of the lake water and the δD of long-chain *n*-alkanes recording the δD of the meteoric water. We show the potential of modern analysis tools for data-driven paleoenvironmental reconstructions and advocate for their more frequent implementation in multi-proxy studies.

**Keywords: paleoenvironment, climate reconstructions, biomarkers, lake sediments, central asia, multi-proxy data, westerlies**

## INTRODUCTION

Paleoenvironmental reconstructions are essential to elucidate the Earth's natural environmental variability in the past. This knowledge enables projections for future climate changes by providing possible analogs for future scenarios (Aichner et al., 2015). Proxy analyses provide a unique tool, often quantitative, to gain insights into past climate conditions since instrumental records mostly cover only the last ∼170 years (Guillot et al., 2015). In particular molecular organic geochemical proxies, so-called biomarkers that have been preserved in natural archives have been extensively used in the field of paleoclimatology and paleoenvironment, especially over the last two decades (Eglinton and Eglinton, 2008; Wang et al., 2016). Biomarkers derive from distinct biotic sources and their abundance and composition is diagnostic for environmental parameters of their formation (Meyers, 2003). Although they typically constitute only <5% of bulk organic matter, biomarkers are widely deployed tools for reconstructing past environmental conditions (Aichner et al., 2010; Feng et al., 2015). Combining the analyses of multiple biomarkers has proven to be more robust as opposed to single-proxy analyses because complementary information and thus a broader perspective can be obtained (Birks and Birks, 2006). However, despite the recent methodological advances, the subsequent data-evaluation and interpretation of biomarker analyses are frequently carried out rather subjectively ("by eye") with little statistical or computational techniques. Consequently, this approach can be misleading and does not exploit the full potential of these complex datasets. Yet, as the number of large datasets increases and the temporal resolution of the data becomes higher, the need for a concordant approach to summarize patterns in complex multi-proxy datasets becomes even greater. Even though techniques for reducing the dimensionality of multi-proxy data already exist and may be suitable for paleoenvironmental datasets, there are still reservations about their applications. Traditionally, the most commonly used method for dimensionality reduction has been Principal Component Analysis (PCA). PCA is a multivariate statistical analysis that utilizes matrix factorization for projecting high-dimensional data on a lower dimensional subspace comprized of the so-called principal components, while retaining the maximum variability present in the original variables (Ringnér, 2008; Abdi and Williams, 2010; Naik, 2018). Thus, by creating new variables, which are linear combinations of the original variables, PCA allows comparing similarities and potential interdependencies between the original variables (Abdi and Williams, 2010). In the context of paleoenvironmental reconstructions, the described function of PCA could be problematic for two reasons: First, as the variance in multi-proxy data spans across scales and PCA primarily seeks major variability components, small-scale variance may be disregarded even though it might still contain important environmental information. And second, paleoenvironmental data are often nonlinear, especially around phase transitions. In many paleoenvironmental studies, the identification of phases and their boundaries is one of the major objectives, yet PCA may be unable to represent the variability at these critical points in time adequately. Therefore, a novel nonlinear dimension reduction technique for visualization has recently been proposed. This technique, Uniform Manifold Approximation and Projection (UMAP), is generally valued for being both locally and globally optimized (McInnes et al., 2018). This means that while it is a neighbor-embedding method that seeks to resolve the local structure within clusters of data points, it can also define the distance between these clusters in a low-dimensional space in such a way that the original global data structure is optimally represented (McInnes et al., 2018). Since its introduction, UMAP has received considerable attention in a variety of fields (Becht et al., 2018; Diaz-Papkovich et al., 2019; Smets et al., 2019), yet has so far not received full attention in paleoenvironmental reconstructions. In a previous study we showed the effectiveness of applying UMAP to biomolecular data obtained from a lake sediment core, allowing to clearly divide the record into distinct phases in a data-driven manner (Schroeter et al., 2020). Nevertheless, it is unclear whether phase boundaries ascertained by UMAP reflect true abrupt shifts in time series, often classified as tipping points (Lenton et al., 2008; Lenton, 2011; Scheffer et al., 2012), or if these changes can also occur gradually within a determined phase. The identification of tipping points is of particular interest since they can shift a system from one state to another, but the objective identification of them in a time series remains challenging (Marwan et al., 2018). Recently, Boulton and Lenton (2019) introduced a statistical method, implemented in R, for detecting abrupt shifts in time series, which is called *asdetect*. As opposed to other methods of anomalous change detection that search for significant changes in mean values, *asdetect* differs by looking for significant changes of gradients within the series (Boulton and Lenton, 2019). However, as *asdetect* was originally designed for single-proxy investigations, the authors emphasize the need for novel or extended statistical analyses that can be applied to multi-proxy datasets.

Here we combine the results of PCA, UMAP and *asdetect* as an innovative statistical approach to define and characterize phase boundaries in a more robust approach than previously applied in paleoenvironmental studies. We utilized a multi-proxy dataset of terrestrial and aquatic biomarkers obtained from a sediment core from Lake Chatyr Kol, Kyrgyzstan, Central Asia, reflecting hydrological, and environmental changes of the lake and its catchment area, respectively. Located in Central Asia, the Tian Shan is one of the largest mountain ranges in the world, playing an important role in determining the hydrological and climatological regime of northern Central Asia. Owing to the lake's position at the intercept between the extent of the mid-latitude Westerlies, the Siberian Anticyclone and partially also the Asian monsoon system (Aizen et al., 2001; Cheng et al., 2012), the Tian Shan represents a key location to study paleoenvironmental changes at high resolution. Although different types of natural archives, such as speleothems (Cheng et al., 2012; Wolff et al., 2017), tree-rings (Esper et al., 2002), loess sequences (Machalett et al., 2008) and lake sediments (Ricketts et al., 2001; Beer et al., 2007; Lauterbach et al., 2014; Mathis et al., 2014; Schwarz et al., 2017) have been analyzed during the last two decades to understand climatic and environmental fluctuations in

Central Asia, knowledge about the regional climate development during the Holocene and the underlying mechanisms is still relatively scarce.

The multi-proxy assessment in this study includes the analysis of long-chain alkenones (LCAs) and the respective alkenone unsaturation index $\left(U_{37}^{K}\right)$as a temperature proxy (Brassell et al., 1986). By analyzing long-chain alkyl diols (LCDs) as an indicator for the presence of algae (Rampen et al., 2012), we connect the intra-lake bio-productivity to variable environmental conditions. We further investigated *n*-alkanes and their stable hydrogen isotope composition (δD) to assess the lake water budget as well as to evaluate contributions of aquatic and terrestrial sources of organic matter. By applying PCA, UMAP, and *asdetect* to this multi-proxy dataset, we evaluate the potential of these data analysis approaches for multi-proxy datasets, particularly regarding their ability to differentiate between event-based phase transitions and more gradual shifts. Based on our results, we emphasize the necessity of utilizing data-driven and statistical methods for paleoenvironmental and paleoclimatological studies.

## STUDY AREA

Lake Chatyr Kol is an endorheic lake located at 3545 m above sea level (a.s.l.) in the southern Kyrgyz Tian Shan (40°37′N, 75°18′E) (**Figure 1**). Extending ∼12 km in width (NW-SE) and ∼23 km in length (SW–NE), it encompasses a surface area of ∼159 km$^2$, thus being the third largest lake in Kyrgyzstan. The maximum water depth is 20 m. To the north and south, the basin (catchment area 1084 km$^2$) is limited by the At Bashy Range (∼4600 m) and the Torugart Range (>4800 m), respectively. The extensive pasture-covered plains surrounding the lake predominantly consist of eroded Quaternary material from the mountain ranges. Besides several small tributaries and rivers, the Kekagyr River is the largest and only permanent inflow. During summer, the water balance is predominantly influenced by glacier surface melting and summer storm precipitation. The current climatic regime in the Kyrgyz Tian Shan is primarily determined by the interaction between the Siberian anticyclonic circulation and the mid-latitude Westerlies (Aizen et al., 1997; Lauterbach et al., 2014), whose moisture likely originates in the North Atlantic, the Mediterranean and Caspian Sea (Aizen et al., 2001, 2006; Cheng et al., 2016). Mean annual precipitation amounts to ∼300 mm year$^{-1}$ in this region (Koppes et al., 2008). The high mountain ranges surrounding Lake Chatyr Kol largely prevent the transport of moisture, resulting in dry conditions and reduced winter precipitation, especially in January and February (Aizen et al., 1995, 2001). In summer, convection increases and strengthens unstable atmospheric stratification, leading to a summer maximum of precipitation brought by cold and moist westerly air masses (Aizen et al., 1995, 2001; Bershaw and Lechler, 2019). Mean annual air temperatures in this region are variable; ranging from −0.34°C in Naryn (∼103 km northeast of Lake Chatyr Kol, 2045 m a.s.l.) (Ilyasov et al., 2013) to −7.2°C in Ak Say (∼30 km east of Lake Chatyr Kol, 3135 m a.s.l.) (Giese et al., 2007), with highest temperatures occurring in July and August. These cold and arid conditions also favor the preservation of permafrost soils (Shnitnikov et al., 1978) and thermokarst formations are widely distributed in this region (Abuduwaili et al., 2019). Vegetation in the region is sparse and characterized by desert and semi-desert vegetation with dominance of montane grassland and no trees (Taft et al., 2011). Since the lake is not inhabited by fish, a considerable number of the amphipod species *Gammarus alius* sp. nov., which is mostly confined to continental freshwater/brackish habitats, have colonized aquatic plants up to a depth of 50 cm (Sidorov, 2012).

## MATERIALS AND METHODS

### Coring and Chronology

Several vertically overlapping piston cores of 3 m length were retrieved in summer 2012 from a coring site at ∼20 m water depth in the southwestern part of Lake Chatyr Kol (40°36.37′N, 75°14.02′E) by using a 60 mm UWITEC piston corer. In addition, seven gravity cores were collected in autumn 2017 by using a 90 mm UWITEC gravity corer with hammer weight (SC17_1–7). By identification and comparison of distinct macroscopic marker layers, the individual sediment cores could be correlated and merged into a continuous 623.5-cm-long composite profile (Kalanke et al., 2020). By seasonal deposition, the sediments are almost continuously annually laminated (varved) except for the upper 63 cm, allowing the establishment of a floating varve chronology ("Chatvd19") through microscopic varve counting below 63 cm composite depth (**Figure 2**). The formation of varves at Lake Chatyr Kol is highly linked to the seasonality of ice coverage during winter and annual variations in temperature and precipitation (Kalanke et al., 2020). A detailed description of the sediments and the age model can be found in Kalanke et al. (2020) and Schroeter et al. (2020). Briefly, microfacies analysis was performed by examining petrographic thin sections, which were prepared at the GFZ German Research Center for Geosciences, Potsdam, Germany, following the method described by Brauer and Casanova (2001). Analysis included counting of individual varves, varve thickness measurements, varve type identification and varve boundary assessment. A total of 11,259 varves were counted twice and interpolated and the mean deviation (∼5%) between the two countings was implemented as the counting uncertainty. Based on the age model, the core has a basal age of 11,619 ± 603 a BP. The floating varve chronology is further supported by accelerator mass spectrometry (AMS) $^{14}$C measurements (Poznań Radiocarbon Laboratory, Poznań, Poland) of two wood remains at 380.5 and 528.0 cm composite depth, dating to 6140 ± 137 cal. a BP (Poz-63307) and 9988 ± 203 cal. a BP (Poz-54302), respectively. Calibrated $^{14}$C ages (cal. a BP) were calculated in OxCal 4.3 (Bronk Ramsey, 2009) using IntCal13 (Reimer et al., 2013). Gamma spectrometric analysis of $^{210}$Pb and $^{137}$Cs on continuous 0.5-cm-thick sediment slices of gravity core SC17_7 was performed at the GFZ German Research Center for Geosciences, Potsdam, Germany in order to complement the chronology in the uppermost, non-varved 63 cm of the composite profile (Kalanke et al., 2020). Activity concentrations of $^{210}$Pb

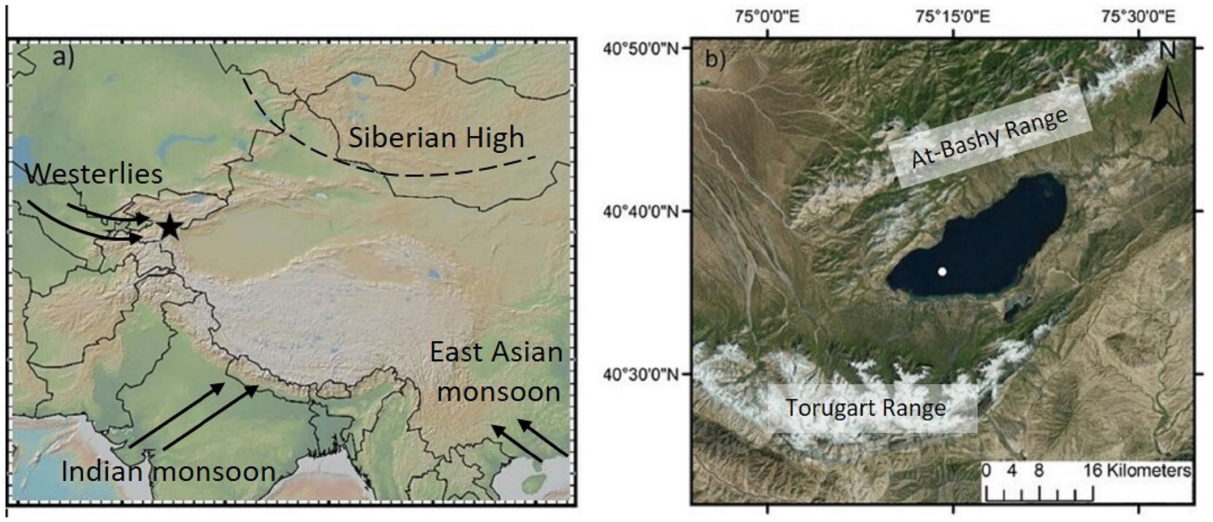


**FIGURE 1 | (a)** Location of the study site Lake Chatyr Kol (black star) and the dominant circulation systems. **(b)** Map of Lake Chatyr Kol with coring location (white dot). Figure made with GeoMapApp (www.geomapapp.org).

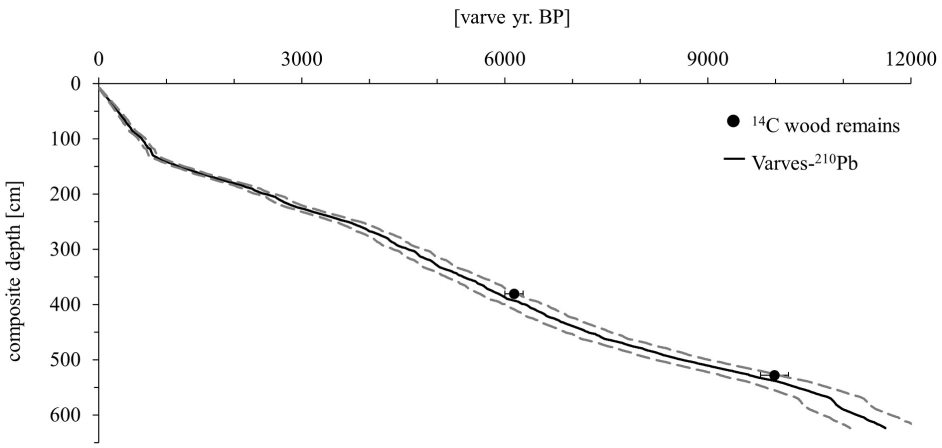


**FIGURE 2 |** Age model of the Lake Chatyr Kol sediment record. Black dots represent $^{14}C$ ages of terrestrial macro remains with two σ error ranges. The age model (solid black line) is based on varve counting combined with $^{210}Pb$ measurements. Dashed lines represent the uncertainty of the varve chronology (Kalanke et al., 2020).

were incorporated both in a constant initial concentration (CIC) model (Robbins, 1978) and in a constant rate of supply (CRS) model (Appleby and Oldfield, 1978). The onset of enhanced $^{137}Cs$ concentrations, originating from global nuclear weapon tests (Pennington et al., 1973; Kudo et al., 1998; Wright et al., 1999), was dated to 1945 by both CIC and CRS model assumptions. Consequently, AD 1945 was chosen to constrain the age-depth relationship of the upper homogenous sediments (Kalanke et al., 2020). All ages of Lake Chatyr Kol sediment record mentioned in this study refer to the described age model (Kalanke et al., 2020).

## Analysis of Lipid Biomarkers

In total, 89 bulk sediment samples of 1 cm thickness were taken from the composite profile at a mean interval of ∼5 cm. These sediment samples were freeze-dried and extracted in a dichloromethane (DCM) and methanol (MeOH) solvent mixture (9:1, v:v) on a pressurized solvent speed extractor (E-916, BÜCHI, Essen, Germany), which was operated at 100°C and 120 bar for 15 min in two cycles. Biomarker separation was conducted according to Richey and Tierney (2016). The resulting total lipid extract was separated into acid and neutral fractions using aminopropyl gel columns (CHROMABOND® $NH_2$ polypropylene columns, 60 Å, Macherey-Nagel GmbH & Co., KG, Düren, Germany), with neutral compounds eluting in 3:1 DCM:isopropanol and acids eluting in 19:1 diethyl ether:acetic acid. Neutral fractions were further separated over an activated silica gel column (∼2 g, 0.040–0.063 mm mesh, Merck, Darmstadt, Germany) into hydrocarbon (*n*-alkanes), ketone (alkenones), and polar (diols) fractions by elution with

hexane, DCM and MeOH, respectively. Elemental sulfur was removed by adding HCl- activated copper.

## Analysis of Sedimentary *n*-Alkanes

Quantification and identification of *n*-alkanes were performed on a gas chromatograph with flame ionization detector (GC-FID, Agilent 7890B Gas Chromatograph), based on retention time and peak area comparison with an external *n*-alkanes standard mixture ($n$C$_{15}$ to $n$C$_{33}$). Separation of the hydrocarbon fraction was achieved on an Ultra two column (50 m length, 0.32 mm inner diameter, 0.52 μm film thickness, Agilent Technologies, Santa Clara, United States) at a constant helium carrier gas flow of 2 mL min$^{-1}$. The PTV injector in splitless mode started at 45°C for 0.1 min, then heating up to 300°C with a ramp of 14.5 °C s$^{-1}$ (held for 3 min). The GC oven temperature program increased from 140°C (held for 1 min) to 310 at 4°C min$^{-1}$ (held for 15 min) and finally to 325°C with a ramp of 30°C min$^{-1}$. The final temperature of 325°C was held for 3 min.

The average chain length (ACL) (Poynter and Eglinton, 1990) was calculated according to the following equation:

$$\mathrm{ACL}_{15-33} = \frac{\sum(C_n \times n)}{\sum C_n} \quad (1)$$

## Analysis of δD of Sedimentary *n*-Alkanes

δD of the *n*-alkanes was measured using a coupled GC-IRMS system (GC: HP 7890, Agilent Technologies, Palo Alto United States; IRMS: Delta V Plus, Thermo Fisher Scientific, Bremen, Germany) equipped with a DB1 ms column (length 30 m, 0.25 mm inner diameter, 0.25 μm film thickness; Agilent Technologies, Palo Alto, United States). Column flow was constant at 1.3 ml min$^{-1}$ and the injector was operated at 280 °C in splitless mode. The oven program started at 110°C (held for 1 min), heated to 320°C (held for 8 min) at a rate of 5°C min$^{-1}$ and finally to 350°C (held for 3 min) at 30°C min$^{-1}$. Injection volume was 2 μL and each sample was measured in triplicate followed by a measurement of an external *n*-alkane standard mixture ($n$C$_{15}$ to $n$C$_{33}$). The $H_3^+$ factor was determined daily to confirm stable ion source conditions and was about 6.8 ± 0.4 over the course of analysis. δD values are reported as per mille relative to VSMOW using the standard δ notation:

$$\delta D\,(\%) = \left(\frac{R_{\mathrm{Sample}}}{R_{\mathrm{VSMOW}}} - 1\right) \times 1000 \quad (2)$$

where, $R$ = the ratio of deuterium to hydrogen ($^2$H/$^1$H) and VSMOW = Vienna Standard Mean Ocean Water.

The Evaporation-to-Inflow ratio (E/I) was calculated based on the stable isotope approach by Gat and Levy (1978):

$$E/I = \left(\frac{1-h}{h}\right) \times \left(\frac{\delta DnC_{23} - \delta DnC_{29}}{\delta D^{\circ} - \delta DnC_{23}}\right) \quad (3)$$

with $h$ = relative humidity [0.44 for Lake Chatyr Kol, obtained for the Kashi station 1971–2011 AD, NOAA IGRA (Durre et al., 2006)], δD = stable hydrogen isotope values of lake water (δD$n$C$_{23}$) and inflow water (δD$n$C$_{29}$) and δD° = limiting isotopic enrichment for a desiccating water body. An average Lake Surface Temperature of 9°C was selected for the calculations. A more detailed explanation of the calculation is provided in Günther et al. (2016).

## Analysis of Sedimentary Long-Chain Alkenones

Prior to analysis, ketone fractions containing LCAs were saponified in 0.5 M potassium hydroxide in a MeOH/water solution (95:5, v:v) at 60°C for 12 h (Plancq et al., 2018) to remove alkenoates that could interfere with the identification of LCAs. LCAs were recovered by liquid-liquid extraction using 3 × 1 mL hexane and subsequently analyzed using GC-FID. The analysis was performed at the University of Glasgow, United Kingdom, on an Agilent 7890B GC System equipped with an Agilent VF-200 ms capillary column (60 m length, 0.25 mm inner diameter, 0.10 μm film thickness) (Longo et al., 2013) using hydrogen as carrier gas at a column flow rate of 36 cm s$^{-1}$. The oven temperature was programmed from 50°C (held for 1 min) to 255 °C at 20 °C min$^{-1}$, then to 300°C at 3°C min$^{-1}$ and finally to 320°C at 10°C min$^{-1}$ followed by 10 min hold time. Peak identification was achieved by gas chromatography-mass spectrometry (GC-MS) using an Agilent 7890B GC coupled with a 5977A GC-EI mass spectrometer and comparing peak retention times and mass spectral data with published data (de Leeuw et al., 1980; Marlowe et al., 1984). The GC conditions were the same as for GC-FID analyses. The MS conditions were as follows: ion energy 70 eV; mass range 40–600 m/z. LCA concentrations were assigned using hexatriacontane ($n$C$_{36}$ alkane) as an internal standard. The alkenone unsaturation index was calculated as follows:

$$U_{37}^{K} = \frac{(C_{37:2} - C_{37:4})}{(C_{37:4} + C_{37:3} + C_{37:2})} \text{(Brassell et al., 1986)} \quad (4)$$

A potential alternative alkenone unsaturation index is the $U_{37}^{K'}$ index, which excludes contributions of the tetra-unsaturated $n$C$_{37}$ methyl alkenone and is frequently utilized in marine settings (e.g. Prahl and Wakeham, 1987; Sikes and Volkman, 1993; Müller et al., 1998; Conte et al., 2006). In lacustrine environments, several studies found a significant relationship of the $U_{37}^{K}$ index and lake water temperature but no correlation between the $U_{37}^{K'}$ index and lake water temperature (Toney et al., 2010; Nakamura et al., 2014; Zhao et al., 2017). We therefore chose the $U_{37}^{K}$ index over the $U_{37}^{K'}$ index in this study.

## Analysis of Sedimentary Long-Chain Alkyl Diols

Polar fractions were analyzed for their LCDs concentration at the Royal Netherlands Institute for Sea Research (NIOZ), Texel, Netherlands. Samples were evaporated to dryness under nitrogen and silylated with a mixture of 10 μL N,O-bis(trimethylsilyl)trifluoroacetamide (BSTFA) and 10 μL pyridine at 60°C for 30 min. Squalane was added as an internal standard. Samples were dissolved in 80 μL ethyl acetate and analyzed by GC-MS using an Agilent 7890B GC equipped with a Agilent CP Sil-5 fused silica capillary column (25 m length, 0.32 mm inner diameter, 0.12 μm film thickness), coupled

to an Agilent 5977A MSD mass spectrometer. Instrumental conditions were the same as described by de Bar et al. (2019): the temperature program started at 70°C, increased to 130°C at a rate of 20°C $min^{-1}$, heated to 320°C at 4°C $min^{-1}$ and was held at 320°C for 25 min. Flow rate was 2 mL $min^{-1}$. The quadrupole was held at 150°C and the electron impact ionization energy of the MS source was 70 eV. Fractional abundances were obtained using SIM of $m/z$ = 313.3 ($C_{28}$ 1,13-diol, $C_{30}$ 1,15-diol, $C_{34}$ 1,19-diol) and 341.3 ($C_{30}$ 1,13-diol, $C_{32}$ 1,15-diol, $C_{34}$ 1,17-diol, $C_{36}$ 1,19-diol) ions (Versteegh et al., 1997; Rampen et al., 2012).

## Analysis of Diatoms

Subsamples for diatom analyses (∼0.1 g) were taken in 1–32 cm intervals, depending on diatom preservation. If the valves were well preserved, a sample was analyzed at least every 8 cm. Diatom sample preparation followed Kalbe and Werner (1974). The diatom concentration was established by adding known quantities of microspheres (Battarbee and Kneen, 1982). If possible, at least 400 valves were counted in each sample at 1000× magnification and differential interference contrast (DIC) using a Leica DM 5000B microscope. Diatom species were identified based on Lange-Bertalot and Moser (1994); Lange-Bertalot (2001), Oliva et al. (2008); Krammer and Lange-Bertalot (2008), Krammer and Lange-Bertalot (2010); Houk et al. (2010), Hofmann et al. (2011), and Genkal (2012).

## Data Analysis

### Linear Dimension Reduction by PCA

A PCA was generated using the function "prcomp" in R 3.6 (R Core Team, 2019). The settings for "prcomp" were: scale = TRUE, center = TRUE. The function was supplied with concentrations of the lipid biomarkers and winter solar insolation data at 40°N over the course of the Holocene (Berger and Loutre, 1991). Data visualization was performed using the R package factoextra 1.0.6. (Kassambara and Mundt, 2019) with the function "fviz_pca_var" (repel = TRUE). A scree plot showing the cumulative variance explained by each principal component can be found in **Supplementary Figure S1**.

### Nonlinear Dimension Reduction by UMAP

UMAP was performed using a R 3.6 implementation as package umap 0.2.3.1 (Konopka, 2019; R Core Team, 2019). The UMAP algorithm was supplied with the concentrations of *n*-alkanes, LCAs, LCDs, the E/I data, the $U_{37}^{K}$ index and the ratio of planktonic and periphytic diatoms. If not specified differently, default options were adopted. To compute the UMAP layout, we used a Manhattan distance metric and fixed the starting conditions to random state = 3 for future reproducibility. A density-based spatial clustering was applied on the resulting layout using the function "hdbscan" within the R package dbscan 1.1-5 and a minimum number of six points per cluster (minPts = 6) (Hahsler et al., 2019). Visualizations of the results were created in the R package ggplot2 3.2.1 (Wickham, 2016).

We also compared the results of UMAP with those of the more commonly used dimensionality reduction technique t-Distributed Stochastic Neighbor Embedding (t-SNE) (**Supplementary Figure 2**). Both dimension reduction techniques captured the same overall variability pattern. However, UMAP performed better on our dataset as it preserved more of the global structure than t-SNE, resulting in a more distinct clustering using the same settings (**Figure 6** and **Supplementary Figure S2**). Consequently, lake phases were separated more clearly in the UMAP embedding. We therefore implemented the results of UMAP in our further discussion.

### Abrupt Shift Detection

Time series analysis was performed using the package *asdetect* 0.1.0 in R 3.6 (Boulton and Lenton, 2019; R Core Team, 2019). *Asdetect* was installed using GitHub. The package *asdetect* was run for each biomarker individually using the default time steps and window lengths fixed between 3 (lowwl) and 1/6 (highwl) of the respective time series. Points in the time series that contribute to significant gradients have a value of 1 added or subtracted to a detection time series, which is then divided by the window length l, resulting in a function-specific detection value.

# RESULTS and DISCUSSION

## Biomarker Results

### Sedimentary *n*-Alkanes

*n*-alkanes are aliphatic hydrocarbons that are relatively resistant to degradation (Meyers, 2003). Generally, their distribution and the ACL are used to distinguish different origins of organic matter sources. Long-chain *n*-alkanes (including $nC_{27}$, $nC_{29}$, $nC_{31}$) with a strong odd-over-even predominance are common components of vascular plant epicuticular waxes (Eglinton and Hamilton, 1967). Therefore, an increase in their concentration would entail higher terrestrial organic productivity (Meyers, 2003). In contrast, short-chain *n*-alkanes ($nC_{15}$ to $nC_{19}$) are synthesized by photosynthetic bacteria and algae (Cranwell et al., 1987; Meyers and Ishiwatari, 1993), whereas submerged and floating aquatic plants produce higher amounts of the mid-chain *n*-alkanes $nC_{21}$ to $nC_{25}$ (Ficken et al., 2000). Consequently, these compounds reflect lacustrine productivity levels (Meyers, 2003).

The sediments of Lake Chatyr Kol contained mainly $nC_{17}$ and $nC_{23}$ – $nC_{31}$ *n*-alkanes with a strong odd-over-even predominance and a changing distribution pattern within the sediment record (**Figure 3**). This suggests that the source of *n*-alkanes primarily derived from allochthonous material (e.g., terrestrial plants). Total *n*-alkane concentrations ranged from 1.1 to 172.4 μg $g^{-1}$ dry weight (d.w.) (median: 19.7 μg $g^{-1}$ d.w., **Figure 4**). The ACL varied between 17.9 and 29.3, with a median of 25.4. A k-means cluster analysis revealed that the Lake Chatyr Kol sediment record consists of three clusters based on the *n*-alkane distribution (**Figure 3**). Sediment samples combined in cluster 1 ($n$ = 13) are characterized by a bimodal pattern of $nC_{23}/nC_{25}$ and $nC_{29}/nC_{31}$ (ACL = 26.5), thus reflecting a higher contribution from aquatic macrophytes. Cluster 2 is the most abundant cluster ($n$ = 55), containing primarily long-chain *n*-alkanes $nC_{27}$ to $nC_{31}$ (ACL = 27). Consequently, cluster 2 indicates predominantly terrestrial vegetation input.

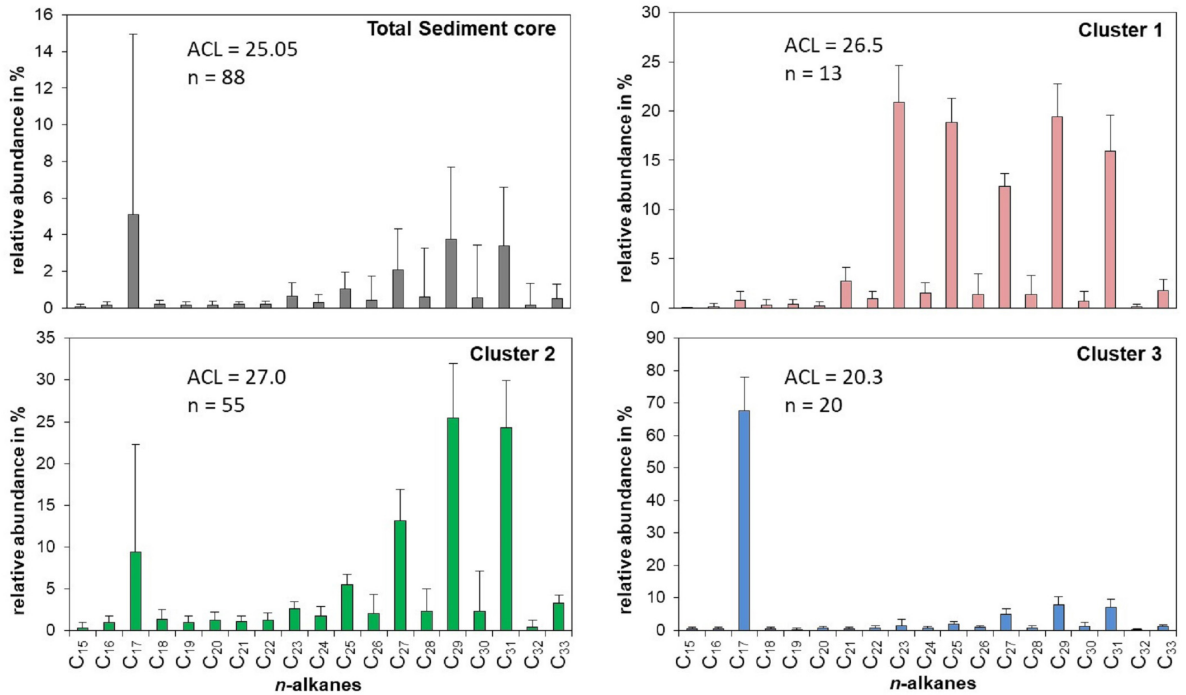


**FIGURE 3 |** Relative distribution, abundance and ACL [average chain length = $\Sigma(Cn \times n)/\Sigma Cn)$] of *n*-alkanes for the entire Lake Chatyr Kol sediment core as well as for the three principal clusters.

Cluster 3 is characterized by a dominance of the short-chain *n*-alkane $nC_{17}$, therefore suggesting higher proportions of microorganism-derived material, likely from cyanobacteria (Lea-Smith et al., 2015).

## δD of Sedimentary *n*-Alkanes

δD values of *n*-alkanes are valuable for paleohydrological reconstructions since they mainly record the δD of the source water (Sachse et al., 2012). The δD of the terrestrial *n*-alkane $nC_{29}$ thereby reflects the δD signature of the meteoric water (precipitation) modified by evapotranspiration, whereas the δD of the aquatic *n*-alkane $nC_{23}$ displays the isotope signal of the ambient lake water, modified by evaporation (Sachse et al., 2012; Guenther et al., 2013). Based on the isotopic differences, the E/I can be applied as a parameter for hydroclimatic balances of a lake system (Mügler et al., 2008). Higher E/I values would indicate higher evaporation relative to input water, therefore reflecting semi-arid or arid environmental conditions. By contrast, humid conditions are characterized by lower E/I values, when inflow water exceeds evaporation (Mügler et al., 2008).

δD of $nC_{23}$ varied between −56 ‰ at ∼1450 a BP and −165 ‰ at ∼7200 a BP (**Supplementary Figure S3**). δD of $nC_{29}$ ranged from −195 ‰ at ∼5900 a BP to −100 ‰ at ∼11,500 a BP, exhibiting smaller fluctuations than the δD of the aquatic $nC_{23}$ (**Supplementary Figure S3**). A significant correlation between $\delta D nC_{23}$ and $\delta D nC_{17}$ throughout the entire sediment record (Pearson correlation coefficient $r = 0.48$, $p < 0.01$, **Supplementary Figures S3, S4**) reinforced the potential of $\delta D nC_{23}$ to record changes in the lake water isotopic composition. Reconstructed E/I varied from 0.4 between ∼11,000 and 5000 a BP, pointing to humid conditions, to 0.8 between ∼5000 and 1200 a BP, indicating more arid conditions (**Figure 4**). The youngest part of the record (∼1000 – 30 a BP) was characterized by an E/I of 0.3, representing more humid conditions (Günther et al., 2016).

## Sedimentary Long-Chain Alkenones

LCAs are $nC_{35}$–$nC_{42}$ aliphatic unsaturated ketones that are biosynthesized by haptophyte algae from the Isochrysidales order (Theroux et al., 2010). Previous investigations have shown that the occurrence of LCAs in lakes are strongly associated with salinity and stratification (Song et al., 2016; Plancq et al., 2018). Furthermore, the bloom of lacustrine alkenone producers is favored by cold water temperatures and enhanced nutrient availability (Toney et al., 2010). The alkenone unsaturation index $\left(U^{K}_{37}\right)$, which is based on the correlation of the degree of LCA unsaturation with the temperature of water, is increasingly used to reconstruct surface temperatures in lacustrine settings (Zink et al., 2001; Chu et al., 2005; Toney et al., 2010; Sun et al., 2012). Since LCAs are absent in surface sediments and we cannot exclude multiple haptophyte species inhabiting the lake, which would require DNA analysis, we utilized the $U^{K}_{37}$ index as an indicator for temperature but do not report absolute temperature values.

The concentrations of $nC_{37}$ and $nC_{38}$ in the Lake Chatyr Kol sediment record exhibited large variations between 0.3 and 1571 $\mu g\ g^{-1}$ d.w. with a mean of 245 $\mu g\ g^{-1}$ d.w. (**Figure 4**). Total LCA concentrations included concentrations of the tetra-,

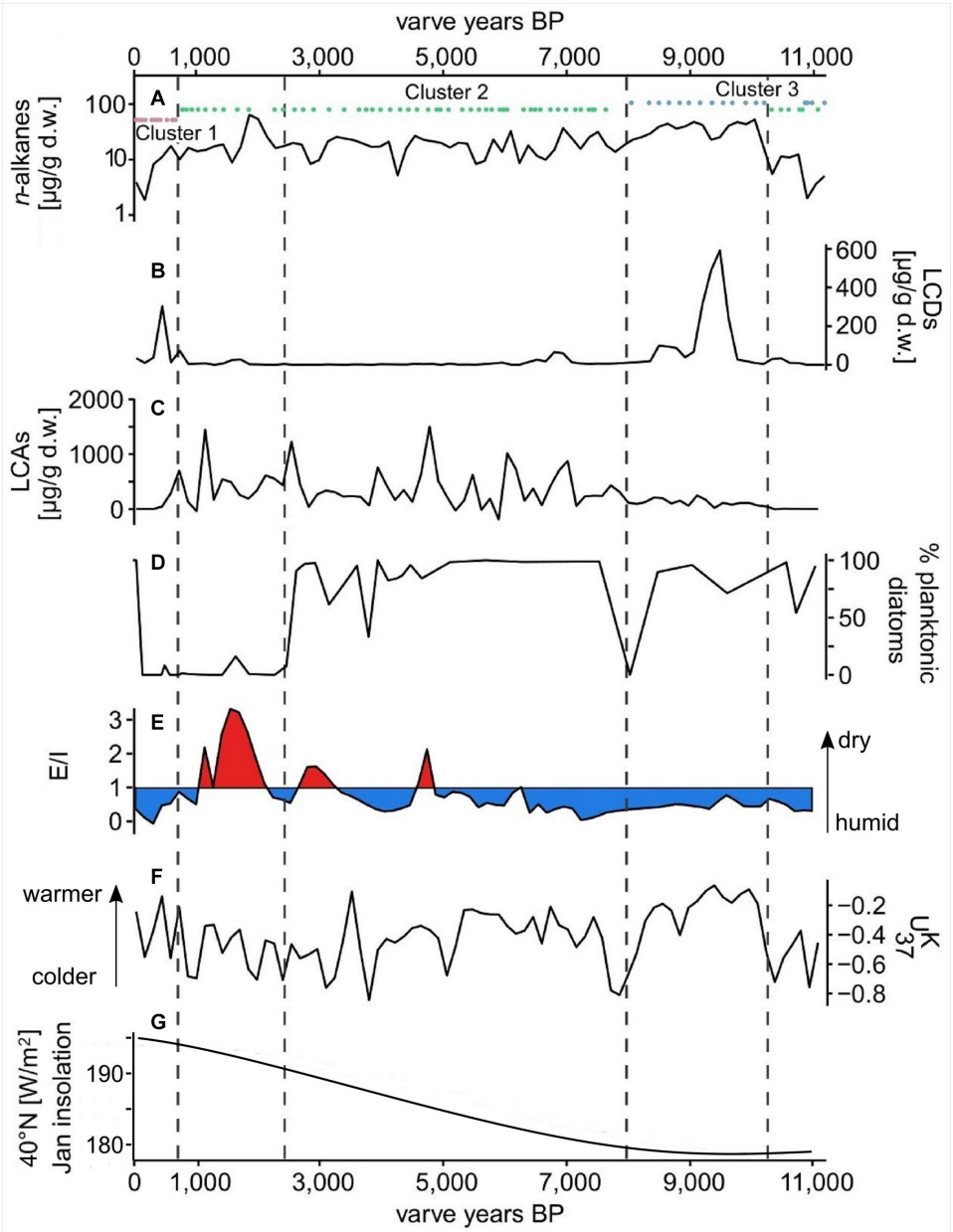


**FIGURE 4 |** Proxy data from the Lake Chatyr Kol sediment record. **(A)** total *n*-alkane amount with *n*-alkane clusters 1–3; **(B)** total long-chain alkyl diol amount (LCDs); **(C)** total long-chain alkenone amount (LCAs); **(D)** % of planktonic over periphytic diatoms **(E)** Evaporation-to-inflow ratio (E/I); **(F)** alkenone unsaturation index ($U^{K}_{37}$); **(G)** January insolation at 40°N (Berger and Loutre, 1991). Dashed vertical lines mark phase boundaries defined by UMAP.

tri-, di-unsaturated $nC_{37}$ methyl alkenones and $nC_{38}$ ethyl alkenones, as well as tri-unsaturated isomers of $nC_{37}$ and $nC_{38}$ alkenones. Values for $U^{K}_{37}$ ranged from −0.873 to −0.057 (median −0.38, **Figure 4**).

## Sedimentary Long-Chain Alkyl Diols

LCDs are a group of lipids that occur widespread in marine environments and consist mainly of saturated $C_{28}$ and $C_{30}$ 1,13-diols, $C_{28}$ and $C_{30}$ 1,14-diols, and $C_{30}$ and $C_{32}$ 1,15-diols (Volkman et al., 1992, 1999; Sinninghe Damsté et al., 2003; Rampen et al., 2014b). These compounds are likely produced by phytoplankton and also appear in freshwater environments (Shimokawara et al., 2010; Castañeda et al., 2011; Romero-Viana et al., 2012; Rampen et al., 2014a; Villanueva et al., 2014; Lattaud et al., 2017, 2018). A major biological source of LCDs in freshwater environments might be the Eustigmatophyceae class of algae, as previous studies have shown a link between the distribution of LCDs and eustigmatophytes (Shimokawara et al., 2010; Rampen et al., 2014a; Villanueva et al., 2014; Lattaud et al., 2018). However,

the sources of LCDs as well as environmental controls on the distribution and abundance of LCDs are still poorly known (Rampen et al., 2012, 2014a). In marine settings, sea surface temperatures play an important role in determining abundance and distribution of LCDs (Rampen et al., 2012).

The most abundant LCDs in our sediment core, were the $C_{32}$ 1,15-diol, followed by the $C_{30}$ 1,13-diol. Total LCD content (sum of $C_{28}$ 1,13-diol, $C_{30}$ 1,15-diol, $C_{30}$ 1,13-diol, $C_{32}$ 1,15-diol, $C_{34}$ 1,17-diol, $C_{34}$ 1,19-diol, and $C_{36}$ 1,19-diol) varied between being not detectable and 619 $\mu g\ g^{-1}$ d.w. (**Figure 4**).

### Planktonic and Periphytic Diatoms

Diatoms are frequently utilized as indicators of paleoenvironmental changes (Pérez et al., 2013). Based on the different adaptive strategies, diatoms can be divided into periphytic and planktonic diatoms. Periphytic diatoms colonize and attach to substrates, whereas planktonic diatoms are adapted to floating (Dunck et al., 2013).

In our sediment core, due to temporal changes in valve preservation during the period examined, the diatom concentration strongly varies between 0.0 and 5171.3 $\times$ $10^5$ valves $g^{-1}$ dry weight (**Supplementary Figure S5**). Zonation of diatom stratification was based on UMAP clustering (see chapter "Lake phases separation") and additionally visual inspection. Poor diatom preservation up to complete valve dissolution started from about 370 a BP.

Phase I (∼11,000 – 10,200 a BP) and Phase II (∼10,200 – 8050 a BP) are characterized by dominance of planktonic diatoms, mainly *Cyclotella choctawhatcheeana* Prasad. Periphytic diatoms, e.g., *Cocconeis placentula* Ehrenberg, are present with varying frequencies. At the beginning of Phase IIIa (∼8050 a BP), periphytic *Nitzschia lacuum* Lange-Bertalot occurs with higher abundance. Otherwise, the plankton dominance (*C. choctawhatcheeana*) increases to almost 100% in Phase IIIa. From about 5000 a BP (Phase IIIb) more periphytic diatoms that indicate saline or electrolyte-rich water, such as *Achnanthes brevipes* var. *brevipes* Agardh and *Navicymbula pusilla* (Grunow) Krammer 2003, appear. With the onset of Phase IV (∼2600 – 780 a BP), the diatom assemblages clearly show changes in species composition, planktonic diatoms almost completely disappeared and periphytic species were dominant. From 780 a BP (Phase V) only freshwater periphytic diatoms, mainly *C. placentula*, occurred in Chatyr Kol. The few valves obtained initially represent periphytic and freshwater-preferring species. In the recent sediments, again planktonic species dominate.

## Data Evaluation

### Interdependencies Between Biomarkers

The PCA of our biomarker dataset revealed interdependencies between the various biomarker groups and parameters (**Figure 5**). The winter solar insolation was likely a controlling parameter of the E/I in our sediment record, which in turn affected the concentration of LCAs. Similarly, based on various lake energy and water-balance models, Li and Morrill (2010) found a close relationship between increasing winter solar insolation and increasing lake evaporation throughout the Holocene for monsoonal Asia. Higher E/I values (more arid conditions) would ultimately lead to a higher lake salinity, which likely promoted higher LCA concentrations in our record. Indeed, water salinity has been proposed as one of the determining factors for the occurrence of LCAs in lacustrine environments (Pearson et al., 2008; Toney et al., 2010; Liu et al., 2011; Song et al., 2016). Commonly, LCAs are barely present in both freshwater (0–3 $g\ L^{-1}$) and hypersaline (>100 $g\ L^{-1}$) lakes, but LCAs are typically found in intermediate salinity freshwater (2.41–44.43 $g\ L^{-1}$) settings (Zink et al., 2001; Chu et al., 2005; Liu et al., 2011; Plancq et al., 2018). We therefore deduce a salinity-dependent occurrence of LCAs in Lake Chatyr Kol since LCAs are absent in the lake at the current salinity level of 1.18 g $L^{-1}$ (measured in July 2018).

Conversely, the concentration of both LCDs and *n*-alkanes seemed to vary with the $U^K_{37}$ index (**Figure 5**). Higher $U^K_{37}$ values, suggesting higher temperatures, likely promoted higher occurrences of LCDs as well as *n*-alkanes. The temperature control on the distribution of LCDs is well observed in marine environments although the sources of the compounds are not clear (Rampen et al., 2012). In contrast, the biological sources of LCDs are likely eustigmatophyte algae (Rampen et al., 2014a; Villanueva et al., 2014). Our results suggest that the productivity of eustigmatophyte algae may have been stimulated by warmer temperatures.

Similar to the occurrence of LCDs, the contribution of *n*-alkanes seemed to be linked to temperature (**Figure 5**). Since *n*-alkanes are dominated by their long-chain homologues

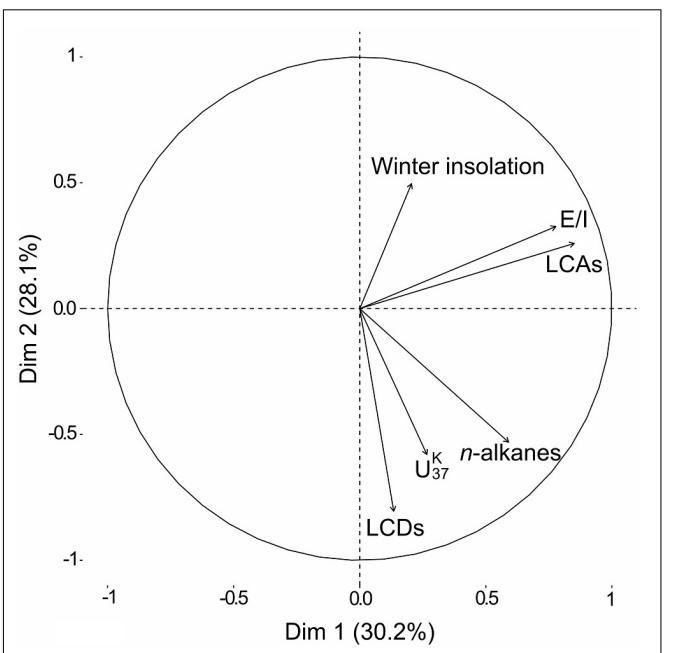


**FIGURE 5 |** Principal Component Analysis (PCA) visualization of lipid biomarker composition and January insolation at 40°N (Berger and Loutre, 1991) over the Holocene. Accordingly, the winter solar insolation was likely a controlling parameter of the Evaporation-to-Inflow ratio E/I, which in turn affected the presence of LCAs. Conversely, the concentration of both LCDs and n-alkanes seemed to be controlled by temperature ($U^K_{37}$ index).

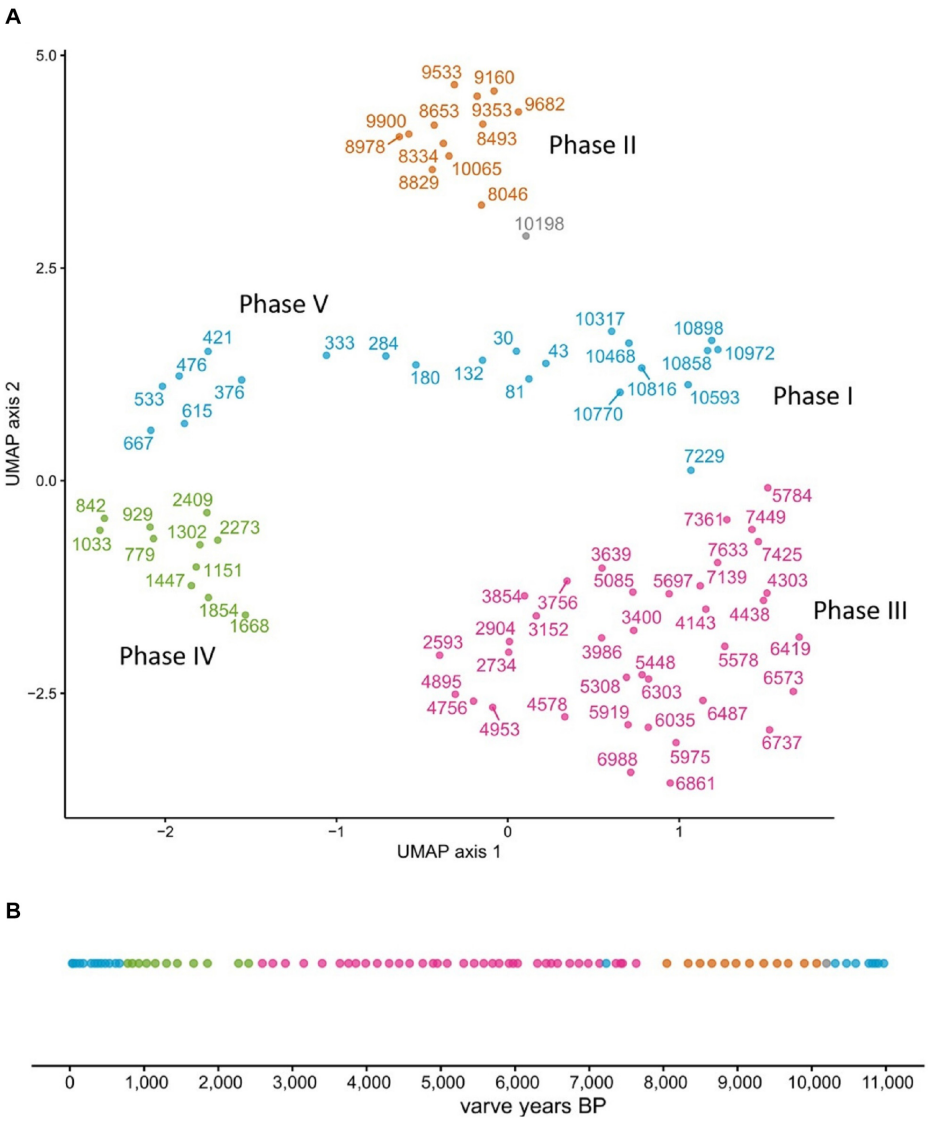


**FIGURE 6 |** Lake phases separation by UMAP. The core was clustered into 4 separate groupings **(A)**, which when resolved temporally yield five distinct lake phases **(B)**. Note that one data point could not be assigned to a grouping (gray point).

in our record, an increase in their concentration would imply an enhanced deposition of allochthonous material. This can be attributed to either higher erosion and/or growth of terrestrial vegetation favored by a warmer climate. Consequently, this could have led to an input of nutrients stimulating eustigmatophyte growth.

## Lake Phases Separation

We ran UMAP on the combined dataset of *n*-alkanes, LCAs, LCDs, E/I, $U_{37}^{K}$ and the ratio of planktonic and periphytic diatoms, containing in total 581 independent data points. A density-based clustering of the resulting UMAP layout separated the sediment core into five distinct phases (I–V), with Phase I: ∼11,000 – 10,200 a BP, Phase II: ∼10,200 – 8050 a BP, Phase III: ∼8050 – 2600 a BP, Phase IV: ∼2600 – 780 a BP, and Phase V: ∼780 – present. Only one data point between Phase I and II remained unclustered (**Figure 6**).

Interestingly, Phase I (∼11,000 – 10,200 a BP) and Phase V (∼780 a BP – present) were assigned to the same cluster (**Figure 6**), indicating similar environmental conditions. While UMAP clearly identified five temporally separated lake phases, the nature of the transitions between these phases needs further discussion.

## Abrupt Shift Detection

To characterize the transitions at the previously identified phase boundaries, we ran *asdetect* on each proxy separately. Since we had already identified the phase boundaries, we did not apply a threshold to *asdetect*, but compared the individual results in a combined approach (**Figure 7**, **Supplementary**

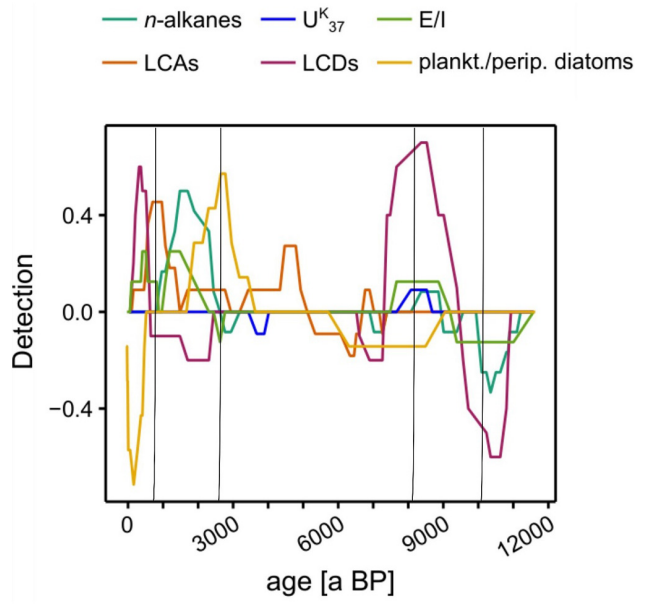


**FIGURE 7 |** Shift detection results by asdetect. The algorithm was performed on every proxy individually and subsequently stacked. Black lines indicate Phase boundaries defined by UMAP (see **Figure 6**).

**Figure S6**). We hypothesized that phase transitions could show two major characteristics. On the one hand a tipping-point type of transition in which an event affects most of biomarker signals simultaneously. On the other hand a gradual phase transition characterized by a consecutive temporal succession of biomarker shifts.

During the Early Holocene, the phase boundaries at ∼10,200 and ∼8050 a BP were characterized by overlapping shift indicators of multiple proxies with their respective maxima/minima at the previously defined phase boundaries (**Figure 7**). Our data indicate that Early Holocene phase boundaries were likely event-based and could be classified as potential tipping points. In contrast, the phase boundaries in the Late Holocene at ∼2600 and 780 a BP showed less pronounced overlaps of biomarker shifts (**Figure 7**). Instead, a continuous succession of proxy changes suggests more gradual phase transitions during this period.

## Holocene Lake Development

Based on the biomarker results and both lake phases and phase boundary identification, a reconstruction of the lake development over the course of the Holocene was conducted. In accordance with the phase separations, the lake development is discussed in separate sections.

### Phase I (∼11,000 – 10,200 a BP)

Phase I comprises the oldest part of the sediment record and is characterized by relatively low concentrations of all biomarkers (**Figures 4**, **8**). Relatively low $U^K_{37}$ values and less negative δD values of $nC_{29}$ (−139 ± 23 ‰) likely reflect cold and arid climate conditions, respectively. Since aquatic plants were most probably not very abundant due to generally low in-lake productivity, concentrations of $nC_{23}$ are periodically below the limit necessary for reliable δD measurements. Less negative δD values of $nC_{23}$ at ∼11,000 to 10,900 a BP likely indicate a dry environment.

Dominant *n*-alkane clusters are the terrestrial cluster 2 and the microbial cluster 3 with a dominance of cluster 2 from ∼10,800 to 10,300 a BP. The change at ∼10,900 a BP from cluster 3 to cluster 2 indicates enhanced terrestrial input to the lake system. Concentrations of long-chain *n*-alkanes were, however, still relatively low. Nevertheless, an increase in the LCD concentration between ∼10,800 and ∼10,300 a BP indicates a slightly increasing biological productivity (**Figure 4**).

### Phase II (∼10,200 – 8050 a BP)

The transition from Phase I to Phase II was likely abrupt. Simultaneous shifts in LCDs, n-alkanes and E/I characterize the transition to Phase II as a potentially event-based tipping point (**Figure 7**). Rising temperatures as indicated by a sharp increase of $U^K_{37}$, most probably triggered by high summer solar insolation, promoted enhanced terrestrial input and algal productivity as seen in increasing *n*-alkane and the LCA amounts, respectively. A shift to a dominance of cluster 3, enhanced LCA production and the highest concentrations of LCDs, reflect high productivity of microorganisms due to more favorable lake conditions (**Figure 4**). The changes in the concentration and distribution of the biomarkers potentially recorded the abrupt crossing of a lake-internal system threshold as a local response to the effects of the Holocene Climate Optimum at ∼10,200 a BP (**Figure 4**). Low concentrations of $nC_{23}$ and thus low abundance of aquatic plants most likely reflect a higher lake level and thus a generally deeper lake as in the modern system aquatic plants occur primarily in the shallow water zone (Kalanke et al., 2020). A higher lake level can equally be inferred from the stronger dominance of planktonic over periphytic diatoms in comparison to Phase I (**Figures 4**, **8**). Favorable lake conditions at this time interval were also inferred by Kalanke et al. (2020), who linked the dominating calcite precipitation with enhanced biological activity of e.g., Chrysophyceae and Characeae. Higher temperatures likely led to an isotopic enrichment of the Westerlies-derived precipitation, causing less negative δD values of $nC_{23}$ ($\delta D nC_{23} = -132 \pm 0.3$‰). E/I decreased at ∼10,200 a BP from 0.7 to 0.5, indicating higher moisture availability (**Figure 4**).

### Phase III (∼8050 – 2600 a BP)

A further potential event-based tipping point, identified by simultaneous shifts in LCDs, *n*-alkanes, E/I and $U^K_{37}$ as well as in the planktonic/periphytic diatom ratio marks the onset of Phase III (**Figures 7**, **8**). Warm and relatively stable environmental conditions during Phase II were interrupted by a significant drop of $U^K_{37}$ at ∼8050 a BP indicating a shift to colder temperatures (**Figure 4**). Planktonic diatoms, for instance, were not present at ∼8050 a BP, whereas the dominance of the periphytic diatom *Nitzschia lacuum* suggests a cooling effect (**Supplementary Figure S5**). The absence of planktonic diatoms could indicate a strong shortening of the mixing phase, which is the main growth period of planktonic diatoms probably reflected by colder winters (Dreßler et al., 2011). Taking dating uncertainty

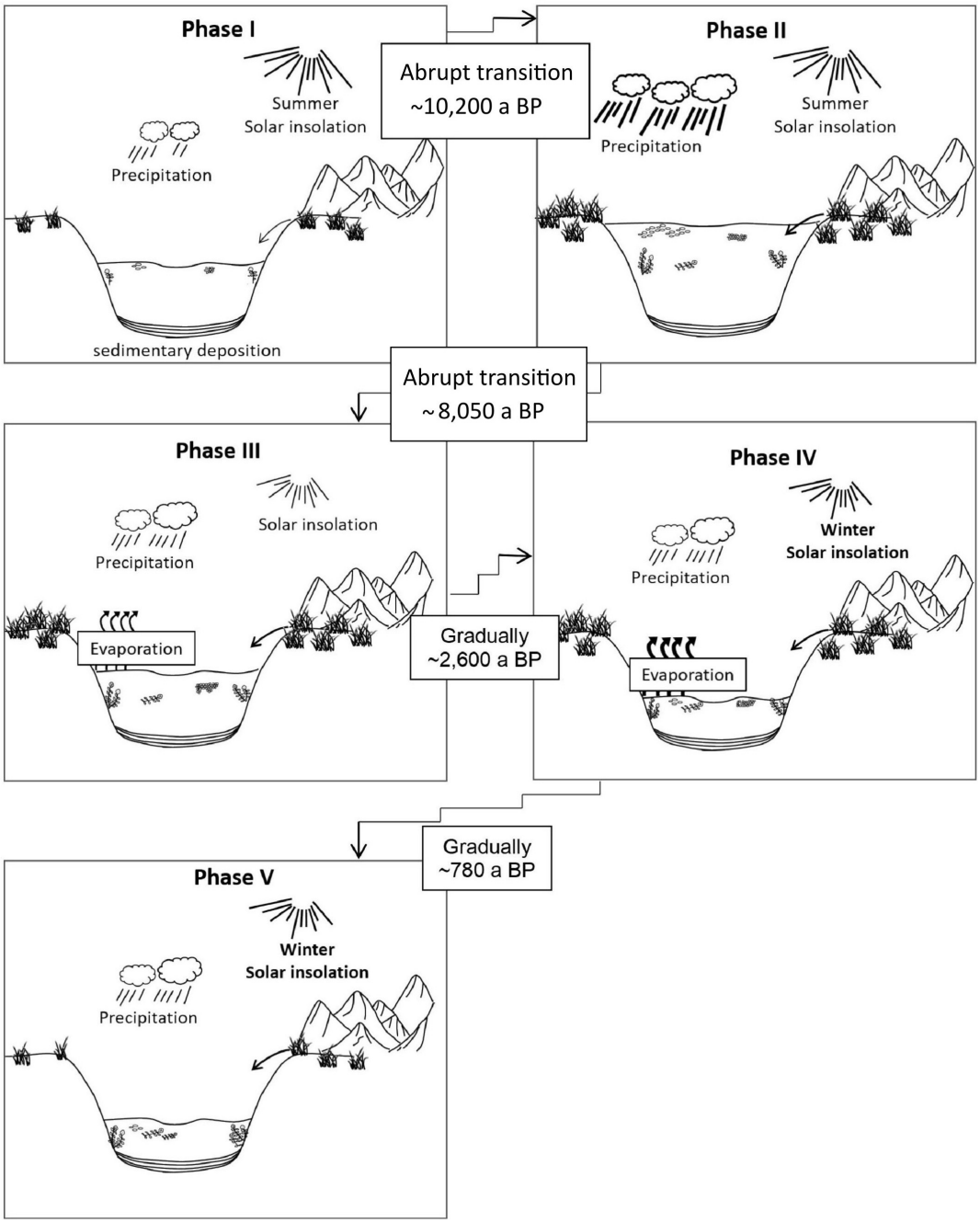


**FIGURE 8 |** Development of Lake Chatyr Kol during the Holocene. Phases I-V refer to Phase definition by UMAP. Phase boundaries in the Early Holocene (I–II and II–III) were likely event-based while phase boundaries in the Late Holocene (III–IV and IV–V) were likely gradual shifts.

into account, this cold interval possibly coincides with the North Atlantic 8.2 ka BP event (Alley and Agustsdottir, 2005; Kobashi et al., 2007). Another possibility which would explain the time lag is the hydrogeomorphology of high mountain lakes. The water balance of Lake Chatyr Kol is predominantly regulated by glacier surface melting, which in turn is influenced by air temperatures, solar radiation and precipitation (e.g., Oerlemans, 2005; Pan et al., 2012). However, oftentimes glaciers respond to climate change with a certain time lag (Jóhannesson et al., 1989; Pan et al., 2012), which would ultimately result in a response time lag of the lake. Cold and dry climate conditions during this period were also postulated for the Tibetan Plateau, mostly inferred from pollen data, such as for Lake Qinghai (∼2100 km northeast of Lake Chatyr Kol) at 8.2 cal. ka BP (Shen et al., 2005), Lake Zigetang Co (∼1700 km southeast of Lake Chatyr Kol) at 8700 – 8300 cal. a BP (Herzschuh et al., 2006) and the

high mountains of the northeastern Tibetan Plateau (∼2,300 km northeast of Lake Chatyr Kol) at 8300 – 8000 cal. a BP (Miao et al., 2014). Furthermore, the event was observed in stalagmites across China (Dykoski et al., 2005; Wu et al., 2012; Liu et al., 2013). The overlapping timing of the reconstructed dry event ∼8200 years ago in Central Asia, that lasted ∼150 years and the 8.2 ka BP cold event of ∼160 years 8200 years ago observed in Greenland ice cores (Thomas et al., 2007), indicates an atmospheric teleconnection between North Atlantic temperature changes and precipitation in Central Asia. It is suggested that a weakening of the Atlantic Meridional Overturning Circulation affected the North Atlantic, which conversely affected the Asian Monsoon and may be related to changing mean latitudinal position of the Intertropical Convergence Zone (ITCZ) (Hu et al., 2008; Cheng et al., 2009).

A likewise decrease in temperature at Lake Chatyr Kol was also proposed by Kalanke et al. (2020) at ∼8040 a BP based on a shift in the varve microfacies. Phase III also marks the decline of the dominance of microorganisms as seen by a strong decrease in the LCD concentration as well as by a shift to a prevalence of the terrestrial *n*-alkane cluster 2. Contrary to the decline of microorganisms, concentrations of LCAs increased during Phase III relative to Phase II. Increases in LCA concentrations have been proposed as a stress response to cooler temperatures (Toney et al., 2010).

At ∼6300 – 5800 a BP, δD values of $nC_{29}$ show the strongest negative values (−191 ± 4‰), possibly associated with high amounts of precipitation and higher lake levels. This would be in agreement with the dating of an exposed lake terrace, which shows a mid-Holocene age of 5786 ± 122 cal. a BP (Kalanke et al., 2020). A dominance of planktonic diatoms (*C. choctawhatcheeana*) and almost complete disappearance of periphytic diatoms, also indicates higher lake levels around this time. Likewise, more negative $\delta D nC_{29}$ values at Lake Son Kol (Central Tian Shan of Kyrgyzstan) suggest predominantly humid summers between 6000 and 4950 cal. a BP (Lauterbach et al., 2014; Schwarz et al., 2017).

Throughout Phase III, however, E/I values increased, indicating increasing dryness likely with a lower lake level. The increase of periphytic diatoms, such as the saline or electrolyte-rich water indicating species *A. brevipes* var. *brevipes* and *N. pusilla* (Hofmann et al., 2011), also suggests lower water levels (**Supplementary Figure S5**). Lowest $U^K_{37}$ values were observed at ∼3900 a BP, which lasted until ∼3600 a BP (**Figure 4**). Furthermore, Mischke et al. (2010) observed a shift to colder conditions around 3500 cal. a BP for Lake Karakul, NE Tajikistan (∼220 km southwest of Lake Chatyr Kol) by multi-proxy analyses. An alkenone-based study from Lake Balikun, located in the eastern Tian Shan (∼1500 km northeast of Lake Chatyr Kol), showed a similar major cooling between 4800 and 3800 cal. a BP (Zhao et al., 2017). Additionally, a period of dry summers between 4950 and 3900 cal. a BP has been inferred for Lake Son Kol (∼120 km north of Lake Chatyr Kol) (Lauterbach et al., 2014). Cold-arid conditions between 4500 and 3500 cal. a BP have been globally documented and identified as the 4.2 ka BP event (Booth et al., 2005; Staubwasser and Weiss, 2006; Walker et al., 2012). The causes and forcing mechanisms behind the 4.2 ka BP event are still not well understood, but potential explanations include, amongst others, a southward shift of the ITCZ (Mayewski et al., 2004), cooler conditions in the North Atlantic (Bond et al., 1997) and a strengthening of the El Niño Southern Oscillation (Walker et al., 2012; Toth and Aronson, 2019). Recently, Perşoiu et al. (2019) hypothesized that the cold and arid conditions, which prevailed on the Eurasian landmass during the 4.2 ka BP event, resulted from a strengthening and expansion of the Siberian High, which hindered the transport of moisture by blocking the Westerlies. Consequently, this could have caused dry and cold conditions in our study area. Interestingly, both UMAP and *asdetect* do not characterize this event as a phase boundary nor as an abrupt shift, indicating that the 4.2 ka BP event did not lead to a lake system change in our study area. We therefore hypothesize that an event-based phase transition only occurs after an internal system threshold is exceeded.

### Phase IV (∼2600 – 780 a BP)

The transition to Phase IV was initiated by a shift in only a minority of the proxies, which, however, was followed by a consecutive temporal succession of biomarker shifts (**Figure 7**). At the transition, $\delta D nC_{23}$ is more negative, resulting in lower E/I values, pointing to a short-term humid phase (**Figure 4**). Additionally, the percentage of planktonic diatoms recorded a significant decline. Subsequently, strongly increased E/I values at ∼2300 and ∼1500 a BP characterize arid and warm periods, which led to high evaporation ($\delta D nC_{23}$ = −93 ± 21‰) and promoted higher concentrations of LCAs. Over the course of Phase IV, solely periphytic and primarily halophilic diatom species occurred, similarly pointing to lower lake levels and higher salinity, most likely because of higher evaporation (**Figure 8**). The prevailing warm and dry environmental conditions at ∼2300 and ∼1500 – 1000 a BP coincide with the Roman Warm Period (RWP) and the Medieval Climate Anomaly (MCA), respectively. Similarly, Aichner et al. (2015) found warm and dry episodes at 2500 – 1900 and 1500 – 600 cal. a BP at Lake Karakuli, located at the westernmost edge of Xinjiang Province, China (∼240 km south of Lake Chatyr Kol). Warm conditions during the MCA are also well recorded in tree rings from Western Central Asia, including the Southern Tian Shan (Esper et al., 2002), in pollen data from the Kashgar oasis (∼150 km south of Lake Chatyr Kol) on the western margin of the Tarim Basin (Zhao et al., 2012) and for Lake Bangong Co (∼900 km southeast of Lake Chatyr Kol) (Gasse et al., 1996). During the RWP and the MCA, the lake level was likely lower, which is supported by higher abundances of periphytic diatoms and aquatic plant remains (Kalanke et al., 2020).

Decreased values for both $U^K_{37}$ and E/I between ∼1030 and ∼780 a BP imply cold and wet conditions, which is also documented in a number of other paleoclimate records in Central Asia (e.g., Esper et al., 2002; Yang et al., 2009; Chen et al., 2010; Zhao et al., 2012; Aichner et al., 2015) and likely reflects the Little Ice Age (LIA). The predominance of wetter conditions during this interval is in agreement with the presence of exposed paleo-lake deposits that date to 1097 ± 166 cal. a BP and 906 ± 160 cal. a BP (Kalanke et al., 2020).

### Phase V (~780 a BP – Present)

The transition to Phase V was again initiated by a singular proxy shift followed by a lagged response of the remaining proxies (**Figure 7**). As inferred by UMAP, biomarker profiles during Phase V were comparable to those during Phase I (**Figure 6**).

The onset of Phase V is reflected by enhanced aquatic productivity, particularly by a shift from the terrestrial *n*-alkane cluster 2 to the aquatic *n*-alkane cluster 1 as well as by an increase in LCD concentrations (**Figure 4**). The shift in the *n*-alkane composition points to a dominance of submerged macrophytes, whereas, higher amounts of LCDs can be linked to higher $U^K_{37}$ values, i.e., increased temperature. In addition, macrophytes dominance is also evidenced by the occurrence of the almost exclusively periphytic *C. placentula* (Hofmann et al., 2011).

Throughout Phase V, $\delta D n C_{29}$ is more negative and an average E/I of 0.3 points toward wetter conditions and higher precipitation in a warmer climate. These conditions likely discriminated against the occurrence of LCAs since their concentration decreased to a minimum (**Figure 4**). The reconstructed predominantly wet conditions during Phase V are in good agreement with the presence of paleo-lake deposits that date to 530 ± 204 cal. a BP (Kalanke et al., 2020).

At ~284 a BP the concentrations of LCDs and *n*-alkanes declined sharply, which could be attributed to decreased $U^K_{37}$ values, thus cooler temperatures. Similarly, the concentrations of LCAs remained low, likely induced by a lower E/I, indicating wetter conditions and fresher lake conditions. The inferred predominance of wetter conditions during this interval is in good agreement with the return of planktonic diatoms, which point to rising lake levels (**Figures 4**, **8**).

## CONCLUSION

The present study highlights the applicability of numerical methods for summarizing patterns in complex multi-proxy datasets. By reducing their dimensionality using PCA and UMAP, we increased their interpretability with minimal information loss. PCA allowed for elucidating proxy interdependencies while UMAP and *asdetect* enabled the objective identification and characterization of lake phases and corresponding phase boundaries, respectively. Over the course of the Holocene, we identified five temporally separated lake phases. In the Early Holocene, phase transitions were likely induced by supra-regional events such as the onset of the Holocene Climate Optimum and the temperature decrease associated with the 8.2 ka BP event. Conversely, during the Late Holocene, phase transitions appeared to have been rather gradual, induced by rather local environmental changes within the catchment area of the lake. Whether event based or gradual, phase transitions at our study site occurred when system-internal thresholds were exceeded as a result of diverse environmental changes.

As one of the rare paleoenvironmental studies integrating data-driven methods, we were able to elucidate the high complexity of lake phase transitions and interdependencies of proxies. We advocate for the use of data-driven approaches to decipher multi-proxy paleoenvironmental records in future studies as an alternative approach to common visual inspection.

## DATA AVAILABILITY STATEMENT

The raw data supporting the conclusions of this article will be made available by the authors, without undue reservation.

## AUTHOR CONTRIBUTIONS

GG designed the research idea. SL participated in field work. AS contributed diatom data. JK generated the age chronology. NS carried out laboratory analysis and the data analysis with support from JT and SS. NS prepared the manuscript. All authors discussed the results and improved the manuscript.

## FUNDING

This study was funded by the BMBF-funded research projects CADY (Central Asian Climate Dynamics, Grant No. 03G0813) and CAHOL (Central Asian Holocene Climate, Grant No. 03G0864). NS acknowledges the Max Planck Society and the International Max Planck Research School for Global Biogeochemical Cycles (IMPRS-gBGC) for further project funding.

## ACKNOWLEDGMENTS

We thank Michael Köhler, Sylvia Pinkerneil, Robert Schedel, Denis Henning, Mirlan Daiyrov, and Roman Witt for their involvement in field work. Furthermore we thank Julien Plancq, Steffen Rühlow, Mohammad Ali Salik, and Caglar Yildiz for their assistance during analyses. We also thank Jens Mingram and Achim Brauer for their involvement in the project.

## SUPPLEMENTARY MATERIAL

The Supplementary Material for this article can be found online at: https://www.frontiersin.org/articles/10.3389/feart.2020.00353/full#supplementary-material

## REFERENCES

Abdi, H., and Williams, L. J. (2010). Principal component analysis. *Wiley Interdiscip. Rev. Comput. Stat.* 2, 433–459. doi: 10.1002/wics.101

Abuduwaili, J., Issanova, G., and Saparov, G. (2019). *Lakes in Kyrgyzstan, Hydrology and Limnology of Central Asia*. Singapore: Springer, 288–294. doi: 10.1007/978-981-13-0929-8

Aichner, B., Feakins, S. J., Lee, J. E., Herzschuh, U., and Liu, X. (2015). High-resolution leaf wax carbon and hydrogen isotopic record of the late Holocene

paleoclimate in arid Central Asia. *Clim. Past* 11, 619–633. doi: 10.5194/cp-11-619-2015

Aichner, B., Wilkes, H., Herzschuh, U., Mischke, S., and Zhang, C. (2010). Biomarker and compound-specific δ13C evidence for changing environmental conditions and carbon limitation at Lake Koucha, Eastern Tibetan Plateau. *J. Paleolimnol.* 43, 873–899. doi: 10.1007/s10933-009-9375-y

Aizen, E. M., Aizen, B., Melack, J. M., Nakamura, T., and Ohta, T. (2001). Precipitation and atmospheric circulation patterns at mid-latitudes of Asia. *Int. J. Climatol.* 21, 535–556. doi: 10.1002/joc.626

Aizen, V. B., Aizen, E., Joswiak, D. R., Fujita, K., Takeuchi, N., and Nikitin, S. A. (2006). Climatic and atmospheric circulation pattern variability from ice-core isotope/geochemistry records (Altai, Tien Shan and Tibet). *Ann. Glaciol.* 43, 49–60. doi: 10.3189/172756406781812078

Aizen, V. B., Aizen, E., and Melack, J. (1995). Climate, Snow cover, Glaciers, and Runoff in the Tien Shan, Central Asia. *Water Resour. Bull.* 31, 1113–1129. doi: 10.1111/j.1752-1688.1995.tb03426.x

Aizen, V. B., Aizen, E., Melack, J., and Dozier, J. (1997). Climatic and hydrologic changes in the Tien Shan, Central Asia. . *J. Clim.* 10, 1393–1404. doi: 10.1175/1520-0442(1997)010<1393:cahcit>2.0.co;2

Alley, R., and Agustsdottir, A. (2005). The 8k event: cause and consequences of a major Holocene abrupt climate change. *Quat. Sci. Rev.* 24, 1123–1149. doi: 10.1016/j.quascirev.2004.12.004

Appleby, G., and Oldfield, F. (1978). The calculation of lead-210 dates assuming a constant rate of supply of unsupported 210Pb to the sediment. *Catena* 5, 1–8. doi: 10.1016/S0341-8162(78)80002-2

Battarbee, R. W., and Kneen, M. J. (1982). The use of electronically counted microspheres in absolute diatom analysis. *Limnol. Oceanogr.* 27, 184–188. doi: 10.4319/lo.1982.27.1.0184

Becht, E., McInnes, L., Healy, J., Dutertre, C. A., Kwok, I. W. H., Ng, L. G., et al. (2018). Dimensionality reduction for visualizing single-cell data using UMAP. *Nat. Biotechnol.* 37, 38–44. doi: 10.1038/nbt.4314

Beer, R., Heiri, O., and Tinner, W. (2007). Vegetation history, fire history and lake development recorded for 6300 years by pollen, charcoal, loss on ignition and chironomids at a small lake in southern Kyrgyzstan (Alay Range, Central Asia). *Holocene* 17, 977–985. doi: 10.1177/0959683607082413

Berger, A., and Loutre, M. F. (1991). Insolation values for the climate of the last 10 million years. *Quat. Sci. Rev.* 10, 297–317. doi: 10.1016/0277-3791(91)90033-Q

Bershaw, J., and Lechler, A. R. (2019). The isotopic composition of meteoric water along altitudinal transects in the Tian Shan of Central Asia. *Chem. Geol.* 516, 68–78. doi: 10.1016/j.chemgeo.2019.03.032

Birks, H. H., and Birks, H. J. B. (2006). Multi-proxy studies in palaeolimnology. *Veg. Hist. Archaeobot.* 15, 235–251. doi: 10.1007/s00334-006-0066-6

Bond, G., Showers, W., Cheseby, M., Lotti, R., Almasi, P., DeMenocal, B., et al. (1997). A Pervasive Millennial-Scale Cycle in North Atlantic Holocene and Glacial Climates. *Science* 278, 1257–1266. doi: 10.1126/science.278.5341.1257

Booth, R. K., Jackson, S. T., Forman, S. L., Kutzbach, J. E., Bettis, E. A., Kreig, J., et al. (2005). A severe centennial-scale drought in mid-continental North America 4200 years ago and apparent global linkages. *Holocene* 15, 321–328. doi: 10.1191/0959683605hl825ft

Boulton, C. A., and Lenton, T. M. (2019). A new method for detecting abrupt shifts in time series [version 1; peer review: 2 approved with reservations]. *F1000 Res.* 8:746. doi: 10.12688/f1000research.19310.1

Brassell, S. C., Eglinton, G., Marlowe, I. T., Pflaumann, U., and Sarnthein, M. (1986). Molecular stratigraphy: a new tool for climatic assessment. *Nature* 320, 129–133. doi: 10.1038/320129a0

Brauer, A., and Casanova, J. (2001). Chronology and depositional processes of the laminated sediment record from Lac d'Annecy, French Alps. *J. Paleolimnol.* 25, 163–177. doi: 10.1023/A:1008136029735

Bronk Ramsey, C. (2009). Bayesian analysis of radiocarbon dates. *Radiocarbon* 51, 337–360. doi: 10.1017/s0033822200033865

Castañeda, I. S., Werne, J. P., Johnson, T. C., and Powers, L. A. (2011). Organic geochemical records from Lake Malawi (East Africa) of the last 700years, part II: Biomarker evidence for recent changes in primary productivity. *Palaeogeogr. Palaeoclimatol. Palaeoecol.* 303, 140–154. doi: 10.1016/j.palaeo.2010.01.006

Chen, F.-H., Chen, J.-H., Holmes, J., Boomer, I., Austin, P., Gates, J. B., et al. (2010). Moisture changes over the last millennium in arid central Asia: a review, synthesis and comparison with monsoon region. *Quat. Sci. Rev.* 29, 1055–1068. doi: 10.1016/j.quascirev.2010.01.005

Cheng, H., Fleitmann, D., Edwards, R. L., Wang, X., Cruz, F. W., Auler, A. S., et al. (2009). Timing and structure of the 8.2 kyr B.P. event inferred from δ18O records of stalagmites from China, Oman, and Brazil. *Geology* 37, 1007–1010. doi: 10.1130/G30126A.1

Cheng, H., Spotl, C., Breitenbach, S. F., Sinha, A., Wassenburg, J. A., Jochum, K. P., et al. (2016). Climate variations of Central Asia on orbital to millennial timescales. *Sci. Rep.* 5:36975. doi: 10.1038/srep36975

Cheng, H., Zhang, Z., Spötl, C., Edwards, R. L., Cai, Y. J., Zhang, D. Z., et al. (2012). The climatic cyclicity in semiarid-arid central Asia over the past 500,000 years. *Geophys. Res. Lett.* 39:L01705. doi: 10.1029/2011gl050202

Chu, G., Sun, Q., Li, S., Zheng, M., Jia, X., Lu, C., et al. (2005). Long-chain alkenone distributions and temperature dependence in lacustrine surface sediments from China. *Geochim. Cosmochim. Acta* 69, 4985–5003. doi: 10.1016/j.gca.2005.04.008

Conte, M. H., Sicre, M.-A., Rühlemann, C., Weber, J. C., Schulte, S., Schulz-Bull, D., et al. (2006). Global temperature calibration of the alkenone unsaturation index (UK′37) in surface waters and comparison with surface sediments. *Geochem. Geophys. Geosyst.* 7:Q02005. doi: 10.1029/2005GC001054

Cranwell, A., Eglinton, G., and Robinson, N. (1987). Lipids of aquatic organisms as potential contributors to lacustrine sediments – II. *Org. Geochem.* 11, 513–527. doi: 10.1016/0146-6380(87)90007-6

de Bar, M. W., Ullgren, J. E., Thunnell, R. C., Wakeham, S. G., Brummer, G.-J. A., Stuut, J.-B. W., et al. (2019). Long-chain diols in settling particles in tropical oceans: insights into sources, seasonality and proxies. *Biogeosciences* 16, 1705–1727. doi: 10.5194/bg-16-1705-2019

de Leeuw, J. W., v.d. Meer, F. W., Rijpstra, W. I. C., and Schenck, A. (1980). On the occurrence and structural identification of long chain unsaturated ketones and hydrocarbons in sediments. *Phys. Chem. Earth* 12, 211–217. doi: 10.1016/0079-1946(79)90105-8

Diaz-Papkovich, A., Anderson-Trocme, L., Ben-Eghan, C., and Gravel, S. (2019). UMAP reveals cryptic population structure and phenotype heterogeneity in large genomic cohorts. *PLoS Genet.* 15:e1008432. doi: 10.1371/journal.pgen.1008432

Dreßler, M., Schwarz, A., Hübener, T., Adler, S., and Scharf, B. W. (2011). Use of sedimentary diatoms from multiple lakes to distinguish between past changes in trophic state and climate: evidence for climate change in northern Germany during the past 5,000 years. *J. Paleolimnol.* 45, 223–241.

Dunck, B., Bortolini, J. C., Rodrigues, L., Rodrigues, L. C., Jati, S., and Train, S. (2013). Functional diversity and adaptative strategies of planktonic and periphytic algae in isolated tropical floodplain lake. *Braz. J. Bot.* 36, 257–266. doi: 10.1007/s40415-013-0029-y

Durre, I., Vose, R. S., and Wuertz, D. B. (2006). Overview of the Integrated Global Radiosonde Archive. *J. Clim.* 19, 53–68. doi: 10.1175/JCLI3594.1

Dykoski, C., Edwards, R., Cheng, H., Yuan, D., Cai, Y., Zhang, M., et al. (2005). A high-resolution, absolute-dated Holocene and deglacial Asian monsoon record from Dongge Cave, China. *Earth Planet. Sci. Lett.* 233, 71–86. doi: 10.1016/j.epsl.2005.01.036

Eglinton, G., and Hamilton, R. (1967). Leaf Epicuticular Waxes. *Science* 156, 1322–1335. doi: 10.1126/science.156.3780.1322

Eglinton, T. I., and Eglinton, G. (2008). Molecular proxies for paleoclimatology. *Earth Planet. Sci. Lett.* 275, 1–16. doi: 10.1016/j.epsl.2008.07.012

Esper, J., Schweingruber, F. H., and Winiger, M. (2002). 1300 years of climatic history for Western Central Asia inferred from tree-rings. *Holocene* 12, 267–277. doi: 10.1191/0959683602hl543rp

Feng, X., Gustafsson, Ö, Holmes, R. M., Vonk, J. E., van Dongen, B. E., Semiletov, I. P., et al. (2015). Multimolecular tracers of terrestrial carbon transfer across the pan-Arctic:14C characteristics of sedimentary carbon components and their environmental controls. *Glob. Biogeochem. Cycles* 29, 1855–1873. doi: 10.1002/2015gb005204

Ficken, K. J., Li, B., Swain, D. L., and Eglinton, G. (2000). An n-alkane proxy for the sedimentary input of submerged/floating freshwater aquatic macrophytes. *Org. Geochem.* 31, 745–749. doi: 10.1016/S0146-6380(00)00081-4

Gasse, F., Fontes, J. C., Van Campo, E., and Wei, K. (1996). Holocene environmental changes in Bangong Co basin (Western Tibet). Part 4: discussion and conclusions. *Palaeogeogr. Palaeoclimatol. Palaeoecol.* 120, 79–92. doi: 10.1016/0031-0182(95)00035-6

Gat, J. R., and Levy, Y. (1978). Isotope hydrology of inland sabkhas in Bardawil area. *Sinai. Limnol. Oceanogr.* 23, 841–850. doi: 10.4319/lo.1978.23.5.0841

Genkal, S. I. (2012). Morphology, taxonomy, ecology, and distribution of Cyclotella choctawhatcheeana prasad (Bacillariophyta). *Inland Water Biol.* 5, 169–177. doi: 10.1134/S1995082912020046

Giese, E., Mossig, I., Rybski, D., and Bunde, A. (2007). Long-term analysis of air temperature trends in central Asia (Analyse langjähriger Zeitreihen der Lufttemperatur in Zentralasien). *Erdkunde* 61, 186–202. doi: 10.3112/erdkunde.2007.02.05

Guenther, F., Aichner, B., Siegwolf, R., Xu, B., Yao, T., and Gleixner, G. (2013). A synthesis of hydrogen isotope variability and its hydrological significance at the Qinghai–Tibetan Plateau. *Quat. Int.* 313-314, 3–16. doi: 10.1016/j.quaint.2013.07.013

Guillot, D., Rajaratnam, B., and Emile-Geay, J. (2015). Statistical paleoclimate reconstructions via Markov random fields. *Ann. Appl. Stat.* 9, 324–352. doi: 10.1214/14-aoas794

Günther, F., Thiele, A., Biskop, S., Mäusbacher, R., Haberzettl, T., Yao, T., et al. (2016). Late quaternary hydrological changes at Tangra Yumco, Tibetan Plateau: a compound-specific isotope-based quantification of lake level changes. *J. Paleolimnol.* 55, 369–382. doi: 10.1007/s10933-016-9887-1

Hahsler, M., Piekenbrock, M., and Doran, D. (2019). dbscan: Fast Density-Based Clustering with R. *J. Stat. Softw.* 91, 1–30. doi: 10.18637/jss.v091.i01

Herzschuh, U., Winter, K., Wünnemann, B., and Li, S. (2006). A general cooling trend on the central Tibetan Plateau throughout the Holocene recorded by the Lake Zigetang pollen spectra. *Quat. Int.* 154-155, 113–121. doi: 10.1016/j.quaint.2006.02.005

Hofmann, G., Werum, M., and Lange-Bertalot, H. (2011). *Diatomeen im Süßwasser - Benthos von Mitteleuropa.: Bestimmungsflora Kieselalgen für die ökologische Praxis. Über 700 der häufigsten Arten und ihre Ökologie*. Ruggell: A.R.G. Gantner Verlag.

Houk, V., Klee, R., and Tanaka, H. (2010). Atlas of freshwater centric diatoms with a brief key and descriptions. Part III: Stephanodiscaceae A, Cyclotella, Tertiarius, Discostella. *Fottea* 10, 1–498.

Hu, C., Henderson, G. M., Huang, J., Xie, S., Sun, Y., and Johnson, K. R. (2008). Quantification of Holocene Asian monsoon rainfall from spatially separated cave records. *Earth Planet. Sci. Lett.* 266, 221–232. doi: 10.1016/j.epsl.2007.10.015

Ilyasov, S., Zabenko, O., Gaydamak, N., Kirilenko, A., Myrsaliev, N., Shevchenko, V., et al. (2013). *Climate Profile of the Kyrgyz Republic*, Vol. 99. Bishkek: The United Nations Development Programme.

Jóhannesson, T., Raymond, C., and Waddington, E. (1989). Time–scale for adjustment of glaciers to changes in mass balance. *J. Glaciol.* 35, 355–369. doi: 10.3189/s002214300000928x

Kalanke, J., Mingram, J., Lauterbach, S., Usubaliev, R., and Brauer, A. (2020). Seasonal deposition processes and chronology of a varved Holocene lake sediment record from Lake Chatyr Kol (Kyrgyz Republic). *Geochronology* 2, 133–154. doi: 10.5194/gchron-2019-18

Kalbe, L., and Werner, H. (1974). Sediment des Kummerower Sees. Untersuchungen des Chemismus und der Diatomeenflora. *Int. Rev. Gesamten Hydrobiol.* 59, 755–782. doi: 10.1002/iroh.19740590603

Kassambara, A., and Mundt, F. (2019). *factoextra: Extract and Visualize the Results of Multivariate Data Analyses, R package version 1.0.6*. Available online at: https://CRAN.R-project.org/package=factoextra (accessed June 1, 2020).

Kobashi, T., Severinghaus, J. P., Brook, E. J., Barnola, J.-M., and Grachev, A. M. (2007). Precise timing and characterization of abrupt climate change 8200 years ago from air trapped in polar ice. *Quat. Sci. Rev.* 26, 1212–1222. doi: 10.1016/j.quascirev.2007.01.009

Konopka, T. (2019). *umap: Uniform Manifold Approximation and Projection. R package version 0.2.3.1*. Available online at: https://cran.r-project.org/web/packages/umap/index.html (accessed June 1, 2020).

Koppes, M., Gillespie, A. R., Burke, R. M., Thompson, S. C., and Stone, J. (2008). Late Quaternary glaciation in the Kyrgyz Tien Shan. *Quat. Sci. Rev.* 27, 846–866. doi: 10.1016/j.quascirev.2008.01.009

Krammer, K., and Lange-Bertalot, H. (2008). *Süßwasserflora von Mitteleuropa, 2/2: Bacillariaceae, Epithemiaceae, Surirellaceae*. Heidelberg: Spektrum Akademischer Verlag.

Krammer, K., and Lange-Bertalot, H. (2010). *Süßwasserflora von Mitteleuropa, 2/1: Naviculaceae*. Heidelberg: Spektrum Akademischer Verlag.

Kudo, A., Zheng, J., Koerner, R. M., Fisher, D. A., Santry, D. C., Mahara, Y., et al. (1998). Global transport rates of 137Cs and 239+240Pu originating from the Nagasaki A-bomb in 1945 as determined from analysis of Canadian Arctic ice cores. *J. Environ. Radioact.* 40, 289–298. doi: 10.1016/S0265-931X(97)00023-4

Lange-Bertalot, H. (2001). "Navicula sensu stricto 10 genera separated from Navicula sensu lato Frustulia," in *Diatoms of Europe*, Vol. 2, ed. H. Lange-Bertalot (Ruggell: A.R.H. Gantner Verlag).

Lange-Bertalot, H., and Moser, G. (1994). Brachysira Monographie der Gattung. *Bibliotheca Diatomol.* 29, 1–212.

Lattaud, J., Dorhout, D., Schulz, H., Castañeda, I. S., Schefuß, E., Sinninghe Damsté, J. S., et al. (2017). The C32 alkane-1,15-diol as a proxy of late Quaternary riverine input in coastal margins. *Clim. Past* 13, 1049–1061. doi: 10.5194/cp-13-1049-2017

Lattaud, J., Kirkels, F., Peterse, F., Freymond, C. V., Eglinton, T. I., Hefter, J., et al. (2018). Long-chain diols in rivers: distribution and potential biological sources. *Biogeosciences* 15, 4147–4161. doi: 10.5194/bg-15-4147-2018

Lauterbach, S., Witt, R., Plessen, B., Dulski, P., Prasad, S., Mingram, J., et al. (2014). Climatic imprint of the mid-latitude Westerlies in the Central Tian Shan of Kyrgyzstan and teleconnections to North Atlantic climate variability during the last 6000 years. *Holocene* 24, 970–984. doi: 10.1177/0959683614534741

Lea-Smith, D. J., Biller, S. J., Davey, M. P., Cotton, C. A. R., Perez Sepulveda, B. M., Turchyn, A. V., et al. (2015). Contribution of cyanobacterial alkane production to the ocean hydrocarbon cycle. *Proc. Natl. Acad. Sci. U.S.A.* 112, 13591–13596. doi: 10.1073/pnas.1507274112

Lenton, T. M. (2011). Early warning of climate tipping points. *Nat. Clim. Change* 1, 201–209. doi: 10.1038/nclimate1143

Lenton, T. M., Held, H., Kriegler, E., Hall, J. W., Lucht, W., Rahmstorf, S., et al. (2008). Tipping elements in the Earth's climate system. *Proc. Natl. Acad. Sci. U.S.A.* 105, 1786–1793. doi: 10.1073/pnas.0705414105

Li, Y., and Morrill, C. (2010). Multiple factors causing Holocene lake-level change in monsoonal and arid central Asia as identified by model experiments. *Clim. Dyn.* 35, 1119–1132. doi: 10.1007/s00382-010-0861-8

Liu, W., Liu, Z., Wang, H., He, Y., Wang, Z., and Xu, L. (2011). Salinity control on long-chain alkenone distributions in lake surface waters and sediments of the northern Qinghai-Tibetan Plateau, China. *Geochim. Cosmochim. Acta* 75, 1693–1703. doi: 10.1016/j.gca.2010.10.029

Liu, Y. H., Henderson, G. M., Hu, C. Y., Mason, A. J., Charnley, N., Johnson, K. R., et al. (2013). Links between the East Asian monsoon and North Atlantic climate during the 8,200 year event. *Nat. Geosci.* 6, 117–120. doi: 10.1038/ngeo1708

Longo, W. M., Dillon, J. T., Tarozo, R., Salacup, J. M., and Huang, Y. (2013). Unprecedented separation of long chain alkenones from gas chromatography with a poly(trifluoropropylmethylsiloxane) stationary phase. *Org. Geochem.* 65, 94–102. doi: 10.1016/j.orggeochem.2013.10.011

Machalett, B., Oches, E. A., Frechen, M., Zöller, L., Hambach, U., Mavlyanova, N. G., et al. (2008). Aeolian dust dynamics in central Asia during the Pleistocene: driven by the long-term migration, seasonality, and permanency of the Asiatic polar front. *Geochem. Geophys. Geosyst.* 9:Q08Q09. doi: 10.1029/2007gc001938

Marlowe, I. T., Brassell, S. C., Eglinton, G., and Green, J. C. (1984). Long chain unsaturated ketones and esters in living algae and marine sediments. *Org. Geochem.* 6, 135–141. doi: 10.1016/0146-6380(84)90034-2

Marwan, N., Eroglu, D., Ozken, I., Stemler, T., Wyrwoll, K.-H., and Kurths, J. (2018). "Regime change detection in irregularly sampled time series," in *Advances in Nonlinear Geosciences*, ed. A. A. Tsonis (Cham: Springer), 357–368. doi: 10.1007/978-3-319-58895-7_18

Mathis, M., Sorrel, P., Klotz, S., Huang, X., and Oberhänsli, H. (2014). Regional vegetation patterns at lake Son Kul reveal Holocene climatic variability in central Tien Shan (Kyrgyzstan, Central Asia). *Quat. Sci. Rev.* 89, 169–185. doi: 10.1016/j.quascirev.2014.01.023

Mayewski, A., Rohling, E. E., Curt Stager, J., Karlén, W., Maasch, K. A., Meeker, L. D., et al. (2004). Holocene climate variability. *Quat. Res.* 62, 243–255. doi: 10.1016/j.yqres.2004.07.001

McInnes, L., Healy, J., Saul, N., and Großberger, L. (2018). UMAP: uniform manifold approximation and projection. *J. Open Source Softw.* 3:861. doi: 10.21105/joss.00861

Meyers, A. (2003). Applications of Organic Geochemistry to paleolimnological reconstructions: a summary of examples from the Laurentian Great Lakes. . *Org. Geochem*. 34, 261–289. doi: 10.1016/s0146-6380(02)00168-7

Meyers, A., and Ishiwatari, R. (1993). Lacustrine Organic Geochemistry.-an overview of indicators of organic matter sources and diagenesis in lake sediments. *Org. Geochem.* 20, 867–900. doi: 10.1016/0146-6380(93)90100-p

Miao, Y., Jin, H., Liu, B., and Wang, Y. (2014). Natural ecosystem response and recovery after the 8.2 ka cold event: evidence from slope sediments on the northeastern Tibetan Plateau. *J. Arid Environ.* 104, 17–22. doi: 10.1016/j.jaridenv.2014.01.021

Mischke, S., Rajabov, I., Mustaeva, N., Zhang, C., Herzschuh, U., Boomer, I., et al. (2010). Modern hydrology and late Holocene history of Lake Karakul, eastern Pamirs (Tajikistan): a reconnaissance study. *Palaeogeogr. Palaeoclimatol. Palaeoecol*. 289, 10–24. doi: 10.1016/j.palaeo.2010.02.004

Mügler, I., Sachse, D., Werner, M., Xu, B., Wu, G., Yao, T., et al. (2008). Effect of lake evaporation on δD values of lacustrine n-alkanes: a comparison of Nam Co (Tibetan Plateau) and Holzmaar (Germany). *Org. Geochem.* 39, 711–729. doi: 10.1016/j.orggeochem.2008.02.008

Müller, J., Kirst, G., Ruhland, G., von Storch, I., and Rosell-Melé, A. (1998). Calibration of the alkenone paleotemperature index UK'37 based on core-tops from the eastern South Atlantic and the global ocean (60°N-60°S). *Geochim. Cosmochim. Acta* 62, 1757–1772. doi: 10.1016/S0016-7037(98)00097-0

Naik, G. R. (2018). *Advances in Principal Component Analysis*. Singapore: Springer, 252.

Nakamura, H., Sawada, K., Araie, H., Suzuki, I., and Shiraiwa, Y. (2014). Long chain alkenes, alkenones and alkenoates produced by the haptophyte alga Chrysotila lamellosa CCMP1307 isolated from a salt marsh. *Org. Geochem*. 66, 90–97. doi: 10.1016/j.orggeochem.2013.11.007

Oerlemans, J. (2005). Extracting a climate signal from 169 glacier records. *Science* 308, 675–677. doi: 10.1126/science.1107046

Oliva, M. G., Lugo, A., Alcocer, J., and Cantoral-Uriza, E. (2008). Morphological Study of Cyclotella choctawhatcheeana Prasad (Stephanodiscaceae) from a saline Mexican Lake. *Aquat. Biosyst*. 4, 17–25. doi: 10.1186/1746-1448-4-17

Pan, B. T., Zhang, G. L., Wang, J., Cao, B., Geng, H. P., Wang, J., et al. (2012). Glacier changes from 1966–2009 in the Gongga Mountains, on the south-eastern margin of the Qinghai-Tibetan Plateau and their climatic forcing. *Cryosphere* 6, 1087–1101. doi: 10.5194/tc-6-1087-2012

Pearson, E. J., Juggins, S., and Farrimond, P. (2008). Distribution and significance of long-chain alkenones as salinity and temperature indicators in Spanish saline lake sediments. *Geochim. Cosmochim. Acta* 72, 4035–4046. doi: 10.1016/j.gca.2008.05.052

Pennington, W., Tutin, T. G., Cambray, R. S., and Fisher, E. M. (1973). Observations on Lake Sediments using Fallout 137Cs as a Tracer. *Nature* 242, 324–326. doi: 10.1038/242324a0

Pérez, L., Lorenschat, J., Massaferro, J., Pailles, C., Sylvestre, F., Hollwedel, W., et al. (2013). Bioindicators of climate and trophic state in lowland and highland aquatic ecosystems of the northern Neotropics. *Rev. Biol. Trop*. 61, 603–644. doi: 10.15517/rbt.v61i2.11164

Perşoiu, A., Ionita, M., and Weiss, H. (2019). Atmospheric blocking induced by the strengthened Siberian High led to drying in west Asia during the 4.2 ka BP event – a hypothesis. *Clim. Past* 15, 781–793. doi: 10.5194/cp-15-781-2019

Plancq, J., Cavazzin, B., Juggins, S., Haig, H. A., Leavitt, R., and Toney, J. L. (2018). Assessing environmental controls on the distribution of long-chain alkenones in the Canadian Prairies. *Org. Geochem*. 117, 43–55. doi: 10.1016/j.orggeochem.2017.12.005

Poynter, J., and Eglinton, G. (1990). Molecular composition of three sediments from Hole 717C: the Bengal fan. *Proc. Ocean Drill. Program* 116, 155–161. doi: 10.2973/odp.proc.sr.116.151.1990

Prahl, F. G., and Wakeham, S. G. (1987). Calibration of unsaturation patterns in long-chain ketone compositions for palaeotemperature assessment. *Nature* 330, 367–369. doi: 10.1038/330367a0

R Core Team (2019). *R: A Language and Environment for Statistical Computing*. Vienna: R Foundation for Statistical Computing.

Rampen, S. W., Datema, M., Rodrigo-Gámiz, M., Schouten, S., Reichart, G.-J., and Sinninghe Damsté, J. S. (2014a). Sources and proxy potential of long chain alkyl diols in lacustrine environments. *Geochim. Cosmochim. Acta* 144, 59–71. doi: 10.1016/j.gca.2014.08.033

Rampen, S. W., Willmott, V., Kim, J.-H., Rodrigo-Gámiz, M., Uliana, E., Mollenhauer, G., et al. (2014b). Evaluation of long chain 1,14-alkyl diols in marine sediments as indicators for upwelling and temperature. *Org. Geochem*. 76, 39–47. doi: 10.1016/j.orggeochem.2014.07.012

Rampen, S. W., Willmott, V., Kim, J.-H., Uliana, E., Mollenhauer, G., Schefuß, E., et al. (2012). Long chain 1,13- and 1,15-diols as a potential proxy for palaeotemperature reconstruction. *Geochim. Cosmochim. Acta* 84, 204–216. doi: 10.1016/j.gca.2012.01.024

Reimer, J., Bard, E., Bayliss, A., Beck, J. W., Blackwell, G., Ramsey, C. B., et al. (2013). IntCal13 and Marine13 Radiocarbon Age Calibration Curves 0–50,000 Years cal BP. *Radiocarbon* 55, 1869–1887. doi: 10.2458/azu_js_rc.55.16947

Richey, J. N., and Tierney, J. E. (2016). GDGT and alkenone flux in the northern Gulf of Mexico: implications for the TEX86 and UK'37 paleothermometers. *Paleoceanography* 31, 1547–1561. doi: 10.1002/2016pa003032

Ricketts, R. D., Johnson, T. C., Brown, E. T., Rasmussen, K. A., and Romanovsky, V. (2001). The Holocene paleolimnology of Lake Issyk-Kul, Kyrgyzstan: trace element and stable isotope composition of ostracodes. *Palaeogeogr. Palaeoclimatol. Palaeoecol*. 176, 207–227. doi: 10.1016/s0031-0182(01)00339-x

Ringnér, M. (2008). What is principal component analysis? *Nat. Biotechnol*. 26, 303–304. doi: 10.1038/nbt0308-303

Robbins, J. A. (1978). "Geochemical and geophysical applications of radioactive lead," in *Biogeochemistry of Lead in the Environment*, ed. J. O. Nriagu (Amsterdam: Elsevier), 285–393.

Romero-Viana, L., Kienel, U., and Sachse, D. (2012). Lipid biomarker signatures in a hypersaline lake on Isabel Island (Eastern Pacific) as a proxy for past rainfall anomaly (1942–2006AD). *Palaeogeogr. Palaeoclimatol. Palaeoecol*. 350-352, 49–61. doi: 10.1016/j.palaeo.2012.06.011

Sachse, D., Billault, I., Bowen, G. J., Chikaraishi, Y., Dawson, T. E., Feakins, S. J., et al. (2012). Molecular paleohydrology: interpreting the hydrogen-isotopic composition of lipid biomarkers from photosynthesizing organisms. *Annu. Rev. Earth Planet. Sci.* 40, 221–249. doi: 10.1146/annurev-earth-042711-105535

Scheffer, M., Carpenter, S. R., Lenton, T. M., Bascompte, J., Brock, W., Dakos, V., et al. (2012). Anticipating critical transitions. *Science* 338, 344–348. doi: 10.1126/science.1225244

Schroeter, N., Lauterbach, S., Stebich, M., Kalanke, J., Mingram, J., Yildiz, C., et al. (2020). Biomolecular evidence of early human occupation of a high-altitude site in Western Central Asia during the Holocene. *Front. Earth Sci*. 8:20. doi: 10.3389/feart.2020.00020

Schwarz, A., Turner, F., Lauterbach, S., Plessen, B., Krahn, K. J., Glodniok, S., et al. (2017). Mid- to late Holocene climate-driven regime shifts inferred from diatom, ostracod and stable isotope records from Lake Son Kol (Central Tian Shan, Kyrgyzstan). *Quat. Sci. Rev.* 177, 340–356. doi: 10.1016/j.quascirev.2017.10.009

Shen, J., Liu, X., Wang, S., and Matsumoto, R. (2005). Palaeoclimatic changes in the Qinghai Lake area during the last 18,000 years. *Quat. Int*. 136, 131–140. doi: 10.1016/j.quaint.2004.11.014

Shimokawara, M., Nishimura, M., Matsuda, T., Akiyama, N., and Kawai, T. (2010). Bound forms, compositional features, major sources and diagenesis of long chain, alkyl mid-chain diols in Lake Baikal sediments over the past 28,000 years. *Org. Geochem*. 41, 753–766. doi: 10.1016/j.orggeochem.2010.05.013

Shnitnikov, A. V., Livja, A. A., Berdovskaya, G. N., and Sevastianov, D. V. (1978). Paleolimnology of Chatyrkel Lake (Tien-shan). *Pol. Arch. Hydrobiol*. 25, 38 3–390.

Sidorov, D. A. (2012). Two new species of freshwater amphipods (Crustacea: Gammaridae) from Central Asia, with comments on the unusual upper lip morphology. *Zootaxa* 3317, 1–24. doi: 10.11646/zootaxa.3317.1.1

Sikes, E., and Volkman, J. K. (1993). Calibration of alkenone unsaturation ratios (UK'37) for paleotemperature estimation in cold polar waters. *Geochim. Cosmochim. Acta* 57, 1883–1889. doi: 10.1016/0016-7037(93)90120-L

Sinninghe Damsté, J. S., Rampen, S., Irene, W., Rijpstra, C., Abbas, B., Muyzer, G., et al. (2003). A diatomaceous origin for long-chain diols and mid-chain hydroxy methyl alkanoates widely occurring in quaternary marine sediments: indicators for high-nutrient conditions. *Geochim. Cosmochim. Acta* 67, 1339–1348. doi: 10.1016/s0016-7037(02)01225-5

Smets, T., Verbeeck, N., Claesen, M., Asperger, A., Griffioen, G., Tousseyn, T., et al. (2019). Evaluation of distance metrics and spatial autocorrelation in uniform manifold approximation and projection applied to mass spectrometry imaging data. *Anal. Chem.* 91, 5706–5714. doi: 10.1021/acs.analchem.8b05827

Song, M., Zhou, A., He, Y., Zhao, C., Wu, J., Zhao, Y., et al. (2016). Environmental controls on long-chain alkenone occurrence and compositional patterns in lacustrine sediments, northwestern China. *Org. Geochem.* 91, 43–53. doi: 10.1016/j.orggeochem.2015.10.009

Staubwasser, M., and Weiss, H. (2006). Holocene Climate and Cultural Evolution in Late Prehistoric–Early Historic West Asia. *Quat. Res.* 66, 372–387. doi: 10.1016/j.yqres.2006.09.001

Sun, Y.-Y., Zhang, K.-X., Liu, J., He, Y.-X., Song, B.-W., Liu, W.-G., et al. (2012). Long chain alkenones preserved in Miocene lake sediments. *Org. Geochem.* 50, 19–25. doi: 10.1016/j.orggeochem.2012.06.007

Taft, J. B., Phillippe, L. R., Dietrich, C. H., and Robertson, K. R. (2011). Grassland composition, structure, and diversity patterns along major environmental gradients in the Central Tien Shan. *Plant Ecol.* 212, 1349–1361. doi: 10.1007/s11258-011-9911-5

Theroux, S., D'Andrea, W. J., Toney, J., Amaral-Zettler, L., and Huang, Y. (2010). Phylogenetic diversity and evolutionary relatedness of alkenone-producing haptophyte algae in lakes: implications for continental paleotemperature reconstructions. *Earth Planet. Sci. Lett.* 300, 311–320. doi: 10.1016/j.epsl.2010.10.009

Thomas, E. R., Wolff, E. W., Mulvaney, R., Steffensen, J. P., Johnsen, S. J., Arrowsmith, C., et al. (2007). The 8.2ka event from Greenland ice cores. *Quat. Sci. Rev.* 26, 70–81. doi: 10.1016/j.quascirev.2006.07.017

Toney, J. L., Huang, Y., Fritz, S. C., Baker, A., Grimm, E., and Nyren, P. E. (2010). Climatic and environmental controls on the occurrence and distributions of long chain alkenones in lakes of the interior United States. *Geochim. Cosmochim. Acta* 74, 1563–1578. doi: 10.1016/j.gca.2009.11.021

Toth, L. T., and Aronson, R. B. (2019). The 4.2 ka event, ENSO, and coral reef development. *Clim. Past* 15, 105–119. doi: 10.5194/cp-15-105-2019

Versteegh, G. J. M., Bosch, H.-J., and De Leeuw, J. W. (1997). Potential palaeoenvironmental information of C24 to C36 mid-chain diols, keto-ols and mid-chain hydroxy fatty acids; a critical review. *Org. Geochem.* 27, 1–13. doi: 10.1016/s0146-6380(97)00063-6

Villanueva, L., Besseling, M., Rodrigo-Gámiz, M., Rampen, S. W., Verschuren, D., and Sinninghe Damsté, J. S. (2014). Potential biological sources of long chain alkyl diols in a lacustrine system. *Org. Geochem.* 68, 27–30. doi: 10.1016/j.orggeochem.2014.01.001

Volkman, J. K., Barrett, S., and Blackburn, S. (1999). Eustigmatophyte microalgae are potential sources of C29 sterols, C22–C28 n-alcohols and C28–C32 n-alkyl diols in freshwater environments. *Org. Geochem.* 30, 307–318. doi: 10.1016/s0146-6380(99)00009-1

Volkman, J. K., Barrett, S. M., Dunstan, G. A., and Jeffrey, S. W. (1992). C30-C32 alkyl diols and unsaturated alcohols in microalgae of the class Eustigmatophyceae. *Org. Geochem.* 18, 131–138. doi: 10.1016/0146-6380(92)90150-v

Walker, M. J. C., Berkelhammer, M., Björck, S., Cwynar, L. C., Fisher, D. A., Long, A. J., et al. (2012). Formal subdivision of the Holocene Series/Epoch: a Discussion Paper by a Working Group of INTIMATE (Integration of ice-core, marine and terrestrial records) and the Subcommission on Quaternary Stratigraphy (International Commission on Stratigraphy). *J. Quat. Sci.* 27, 649–659. doi: 10.1002/jqs.2565

Wang, X., Huang, X., Sachse, D., Ding, W., and Xue, J. (2016). Molecular paleoclimate reconstructions over the last 9 ka from a peat sequence in South China. *PLoS One* 11:e0160934. doi: 10.1371/journal.pone.0160934

Wickham, H. (2016). *ggplot2: Elegant Graphics for Data Analysis*. New York, NY: Springer, 260.

Wolff, C., Plessen, B., Dudashvilli, A. S., Breitenbach, S. F. M., Cheng, H., Edwards, L. R., et al. (2017). Precipitation evolution of Central Asia during the last 5000 years. *Holocene* 27, 142–154. doi: 10.1177/0959683616652711

Wright, S. M., Howard, B. J., Strand, P., Nylén, T., and Sickel, M. A. K. (1999). Prediction of 137Cs deposition from atmospheric nuclear weapons tests within the Arctic. *Environ. Pollut.* 104, 131–143. doi: 10.1016/S0269-7491(98)00140-7

Wu, J. Y., Wang, Y. J., Cheng, H., Kong, X. G., and Liu, D. B. (2012). Stable isotope and trace element investigation of two contemporaneous annually-laminated stalagmites from northeastern China surrounding the "8.2 ka event". *Clim. Past Discuss.* 8, 1591–1614. doi: 10.5194/cpd-8-1591-2012

Yang, B., Wang, J., Bräuning, A., Dong, Z., and Esper, J. (2009). Late Holocene climatic and environmental changes in arid central Asia. *Quat. Int.* 194, 68–78. doi: 10.1016/j.quaint.2007.11.020

Zhao, J., An, C.-B., Huang, Y., Morrill, C., and Chen, F.-H. (2017). Contrasting early Holocene temperature variations between monsoonal East Asia and westerly dominated Central Asia. *Quat. Sci. Rev.* 178, 14–23. doi: 10.1016/j.quascirev.2017.10.036

Zhao, K., Li, X., Dodson, J., Atahan, P., Zhou, X., and Bertuch, F. (2012). Climatic variations over the last 4000 cal yr BP in the western margin of the Tarim Basin, Xinjiang, reconstructed from pollen data. *Palaeogeogr. Palaeoclimatol. Palaeoecol.* 321-322, 16–23. doi: 10.1016/j.palaeo.2012.01.012

Zink, K. G., Leythaeuser, D., Melkonian, M., and Schwark, L. (2001). Temperature dependency of long-chain alkenone distributions in recent to fossil limnic sediments and in lake waters. *Geochim. Cosmochim. Acta* 65, 253–265. doi: 10.1016/S0016-7037(00)00509-3

**Conflict of Interest:** The authors declare that the research was conducted in the absence of any commercial or financial relationships that could be construed as a potential conflict of interest.

*Copyright © 2020 Schroeter, Toney, Lauterbach, Kalanke, Schwarz, Schouten and Gleixner. This is an open-access article distributed under the terms of the Creative Commons Attribution License (CC BY). The use, distribution or reproduction in other forums is permitted, provided the original author(s) and the copyright owner(s) are credited and that the original publication in this journal is cited, in accordance with accepted academic practice. No use, distribution or reproduction is permitted which does not comply with these terms.*

# *Supplementary Material*

## 1.1 Supplementary Figures

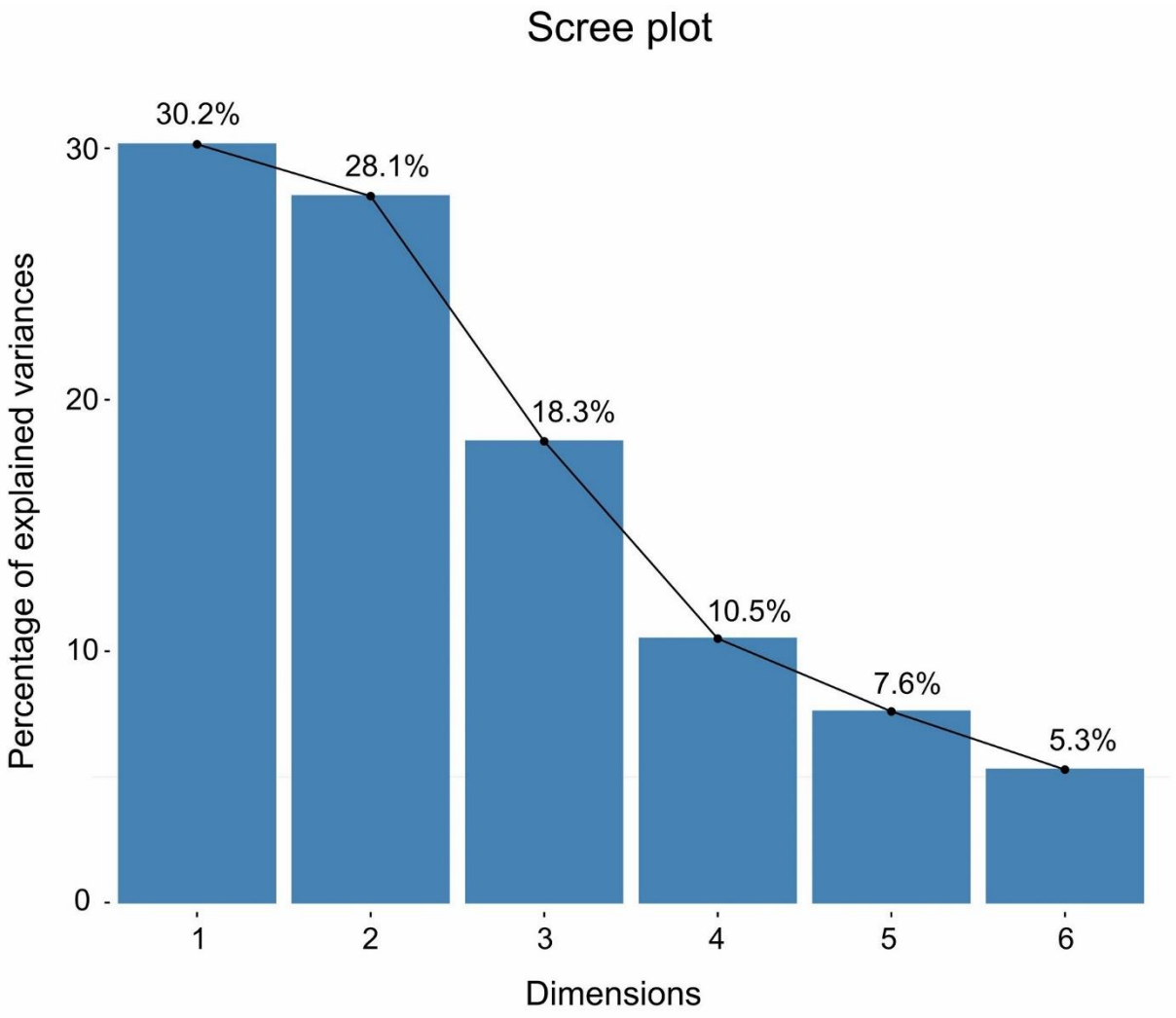


**Supplementary Figure 1** Scree plot of the Principal Component Analysis (PCA) showing the cumulative variance explained by each principal component (PC1–PC6).

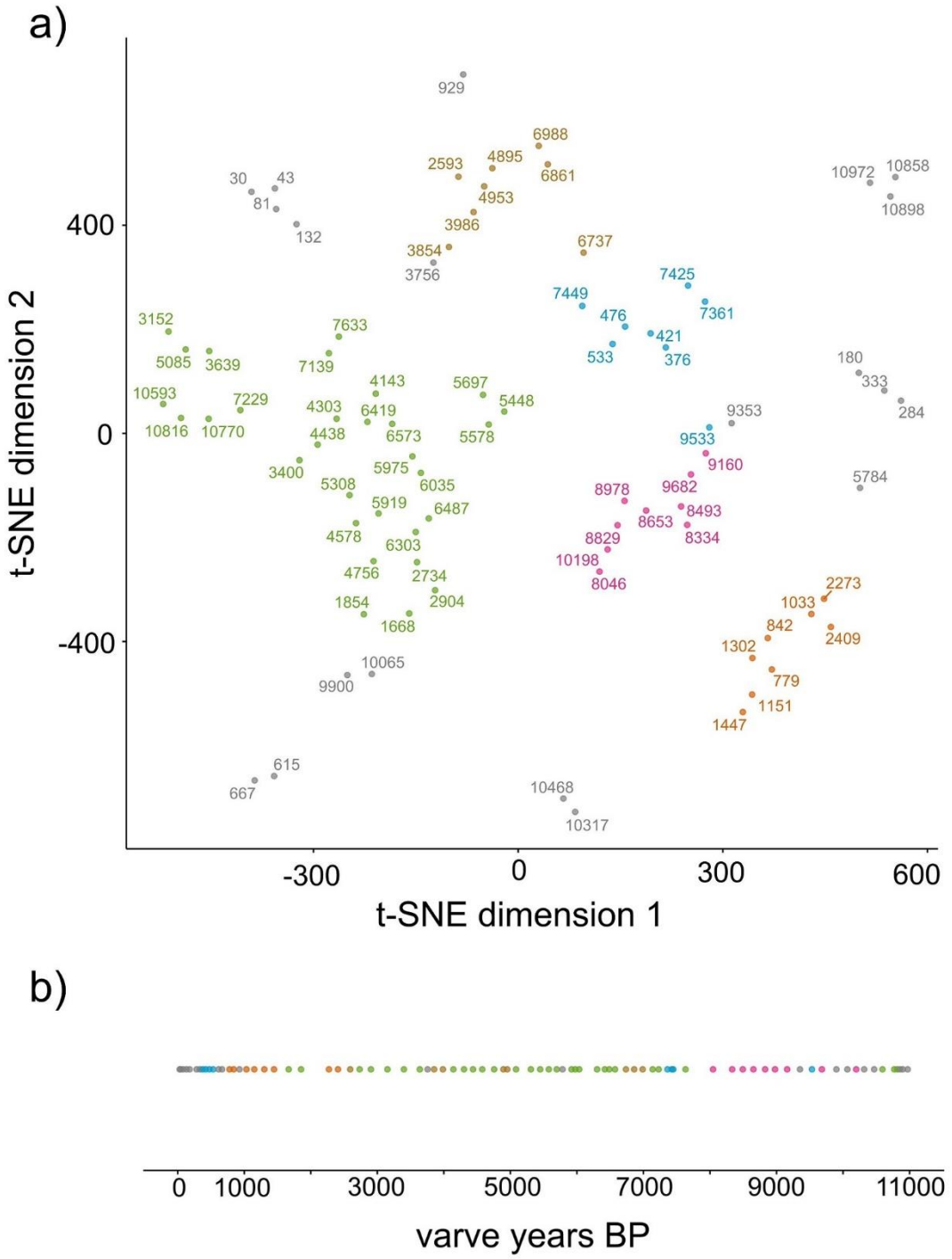


**Supplementary Figure 2.** Lake phases separation by t-SNE. The core was clustered into 5 separate groupings (a). 20 data points could not be assigned to a grouping (grey points). The groupings were temporally not well separated (b). As a result, the lake phase boundaries were not well defined. In comparison, UMAP integrated all but 1 data point in its clustering and revealed sharp lake phase boundaries (Figure 6).

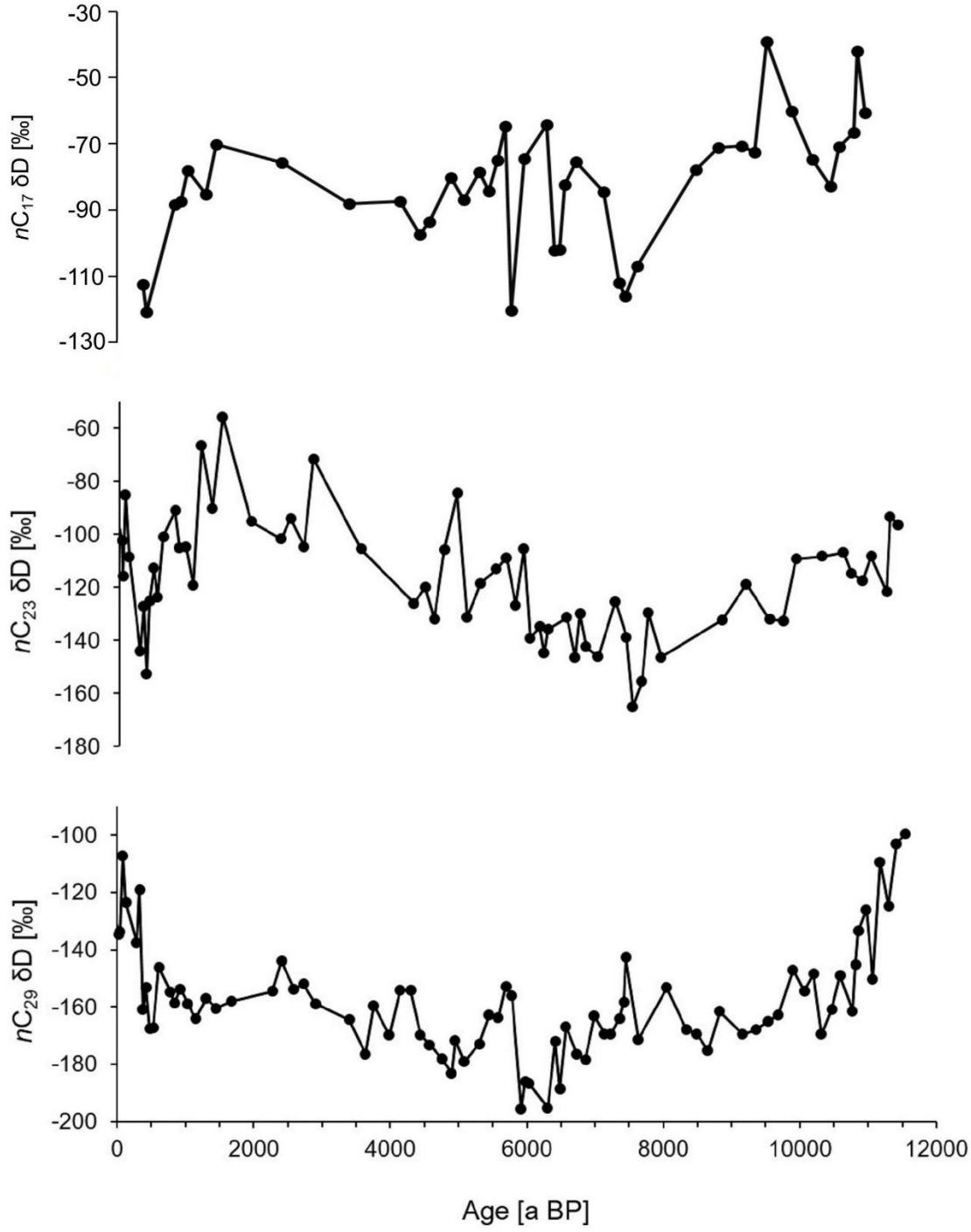


**Supplementary Figure 3.** Compound-specific stable hydrogen isotope composition (δD) of *n*-alkanes $n\mathrm{C}_{17}$, $n\mathrm{C}_{23}$ and $n\mathrm{C}_{29}$.

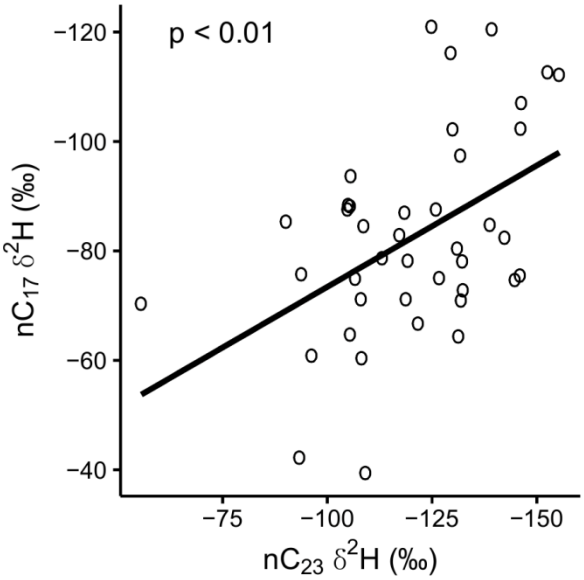


**Supplementary Figure 4.** Pearson correlation between the compound-specific stable hydrogen isotopic composition of *n*-alkanes $nC_{17}$ and $nC_{23}$.

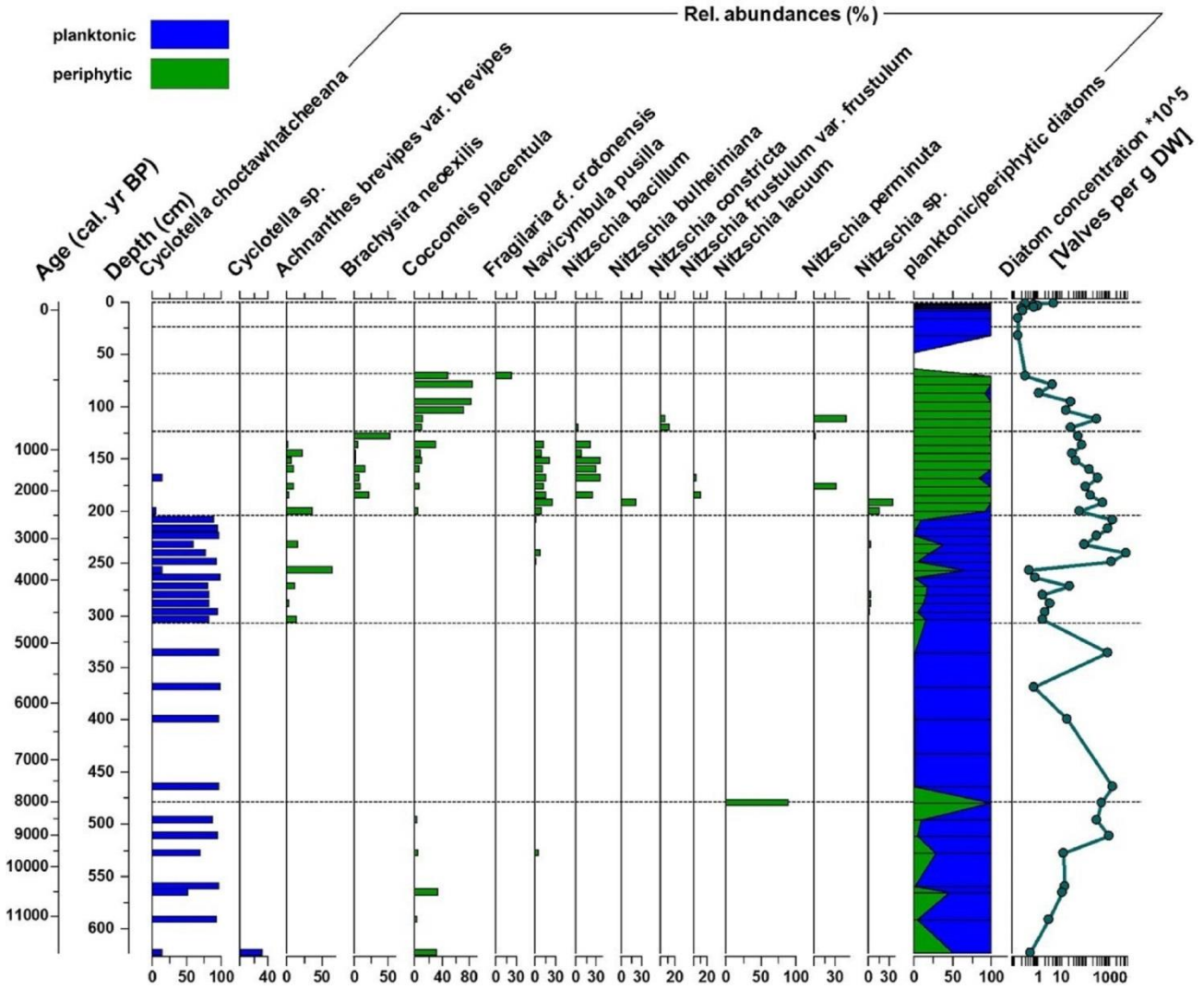


**Supplementary Figure 5.** Analysis of diatom species and ratio between planktonic and periphytic diatoms.

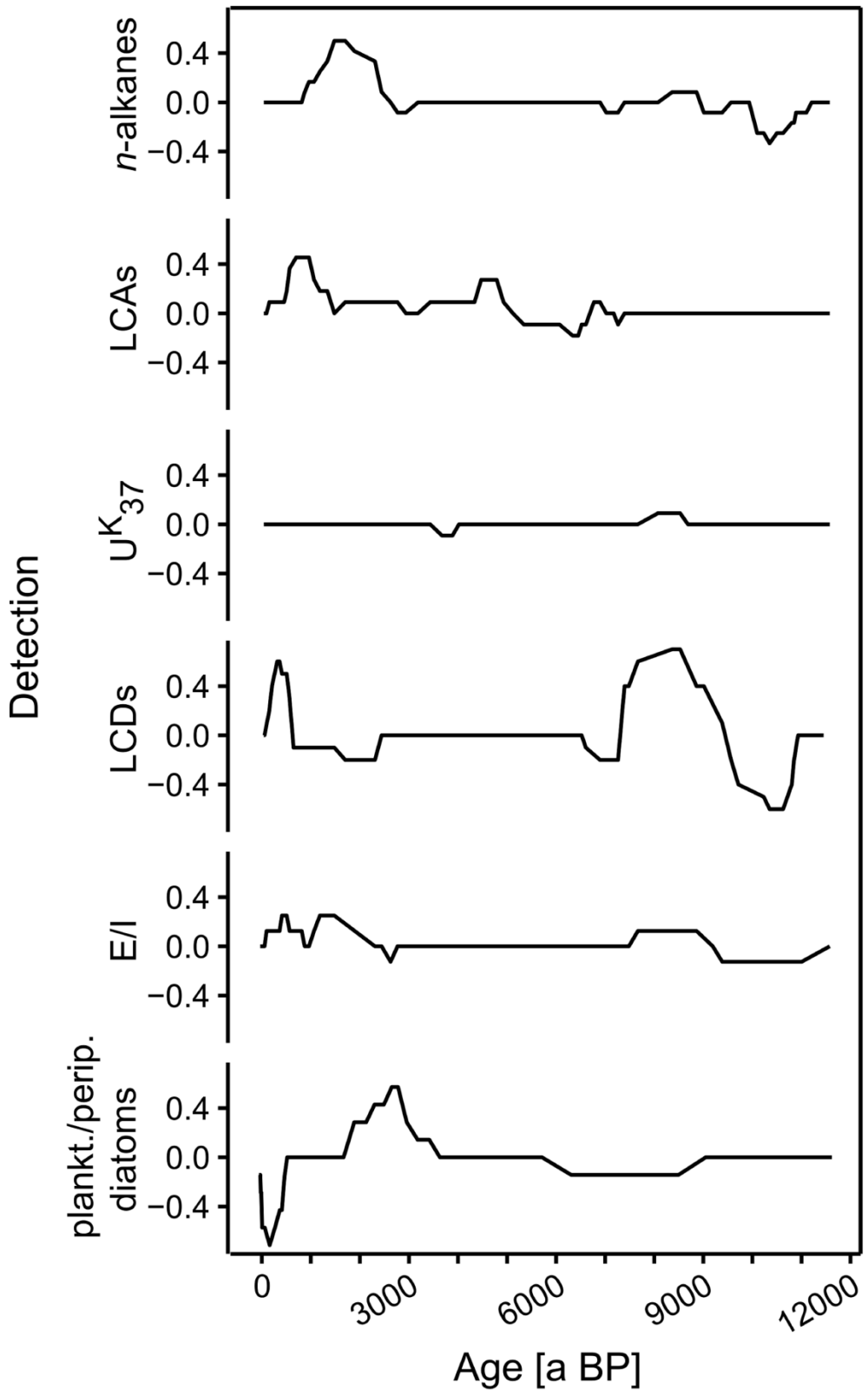


**Supplementary Figure 6.** Results of individual shift detection by asdetect for single proxies.

# The lake reservoir effect varies with the mobilization of pre-aged organic carbon in a high-altitude Central Asian catchment

**Natalie Schroeter[1], Jens Mingram[2], Julia Kalanke[2], Stefan Lauterbach[3,4], Rik Tjallingii[2], Valérie F. Schwab[1], Gerd Gleixner[1]***

[1]Max Planck Institute for Biogeochemistry, Research Group Molecular Biogeochemistry, 07745 Jena, Germany

[2] GFZ German Research Centre for Geosciences, 14473 Potsdam, Germany, Section 4.3 – Climate Dynamics and Landscape Evolution

[3] Kiel University, Leibniz Laboratory for Radiometric Dating and Stable Isotope Research, 24118 Kiel, Germany

[4] Kiel University, Institute of Geosciences, 24118 Kiel, Germany

*** Correspondence:**
Gerd Gleixner
gerd.gleixner@bgc-jena.mpg.de

**Keywords: compound-specific radiocarbon analysis, leaf waxes, Lake Reservoir effect, HPLC, XRF**

## Abstract

Lake sediments provide excellent archives to study past environmental and hydrological changes at high temporal resolution. However, their utility is often restricted by chronological uncertainties due to the "lake reservoir effect" (LRE) or "hard water effect", a phenomenon that results in anomalously old radiocarbon ages of total organic carbon (TOC) samples due to the contribution of pre-aged carbon from aquatic organisms. Although the LRE is a well-known problem especially in high altitude lakes, detailed studies analyzing the temporal variations in the contribution of terrestrial and aquatic organic carbon (OC) on the LRE are scarce. This is partially due to the complexity of isolating individual compounds for subsequent compound-specific radiocarbon analysis (CSRA). We developed a rapid method for isolating individual short-chain ($C_{16}$ & $C_{18}$) and long-chain ($>C_{24}$) saturated fatty acid methyl esters (FAMEs) by using high-pressure liquid chromatography (HPLC). Our method introduces only minor contaminations (0.50 ± 0.22 µg dead carbon on average) and requires only few injections (≤10), therefore offering clear advantages over traditional preparative gas chromatography (prep-GC). Here we show that radiocarbon values ($\Delta^{14}C$) of long-chain FAMEs, which originate from terrestrial higher plant waxes, reflect carbon from a substantially pre-aged OC reservoir, whereas the $\Delta^{14}C$ of short-chain FAMEs that originate from aquatic sources were generally less pre-aged. $^{14}C$ ages obtained from the long-chain FAs are in closer agreement with $^{14}C$ ages of the corresponding bulk TOC fraction, indicating a high control of pre-aged terrestrial OC input from the catchment on TOC-derived $^{14}C$ ages. Evidently, variations in the age offset between terrestrial and aquatic biomarkers are related to changes in bulk sediment log(Ti/K) that reflect variations in detrital input from the catchment. Our results unexpectedly indicate that the chronological offset between terrestrial and aquatic OC in this high-altitude catchment is mainly driven by temporal variations in the mobilization of pre-aged OC from

the catchment. In conclusion, to obtain accurate and process-specific lake sediment chronologies, attention must be given to both the aquatic and terrestrial influences on the LRE.

## 1 Introduction

Lake sediments provide excellent high-resolution archives of regional environmental and climatic changes in the past. A prerequisite for paleoenvironmental reconstructions from lacustrine sediments are, however, reliable chronologies. Radiocarbon ($^{14}C$) dating has been one of the most widely used dating techniques for lake sediment records spanning the last ~50,000 years (Hughen et al., 2004; Reimer et al., 2013). Yet, $^{14}C$ dating of lacustrine sediments has proven to be a challenging task, since many lakes are characterized by anomalously old $^{14}C$ ages of in situ organic material owing to a lake reservoir effect (LRE, also 'old carbon', 'dead carbon' and "hard water" effect) (Hou et al., 2012; Mischke et al., 2013). The most common cause of the LRE is the dissolution of $^{14}C$-depleted inorganic carbon in the lake water and its incorporation by aquatic plants and organisms (Philippsen, 2013; Zhang et al., 2016). However, the remobilization of pre-aged terrestrial OC (Howarth et al., 2013) and carbonate rocks in the catchment may also contribute to the LRE (Hou et al., 2012; Mischke et al., 2013). Terrestrial plant macrofossils, if deposited soon after their death, are the most suitable material for accurate $^{14}C$ dating, since they incorporate carbon in equilibrium with atmospheric $CO_2$ (Bertrand et al., 2012) and therefore do not require a reservoir effect correction. Yet, especially in arid and cold high-altitude and -altitude regions where the terrestrial vegetation cover is commonly sparse, total organic carbon (TOC) or aquatic organic matter are often the only available material that can be used for $^{14}C$ dating. This, however, results in large temporal and spatial uncertainties of the LRE since TOC contains a mixture of allochthonous and autochthonous carbon and therefore contributions from $^{14}C$-dead or $^{14}C$-depleted sources (Hou et al., 2012). As a consequence, age models for lacustrine sequences from such settings are commonly established by assessing the present-day LRE and correcting chronologies based on $^{14}C$-dating of TOC or aquatic organic matter by assuming a constant LRE over time, which may be misleading (Geyh et al., 1998). Even though the LRE has been now known for over 60 years (Philippsen, 2013), detailed studies regarding the temporally variable influence of terrestrial OC and aquatic OC on the LRE are rarely conducted. A substantial part of the existing knowledge on a variable LRE magnitude has been compiled in Central Asia (Hou et al., 2012). Central Asia has been and continues to be in the focus of paleoenvironmental research using various types of archives, such as tree rings (Liang et al., 2009; Sheppard et al., 2004; Yang et al., 2014), ice cores (Thompson et al., 2006a; Thompson et al., 2006b; Thompson et al., 1997; Yao et al., 1996) and lake sediments (Doberschütz et al., 2014; Günther et al., 2016; Lauterbach et al., 2014; Mügler et al., 2010; Zhang et al., 2017). To determine temporal variations in the LRE, compound-specific radiocarbon analysis (CSRA) of individual terrestrial and aquatic biomarkers is increasingly employed, as this method overcomes the mixed $^{14}C$ signal of TOC dating. To date, however, only a relatively small number of studies carried out $^{14}C$ analysis of individual lipid biomarkers. Major progress in accelerator mass spectrometry (AMS) within the last two decades has made CSRA more feasible and greatly reduced the required sample size for obtaining reliable $^{14}C$ ages to <100 µg carbon (Eglinton et al., 1996; Ishikawa et al., 2018; Pearson et al., 1998; Santos et al., 2007; Yokoyama et al., 2010). For the isolation of individual compounds, preparative gas chromatography (prep-GC) is traditionally used (Eglinton et al., 1996; Kramer and Gleixner, 2006), but this time-consuming procedure often yields relatively low recovery rates (Haas et al., 2017) and may suffer from column bleed. Conversely, high-pressure liquid chromatography (HPLC) strongly reduces the number of necessary injections required to isolate sufficient amounts of carbon (Bour et al., 2016; Ingalls et al., 2010; Schwab et al., 2019a).



This is a provisional file, not the final typeset article

Here, we present the results of extensive tests of a new method for the isolation of short- ($C_{16}$ & $C_{18}$ homologues) and long-chain fatty acids ($C_{24}$, $C_{26}$ & $C_{28}$ homologues) from the sediments of Lake Chatyr Kol, Kyrgyzstan, by preparative HPLC for subsequent CSRA. Our method introduces only minor contamination of extraneous carbon and can be easily adopted in future studies. By comparing $^{14}C$ data of terrestrial and aquatic biomarkers with an independent varve chronology (Kalanke et al., 2020), we assess the temporal variability of the LRE and ascertain the relative influence of aquatic and terrestrial OC on the $^{14}C$ dating of bulk sediment TOC.

## 2 Study area

Endorheic Lake Chatyr Kol (40°37'N, 75°18'E), the third largest lake in Kyrgyzstan (Thorpe et al., 2009), is located at 3545 m above sea level in the south-western Tian Shan (Fig.1). The lake, which has a surface area of ~175 $km^2$ (Mosello, 2015), a width of ~12 km and a length of ~23 km, occupies the westernmost past of a large intra-montane basin (catchment area ~1084 $km^2$), which is confined by the At Bashy Range in the north and the Torugart Range in the south. Quaternary sediments, eroded from these mountain ranges, cover the surrounding plains, which are used as pastures. Climate conditions in the Kyrgyz Tian Shan are predominantly controlled by the interaction of the Siberian High and the mid-latitude Westerlies (Aizen et al., 1997; Lauterbach et al., 2014), which results in a generally low mean annual air temperature of -0.34 °C (Ilyasov et al., 2013) and lake ice cover from October to April. Precipitation is highest during the summer months due to convection and unstable atmospheric stratification (Aizen et al., 2001; Aizen et al., 1995); the average annual precipitation amounts to ~300 mm $a^{-1}$ (Koppes et al., 2008). The prevailing cold climate at Lake Chatyr Kol promotes the preservation of permafrost soils and widespread thermokarst formations (Abuduwaili et al., 2019; Shnitnikov et al., 1978). The sparse desert and semi-desert vegetation around the lake is dominated by montane grassland without trees (Taft et al., 2011). Due to the absence of fish stock, large numbers of the amphipod species *Gammarus alius* sp. nov., which is constrained to fresh and brackish water habitats, colonize aquatic plants(Sidorov, 2012).

## 3 Materials & Methods

### 3.1 Coring & Chronology

Five sediment cores, each consisting of one or two consecutive segments of 3 m length that partially overlapped with the segments of the other cores, were recovered in July 2012 from the south-western part of Lake Chatyr Kol (40° 36.37' N, 75° 14.02' E, ~20 m water depth) by using a 60-mm-diameter UWITEC piston corer (Kalanke et al., 2020). Furthermore, six surface sediment cores were recovered in July 2012 and seven surface sediment cores were retrieved in September 2017 from different sites across the lake basin using a UWITEC gravity corer equipped with additional hammer weight (Kalanke et al., 2020). Using the piston cores recovered in 2012, a continuous composite profile (CHAT12) with a total length of 623.5 cm was compiled through correlation of the individual core segments via prominent macroscopically visible marker layers (Kalanke et al., 2020). As the sediments are annually laminated (varved) except for the uppermost 63.0 cm of the composite profile, a floating varve chronology (Chatvd19) was established by microscopic analysis of large-scale petrographic thin sections (Kalanke et al., 2020). This included the identification and characterization of different varve types, thickness measurements as well as the counting of varves. Based on the difference between two consecutive varve counts, the uncertainty of the Chatvd19 varve chronology was estimated to ~5%

(Kalanke et al., 2020). In order to extend the floating varve chronology until recent times, gamma spectrometry measurements (210Pb, 137Cs) were carried out on the uppermost non-varved sediments of the CHAT12 composite profile (Kalanke et al., 2020). The measured $^{210}$Pb activity concentrations were implemented in both a constant initial concentration (CIC) model (Robbins, 1978) and a constant rate of supply (CRS) model (Appleby and Oldfield, 1978). Both models are concordant with commencing elevated $^{137}$Cs concentrations associated with nuclear weapon testing after AD1945 (Kudo et al., 1998; Pennington et al., 1973; Wright et al., 1999). By extrapolating the $^{210}$Pb-derived sedimentation rate, the gamma spectrometry chronology was linked at 63.0 cm composite depth to the floating varve chronology, allowing to establish a continuous age-depth model for the CHAT12 composite profile, which spans the last ~11620 years with a mean sedimentation rate of 0.55 mm $a^{-1}$ (Kalanke et al., 2020). The mainly varve counting-based chronology of the CHAT12 composite profile is independently confirmed by AMS $^{14}$C dating of two terrestrial macrofossil samples (wood) obtained at 380.5 and 528.0 cm composite depth, which yielded conventional $^{14}$C ages of 5360 ± 40 $^{14}$C a BP and 8890 ± 50 $^{14}$C a BP, respectively. These were calibrated using OxCal 4.3 (Bronk Ramsey, 1995, 2009) with the IntCal13 calibration data set (Reimer et al., 2013), yielding calibrated ages of 6140 ± 137 cal. a BP and 9988 ± 203 cal. a BP, respectively (Kalanke et al., 2020).

### 3.2 Lipid extraction and purification of fatty acid methyl esters (FAMEs)

In order to extract lipids for CSRA, ten 1-cm-thick sediment samples were taken at different depths from the CHAT12 composite profile (Supplementary Table 1), freeze-dried, homogenized, and subsequently processed using a pressurized solvent speed extractor (E-916, BÜCHI, Essen, Germany) with a dichloromethane/methanol mixture (9:1) at 100 °C and 120 bar for 15 min in 2 cycles. Free fatty acids (FAs) were separated from the total lipid extract by elution with diethyl ether/acetic acid (19:1) over columns with aminopropyl-modified silica gel (CHROMABOND® $NH_2$ polypropylene columns, 60 Å, Macherey-Nagel, Düren, Germany). FAs were then methylated using 5% hydrochloric acid in methanol of known isotopic composition at 80 °C for 12 h to yield corresponding fatty acid methyl esters (FAMEs). Subsequently, FAMEs were obtained by liquid-liquid extraction with 5% NaCl and hexane and further purified by elution with dichloromethane over silica gel columns (~2 g). In order to minimize organic contaminants, all glassware was pre-heated to 450 °C for 5 h prior to use. A schematic overview of the workflow is depicted in Fig. 2.

### 3.3 Bulk sediment geochemical analyses and AMS $^{14}$C dating of organic material from the Lake Chatyr Kol sediments

To assess the influence of variations in terrigenous input on the compound-specific $^{14}$C ages, we analysed the major element composition of the CHAT12 sediments. These analyses were performed on the foil-covered fresh surface of the split sediment cores at 200 µm resolution using an ITRAX X-ray fluorescence (XRF) core scanner (Cox Analytical Systems, Mölndal, Sweden) equipped with a Cr X-ray tube operating at 40 kV and 40 mA. The measurement time per scanning step was 10 s. Here we only report the log-ratio of the measured intensities for potassium and titanium, reflecting relative variations of element concentrations without the potential bias of measurement and matrix effects (Weltje and Tjallingii, 2008). To better visualize the relation between the compound-specific $^{14}$C ages and variations in the high-resolution XRF element data, log(K/Ti) was averaged over 1.2-cm-intervals across the positions where the individual 1-cm-thick samples for CSRA were taken.
In addition to the two pieces of wood that have been AMS $^{14}$C-dated to support the Chatvd19 varve chronology (see chapter 3.1), eleven depth-matched sediments of bulk TOC were subjected to the Poznań Radiocarbon Laboratory, Poland, for AMS $^{14}$C dating (Kalanke et al., 2020). The conventional $^{14}$C ages obtained from these samples were calibrated using OxCal 4.3 (Bronk Ramsey, 1995, 2009)



This is a provisional file, not the final typeset article

with the IntCal13 calibration data set (Reimer et al., 2013) and are reported in Supplementary Table 2 as well as in Kalanke et al. (2020).

### 3.4 Isolation of FAMEs by HPLC

Individual FAMEs were isolated using an Agilent Technologies 1200 Series HPLC system consisting of a vacuum degasser, a quaternary pump, a thermostat-controlled column compartment, an injection autosampler, a UV detector and a fraction collector (Fig. 2). Separation was achieved on a reverse-phase column (Nucleodur® C8 Gravity, 250 mm × 4.6 mm, 5 µm particle size, Macherey-Nagel, Düren, Germany) along with a guard column (Macherey-Nagel, Düren, Germany), using an isocratic elution with 100% acetonitrile (ACN) at a flow rate of 1.0 mL $min^{-1}$. The column was maintained at a constant temperature of 40 °C and compounds were detected at a wavelength of 230 nm. Elution times of the short- and long-chain FAMEs and their stability have been determined beforehand by standard runs and were adjusted daily. Up to 10 injections of each sample with an injection volume of 10 µL were made to ensure quantities of 20 – 150 µg carbon required for CSRA using EA/AMS. Collected fractions of the same compounds were pooled into gas chromatography vials and evaporated to a volume of ~ 2 mL under a stream of ultra-high-purity $N_2$. In order to assure the purity of the collected FAMEs and to determine the recovery of carbon prior to $^{14}C$ measurements, aliquots of 5 µL of several samples were run on a gas chromatograph (GC) equipped with a flame ionization detector (GC-FID, Agilent 7890B, Agilent Technologies, Santa Clara, USA) (Fig. 2). The identification of the individual compounds was achieved relative to a FAME standard mixture on an Ultra 2 column (50m, 0.32 mm ID, 0.52-µm film thickness, Agilent Technologies, Santa Clara, USA). The PTV injector was operated in splitless mode, starting at 45 °C for 0.1 min and heating up to 300 °C at 14.5 °C $s^{-1}$ (hold for 3 min). The GC oven increased from 140 °C (hold for 1 min) to 310 °C at a rate of 4 °C $min^{-1}$ (hold for 15 min) and finally to 325 °C at 30 °C/min (hold for 3 min). Since the concentrations of long-chain FAMEs in the Lake Chatyr Kol sediments were relatively low, long-chain FAMEs $C_{24}$, $C_{26}$ and $C_{28}$ were recombined in order to provide sufficient amounts for $\Delta^{14}C$ analysis. Purified FAMEs were transferred to tin capsules and all solvent residues were allowed to evaporate to complete dryness.

### 3.5 AMS measurements on FAMEs

$\Delta^{14}C$ analysis of the FAMEs was performed at the Max Planck Institute for Biogeochemistry, Jena, using a MICADAS (Ionplus, Dietikon, Switzerland) connected via a gas interface system to a Vario Isotope Select elemental analyzer (Elementar Analysensysteme, Langenselbold, Germany) that was used as a combustion unit (Fig. 2). The settings for the MICADAS were ensured by measuring the Oxalic acid II standard (NIST SRM 4990) to account for fractionation and standard normalization. $^{14}C$ background of the MICADAS was quantified by $^{14}C$-free $CO_2$ reference gas.

Results are normalized to Oxalic Acid II (National Institute of Standards and Technology) primary standard. All obtained $^{14}C$ values were corrected for the contribution of the methyl carbon derived from the methanol ($\Delta^{14}C$ = -998±0 ‰) used during the derivatization of the fatty acids by an isotopic mass balance equation:

$$\Delta^{14}C_{fame} = \frac{[(n+1)\,\Delta^{14}C_{measured}] - \Delta^{14}C_{MeOH}}{n}$$

where n is the number of carbon atoms in the original fatty acid. All conventional $^{14}C$ ages were calibrated using OxCal 4.3 software (Bronk Ramsey, 2009) with the IntCal13 calibration data set

(Reimer et al., 2013) and are reported as calendar years before present (cal. a BP); all data are reported in Supplementary Table 1.

### 3.6 Correction for extraneous carbon

Because $^{14}C$ analysis is sensitive to contributions from extraneous carbon ($C_{ex}$), it is mandatory to assess the amount of $C_{ex}$ that is added to the sample during compound isolation and subsequent processing (Hanke et al., 2017; Mollenhauer and Rethemeyer, 2009; Santos et al., 2007; Shah and Pearson, 2007; Ziolkowski and Druffel, 2009). We therefore performed extensive blank corrections using commercially available modern-$^{14}C$-content (MC) and $^{14}C$- dead (DC) reference materials to monitor the modern and $^{14}C$-free constituents of $C_{ex}$, respectively. Detailed information about blank assessment can be found in Santos et al. (2010) and Hanke et al. (2017). FAMEs $C_{16:0}$ (Sigma-Aldrich, 76119, $\Delta^{14}C$ value of 111±28‰) and phenanthrene (Sigma-Aldrich, lot MKBB7303, $\Delta^{14}C$ value of -997±0.1‰) were used as modern and $^{14}C$-free standards to quantify the HPLC contamination and AMS contamination (all process). The NOX and Fluka standards and the NOX and phenanthrene were used to quantify the EA and AMS contamination. In our approach, contaminating carbon might be taken up during process steps such as HPLC isolation ($C_{HPLC}$) and during AMS sample preparation and analysis itself ($C_{AMS}$). Accordingly, the $C_{HPLC}$ contamination is $C_{ex}$ minus $C_{AMS}$.

## 4 Results & Discussion

### 4.1 HPLC isolation & purification

Typical chromatograms of HPLC runs and corresponding collection times of FAMEs $C_{16:0}$, $C_{18:0}$, $C_{24:0}$, $C_{26:0}$ and $C_{28:0}$ are illustrated in Fig. 3. Using an isocratic elution with ACN, short- and long-chain FAMEs were well separated on the reverse-phase column. Short-chain FAMEs eluted between 5 and 8 min, while long-chain FAMEs eluted between 12 and 18 min (Fig. 3). The available carbon amounts varied between 15 and 89 µg C for the short-chain FAs and between 55 and 149 µg C for the long-chain FAs throughout the sediment record (Supplementary Table 1). GC-FID chromatograms of the collected fractions affirmed the purity of the isolation by HPLC (Supplementary Figure S1).

### 4.2 $C_{ex}$ from AMS Sample Preparation ($C_{AMS}$) and HPLC isolation ($C_{HPLC}$)

Contributions from $C_{AMS}$ were assessed by preparing and measuring standards ranging from $^{14}C$-dead to modern values (phenanthrene, Fluka, Oxalic acid (OX-1), FAME standards $C_{16:0}$ and $C_{26:0}$) at similar measurement conditions as the samples. The amount of carbon introduced during AMS sample preparation was 0.28 µg of MC and 0.20 µg of DC. $C_{HPLC}$ was quantified using FAME standards $C_{16:0}$ and $C_{26:0}$ and phenanthrene. These standards were injected directly on the C8 reverse-phase column of the HPLC in different concentrations. Each injection on the HPLC was collected separately and merged to cover carbon amounts between 20 µg (1 HPLC injection) and 80 µg (10 HPLC injections) to coincide with the weight range of the carbon in the samples. The isolation via HPLC introduced DC contaminations of 0.50 ± 0.22 µg on average. The $F^{14}C$ results of our DC standards were not significantly altered by HPLC isolation, suggesting that no substantial MC contaminations were introduced by HPLC. Previous HPLC-based isolations of phospholipids resulted in highly similar contaminations of 0.57 ± 0.29 µg DC with no substantial MC being introduced (Schwab et al., 2019b). Despite the low amounts of $C_{ex}$ that were introduced during our laboratory procedures, the $F^{14}C$ values of our sediment samples were corrected according to the DC contaminations identified through our standard measurements (Supplementary Table 1).

### 4.3 Implication of mixed OC pools for TOC dating



This is a provisional file, not the final typeset article

To assess the LRE on the AMS $^{14}C$ ages obtained from bulk sediment TOC (Supplementary Table 2) as well as on the $^{14}C$ ages obtained from FAMEs by CSRA (Supplementary Table 1), we compared these ages to the Chatvd19 varve chronology established by Kalanke et al. (2020). We found that the $^{14}C$ ages of TOC were substantially higher than what would be expected from the varve count at the respective depth (Fig. 4; and Kalanke et al. (2020), Fig. 7). Over the last ~10,000 years (based on the varve chronology), these $^{14}C$ ages were between ~960 and ~5000 years older than the corresponding varve ages. The deviation increases with sediment depth, possibly related to increased input of pre-aged OC from glacial erosion material during the early Holocene. This reveals that (i) the sediments of Lake Chatyr Kol were strongly affected by the LRE in the past and (ii) the magnitude of the LRE was highly variable through time.

The CSRA of the short- and long-chain FAMEs yielded $^{14}C$ ages ranging between the TOC- and aquatic macro remain-derived $^{14}C$ ages and the ages inferred from the varve chronology for most of the composite sediment core. The $^{14}C$ ages of the long-chain FAMEs are systematically older than those of the short-chain FAMEs (average ~1680 years, maximum ~4940 years) and the varve chronology and closer to the TOC- and aquatic macro remain-derived $^{14}C$ ages, indicating a major terrestrial OC source contributing to the complex TOC mixture. In contrast, the $^{14}C$ ages of the short-chain FAMEs reveal a smaller offset compared to the varve chronology than those of the long-chain FAMEs, suggesting that compound-specific sources, transport and pre-deposition aging processes control the magnitude and variability of the LRE in the Lake Chatyr Kol sediments. Long-chain FAs ($>C_{24}$) are generally considered to derive from terrigenous sources such as soils and higher plant leaf waxes (McIntosh et al., 2015; Meyers, 1997; Parkes and Taylor, 1983) and can thus be utilized as tracers of terrestrial vascular plant carbon. In contrast, short-chain FAs ($C_{16}$ & $C_{18}$) are, though being ubiquitous lipids, mostly ascribed to in situ autotrophic and heterotrophic microbes (Cranwell et al., 1987; Meyers, 1997; Tao et al., 2017). In addition, their respective transport mechanisms greatly depend on the FAs chemical properties: short-chain FAs are more water-soluble than long-chain FAs and hence can be mobilized more easily from soils and are preferentially degraded by microorganisms (Matsumoto et al., 2007). In contrast, long-chain FAs are less water-soluble and consequently more resistant to microbial degradation (Matsumoto et al., 2007; Moucawi et al., 1981). Their relative persistence and delayed transport properties, which derive from their chemical characteristics, could likely explain the higher $^{14}C$ ages of the long-chain FAs in the Lake Chatyr Kol sediment record compared to their short-chain homologues. Nevertheless, also the short-chain FAs are characterized by higher $^{14}C$ ages than inferred from the varve counting at the respective depths in the composite profile. Short-chain FAs are likely influenced by the $^{14}C$ content prevailing in the lake, which can, for example, be influenced by the input of surface water and/or groundwater containing old $^{14}C$ (Zhou et al., 2015; Zhou et al., 2020) as well as by the exchange rate between the lakes surface and atmospheric $CO_2$ resulting in $^{14}C$ depleted lake water compared to the atmosphere (Sayle et al., 2016; Zhou et al., 2020). Consequently, aquatic plants may assimilate $^{14}C$-depleted dissolved inorganic carbon during photosynthesis and therefore may appear older than the deposition age. This is evidenced by the discrepancy between the aquatic macro remain-derived $^{14}C$ ages and the Chatvd19 varve chronology (Fig. 4). Furthermore, also remobilization of pre-aged terrestrial OC that enters the lake needs to be considered as an influence on the $^{14}C$ ages derived from short-chain FAs (Howarth et al., 2013). While we cannot disentangle the individual effects of $^{14}C$-depletion on TOC in both short- and long-chain FAs, our data indicate a common trend towards an increasing magnitude of the LRE with sediment depth. We therefore hypothesize that instead of compound-specific characteristics, the overarching temporal trend potentially resulted from system-wide shifts in OC input from the catchment.

To assess the mobilization of OC from the catchment, we utilized the elemental composition, i.e. the Ti/K log-ratio, of the sediments (Supplementary Figure 2). The elements K and Ti are both confined to the detrital sediment fraction and variations in the log(Ti/K) record therefore indicate relative variations in its composition. Ti/K has previously been used as a proxy for grain-size variability

(Gascon Diez et al., 2017; Marshall et al., 2011) as it reflects mineralogical variations associated with size-selective transport. In general, fine-grained detrital sediments such as clay contain relatively high amounts of K, whereas relatively high amounts of Ti are found in coarser detrital sediments such as coarse silt and very fine sand (Bloemsma et al., 2012; Henares et al., 2019; Rothwell and Croudace, 2015). Additionally, Boyle et al. (2011) showed the potential of Ti/K in lake sediments to reflect changes in the proportion of subsoil erosion. Consequently, an increase in log(Ti/K) in the lake sediments would indicate the mobilization of subsoil-derived material with potentially higher proportions of pre-aged OC. Indeed, the age offsets between long- and short-chain FAMEs in the Holocene Lake Chatyr Kol sediments are positively correlated to log(Ti/K) (Spearman rank correlation coefficient $\rho_s = 0.70$, $p < 0.025$; Fig. 5). High log(Ti/K) values are consistent with higher age offsets, suggesting that variations in sediment supply from the catchment are a major driver of the LRE magnitude at Lake Chatyr Kol.

## 5 Conclusions

The data from the Lake Chatyr Kol sediment record show that in lacustrine systems with temporally variable influx from the catchment, the magnitude of the LRE can be highly variable. Therefore, assuming a linear LRE and applying a respective age correction – as commonly done in many studies utilizing lake sediments as paleoclimate archives – may be misleading and can result in severely offset chronologies. In the case of Lake Chatyr Kol, the CSRA results quantify the discrepancies between aquatic and terrestrial biomarker $^{14}C$ ages to up to ~4940 years and furthermore provide insights into the relationship between catchment processes and lacustrine biomarker deposition. Therefore, several factors of OC dynamics and transport mechanisms need to be considered in the study of OC cycling. Although CSRA is generally considered very time-consuming and analytically challenging, this study introduces a rapid HPLC-based method for isolating short- and long-chain FAs. With only few injections, the reported HPLC approach can provide sufficient amounts of carbon for $^{14}C$ analysis while minimizing the risk of contaminations at the same time. We therefore advocate for the regular implementation of compound-specific $^{14}C$ dating, as methodological advances give easier access to CSRA and $^{14}C$ dating of bulk sediment TOC is often less reliable. The data from Lake Chatyr Kol exemplify the substantial potential of compound-specific $^{14}C$ dating to detect temporal variations in the LRE and consequently develop more robust chronologies for lake sediment records from sparsely vegetated high-latitude and -altitude regions.

## 6 Data Availability Statement

The raw data supporting the conclusions of this article will be made available by the authors, without undue reservation.

## 7 Author contribution

GG designed the research idea. JM and JK finalized the age model. SL conducted the field work, compiled the composite profile and selected bulk sediment and plant macro remain samples for AMS $^{14}C$ dating. RT interpreted the XRF data. NS performed laboratory analyses with the help of VFS and subsequent data interpretation with support from VSF and GG. NS wrote the manuscript. All authors contributed to reviewing the manuscript.

## 8 Funding

This study was funded by the BMBF through the research projects CADY (Central Asian Climate Dynamics, Grant No. 03G0813) and CAHOL (Central Asian Holocene Climate, Grant No. 03G0864).



This is a provisional file, not the final typeset article

NS also acknowledges the Max Planck Society and the International Max Planck Research School for Global Biogeochemical Cycles (IMPRS-gBGC). VS acknowledges support from the European Research Council (ERC) Advanced Grant 695101 14Constraint.

## 9 Conflict of interest

The authors declare that the research was conducted in the absence of any commercial or financial relationships that could be construed as a potential conflict of interest.

## 10 Acknowledgments

We thank Michael Köhler, Sylvia Pinkerneil, Robert Schedel, Denis Henning, Mirlan Daiyrov, and Roman Witt for participation in the field work and Peter Dulski for carrying out the XRF measurements. Furthermore, we thank the group of Axel Steinhof for the MICADAS radiocarbon measurements and Achim Brauer for his project engagement.

## 11 References

Abuduwaili, J., Issanova, G., and Saparov, G., 2019, Lakes in Kyrgyzstan, Hydrology and Limnology of Central Asia, Springer, Singapore, p. 288–294.

Aizen, E. M., Aizen, V. B., Melack, J. M., Nakamura, T., and Ohta, T., 2001, Precipitation and atmospheric circulation patterns at mid-latitudes of Asia: International Journal of Climatology, v. 21, no. 5, p. 535–556, doi: 10.1002/joc.626

Aizen, V., Aizen, E., and Melack, J., 1995, Climate, Snow cover, Glaciers, and Runoff in the Tien Shan, Central Asia: Water Resources Bulletin, v. 31, p. 1113–1129, doi: 10.1111/j.1752-1688.1995.tb03426.x

Aizen, V., Aizen, E., Melack, J., and Dozier, J., 1997, Climatic and hydrologic changes in the Tien Shan, Central Asia: Journal of Climate, v. 10, p. 1393–1404, doi: 10.1175/1520-0442(1997)010<1393:CAHCIT>2.0.CO;2

Appleby, P. G., and Oldfield, F., 1978, The calculation of lead-210 dates assuming a constant rate of supply of unsupported $^{210}$Pb to the sediment: Catena, v. 5, no. 1, p. 1–8, doi: 10.1016/S0341-8162(78)80002-2

Bertrand, S., Araneda, A., Vargas, P., Jana, P., Fagel, N., and Urrutia, R., 2012, Using the N/C ratio to correct bulk radiocarbon ages from lake sediments: Insights from Chilean Patagonia: Quaternary Geochronology, v. 12, p. 23–29, doi: 10.1016/j.quageo.2012.06.003

Bloemsma, M. R., Zabel, M., Stuut, J.-B. W., Tjallingii, R., Collins, J. A., and Weltje, G. J., 2012, Modelling the joint variability of grain size and chemical composition in sediments: Sedimentary Geology, v. 280, p. 135–148, doi: 10.1016/j.sedgeo.2012.04.009

Bour, A. L., Walker, B. D., Broek, T. A., and McCarthy, M. D., 2016, Radiocarbon Analysis of Individual Amino Acids: Carbon Blank Quantification for a Small-Sample High-Pressure Liquid Chromatography Purification Method: Analytical Chemistry, v. 88, no. 7, p. 3521–3528, doi: 10.1021/acs.analchem.5b03619

Boyle, J. F., Plater, A. J., Mayers, C., Turner, S. D., Stroud, R. W., and Weber, J. E., 2011, Land use, soil erosion, and sediment yield at Pinto Lake, California: comparison of a simplified USLE model with the lake sediment record: Journal of Paleolimnology, v. 45, p. 199–212, doi: 10.1007/s10933-010-9491-8

386 Bronk Ramsey, C., 1995, Radiocarbon Calibration and Analysis of Stratigraphy: The OxCal
387 Program: Radiocarbon, v. 37, no. 2, p. 425–430, doi: 10.1017/s0033822200030903

388 Bronk Ramsey, C., 2009, Bayesian Analysis of Radiocarbon Dates: Radiocarbon, v. 51, no. 01, p.
389 337–360, doi: 10.1017/s0033822200033865

390 Cranwell, P. A., Eglinton, G., and Robinson, N., 1987, Lipids of aquatic organisms as potential
391 contributors to lacustrine sediments – ll∗: Organic Geochemistry, v. 11, p. 513–527, doi:
392 10.1016/0146-6380(87)90007-6

393 Doberschütz, S., Kasper, T., Daut, G., Frenzel, P., Wang, J., Schwalb, A., Haberzettl, T., Zhu, L., and
394 Mäusbacher, R., 2014, Monsoonal forcing of Holocene paleoenvironmental change on the
395 central Tibetan Plateau inferred using a sediment record from Lake Nam Co (Xizang, China):
396 Journal of Paleolimnology, v. 51, p. 253–266, doi: 10.1007/s10933-013-9702-1)

397 Eglinton, T., Aluwihare, L. I., Bauer, J. E., Druffel, E. R., and McNichol, A. P., 1996, Gas
398 Chromatographic Isolation of Individual Compounds from Complex Matrices for
399 Radiocarbon Dating: Analytical Chemistry, v. 68, no. 5, p. 904–912

400 Gascon Diez, E., Corella, J. P., Adatte, T., Thevenon, F., and Loizeau, J.-L., 2017, High-resolution
401 reconstruction of the 20th century history of trace metals, major elements, and organic matter
402 in sediments in a contaminated area of Lake Geneva, Switzerland: Applied Geochemistry, v.
403 78, p. 1–11, doi: 10.1016/j.apgeochem.2016.12.007

404 Geyh, M. A., Schotterer, U., and Grosjean, M., 1998, Temporal Changes of the $^{14}C$ Reservoir Effect
405 in Lakes: Radiocarbon, v. 40, no. 2, p. 921–931

406 Günther, F., Thiele, A., Biskop, S., Mäusbacher, R., Haberzettl, T., Yao, T., and Gleixner, G., 2016,
407 Late quaternary hydrological changes at Tangra Yumco, Tibetan Plateau: a compound-
408 specific isotope-based quantification of lake level changes: Journal of Paleolimnology, v. 55,
409 no. 4, p. 369–382, doi: 10.1007/s10933-016-9887-1

410 Haas, M., Bliedtner, M., Borodynkin, I., Salazar, G., Szidat, S., Eglinton, T. I., and Zech, R., 2017,
411 Radiocarbon Dating of Leaf Waxes in the Loess-Paleosol Sequence Kurtak, Central Siberia:
412 Radiocarbon, v. 59, no. 01, p. 165–176, doi: 10.1017/rdc.2017.1

413 Hanke, U. M., Wacker, L., Haghipour, N., Schmidt, M. W. I., Eglinton, T. I., and McIntyre, C. P.,
414 2017, Comprehensive radiocarbon analysis of benzene polycarboxylic acids (BPCAs) derived
415 from pyrogenic carbon in environmental samples: Radiocarbon, v. 59, no. 04, p. 1103–1116,
416 doi: 10.1017/rdc.2017.44

417 Henares, S., Donselaar, M. E., Bloemsma, M. R., Tjallingii, R., De Wijn, B., and Weltje, G. J., 2019,
418 Quantitative integration of sedimentological core descriptions and petrophysical data using
419 high-resolution XRF core scans: Marine and Petroleum Geology, v. 110, p. 450–462, doi:
420 10.1016/j.marpetgeo.2019.07.034

421 Hou, J., D'Andrea, W. J., and Liu, Z., 2012, The influence of $^{14}C$ reservoir age on interpretation of
422 paleolimnological records from the Tibetan Plateau: Quaternary Science Reviews, v. 48, p.
423 67–79, doi: 10.1016/j.quascirev.2012.06.008

424 Howarth, J. D., Fitzsimons, S. J., Jacobsen, G. E., Vandergoes, M. J., and Norris, R. J., 2013,
425 Identifying a reliable target fraction for radiocarbon dating sedimentary records from lakes:
426 Quaternary Geochronology, v. 17, p. 68–80, doi: 10.1016/j.quageo.2013.02.001



This is a provisional file, not the final typeset article

427 Hughen, K. A., Lehman, S., Southon, J. R., Overpeck, J. T., Marchal, O., Herring, C., and Turnbull,
428 D., 2004, $^{14}C$ activity and global carbon cycle changes over the past 50,000 years: Science, v.
429 393, no. 5655, p. 202–207

430 Ilyasov, S., Zabenko, O., Gaydamak, N., Kirilenko, A., Myrsaliev, N., Shevchenko, V., and Penkina,
431 L., 2013, Climate profile of the Kyrgyz Republic, p. 99

432 Ingalls, A. E., Ellis, E. E., Santos, G. M., McDuffee, K. E., Truxal, L., Keil, R. G., and Druffel, E. R.,
433 2010, HPLC Purification of Higher Plant-Dervied Lignin Phenols for Compound Specific
434 Radiocarbon Analysis: Analytical Chemistry, v. 82, no. 21, p. 8931–8938

435 Ishikawa, N. F., Itahashi, Y., Blattmann, T. M., Takano, Y., Ogawa, N. O., Yamane, M., Yokoyama,
436 Y., Nagata, T., Yoneda, M., Haghipour, N., Eglinton, T. I., and Ohkouchi, N., 2018,
437 Improved Method for Isolation and Purification of Underivatized Amino Acids for
438 Radiocarbon Analysis: Analytical Chemistry, v. 90, no. 20, p. 12035–12041, doi:
439 10.1021/acs.analchem.8b02693

440 Kalanke, J., Mingram, J., Lauterbach, S., Usubaliev, R., Tjallingii, R., and Brauer, A., 2020, Seasonal
441 deposition processes and chronology of a varved Holocene lake sediment record from Lake
442 Chatyr Kol (Kyrgyz Republic) Geochronology Discuss, v. 2, p. 133–154, doi:
443 10.5194/gchron-2-133-2020

444 Koppes, M., Gillespie, A. R., Burke, R. M., Thompson, S. C., and Stone, J., 2008, Late Quaternary
445 glaciation in the Kyrgyz Tien Shan: Quaternary Science Reviews, v. 27, no. 7-8, p. 846–866,
446 doi: 10.1016/j.quascirev.2008.01.009

447 Kramer, C., and Gleixner, G., 2006, Variable use of plant- and soil-derived carbon by
448 microorganisms in agricultural soils: Soil Biology and Biochemistry, v. 38, no. 11, p. 3267–
449 3278, doi: 10.1016/j.soilbio.2006.04.006

450 Kudo, A., Zheng, J., Koerner, R. M., Fisher, D. A., Santry, D. C., Mahara, Y., and Sugahara, M.,
451 1998, Global transport rates of $^{137}Cs$ and $^{239+240}Pu$ originating from the Nagasaki A-bomb in
452 1945 as determined from analysis of Canadian Arctic ice cores: Journal of Environmental
453 Radioactivity, v. 40, no. 3, p. 289–298, doi: 10.1016/S0265-931X(97)00023-4

454 Lauterbach, S., Witt, R., Plessen, B., Dulski, P., Prasad, S., Mingram, J., Gleixner, G., Hettler-Riedel,
455 S., Stebich, M., Schnetger, B., Schwalb, A., and Schwarz, A., 2014, Climatic imprint of the
456 mid-latitude Westerlies in the Central Tian Shan of Kyrgyzstan and teleconnections to North
457 Atlantic climate variability during the last 6000 years: The Holocene, v. 24, no. 8, p. 970–
458 984, doi: 10.1177/0959683614534741

459 Liang, E. Y., Shao, X. M., and Xu, Y., 2009, Tree-ring evidence of recent abnormal warming on the
460 southeast Tibetan Plateau: Theoretical and Applied Climatology, v. 98, no. 1-2, p. 9–18, doi:
461 10.1007/s00704-008-0085-6

462 Marshall, M. H., Lamb, H. F., Huws, D., Davies, S. J., Bates, C. R., Bloemendal, J., Boyle, J., Leng,
463 M. J., Umer, M., and Bryant, C., 2011, Late Pleistocene and Holocene drought events at Lake
464 Tana, the source of the Blue Nile: Global and Planetary Change, v. 78, no. 3–4, p. 147–161,
465 doi: 10.1016/j.gloplacha.2011.06.004

466 Matsumoto, K., Kawamura, K., Uchida, M., and Shibata, Y., 2007, Radiocarbon content and stable
467 carbon isotopic ratios of individual fatty acids in subsurface soil: Implication for selective
468 microbial degradation and modification of soil organic matter: Geochemical Journal, v. 41,
469 no. 6, p. 483–492, doi: 10.2343/geochemj.41.483

McIntosh, H. A., McNichol, A. P., Xu, L., and Canuel, E. A., 2015, Source-age dynamics of estuarine particulate organic matter using fatty acid $\delta^{13}C$ and $\Delta^{14}C$ composition: Limnology and Oceanography, v. 60, no. 2, p. 611–628, doi: 10.1002/lno.10053

Meyers, P. A., 1997, Organic geochemical proxies of paleoceanographic, paleolimnologic, and paleoclimatic processes: Organic Geochemistry, v. 27, no. 5–6, p. 213–250, doi: 10.1016/S0146-6380(97)00049-1

Mischke, S., Weynell, M., Zhang, C., and Wiechert, U., 2013, Spatial variability of $^{14}C$ reservoir effects in Tibetan Plateau lakes: Quaternary International, v. 313-314, p. 147–155, doi: 10.1016/j.quaint.2013.01.030

Mollenhauer, G., and Rethemeyer, J., 2009, Compound-specific radiocarbon analysis – Analytical challenges and applications: IOP Conference Series: Earth and Environmental Science, v. 5, p. 012006, doi: 10.1088/1755-1307/5/1/012006

Mosello, B., 2015, The Syr Darya River Basin, How to Deal with Climate Change?, Springer International Publishing, p. 117–162.

Moucawi, J., Fustec, E., Jambu, P., and Jacquesy, R., 1981, Decomposition of lipids in soils: Free and esterified fatty acids, alcohols and ketones: Soil Biology and Biochemistry, v. 13, no. 6, p. 461–468, doi: 10.1016/0038-0717(81)90035-3

Mügler, I., Gleixner, G., Günther, F., Mäusbacher, R., Daut, G., Schütt, B., Berking, J., Schwalb, A., Schwark, L., Xu, B., Yao, T., Zhu, L., and Yi, C., 2010, A multi-proxy approach to reconstruct hydrological changes and Holocene climate development of Nam Co, Central Tibet: Journal of Paleolimnology, v. 43, no. 4, p. 625–648, doi: 10.1007/s10933-009-9357-0

Parkes, R. J., and Taylor, J., 1983, The relationship between fatty acid distributions and bacterial respiratory types in contemporary marine sediments: Estuarine, Coastal and Shelf Science, v. 16, no. 2, p. 173–189, doi: 10.1016/0272-7714(83)90139-7

Pearson, A., McNichol, A. P., Schneider, R. J., Von Reden, K. F., and Zheng, Y., 1998, Microscale AMS $^{14}C$ Measurement at NOSAMS: Radiocarbon, v. 40, no. 01, p. 61–75, doi: 10.1017/s0033822200017902

Pennington, W., Tutin, T. G., Cambray, R. S., and Fisher, E. M., 1973, Observations on Lake Sediments using Fallout $^{137}Cs$ as a Tracer: Nature, v. 242, p. 324–326, doi: 10.1038/242324a0

Philippsen, B., 2013, The freshwater reservoir effect in radiocarbon dating: Heritage Science, v. 1, no. 24, p. 1–19, doi: 10.1186/2050-7445-1-24

Reimer, P. J., Bard, E., Bayliss, A., Beck, J. W., Blackwell, P. G., Ramsey, C. B., Buck, C. E., Cheng, H., Edwards, R. L., Friedrich, M., Grootes, P. M., Guilderson, T. P., Haflidason, H., Hajdas, I., Hatté, C., Heaton, T. J., Hoffmann, D. L., Hogg, A. G., Hughen, K. A., Kaiser, K. F., Kromer, B., Manning, S. W., Niu, M., Reimer, R. W., Richards, D. A., Scott, E. M., Southon, J. R., Staff, R. A., Turney, C. S. M., and van der Plicht, J., 2013, IntCal13 and Marine13 Radiocarbon Age Calibration Curves 0–50,000 Years cal BP: Radiocarbon, v. 55, no. 04, p. 1869–1887, doi: 10.2458/azu_js_rc.55.16947

Robbins, J. A., 1978, Geochemical and geophysical applications of radioactive lead, *in* Nriagu, J. O., ed., Biogeochemistry of Lead in the Environment: Amsterdam, Elsevier Scientific, p. 285–393.

Rothwell, R. G., and Croudace, I. W., 2015, Twenty Years of XRF Core Scanning Marine Sediments: What Do Geochemical Proxies Tell Us?, *in* Croudace, I. W., and Rothwell, R. G.,



This is a provisional file, not the final typeset article

513 eds., Micro-XRF Studies of Sediment Cores. Developments in Paleoenvironmental Research,
514 Volume 17: Dordrecht, Springer.

515 Santos, G. M., Southon, J. R., Drenzek, N. J., Ziolkowski, L. A., Druffel, E. R., Xu, X., Zhang, D.,
516 Trumbore, S., Eglinton, T. I., and Hughen, K. A., 2010, Blank Assessment for ultra-small
517 radiocarbon samples: chemical extraction and seperation versus AMS: Radiocarbon, v. 52,
518 no. 2-3, p. 1322–1335

519 Santos, G. M., Southon, J. R., Griffin, S., Beaupre, S. R., and Druffel, E. R. M., 2007, Ultra small-
520 mass AMS $^{14}$C sample preparation and analyses at KCCAMS/UCI Facility: Nuclear
521 Instruments and Methods in Physics Research Section B: Beam Interactions with Materials
522 and Atoms, v. 259, no. 1, p. 293–302, doi: 10.1016/j.nimb.2007.01.172

523 Sayle, K. L., Hamilton, W. D., Gestsdóttir, H., and Cook, G. T., 2016, Modelling Lake Mývatn's
524 freshwater reservoir effect: Utilisation of the statistical program FRUITS to assist in the re-
525 interpretation of radiocarbon dates from a cemetery at Hofstaðir, north-east Iceland:
526 Quaternary Geochronology, v. 36, p. 1–11, doi: 10.1016/j.quageo.2016.07.001

527 Schwab, V. F., Nowak, M. E., Elder, C. D., Trumbore, S., Xu, X., Gleixner, G., Lehmann, R.,
528 Pohnert, G., Muhr, J., Küsel, K., and Totsche, K. U., 2019a, $^{14}$C-Free Carbon Is a Major
529 Contributor to Cellular Biomass in Geochemically Distinct Groundwater of Shallow
530 Sedimentary Bedrock Aquifers: Water Resources Research, v. 55, no. 3, p. 2104–2121, doi:
531 10.1029/2017WR022067

532 Schwab, V. F., Nowak, M. E., Trumbore, S. E., Xu, X., Gleixner, G., Muhr, J., Küsel, K., and
533 Totsche, K. U., 2019b, Isolation of Individual Saturated Fatty Acid Methyl Esters Derived
534 From Groundwater Phospholipids by Preparative High-Pressure Liquid Chromatography for
535 Compound-Specific Radiocarbon Analyses: Water Resources Research, v. 55, no. 11, p.
536 2521–2531, doi: 10.1029/2018WR024076

537 Shah, S. R., and Pearson, A., 2007, Ultra-microscale (5-25 μg C) analysis of individual lipids by $^{14}$C
538 AMS: Assessment and correction for sample processing blanks: Radiocarbon, v. 49, no. 1, p.
539 69–82, doi: 10.2458/azu_js_rc.49.2900

540 Sheppard, P. R., Tarasov, P. E., Graumlich, L. J., Heussner, K. U., Wagner, M., Österle, H., and
541 Thompson, L. G., 2004, Annual precipitation since 515 BC reconstructed from living and
542 fossil juniper growth of northeastern Qinghai Province, China: Climate Dynamics, v. 23, no.
543 7-8, p. 869–881, doi: 10.1007/s00382-004-0473-2

544 Shnitnikov, A. V., Livja, A. A., Berdovskaya, G. N., and Sevastianov, D. V., 1978, Paleolimnology
545 of Chatyrkel Lake (Tien-shan): Polskie Archiwum Hydrobiologii, v. 25, p. 383–390

546 Sidorov, D. A., 2012, Two new species of freshwater amphipods (Crustacea: Gammaridae) from
547 Central Asia, with comments on the unusual upper lip morphology: Zootaxa, v. 3317, p. 1–
548 24, doi: 10.11646/zootaxa.3317.1.1

549 Taft, J. B., Phillippe, L. R., Dietrich, C. H., and Robertson, K. R., 2011, Grassland composition,
550 structure, and diversity patterns along major environmental gradients in the Central Tien
551 Shan: Plant Ecology, v. 212, no. 8, p. 1349–1361, doi: 10.1007/s11258-011-9911-5)

552 Tao, S., Yin, X., Jiao, L., Zhao, S., and Chen, L., 2017, Temporal Variability of Source-Specific
553 Solvent-Extractable Organic Compounds in Coastal Aerosols over Xiamen, China:
554 Atmosphere, v. 8, no. 33, doi: 10.3390/atmos8020033

555 Thompson, L. G., Mosley-Thompson, E., Davis, M. E., Mashiotta, T. A., Henderson, K. A., Lin, P.-
556 N., and Tandong, Y., 2006a, Ice core evidence for asynchronous glaciation on the Tibetan
557 Plateau: Quaternary International, v. 154-155, p. 3-10, doi: 10.1016/j.quaint.2006.02.001

558 Thompson, L. G., Tandong, Y., Davis, M., Mosley-Thompson, E., Mashiotta, T. A., Lin, P.-N.,
559 Mikhalenko, V. N., and Zagorodnov, V. S., 2006b, Holocene climate variability archived in
560 the Puruogangri ice cap on the central Tibetan Plateau: Annals of Glaciology, v. 43, p. 61-69

561 Thompson, L. G., Yao, T., Davis, M., Henderson, K. A., Mosley-Thompson, E., Lin, P.-N., Beer, J.,
562 Synal, H.-A., Cole-Dai, J., and Bolzan, J. F., 1997, Tropical Climate Instability:The Last
563 Glacial Cycle from a Qinghai-Tibetan Ice Core: Science, v. 276, no. 5320, p. 1821–1825, doi:
564 10.1126/science.276.5320.1821

565 Thorpe, A., van Anrooy, R., Niyazov, B. N., Sarieva, M. K., Valbo-Jørgensen, J., and Millar, A. M.,
566 2009, The collapse of the fisheries sector in Kyrgyzstan: An analysis of its roots and its
567 prospects for revival: Communist and Post-Communist Studies, v. 42, no. 1, p. 141–163, doi:
568 10.1016/j.postcomstud.2009.02.007

569 Weltje, G. J., and Tjallingii, R., 2008, Calibration of XRF core scanners for quantitative geochemical
570 logging of sediment cores: Theory and application: Earth and Planetary Science Letters, v.
571 274, no. 3–4, p. 423–438, doi: 10.1016/j.epsl.2008.07.054

572 Wright, S. M., Howard, B. J., Strand, P., Nylén, T., and Sickel, M. A. K., 1999, Prediction of $^{137}Cs$
573 deposition from atmospheric nuclear weapons tests within the Arctic: Environmental
574 Pollution, v. 104, no. 1, p. 131–143, doi: 10.1016/S0269-7491(98)00140-7

575 Yang, B., Qin, C., Wang, J., He, M., Melvin, T. M., Osborn, T. J., and Briffa, K. R., 2014, A 3,500-
576 year tree-ring record of annual precipitation on the northeastern Tibetan Plateau: Proc Natl
577 Acad Sci U S A, v. 111, no. 8, p. 2903–2908, doi: 10.1073/pnas.1319238111

578 Yao, T., Thompson, L. G., Mosley-Thompson, E., Zhihong, Y., Xingping, Z., and Lin, P.-N., 1996,
579 Climatological significance of $\delta^{18}O$ in north Tibetan ice cores: Journal of Geophysical
580 Research: Atmospheres, v. 101, no. D23, p. 29531–29537, doi: 10.1029/96jd02683

581 Yokoyama, Y., Koizumi, M., Matsuzaki, H., Miyairi, Y., and Ohkouchi, N., 2010, Developing Ultra
582 Small-Scale Radiocarbon Sample Measurement at the University of Tokyo: Radiocarbon, v.
583 52, no. 2-3, p. 310-318

584 Zhang, H., Wang, R., and Xiao, W., 2017, Paleoenvironmental implications of Holocene long-chain
585 *n*-alkanes on the northern Bering Sea Slope: Acta Oceanologica Sinica, v. 36, no. 8, p. 137–
586 145, doi: 10.1007/s13131-017-1032-0

587 Zhang, J., Ma, X., Qiang, M., Huang, X., Li, S., Guo, X., Henderson, A. C. G., Holmes, J. A., and
588 Chen, F., 2016, Developing inorganic carbon-based radiocarbon chronologies for Holocene
589 lake sediments in arid NW China: Quaternary Science Reviews, v. 144, p. 66–82, doi:
590 10.1016/j.quascirev.2016.05.034

591 Zhou, A., He, Y., Wu, D., Zhang, X., Zhang, C., Liu, Z., and Yu, J., 2015, Changes in the
592 radiocarbon reservoir age in Lake Xingyun, Southwestern China during the Holocene: PLoS
593 One, v. 10, no. 3, p. e0121532, doi: 10.1371/journal.pone.0121532

594 Zhou, K. e., Xu, H., Lan, J., Yan, D., Sheng, E., Yu, K., Song, Y., Zhang, J., Fu, P., and Xu, S., 2020,
595 Variable Late Holocene $^{14}C$ Reservoir Ages in Lake Bosten, Northwestern China: Front.
596 Earth Sci., v. 7, no. 328, doi: 10.3389/feart.2019.00328



This is a provisional file, not the final typeset article

Ziolkowski, L. A., and Druffel, E. R., 2009, Quantification of Extraneous Carbon during Compound Specific Radiocarbon Analysis of Black Carbon: Analytical Chemistry, v. 81, no. 24, p. 10156–10161

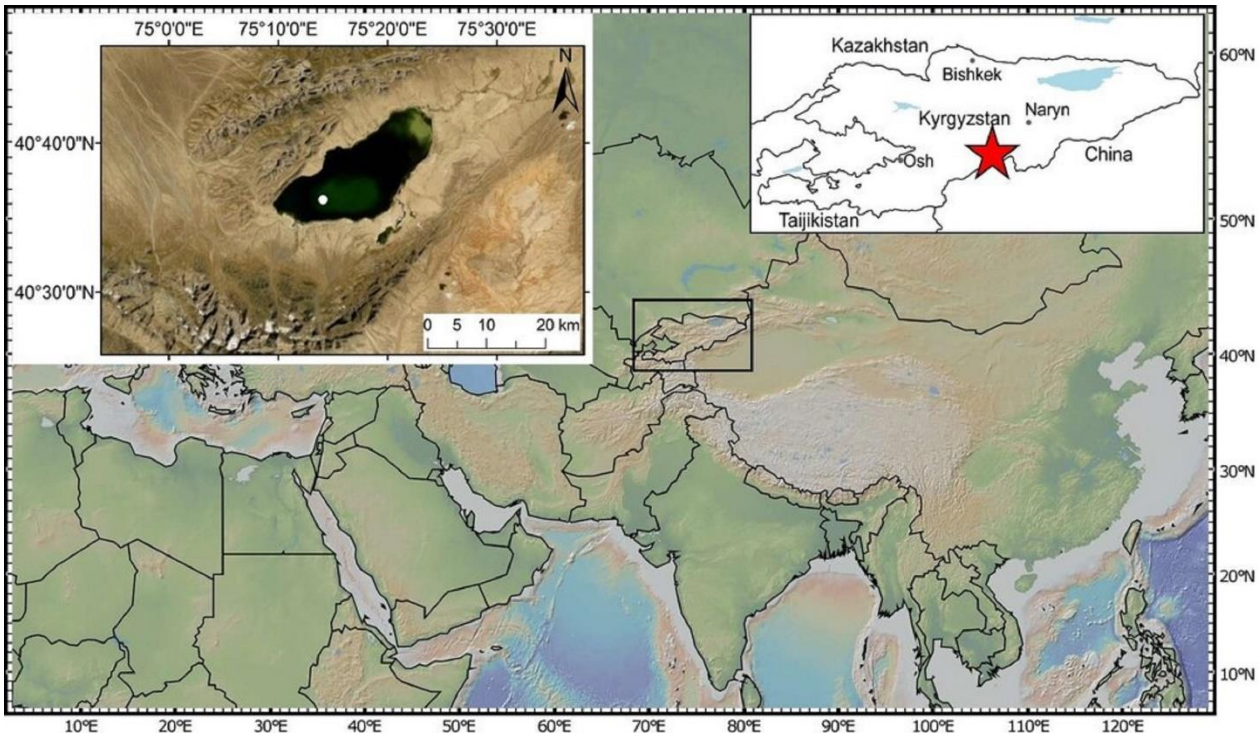


**Figure 1** Location of the study area. The small insert map on the right shows the location of Lake Chatyr Kol (red star) in Kyrgyzstan. The small insert map on the left shows a close-up view of the lake with the coring location (white dot). Figures made with GeoMapApp (www.geomapapp.org) and SimpleMappr (www.simplemappr.net).

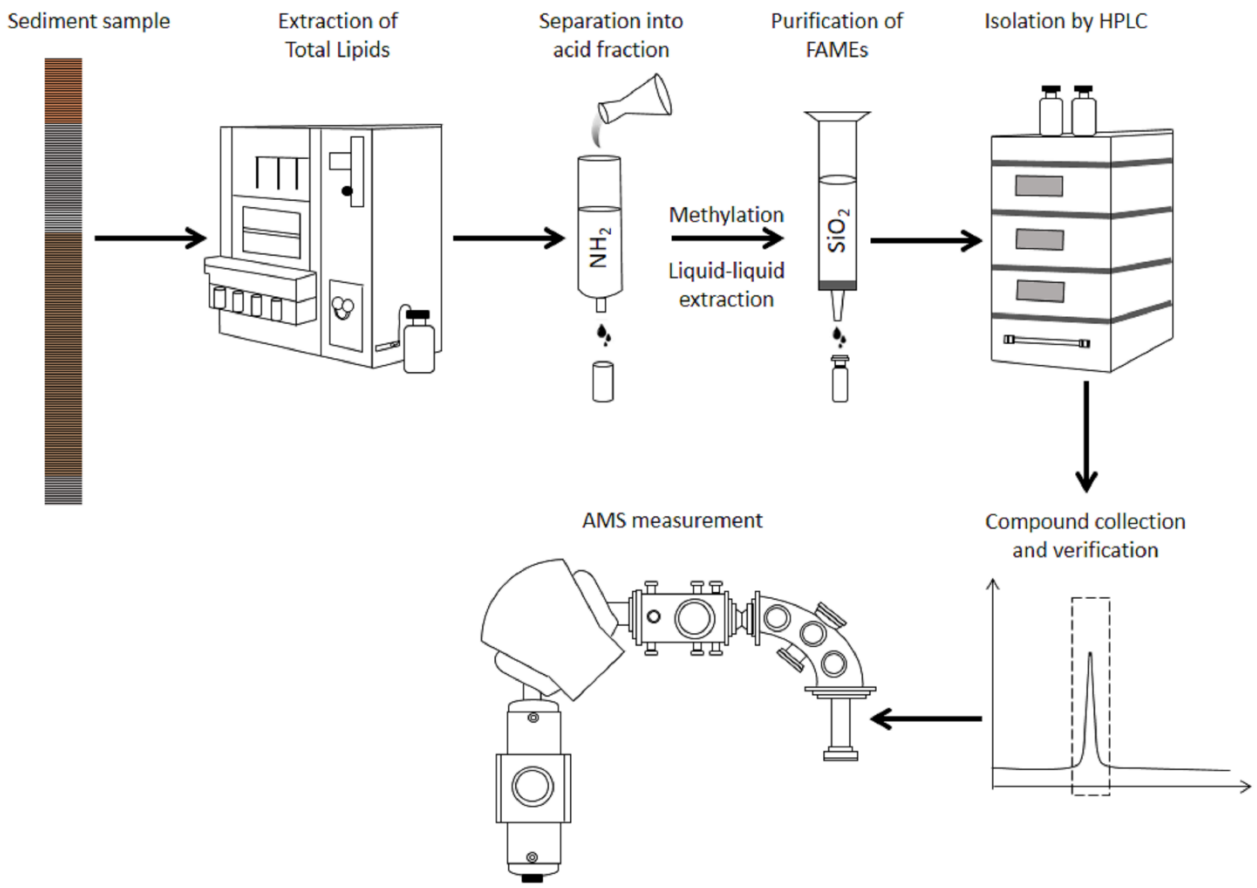


**Figure 2** Schematic workflow diagram of biomarker extraction, purification, isolation and CSRA.

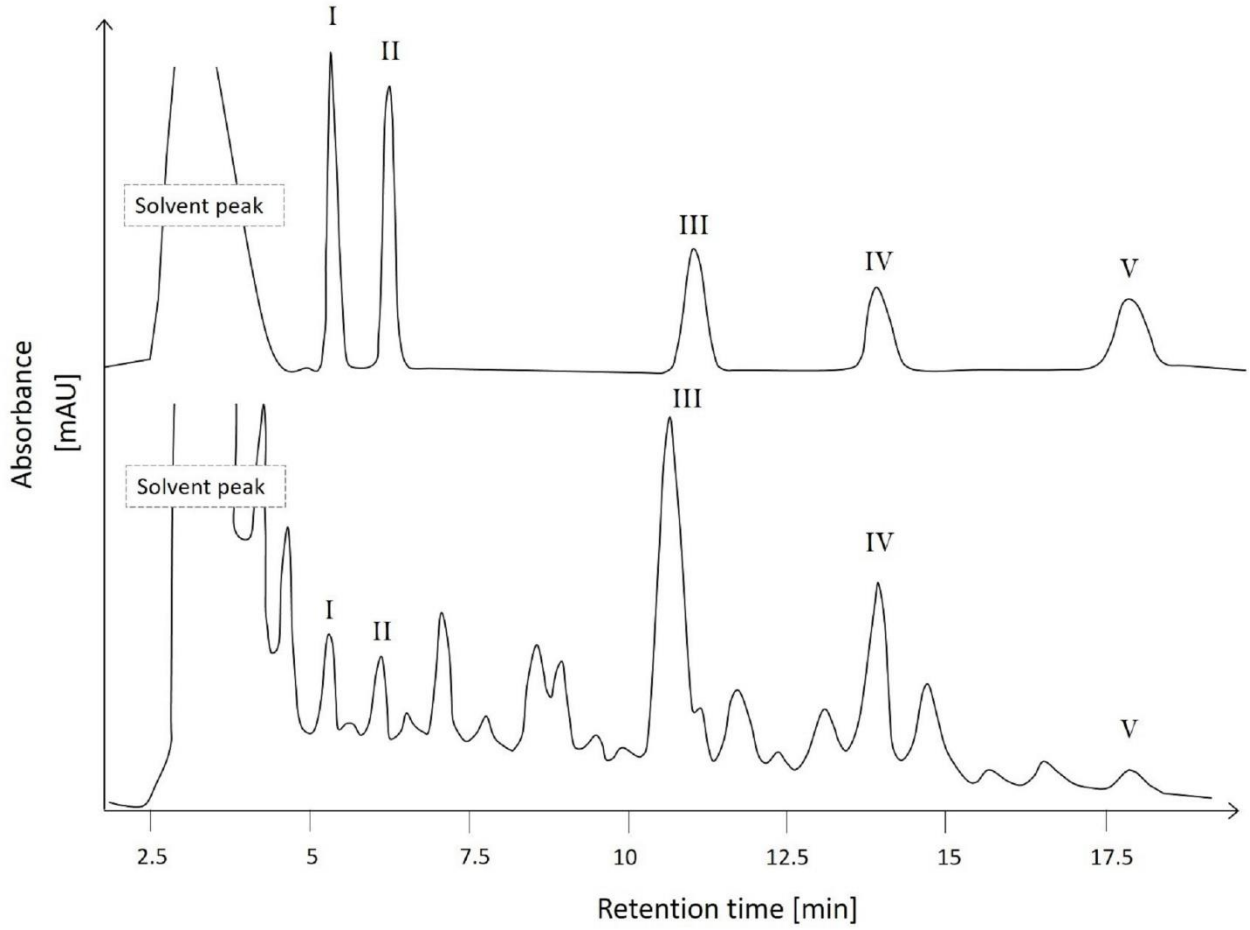


**Figure 3** Typical HPLC-UV/VIS chromatograms of a standard run (upper picture) and a sample run (lower picture). Roman numbers stand for targeted saturated fatty acid methyl esters (FAMEs) with I: C16:0, II: C18:0, III: C24:0, IV: C26:0, V: C28:0.

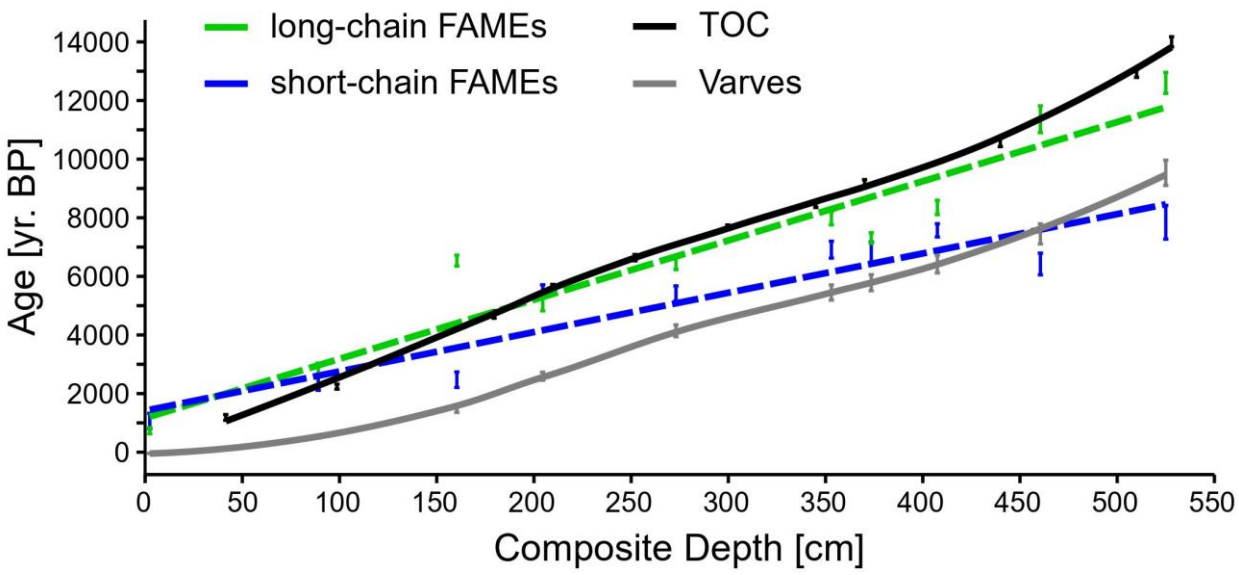


**Figure 4** $^{14}C$ ages of bulk sediment TOC as well as, short-chain and long-chain FAMEs obtained from the CHAT12 sediments in comparison to the varve chronology (Kalanke et al, 2020) reveal a temporally variable lake reservoir effect at Lake Chatyr Kol.

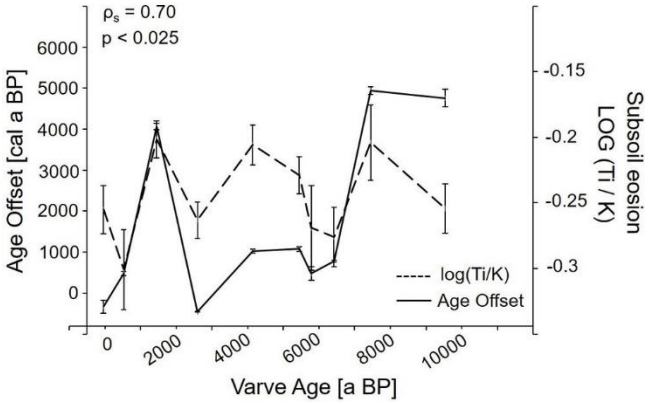


**Figure 5** The observed offset between the long- and short-chain FAMEs is highly correlated to changes in the log(Ti/K) of the sediment, indicating that mobilization of pre-aged OC from the catchment is a major determinant of LRE magnitude. Error bars on the log(Ti/K) data show the standard deviation within a 1.2-cm sediment interval across the positions where samples for CSRA were taken.

# *Supplementary Material*

## 1 Supplementary Data

### 1.1 Supplementary Figures

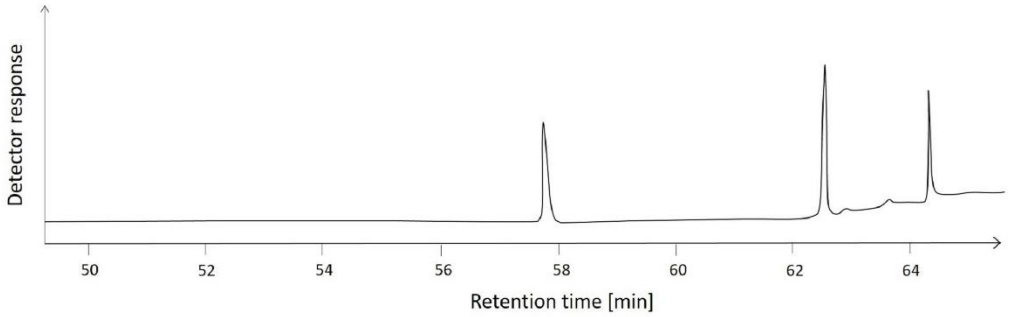


**Supplementary Figure 1.** Typical chromatogram of isolated long-chain fatty acid methyl esters to check for purity. Peaks correspond to C24:0 FAME, C26:0 FAME and C28:0, respectively.

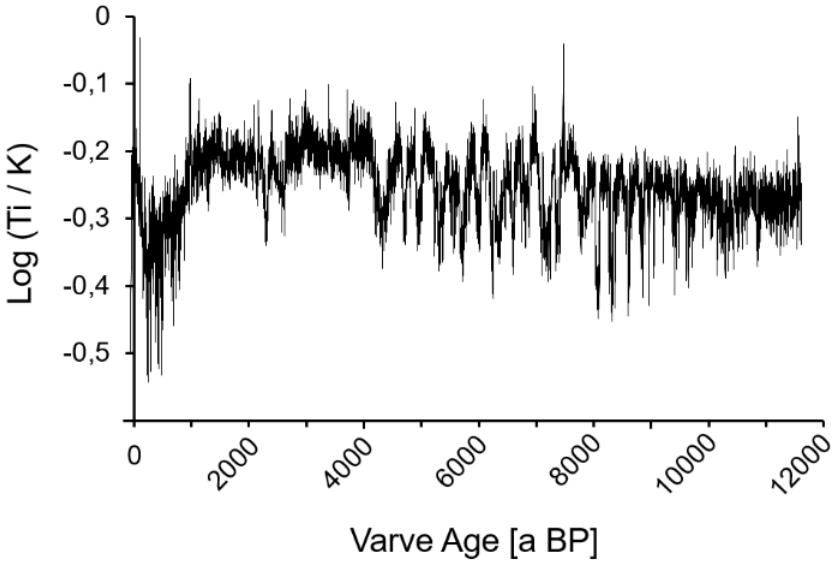


**Supplementary Figure 2**. Ti/K ratio measured with X-ray fluorescence (XRF).

## 1.2 Supplementary Tables

**Supplementary Table 1**. Correction of $F^{14}C$ values for contaminations introduced during compound isolation by HPLC and EA/AMS analysis.

| Fatty acids | Lab code | Depth (cm) | Size (µg C) | $F^{14}C$ AMS uncorrected | Error AMS | $F^{14}C$ corrected | Error corrected | Cal a BP | σ Cal a BP |
|---|---|---|---|---|---|---|---|---|---|
| $C_{16}$, $C_{18}$ | 22331 | 2.4 | 17 | 0.79049 | 0.01363 | 0.86969 | 0.03034 | 1061 | 264 |
| $C_{24}$,$C_{26}$,$C_{28}$ | 22321 | 2.4 | 130 | 0.87197 | 0.01077 | 0.90720 | 0.01342 | 734 | 104 |
| $C_{16}$, $C_{18}$ | 22332 | 89.05 | 34 | 0.69588 | 0.01062 | 0.74955 | 0.01874 | 2362 | 250 |
| $C_{24}$,$C_{26}$,$C_{28}$ | 22322 | 89.05 | 71 | 0.68287 | 0.00947 | 0.71364 | 0.01321 | 2839 | 199 |
| $C_{16}$, $C_{18}$ | 22333 | 160.35 | 30 | 0.68598 | 0.01098 | 0.74096 | 0.02025 | 2473 | 265 |
| $C_{24}$,$C_{26}$,$C_{28}$ | 22310 | 160.35 | 149 | 0.47192 | 0.00777 | 0.49061 | 0.01014 | 6536 | 186 |
| $C_{16}$, $C_{18}$ | 22334 | 204.5 | 89 | 0.51875 | 0.00810 | 0.55158 | 0.01150 | 5497 | 213 |
| $C_{24}$,$C_{26}$,$C_{28}$ | 22323 | 204.5 | 105 | 0.55485 | 0.00839 | 0.57798 | 0.01128 | 5041 | 218 |
| $C_{16}$, $C_{18}$ | 22335 | 273.05 | 49 | 0.51929 | 0.00867 | 0.55574 | 0.01411 | 5415 | 258 |
| $C_{24}$,$C_{26}$,$C_{28}$ | 22311 | 273.05 | 88 | 0.47598 | 0.00791 | 0.49645 | 0.01110 | 6436 | 204 |
| $C_{16}$, $C_{18}$ | 22336 | 353 | 37 | 0.43833 | 0.00818 | 0.47128 | 0.01548 | 6910 | 288 |

| | | | | | | | | | |
|---|---|---|---|---|---|---|---|---|---|
| $C_{24}$,$C_{26}$,$C_{28}$ | 22324 | 353 | 55 | 0.39191 | 0.00770 | 0.41072 | 0.01221 | 7985 | 226 |
| $C_{16}$, $C_{18}$ | 22337 | 373.5 | 28 | 0.43997 | 0.0091 | 0.47599 | 0.01897 | 6826 | 345 |
| $C_{24}$,$C_{26}$,$C_{28}$ | 22312 | 373.5 | 149 | 0.43329 | 0.00754 | 0.45044 | 0.00990 | 7307 | 182 |
| $C_{16}$, $C_{18}$ | 22338 | 407.5 | 51 | 0.40678 | 0.00778 | 0.43495 | 0.01293 | 7570 | 227 |
| $C_{24}$,$C_{26}$,$C_{28}$ | 22325 | 407.5 | 82 | 0.37515 | 0.00729 | 0.39149 | 0.01061 | 8352 | 244 |
| $C_{16}$, $C_{18}$ | 22339 | 460.5 | 26 | 0.45949 | 0.00939 | 0.49809 | 0.02003 | 6422 | 369 |
| $C_{24}$,$C_{26}$,$C_{28}$ | 22326 | 460.5 | 79 | 0.28116 | 0.00676 | 0.29348 | 0.01014 | 11362 | 458 |
| $C_{16}$, $C_{18}$ | 22340 | 525 | 15 | 0.38071 | 0.00931 | 0.42118 | 0.02801 | 7845 | 575 |
| $C_{24}$,$C_{26}$,$C_{28}$ | 22313 | 525 | 111 | 0.25233 | 0.00655 | 0.26271 | 0.00928 | 12602 | 358 |

**Supplementary Table 2**. $^{14}C$ ages of bulk total organic carbon (TOC).

| Material | Lab code | Depth (cm) | Cal a BP | Error |
|---|---|---|---|---|
| bulk TOC | Poz-56609 | 41.5 | 1186 | 98 |
| bulk TOC | Poz-556592 | 98.7 | 2238 | 86 |
| bulk TOC | Poz-56596 | 179.5 | 4699 | 127 |
| bulk TOC | Poz-56610 | 209.7 | 5661 | 64 |
| bulk TOC | Poz-56595 | 252 | 6639 | 107 |
| bulk TOC | Poz-56593 | 299.7 | 7673 | 81 |
| bulk TOC | Poz-54292 | 345 | 8432 | 82 |
| bulk TOC | Poz-56613 | 370.1 | 9157 | 142 |
| bulk TOC | Poz-56611 | 439.9 | 10570 | 143 |
| bulk TOC | Poz-54300 | 510 | 12926 | 136 |
| bulk TOC | Poz-54301 | 528 | 14003 | 172 |

frontiers in Earth Science

ORIGINAL RESEARCH
published: 07 February 2020
doi: 10.3389/feart.2020.00020

# Biomolecular Evidence of Early Human Occupation of a High-Altitude Site in Western Central Asia During the Holocene

*Natalie Schroeter[1], Stefan Lauterbach[2], Martina Stebich[3], Julia Kalanke[4], Jens Mingram[4], Caglar Yildiz[5], Stefan Schouten[5,6] and Gerd Gleixner[1]**

[1] Research Group Molecular Biogeochemistry, Max Planck Institute for Biogeochemistry, Jena, Germany, [2] Leibniz Laboratory for Radiometric Dating and Stable Isotope Research, Kiel University, Kiel, Germany, [3] Senckenberg Research Institute and Natural History Museum Frankfurt – Research Station of Quarternary Palaeontology, Weimar, Germany, [4] Section 4.3 – Climate Dynamics and Landscape Evolution, GFZ German Research Centre for Geosciences, Potsdam, Germany, [5] Department of Marine Microbiology and Biogeochemistry, NIOZ Royal Netherlands Institute for Sea Research, Texel, Netherlands, [6] Department of Earth Sciences, Faculty of Geosciences, Utrecht University, Utrecht, Netherlands

Reconstructions of early human occupation of high-altitude sites in Central Asia and possible migration routes during the Holocene are limited due to restricted archeological sample material. Consequently, there is a growing interest in alternative approaches to investigate past anthropogenic activity in this area. In this study, fecal biomarkers preserved in lake sediments from Lake Chatyr Kol (Tian Shan, Kyrgyzstan) were analyzed to reconstruct the local presence of humans and pastoral animals in this low-human-impact area in the past. Spanning the last ∼11,700 years, this high-altitude site (∼3,500 m above sea level) provides a continuous record of human occupancy in Western Central Asia. An early increase of human presence in the area during the mid-Holocene is marked by a sharp peak of the human fecal sterol coprostanol and its epimer epicoprostanol in the sediments. An associated increase in 5β-stigmastanol, a fecal biomarker deriving from herbivores indicates a human occupancy that most probably largely depended upon livestock. However, sterol profiles show that grazing animals had already occupied the catchment area of Lake Chatyr Kol before and also after a significant presence of humans. The biomarker evidence in this study demonstrates an early presence of humans in a high-altitude site in Central Asia at ∼5,900–4,000 a BP. Dry environmental conditions during this period likely made high altitude regions more accessible. Moreover, our results help to understand human migration in Western Central Asia during the early and mid-Holocene as part of a prehistoric Silk Road territory.

**Keywords: fecal stanols, geochemistry, paleodemography, lake sediments, biomarkers, Silk Road**

OPEN ACCESS

***Edited by:***
*Karen L. Bacon, National University of Ireland Galway, Ireland*

***Reviewed by:***
*Fabien Arnaud, Centre National de la Recherche Scientifique (CNRS), France*
*Nadia Solovieva, University College London, United Kingdom*

****Correspondence:***
*Gerd Gleixner*
*gerd.gleixner@bgc-jena.mpg.de*

***Specialty section:***
*This article was submitted to Quaternary Science, Geomorphology and Paleoenvironment, a section of the journal Frontiers in Earth Science*

***Received:*** *09 September 2019*
***Accepted:*** *22 January 2020*
***Published:*** *07 February 2020*

***Citation:***
*Schroeter N, Lauterbach S, Stebich M, Kalanke J, Mingram J, Yildiz C, Schouten S and Gleixner G (2020) Biomolecular Evidence of Early Human Occupation of a High-Altitude Site in Western Central Asia During the Holocene. Front. Earth Sci. 8:20. doi: 10.3389/feart.2020.00020*

## INTRODUCTION

There is growing evidence that human occupation of high-altitude sites [>3,500 m above sea level (a.s.l.)] has occurred as early as during the latest Pleistocene and Early Holocene (Brantingham et al., 2013; Rademaker et al., 2014; Shnaider S. et al., 2018; Zhang et al., 2018). The highest located and oldest archeological sites have so far been identified on the Tibetan Plateau and in the southern Peruvian Andes, dating back to at least 30,000 and > 11,500 years ago, respectively

(Rademaker et al., 2014; Zhang et al., 2018). Recently, however, Ossendorf et al. (2019) provided evidence of repeated human occupation of Fincha Habera (∼3,500 m a.s.l.), located in Africa's largest alpine landscape, dating back to 47,000–31,000 years ago, which makes it the earliest known high-altitude residential site. These findings indicate that prehistoric human populations were able to adapt to climatic and environmental extremes at high altitudes, such as low temperatures, high solar radiation and low primary productivity, as well as to related physiological challenges, including hypoxia and cold stress (Rademaker et al., 2014; Meyer et al., 2017). The prehistoric settlement of high-altitude regions was likely facilitated by strong immigration from one resource area to another, and/or by biological adaptation to a variable climate and environment (Madsen et al., 2006). In this context, a key period in human history was the onset of the Holocene since the development of more favorable climate conditions promoted both the rise and decline of many prehistoric civilizations (Dong et al., 2012; Thienemann et al., 2017). Additionally, demographic pressure on resources potentially opened previously uninhabitable high-altitude regions, such as the mountain regions of Central Asia, for settlement and migration.

Owing to its location at the crossroads between East and West and the related importance for migration and cultural exchanges (Agatova et al., 2014) for early humans and later as part of the ancient Silk Road, Central Asia has recently become a focus region with respect to investigating the occupation of high-altitude regions by early human civilizations (Bae et al., 2017; Hessl et al., 2017; Shnaider S. et al., 2018; Yang et al., 2019a). Due to the harsh environment, featuring dry deserts, cold mountains and seasonal grasslands, a nomadic pastoral culture has predominantly prevailed in the mountainous regions of Arid Central Asia, which is contrary to Monsoon Asia where sedentary agriculturalists predominated (Hessl et al., 2017; Yang et al., 2019b). Despite its crucial role in cultural development and human migration patterns, little is known about the early history of human occupation of Western Central Asia as part of the Silk Road territory, especially during the period between the Paleolithic and the mid-Holocene (Shnaider S. V. et al., 2018). Western Central Asia encompasses several high-altitude mountain regions, such as the Tian Shan, the Pamir Mountains and the Alay Mountains (Shnaider S. et al., 2018). There is evidence that the Alay Mountains may represent the high-altitude region in Western Central Asia that has at first been occupied by humans and was at least temporarily inhabited by hunter-gatherers since the Paleolithic (Ranov, 1975; Abdykanova, 2014; Shnaider S. et al., 2018; Taylor et al., 2018). However, the early colonization of high-altitude Central Asia by humans is still not well-constrained (Rademaker et al., 2014). Generally, the success of tracing human presence in such regions largely relies on finding related archeological sites and respective artifacts. However, as this is often hindered by a limited number of settlements and small sample sizes, there has been a growing interest in alternative approaches to detect early anthropogenic activity. In this context, the identification of sterols and stanols as fecal biomarkers is an emergent valuable analytical tool that can provide evidence for the presence of both humans and livestock at a certain site. Fecal sterols and stanols are recalcitrant organic compounds, which can accumulate and persist in sediments for 1000s of years (Bull et al., 2001, 2003). 5β-Stanols, notably coprostanol (5β-cholestan-3β-ol) and 5β-stigmastanol (24β-ethyl-5β-cholestan-3β-ol), are the products of anaerobic microbial reduction of sterols, i.e., cholesterol (Cholest-5-en-3β-ol), in the intestinal tract of mammals (Eyssen et al., 1973; Macdonald et al., 1983). Owing to their herbivorous diet, ruminant feces are largely composed of 5β- stigmastanol and epi-5β-stigmastanol (24β-ethyl-5β-cholestan-3α-ol), which are derived from β-sitosterol (3β-Stigmast-5-en-3-ol) and stigmasterol (Stigmasta-5,22-dien-3β-ol), the most common and the third most common phytosterol (plant sterol), respectively (Evershed et al., 1997; Bull et al., 2002; Rogge et al., 2006). Conversely, coprostanol, a cholesterol derivative, accounts for ∼60% of the total sterols in human feces (Leeming et al., 1996; Bull et al., 2002; Daughton, 2012). Therefore, human fecal input can be distinguished from those of herbivores (Leeming and Nichols, 1996; Leeming et al., 1996; Ortiz et al., 2016), enabling their use in paleoenvironmental and archeological studies (e.g., Baeten et al., 2012; D'Anjou et al., 2012; Gea et al., 2017; Engels et al., 2018; White et al., 2018).

Since sterols and stanols are well-preserved in lacustrine sediments, the latter provide an ideal natural archive for tracing the sources of feces in the environment and for assessing human and livestock occupation of a certain area through time, both qualitatively and quantitatively (D'Anjou et al., 2012; White et al., 2018; Kinder et al., 2019). Furthermore, the vicinity of lakes and rivers provides ideal conditions for natural settlements as well as important pathways for human migration (Thienemann et al., 2017).

In this study we analyzed coprostanol, epicoprostanol, cholesterol, cholestanol and 5β-stigmastanol as fecal biomarkers in the sediments of Lake Chatyr Kol, in the central Tian Shan of Kyrgyzstan to elucidate the local presence of humans and livestock during the Holocene. Investigating the history of human occupation of this part of the Tian Shan can potentially contribute to a better understanding of its cultural importance as a prehistoric trade and migration route along the ancient Silk Road.

## Study Area

Lake Chatyr Kol (40°37′ N, 75°18′ E) is located at 3,535 m a.s.l. in the southern Tian Shan of Kyrgyzstan, close to the border to China (**Figure 1**). The lake occupies the south-western part of a large intra-montane basin between the At Bashy Range in the north and the Torugart pass in the south. To the west of Lake Chatyr Kol lies the Arpa river valley and moraine landscape. Lake Chatyr Kol is the third largest lake in Kyrgyzstan (Thorpe et al., 2009) and has a catchment area of approximately 1,084 $km^2$. The lake extends to a maximum width (NW-SE) of 12 km and a maximum length (SW-NE) of 23 km and has a surface water area of ∼175 $km^2$ (Mosello, 2015). Since Lake Chatyr Kol is a hydrologically closed alpine lake, the lake water is slightly brackish (salinity 1.18 g/l in July 2018) and its water balance is generally controlled by the interplay between snow meltwater and precipitation input and evaporation. The largest and only permanent inflow is the Kekagyr River, which enters

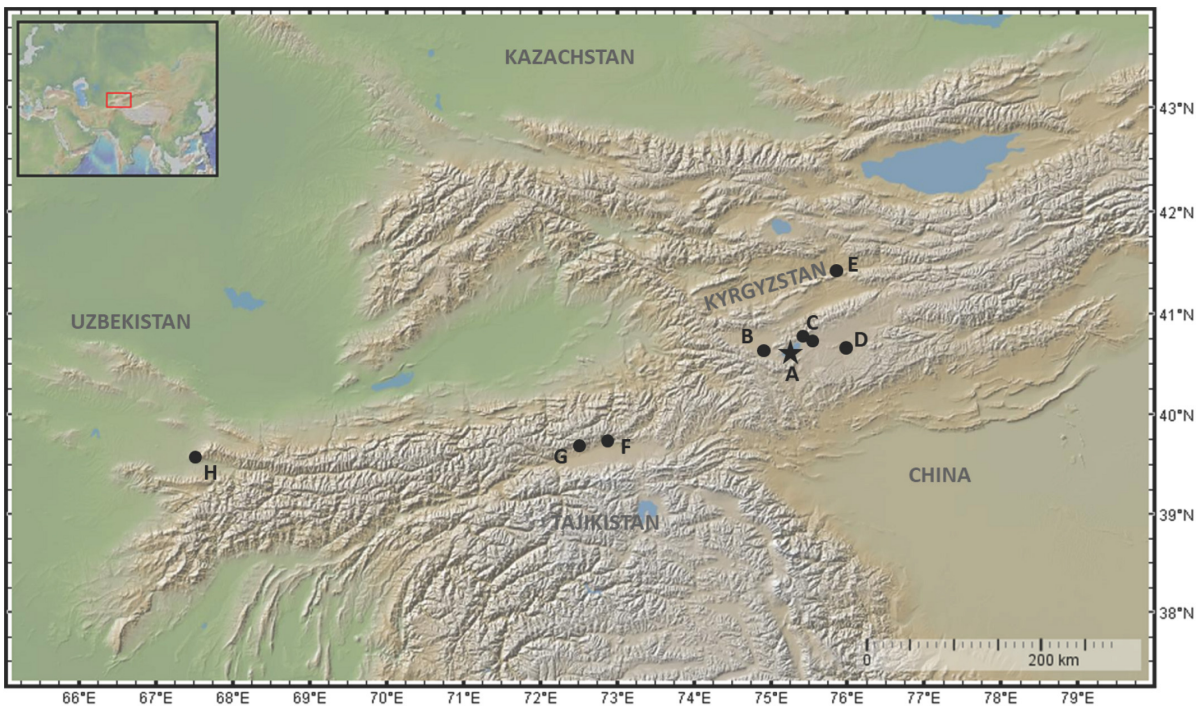


**FIGURE 1 |** Map of Central Asia showing the study site Lake Chatyr Kol (indicated by a black star) and other sites mentioned in this study. A = Lake Chatyr Kol; B = Grotto Semetey (Abdykanova, 2014); C = Kok-Aygyr (Ranov and Kydyrov, 1969); D = Terek-1 (Ranov, 1975); E = Aigyrzhal-2 (Motuzaite Matuzeviciute et al., 2017); F = Alay Valley (Shnaider S. et al., 2018); G = Chegirtke Cave (Taylor et al., 2018); H = Sarazm (Spengler and Willcox, 2013). Figure made with GeoMapApp (www.geomapapp.org, Ryan et al., 2009).

the lake from the north-east. The present-day regional climate is temperate continental (Wang et al., 2017) and dominated by the interaction between the Siberian anticyclonic circulation and the mid-latitude Westerlies (Aizen et al., 1997; Lauterbach et al., 2014). Owing to the high mountain ranges of the Tian Shan that prevent the transport of moisture, rainfall is reduced, especially in January and February (Aizen et al., 1995, 2001). Mean annual precipitation consequently amounts to only ∼300 mm/a (Koppes et al., 2008). The mean annual air temperature (1961–1990) in Naryn, ∼100 km northeast of Lake Chatyr Kol, is −0.34°C (Ilyasov et al., 2013) and the lake is generally ice covered from October to April. The prevailing dry and cold conditions favor the preservation of permafrost soils (Shnitnikov et al., 1978) and thermokarst formations can be frequently observed in this region (Abuduwaili et al., 2019). Due to the harsh climate conditions, vegetation is sparse and classified as desert and semi-desert vegetation. Alpine grasslands dominate this region (Taft et al., 2011) and there are no trees in the surrounding of the lake.

## MATERIALS AND METHODS

### Sediment Material and Chronology

In July/August 2012, several vertically overlapping, 2-m-long sediment cores have been recovered from about 20 m water depth in the deep south-western part of Lake Chatyr Kol (40°36.37′ N, 75°14.02′ E) by using a 60 mm diameter UWITEC piston corer. Additionally, seven parallel gravity cores have been withdrawn in 2017 by utilizing a UWITEC gravity corer with hammer weight (SC17_1–7). The individual sediment cores were stratigraphically linked using distinct macroscopically visible correlation layers, allowing the construction of a continuous, 623.5-cm-long composite profile (Kalanke et al., Under review). With the exception of the upper 63 cm, the sediments are almost continuously annually laminated (varved). The floating varve age model (**Figure 2**), labeled "Chatvd19," was established using replicate microscopic varve counts below 63.0 cm depth, which were performed on petrographic thin sections (Kalanke et al., Under review) prepared at the GFZ German Research Centre for Geosciences, Potsdam, Germany. Replicate varve counts yield a mean deviation of ∼5% which was applied as an uncertainty for the varved composite profile between 623.5–63.0 cm depth. The uppermost homogenous 63.0 cm of the composite profile were chronologically constrained by gamma spectrometric analysis of $^{210}$Pb and $^{137}$Cs performed at the GFZ German Research Centre for Geosciences, Potsdam, Germany, on 0.5 cm thick sediment slices of the parallel gravity core SC17_7. $^{210}$Pb activity concentrations were used for age model constructions based on a constant initial concentration (CIC) model (cf. Appleby, 2002) and on a constant rate of supply (CRS) model (Appleby and Oldfield, 1978) in combination with $^{137}$Cs activity concentrations. Both $^{210}$Pb models are in good accordance with the onset of elevated $^{137}$Cs activity concentrations, representing the onset of global nuclear weapon

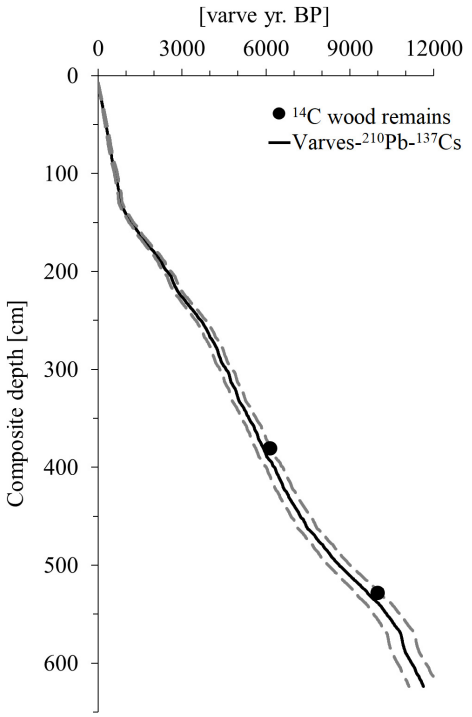


**FIGURE 2 |** Age model of the Lake Chatyr Kol sediment record (Kalanke et al., Under review). The age model (black line) is based on varve counting combined with $^{210}$Pb and $^{137}$Cs measurements. Dashed lines indicate the varve counting error (Kalanke et al., Under review). Black dots with 2 σ error ranges represent AMS $^{14}$C dates of terrestrial plant macro remains.

tests since AD 1945 (Kudo et al., 1998; Wright et al., 1999). The non-varved interval between the time marker AD 1945 and the onset of varve deposition at 63.0 cm depth was interpolated by using a mean sedimentation rate derived from varve thickness measurements of adjacent varved intervals with an assumed uncertainty of 10%. The final floating varve chronology had a basal age of 11619 ± 603 a BP and was independently verified by two AMS $^{14}$C ages of terrestrial wood remains at a composite depth of 380.5 and 528 cm (Poz-63307 and Poz-54302) (Kalanke et al., Under review). AMS $^{14}$C measurements were conducted at the Poznań Radiocarbon Laboratory in Poland and the conventional $^{14}$C ages were calibrated with OxCal 4.3 (Bronk Ramsey, 1995) using the IntCal13 calibration curve (Reimer et al., 2013). All age dates of Lake Chatyr Kol samples reported in this study refer to the described age model.

## Pollen Analyses

Pollen analyses have been carried out on 152 sediment samples. The samples have been collected volumetrically (ranging between 1–2.6 cm$^3$) at intervals of 4 cm on average from sediment depth between 0.5 and 623 cm. The preparation involved treatment with HCl, KOH, HF, hot acetolysis mixture and ultrasonic sieving (mesh size 6 × 8 μm), following the standard methods described by Berglund and Ralska-Jasiewiczowa (1986). Lycopodium spores were added to each sample to calculate the pollen concentrations. Sample residues were stained with safranine, mounted in glycerine and analyzed using an Olympus BX 40 light microscope at ×400–1000 magnification. With the exception of six samples, a minimum of 500 terrestrial pollen grains was counted. The identification of the palynomorphs was carried out with the aid of the palynological reference collection of the Senckenberg Research station of Quaternary Palaeontology, Weimar, supported by different pollen atlases (Beug, 2004; Reille, 1995–1999). Pollen percentages were calculated on the basis of terrestrial pollen, excluding aquatics, spores and non-pollen palynomorphs.

## Fecal Biomarker Analyses

For the present study, bulk sediment samples of 1 cm thickness were taken from the Lake Chatyr Kol composite profile at 5 cm intervals and subsequently freeze-dried. The freeze-dried bulk sediment samples were homogenized and lipids were extracted twice with a dichloromethane/methanol solvent mixture (9:1, v:v) by using a pressurized solvent speed extractor (E-916, BÜCHI, Essen, Germany) operated at 100°C and 120 bar for 15 min. Subsequently, the total lipid extract of each sample was partitioned into a neutral and an acid fraction by elution over aminopropyl gel columns (CHROMABOND® $NH_2$ polypropylene columns, 60 Å, Macherey-Nagel GmbH & Co., KG, Düren, Germany) with dichloromethane/isopropanol (3:1, v:v) and diethyl ether:acetic acid (19:1, v:v), respectively (Richey and Tierney, 2016). The neutral fraction was further separated over activated silica gel columns (∼2 g, 0.040–0.063 mm mesh, Merck, Darmstadt, Germany) into hydrocarbons, ketones and a polar fraction by elution with hexane, dichloromethane and methane, respectively. The hydrocarbon fraction, containing long-chain *n*-alkanes, was analyzed using a gas chromatograph (GC) with flame ionization detection (GC-FID, Agilent 7890B GC) and an Ultra 2 column (50 m length, 0.32 mm ID, 0.52 μm film thickness, Agilent Technologies, Santa Clara, CA, United States). The GC oven temperature program started at 140°C (hold for 1 min), heated up to 310°C at 4°C/min (hold for 15 min) and finally increased to 325°C at 30°C/min (hold for 3 min). The PTV injector was operated in splittless mode and started at 45°C (hold for 0.1 min) and increased to 300°C at 14.5°C/s (hold for 3 min). The quantification of long-chain *n*-alkanes was carried out by peak area comparison with an external *n*-alkane standard mixture ($nC_{15}$–$nC_{33}$).

The polar fraction, containing sterols and stanols, was silylated with 10 μL N,O-*bis*(trimethylsilyl)trifluoroacetamide (BSTFA) and 10 μL pyridine at 60°C for 30 min and afterward dissolved in ethyl acetate. Sterol and stanol concentrations were measured at the Royal Netherlands Institute for Sea Research (NIOZ), Texel, Netherlands, as described by de Bar et al. (2019). Gas chromatographic separation was carried out utilizing an Agilent 7890B GC that was equipped with a fused silica capillary column (Agilent CP Sil-5, length 25 m, diameter 320 μm, film thickness 0.12 μm) and coupled to an Agilent 5977A MSD mass spectrometer (MS). The GC temperature program started at 70°C, increased to 130°C at a rate of 20°C/min, then heated to 320°C at 4°C/min and was held at 320°C for 25 min. The flow rate was 2 mL/min. The MS quadrupole was held at 150°C

and the electron impact ionization energy of the MS source was set to 70 eV. Sterols were identified and quantified via single ion monitoring (SIM) of the mass-to-charge-ratios m/z 368.3 (cholesterol), 398.3 (stigmastanol) and 370.3 (cholestanol). Additionally, characteristic mass spectra fragmentation patterns and relative retention times were compared with the literature for further identification. Coprostanol and epicoprostanol were additionally confirmed using reference standards. An external coprostanol reference standard in five different concentrations was used for quantification of the sterols.

In order to account for microbial degradation processes, we applied the ratio established by Bull et al. (1999):

$$\frac{\text{coprostanol} + \text{epicoprostanol}}{\text{coprostanol} + \text{epicoprostanol} + 5\alpha - \text{cholestanol}} = \text{R1}$$

5α-cholestanol is a product of the degradation of cholesterol by soil microbial communities (Wakeham, 1989; Bull et al., 2001). Therefore, considering both 5α-cholestanol and coprostanol allows to compare input and preservation of stanols in a specific environment to stanol input from feces (White et al., 2018). In particular, higher R1 values indicate increased human fecal input, while lower R1 values reflect low human fecal deposition.

In addition, we utilized the ratio proposed by Evershed and Bethell (1996) to distinguish between human and higher mammal feces:

$$\frac{\text{coprostanol}}{5\beta - \text{stigmastanol}} = \text{R2}$$

with R2 values > 1.5 suggesting human or porcine fecal matter (Evershed and Bethell, 1996).

In order to determine distinct temporal intervals in the Lake Chatyr Kol sediment record, we used Uniform Manifold Approximation and Projection (UMAP), a novel nonmetric manifold learning technique for dimension reduction (McInnes et al., 2018) implemented in R 3.6 as package "umap" 0.2.3.1 (Konopka, 2019; R Core Team, 2019). UMAP was recently shown to preserve more of the global structure compared to previous nonmetric techniques such as t-SNE (van der Maaten and Hinton, 2008; McInnes et al., 2018). The improved preservation of global structures in UMAP allowed the use of k-means clustering on the resulting graph. We supplied the UMAP algorithm with the biomarker profiles as well as their chronology and interpreted the resulting three clusters as distinct temporal intervals in the sediment core (Phases I, II, and III) (**Supplementary Figure S1**). Data visualizations were performed in R package "ggplot2" 3.2.1 (Wickham, 2016).

# RESULTS AND DISCUSSION

## Vegetation Development

The Holocene vegetation development of Lake Chatyr Kol has been derived from 152 pollen samples collected between 0.5 and 623 cm composite core depth. The sampling intervals yield a temporal resolution of 77 years on average. Total pollen concentration is circa 30,000–60,000 grains per $cm^3$ through most of the sequence. Overall, 83 pollen taxa were distinguished, consisting of 20 arboreal and 63 non-arboreal elements. The pollen assemblages are characterized by predominance of non-arboreal taxa contributing between 88.3 and 99.6% to the terrestrial pollen assemblage (**Supplementary Table S1**). The herbaceous flora is mainly composed of *Artemisia* (34–61%), Chenopodiaceae (15–29%), Poaceae (7–24%), and Cyperaceae (0.2–6.9%). Other herbs occur in smaller quantities or only scattered, each contributing between 0 and 8%. Most abundant woody taxa are *Juniperus* (0–6.6%), *Betula* (0–3.4%), *Hippophaë* (0–1.8%) and *Picea* (0–1.7%), while other tree pollen taxa appear in trace amounts (**Supplementary Table S1**).

The dominance of xerophytic herbs and the sparse representation of trees and shrubs reveal an open landscape character in the surroundings of the Chatyr Kol Lake throughout the Holocene (**Figure 3**). According to studies on modern pollen assemblages in central and eastern Asia, herbaceous pollen composition of the Chatyr Kol Lake sediments mainly reflects semi-arid, alpine meadow, steppe, and lake shore communities (Beer et al., 2007; Ma et al., 2008; Qin et al., 2015). In terms of the overall species composition, the pollen signatures show only gradual changes through the entire record. Therefore, the alpine landscape of the study region experienced no major vegetation shifts during the past 11.5 ka.

## Sedimentary Fecal Biomarker Distribution

Several fecal biomarkers were detected in the Lake Chatyr Kol sediments of which five sterols and stanols, i.e., cholesterol, coprostanol, epicoprostanol, 5β-stigmastanol and 5α-cholestanol, were quantified. Their total sum reveals a strong increase from relatively low concentrations in the oldest part of the composite profile [∼146 μg/g dry weight (d.w.)] to higher amounts (5,342 μg/g d.w.) at a composite depth of 319.5 cm (∼4,900 a BP) (**Figure 3**). The total concentration of sterols and stanols ranged between 0.2 and 5,800 μg/g d.w. The most abundant sterol throughout the record is cholesterol (46%), followed by 5β-stigmastanol (21%).

The sediment record was divided into three distinct phases based on three distinct k-means clusters within a UMAP ordination of the fecal biomarker data (**Figure 4** and **Supplementary Figure S1**). Phase I (∼11,400–8,300 a BP) shows conditions of prehuman occupation with low background concentrations of human-specific fecal sterols and stanols (coprostanol, epicoprostanol, and cholesterol). However, considerable amounts of 5α-cholestanol and 5β-stigmastanol are present throughout Phase I, indicating the presence of indigenous higher mammals. First noticeable human activity is recorded during Phase II (∼7,600–2,400 a BP), which is characterized by strong concentration increases in all fecal biomarkers at three time points, dating to ∼5,900, ∼4,800, and ∼2,400 a BP, respectively. This phase represents the beginning of human occupation in the catchment area of Lake Chatyr Kol, possibly with domesticated livestock, since both human-specific and higher mammals-specific fecal biomarkers increase significantly during Phase II. In relation to the total amount of fecal

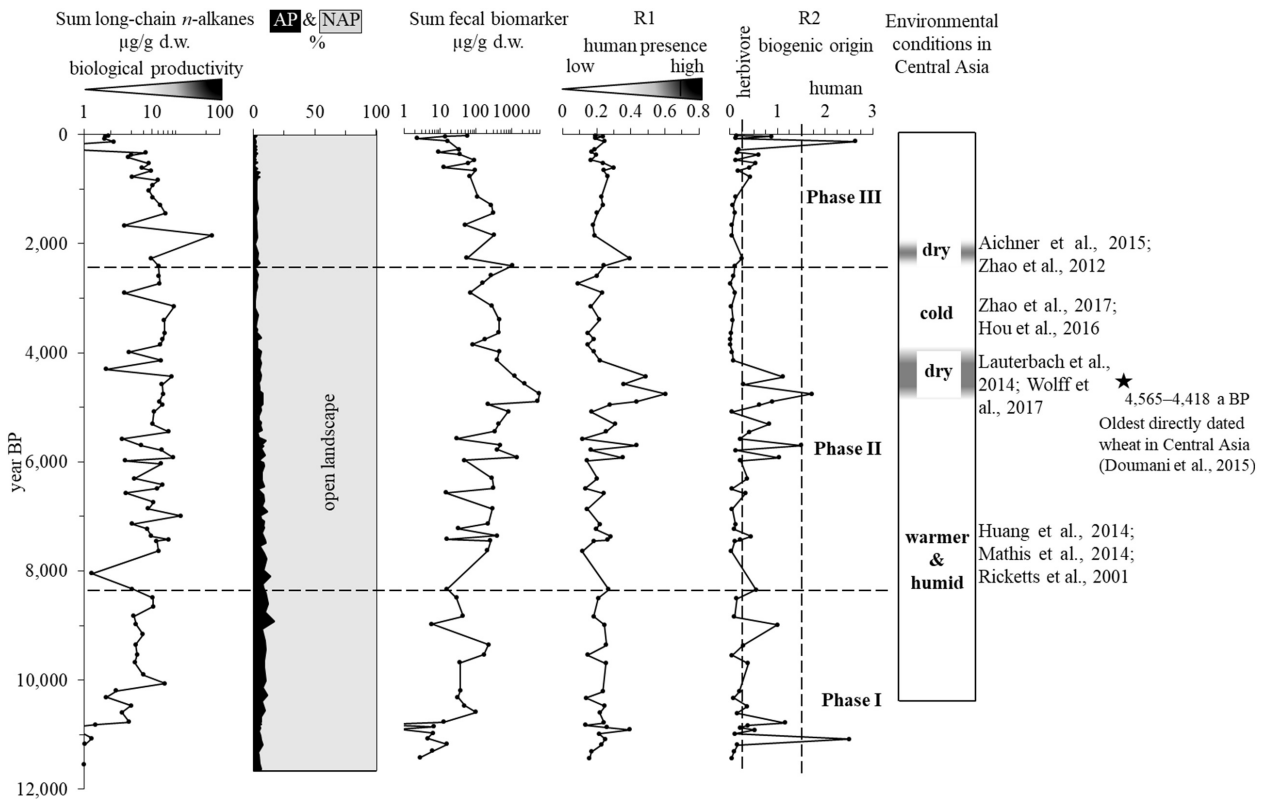


**FIGURE 3 |** Profiles of the sum of long-chain n-alkanes ($nC_{27}$ + $nC_{29}$ + $nC_{31}$), pollen percentages of arboreal pollen (AP, black area) and non-arboreal pollen (NAP, gray area) with AP + NAP = 100%, sum of fecal biomarkers, R1 (coprostanol + epicoprostanol)/(coprostanol + epicoprostanol + 5α–cholestanol), R2 (coprostanol/5β– stigmastanol) and environmental conditions during the Holocene. Time periods of increased human presence at ∼4,800 and ∼2,500 a BP seem to coincide with dry phases.

biomarkers, the imprint of human presence was highest at ∼4,800 a BP, where concentrations reach their maxima. Additionally, there are intervals within Phase II, which show decreased values of human-specific fecal biomarkers, especially during ∼3,800 –2,700 a BP, whereas concentrations of 5β-stigmastanol are still elevated. The beginning of Phase III (<2,300 a BP) is marked by a decline of all biomarkers toward background concentrations comparable to Phase I. Phase III continues to modern times and displays the current low level of human occupation of the catchment area of Lake Chatyr Kol.

## Sources of Analyzed Fecal Biomarkers

In order to disentangle the sources of the sterols and stanols, we applied principal component analysis (PCA). PC1 and PC2 account for 96.2% of the total variance and show a clear distinction between the fecal biomarkers cholesterol, coprostanol and epicoprostanol, which are associated to a carnivorous and omnivorous diet, and the herbivore-derived fecal biomarker 5β-stigmastanol (**Figure 5**). We utilized cholesterol, coprostanol and epicoprostanol as human-specific biomarkers; however it is possible that carnivorous animals may have contributed to this biomarker signal. The strong linear correlation between the concentrations of coprostanol and epicoprostanol ($r^2$ = 0.9) and coprostanol and cholesterol ($r^2$ = 0.92) additionally confirms a combined source of these compounds (**Supplementary Figure S2**). This confirms coprostanol, epicoprostanol, and cholesterol as human biomarkers and 5β-stigmastanol as being indicative of grazing animals including domesticated livestock.

Since 5β-stanol background concentrations are also detectable in soils that were not exposed to fecal deposition, diagnostic ratios of selected sterols that are independent of total concentrations are advantageous for the interpretation of the total fecal biomarker spectrum (Grimalt et al., 1990; Bull et al., 1999, 2001). In this context, several ratios of different sterol and stanol classes have been proposed to determine the origin of organic matter and to detect anthropogenic activity (Grimalt et al., 1990; Bull et al., 2002; Martins et al., 2007). In order to determine the fecal origin of our sterols and stanols, we applied ratio R1 proposed by Bull et al. (1999). By including epicoprostanol, R1 corrects for microbial degradation processes since coprostanol may be microbially degraded *in situ* to epicoprostanol (Bull et al., 1999, 2002; Battistel et al., 2015).

R1 values for the sediments of Lake Chatyr Kol range between 0.09 and 0.6 (**Figure 3**). A R1 value of 0.7 has been proposed as a threshold with higher R1 values indicating human fecal deposition and lower values reflecting scarce human presence (Grimalt et al., 1990). The values in the Lake Chatyr Kol sediments, however, do not exceed this threshold but as it was

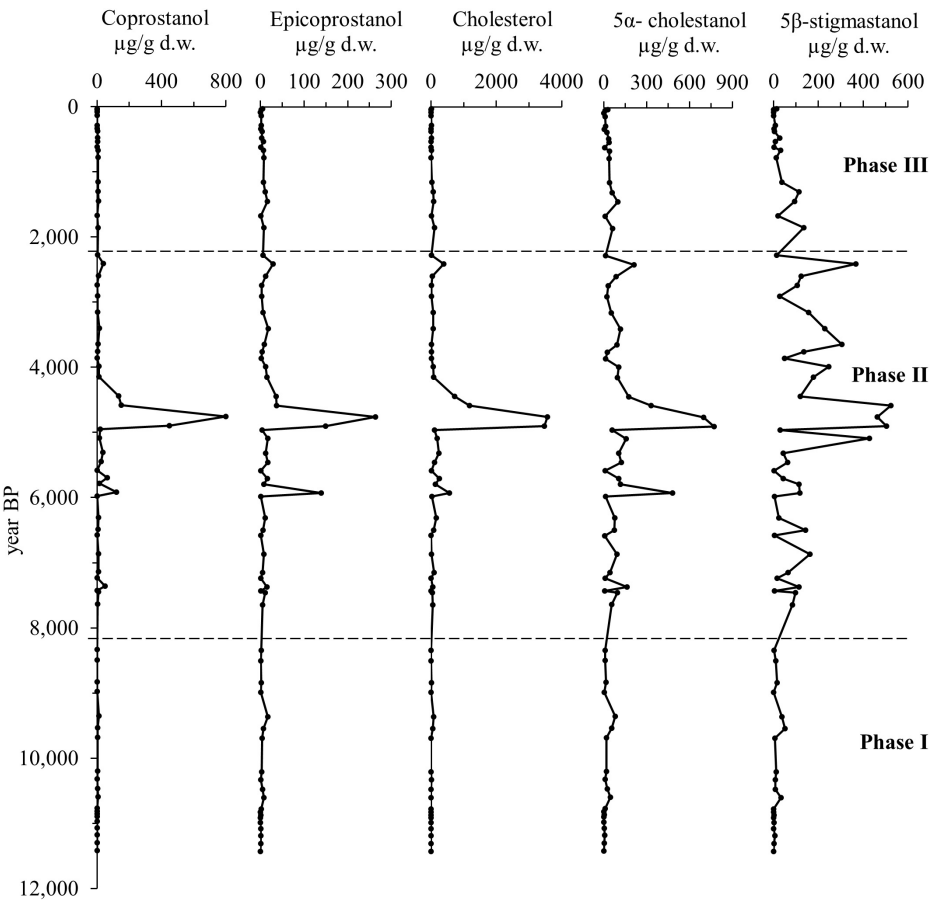


**FIGURE 4 |** Fecal sterol and stanol concentrations in the Lake Chatyr Kol sediments. Dashed horizontal lines indicate different time periods discussed in this study.

originally determined from modern-day urban sewage pollution investigations, it may not be applicable in an archeological context (Bull et al., 2001; Birk et al., 2011; Baeten et al., 2012). Nevertheless, elevated R1 values during Phase II, especially at ∼4,800 a BP (R1 = 0.6), demonstrate the fecal nature of the 5β-stanols and most likely indicate the presence of humans during the mid-Holocene (**Figure 3**).

To allow for the discrimination between human and herbivore fecal deposition, the ratio of coprostanol and 5β-stigmastanol (R2) was established (Evershed and Bethell, 1996), which is based on the divergent biogenic origin of these 5β-stanols. As a result of their herbivorous diet and the associated high uptake of phytosterols, ruminant feces are enriched in 5β-stigmastanol, whereas coprostanol is the major sterol in human and omnivore feces. Typically, R2 values between 1.5 and 5.5 are indicative of humans and pigs, while R2 values in the order of ∼0.25 imply herbivorous fecal input (Baeten et al., 2012).

R2 values in the Lake Chatyr Kol sediment record fluctuate between 0.003 and 2.6 (**Figure 3**). Highest R2 values of 2.5 and 2.6 are observed at ∼11,100 and ∼132 a BP, respectively (**Figure 3**). However, these values are controlled by particularly low amounts of 5β-stigmastanol and may therefore not necessarily reflect human activity. Conversely, slightly elevated R2 values (>1.5) during Phase II at ∼5,700 and ∼4,800 a BP confirm a human origin of the stanols and reinforce the assumption of an early human occupation of the Lake Chatyr Kol catchment area during the mid-Holocene. In this context, generally lower R2 values during Phase I and Phase III indicate predominant herbivore origin of the stanols during the Early and Late Holocene, respectively (**Figure 3**).

## Holocene Human and Mammal Presence in the Lake Chatyr Kol Catchment Area

### Phase I (∼11.4k – 8,300 a BP)

The beginning of the Holocene was characterized by a global temperature rise (Marcott et al., 2013). Such more favorable climate conditions may have boosted human migration as climate is generally considered a key factor for cultural and social development (DeMenocal, 2001; Flohr et al., 2016). Direct evidence of human occupation of Kyrgyzstan during this period was observed in the western part of the Alay Valley in southern Kyrgyzstan at an elevation of ∼2,800 m a.s.l. (Shnaider S. et al., 2018), where findings of stone tool assemblages suggest the local presence of prehistoric humans during the Late Pleistocene or Early Holocene, supposedly mainly

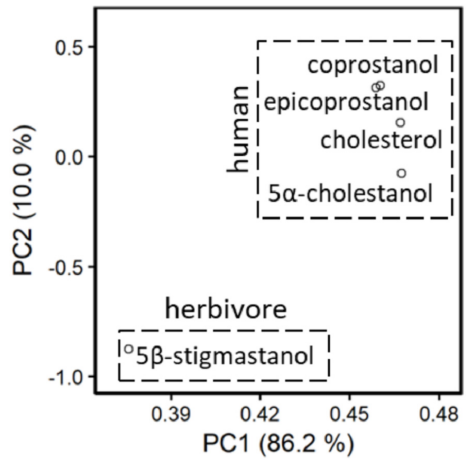


**FIGURE 5 |** Principal component analysis (PCA) of fecal sterols. The separation indicates different sources for coprostanol, epicoprostanol, cholesterol, 5α-cholestanol, and 5β- stigmastanol.

consuming sheep (Shnaider S. et al., 2018; Taylor et al., 2018). Furthermore, archaeological findings close to Lake Chatyr Kol indicated the presence of humans in the area around the lake during the Mesolithic and Neolithic. Ranov and Kydyrov (1969) described findings of stone tools at two archaeological sites at Kok-Aygyr, northeast of Lake Chatyr Kol. The relative ages of these archaeological sites were established by assigning a series of characteristic artifacts to a local culture dated to 9,530 ± 130 a. Furthermore, Ranov (1975) reported findings from the archaeological site Terek-1, ∼40 km east of Lake Chatyr Kol, described as likely Neolithic based on the composition and craftwork of the excavated assemblages.

The Lake Chatyr Kol fecal sterol record does not indicate local human presence during the Early Holocene as the amounts of coprostanol, epicoprostanol, and cholesterol remained near the background values (median values for Phase I: 0.72, 1.19, and 1.72 μg/g d.w., respectively) (**Figure 4**). Yet, elevated concentrations of 5α-cholestanol and 5β-stigmastanol indicate an increased presence of indigenous higher mammals in the catchment area during the Early Holocene. The first biomarker evidence for an increased occurrence of higher mammals at Lake Chatyr Kol is found at ∼10,600 and ∼9,500 a BP (**Figure 4**). The occupation by mammals over a prolonged period during the Early Holocene is further supported by generally higher 5β-stigmastanol concentrations between ∼8,300 and ∼8,500 a BP. More temperate climate conditions in Kyrgyzstan during this time were inferred from analyzing the sediments of Lake Son Kul, located ∼125 km north of Lake Chatyr Kol (Huang et al., 2014; Mathis et al., 2014) and Lake Issyk-Kul, located ∼242 km northeast of Lake Chatyr Kol (Ricketts et al., 2001).

In order to estimate the flux of vegetation remains within the catchment area of Lake Chatyr Kol independently from the fecal biomarkers, we analyzed the concentrations of long-chain *n*-alkanes ($nC_{27}$, $nC_{29}$, $nC_{31}$). An increase in the concentration of long-chain *n*-alkanes would imply enhanced organic productivity, since these compounds are commonly found in terrestrial sources, such as terrestrial plants and grasses (Eglinton and Hamilton, 1967; Meyers, 2003). Both long-chain *n*-alkanes and arboreal pollen increase at the beginning of the early Holocene (**Figure 3**). It is therefore likely that more temperate climate conditions promoted the growth of terrestrial vegetation, resulting in improved habitability of the Lake Chatyr Kol catchment area.

## Phase II (∼7,600–2,400 a BP)

The earliest biomolecular evidence of human presence in the Lake Chatyr Kol catchment is provided by significant increases in the concentrations of coprostanol, epicoprostanol, and cholesterol at ∼5,900 a BP and particularly at ∼4,800 a BP (**Figure 4**). This is further supported by elevated R1 and R2 values (**Figure 3**). Since 5β-stigmastanol concentrations also reveal maximum values at the same time, it is likely that human presence at that time was associated with domesticated livestock. Variations in the concentrations of fecal sterols suggest that the population size of the first human occupancy was low in relation to the human presence at ∼4,800 a BP as changes in the human and livestock population would inevitably entail changes in the concentrations of fecal sterols being transported to the lake (cf. D'Anjou et al., 2012).

The biomarker evidence for human presence at Lake Chatyr Kol during Phase II coincides with findings of stone tool assemblages from Grotto Semetey situated in the adjoining Arpa river valley dating to ∼5,700 and ∼6,180 cal a BP (Abdykanova, 2014).

Archeological findings of ceramic fragments and radiocarbon dating of animal bones (4,240–3,990 cal a BP) at Chegirtke Cave in southern Kyrgyzstan indicate that humans started to occupy the mountain foothills of the Alay Valley at least during the early Bronze Age (Taylor et al., 2018). Since the excavated bone fragments at this site belong to sheep, goat, and cattle, it can be concluded that they represent a pastoral assemblage of domestic animals (Taylor et al., 2018). This would support our assumption of a livestock-herding human occupancy around Lake Chatyr Kol at ∼4,800 a BP. Evidence of human occupancy during the Bronze Age is provided by archeological excavations at the closely nearby site Aigyrzhal-2 (2,005 m a.s.l.) in central Kyrgyzstan, ∼97 km northeast of Lake Chatyr Kol (Motuzaite Matuzeviciute et al., 2017). Domestic animal remains, such as horse and ovicaprines, and remains of cereals (grains and chaff), indicate that humans in the Tian Shan mountain valleys developed agricultural interests during this period (Motuzaite Matuzeviciute et al., 2017). Yet, at the high-altitude site Lake Chatyr Kol pollen analysis did not indicate agricultural practice. The oldest directly dated wheat remains in Central Asia have been found in Tasbas, eastern Kazakhstan, and have been dated to ∼4,500 cal a BP (Doumani et al., 2015). Based on archaeobotanical and carbon isotope data of human bones and dating of crop remains found in prehistoric sites in Eurasia, Dong et al. (2017) suggested that western Asian crops spread to eastern Central Asia and northwestern China between 4,500 and 4,000 a BP. Further evidence of early agricultural and herding practice in Central Asia stems from the Eneolithic/Early

Bronze Age site of Sarazm in northwestern Tajikistan (Frachetti, 2012; Spengler and Willcox, 2013). Sarazm was a sedentary agropastoral settlement, which was occupied from the fourth to the end of the third millenium BC and provides evidence for exchange and trade (Spengler and Willcox, 2013).

Paleoenvironmental studies from Kyrgyzstan indicate rather dry conditions during Phase II. Lauterbach et al. (2014) reported a pronounced dry interval for Lake Son Kul between 4,950 and 3,900 cal a BP. In accordance, a stalagmite record from Uluu-2 Cave, ∼250 km west of Lake Chatyr Kol, also suggests dry conditions between 4,700 and 3,900 cal a BP (Wolff et al., 2017). These dry conditions likely entailed the necessity of exploiting new herding grounds and correspondingly affected migration flows. Human settlement and local herding within the catchment area of Lake Chatyr Kol were likely favored by an open landscape and herbaceous vegetation as indicated by pollen data (**Figure 3**).

Phase II is mainly characterized by a high amount of long-chain *n*-alkanes, which is in line with the presence of herbivores in general (**Figure 3**; R2). The high amounts of the human specific fecal biomarkers, however, cover only a short period of time that is defined by a reduced flux of vegetation remains. Further, pollen data do not indicate significant increases or compositional changes of the local vegetation. We therefore suggest the reported dryness likely influenced the presence of humans at Lake Chatyr Kol rather than an enhanced supply of vegetation resources. As there are no pollen data indicative of agricultural practices, the catchment area of Lake Chatyr Kol was likely inhabited by pastoralists rather than agro-pastoralists.

Concentrations of human-specific fecal sterols returned to background values between ∼3,900 a BP and ∼2,400 a BP (**Figure 4**) and 5β-stigmastanol concentrations decreased similarly at ∼3,900 a BP. The decline in the fecal sterol concentrations was probably triggered by a shift to colder climate conditions as reconstructed for Lake Karakul in NE Tajikistan (∼240 km southwest of Lake Chatyr Kol) at ∼3,500 cal a BP, for Lake Balikun, eastern Tian Shan Mountains, between 4,800 and 3,800 cal a BP (Zhao et al., 2017) and for Lake Qinghai, located in the northeast corner of the Tibet-Qinghai Plateau Qinghai, between 5,000 and 3,500 cal a BP (Hou et al., 2016). 5β-Stigmastanol concentrations however increase again shortly afterward to relatively high amounts at ∼3,600 a BP, indicating herbivore activity without a significant presence of human activity.

The latest short-term increase of human-specific fecal sterol concentrations occurred between ∼2,500 and ∼2,400 a BP. As previously observed, this increase is accompanied by a simultaneous increase of 5β-stigmastanol concentrations, suggesting livestock farming. Interpreting these elevated concentrations in the context of local environmental conditions, they again appear to have contemporaneously occurred to dry climate conditions. For example, a warm and dry episode has been identified at Lake Karakuli, ∼240 km south of Lake Chatyr Kol, between 2,500 and 1,900 cal a BP (Aichner et al., 2015). Pollen data from the Kashgar oasis at the western margin of the Tarim Basin show sparse vegetation cover from 2,620 to 1,750 cal a BP, indicating a relatively dry climate (Zhao et al., 2012). Similarly, Mischke et al. (2010) reported low freshwater inflow and a low lake level for Lake Karakul between 2,600 and 1,900 cal a BP.

### Phase III (∼2,300 a BP – Present)

Phase III is characterized by generally low concentrations of coprostanol, epicoprostanol and cholesterol, suggesting scarce human presence within the catchment area of Lake Chatyr Kol. 5β-Stigmastanol concentrations remained on an intermediate level between ∼1,900 and ∼1,300 a BP but significantly dropped thereafter (**Figure 4**).

The economy of Kyrgyzstan largely relies on the agricultural sector and seminomadic lifestyles continue to exist until present-day (Rahimon, 2012). A survey of pastoralists in Kyrgyzstan revealed that in AD 2004 only 12 herding families encamped the vicinity of Lake Chatyr Kol, owning livestock of not more than 12,000 sheep (Farrington, 2005). At present, the basin of Lake Chatyr Kol is little used, with the majority of occupancy occurring during the summer months from June to mid- September (Farrington, 2005). This could explain the low amounts of fecal sterols in the youngest part of the Lake Chatyr Kol sediment record.

## Cultural Importance of the Tian Shan

Being located along the ancient Silk Road, the territory of Kyrgyzstan represented an important corridor for cultural exchange and trade in the past. The Silk Road was a complex network of trade and travel routes, which enabled both cultural interaction and the trading of goods between Central Asia, the Middle East and the Eastern Mediterranean (Hansen, 2012; Yang et al., 2019b). Therefore, it functioned as a "Cultural Bridge" between Asia and Europe (Foltz, 2010; Yang et al., 2019b) and had a profound influence on societal development. Even though the relevance of the Silk Road is conventionally constrained to the second century BC, exchange and migration occurred well before that (Taylor et al., 2019). Archeological studies elucidated that ancient trade and travel routes along this corridor already existed during the Bronze Age (third to second millenium BC) (Frank and Thompson, 2005; Frachetti et al., 2017; Panyushkina et al., 2019), although details about pathways and exact timing are still uncertain.

The progression of mobile pastoralist groups during the Bronze Age is considered to have contributed to the evolvement of high-elevation pathways across the Silk Road, but more research is needed to determine their extent (Frachetti et al., 2017). Nevertheless, interrelations and early diffusions of technologies between mobile pastoralist economies across Eurasia occurred from the third to the second millenium BC (Mei, 2003; Spengler et al., 2014).

This is in good agreement with our observation of elevated fecal sterol amounts at ∼4,800 year. BP, indicating anthropogenic and livestock presence. Indeed, it is suggested that the Tian Shan was already occupied by pastoralists during the Bronze Age (Motuzaite Matuzeviciute et al., 2017). Along with the Pamir, Dzhungar and Altai mountains, the Tian Shan is part of a proposed "Inner Asian Mountain Corridor" (Frachetti, 2012), which promoted the exchange of goods, culture flow (Spengler and Willcox, 2013) and the earliest diffusion of sheep and goat

pastoralism to inner Asia at ∼3,500 BC (Frachetti, 2012). Routes of nomadic societies near Lake Chatyr Kol have been indicated by Frachetti et al. (2017), who used flow accumulation modeling to assess migration along the Silk Road. Specifically, the model results revealed a path crossing the Torugart Pass in the south, highlighting the importance of Lake Chatyr Kol as a likely transit stop along herding routes.

Considering that the human-specific fecal sterols in the Lake Chatyr Kol sediment record diminished at ∼ 3,900 year. BP, it is likely that mobile non-sedentary pastoralists occupied the Lake Chatyr Kol catchment area around ∼4,800 year. BP but later left the area again, probably focusing on other, more habitable regions. The migration from one region to another after the consumption of resources in one area is commonly observed along the Silk Road (Yang et al., 2019b). This does not necessarily entail the collapse of a population, but rather reflects high adaptability and resilience of social groups (Yang et al., 2019b).

In summary, our study indicates human migration in the area around Lake Chatyr Kol as early as during the early Bronze Age, centuries before the establishment of the Silk Road. This reinforces the influence of small-scale migration patterns on the evolution of a macro-scale trade and exchange network (Frachetti et al., 2017).

## CONCLUSION

The present study demonstrates the usefulness of fecal biomarker analyses as a valuable tool to reconstruct temporal anthropogenic presence in an area as an alternative approach in archeological studies. Such biomarker analyses applied to the sediments of Lake Chatyr Kol, Kyrgyzstan reveal a pronounced population evolvement in the Tian Shan at ∼4,800 a BP. Coinciding dry environmental conditions likely increased the accessibility of high-altitude regions and necessitated the exploitation of new herding grounds. This finding suggests climatic change, inter alia, as a potential driver for human migration and underlines the ability of early humans to adapt to variable environmental conditions. Migration through the high-altitude terrains of the Tian Shan reveals its cultural importance as an early travel corridor during the Bronze Age. As one of the rare high-altitude sites providing evidence of early pastoralists, Lake Chatyr Kol is of great importance for the understanding of the human history and migration in Eurasia.

## DATA AVAILABILITY STATEMENT

The datasets generated for this study are available on request to the corresponding author.

## AUTHOR CONTRIBUTIONS

GG conceived the research idea. SL conducted the field work. MS contributed pollen data. JK and JM generated the age model. NS conducted laboratory analysis and data analysis with support from SS and CY. NS prepared the manuscript. All authors discussed the data and improved the manuscript.

## FUNDING

This study was supported by the BMBF-funded research projects CADY (Central Asian Climate Dynamics, Grant No. 03G0813) and CAHOL (Central Asian Holocene Climate, Grant No. 03G0864). NS acknowledges the Max Planck Society and the International Max Planck Research School for Global Biogeochemical Cycles (IMPRS-gBGC) for additional project funding.

## ACKNOWLEDGMENTS

The authors thank Michael Köhler, Sylvia Pinkerneil, Roman Witt, and Robert Schedel for their help during field work and Stefanie Garz for her help during pollen analysis.

## SUPPLEMENTARY MATERIAL

The Supplementary Material for this article can be found online at: https://www.frontiersin.org/articles/10.3389/feart.2020.00020/full#supplementary-material

## REFERENCES

Abdykanova, A. (2014). New data on mesolithic and neolithic in Kyrgyzstan: a brief review. *Bull. IICAS Pub. Int. Inst. Centr. Asian Stud.* 20, 5–19.

Abuduwaili, J., Issanova, G., and Saparov, G. (2019). *Lakes in Kyrgyzstan, Hydrology and Limnology of Central Asia*. Singapore: Springer, 288–294. doi: 10.1007/978-981-13-0929-8

Agatova, A. R., Nepop, R. K., Slyusarenko, I. Y., Myglan, V. S., Nazarov, A. N., and Barinov, V. V. (2014). Glacier dynamics, palaeohydrological changes and seismicity in southeastern Altai (Russia) and their influence on human occupation during the last 3000 years. *Quat. Int.* 324, 6–19. doi: 10.1016/j.quaint.2013.07.018

Aichner, B., Feakins, S. J., Lee, J. E., Herzschuh, U., and Liu, X. (2015). High-resolution leaf wax carbon and hydrogen isotopic record of the late Holocene paleoclimate in arid Central Asia. *Clim. Past* 11, 619–633. doi: 10.5194/cp-11-619-2015

Aizen, E. M., Aizen, V. B., Melack, J. M., Nakamura, T., and Ohta, T. (2001). Precipitation and atmospheric circulation patterns at mid-latitudes of Asia. *Int. J. Climatol.* 21, 535–556. doi: 10.1002/joc.626

Aizen, V., Aizen, E., and Melack, J. (1995). Climate, snow cover, glaciers, and runoff in the Tien Shan, Central Asia. *J. Am. Water Resour. Bull.* 31, 1113–1129. doi: 10.1111/j.1752-1688.1995.tb03426.x

Aizen, V., Aizen, E., Melack, J., and Dozier, J. (1997). Climatic and hydrologic changes in the Tien Shan, Central Asia. *J. Clim.* 10, 1393–1404. doi: 10.1175/1520-0442(1997)010<1393:CAHCIT>2.0.CO;2

Appleby, P. G. (2002). "Chronostratigraphic techniques in recent sediments," in *Tracking Environmental Change Using Lake Sediments*, eds W. M. Last, and J. P. Smol, (Dordrecht: Springer), 171–203. doi: 10.1007/0-306-47669-x_9

Appleby, P. G., and Oldfield, F. (1978). The calculation of lead-210 dates assuming a constant rate of supply of unsupported 210Pb to the sediment. *Catena* 5, 1–8. doi: 10.1016/S0341-8162(78)80002-2

Bae, C. J., Douka, K., and Petraglia, M. D. (2017). On the origin of modern humans: Asian perspectives. *Science* 358:eaai9067. doi: 10.1126/science.aai9067

Baeten, J., Marinova, E., De Laet, V., Degryse, P., De Vos, D., and Waelkens, M. (2012). Faecal biomarker and archaeobotanical analyses of sediments from a public latrine shed new light on ruralisation in Sagalassos, Turkey. *J. Archaeol. Sci.* 39, 1143–1159. doi: 10.1016/j.jas.2011.12.019

Battistel, D., Piazza, R., Argiriadis, E., Marchiori, E., Radaelli, M., and Barbante, C. (2015). GC-MS method for determining faecal sterols as biomarkers of human and pastoral animal presence in freshwater sediments. *Anal. Bioanal. Chem.* 407, 8505–8514. doi: 10.1007/s00216-015-8998-2

Beer, R., Heiri, O., and Tinner, W. (2007). Vegetation history, fire history and lake development recorded for 6300 years by pollen, charcoal, loss on ignition and chironomids at a small lake in southern Kyrgyzstan (Alay Range. Central Asia). *Holocene* 17, 977–985. doi: 10.1177/0959683607082413

Berglund, B. E., and Ralska-Jasiewiczowa, M. (1986). "Pollen analysis and pollen Diagrams," in *Handbook of Holocene Palaeoecology and Palaeohydrology*, ed. B. E. Berglund, (Chichester: Wiley), 455–484.

Beug, H. J. (2004). *Leitfaden der Pollenbestimmung für Mitteleuropa und Angrenzende Gebiete, 21*. Munich: Dr. Friedrich Pfeil.

Birk, J. J., Teixeira, W. G., Neves, E. G., and Glaser, B. (2011). Faeces deposition on Amazonian Anthrosols as assessed from 5β-stanols. *J. Archaeol. Sci.* 38, 1209–1220. doi: 10.1016/j.jas.2010.12.015

Brantingham, P. J., Xing, G., Madsen, D. B., Rhode, D., Perreault, C., van der Woerd, J., et al. (2013). Late occupation of the high-elevation northern Tibetan Plateau based on cosmogenic, luminescence, and radiocarbon ages. *Geoarchaeology* 28, 413–431. doi: 10.1002/gea.21448

Bronk Ramsey, C. (1995). Radiocarbon calibration and analysis of stratigraphy: the OxCal program. *Radiocarbon* 37, 425–430. doi: 10.1017/s0033822200030903

Bull, I. D., Elhmmali, M. M., Roberts, D. J., and Evershed, R. P. (2003). The application of steroidal biomarkers to track the abandonment of a Roman wastewater course at the Agora (Athens, Greece). *Archaeometry* 45, 149–161. doi: 10.1111/1475-4754.00101

Bull, I. D., Evershed, R. P., and Betancourt, P. P. (2001). An organic geochemical investigation of the practice of manuring at a Minoan site on Pseira Island, Crete. *Geoarchaeology* 16, 223–242. doi: 10.1002/1520-6548(200102)16:2<223::aid-gea1002<3.0.co;2-7

Bull, I. D., Lockheart, M. J., Elhmmali, M. M., Roberts, D. J., and Evershed, R. P. (2002). The origin of faeces by means of biomarker detection. *Environ. Int.* 27, 647–654. doi: 10.1016/s0160-4120(01)00124-6

Bull, I. D., Simpson, I. A., Van Bergen, P. F., and Evershed, R. P. (1999). Muck 'n' molecules: organic geochemical methods for detecting ancient manuring. *Antiquity* 73, 86–96. doi: 10.1017/s0003598x0008786x

D'Anjou, R. M., Bradley, R. S., Balascio, N. L., and Finkelstein, D. B. (2012). Climate impacts on human settlement and agricultural activities in northern Norway revealed through sediment biogeochemistry. *Proc. Natl. Acad. Sci. U.S.A.* 109, 20332–20337. doi: 10.1073/pnas.1212730109

Daughton, C. G. (2012). Real-time estimation of small-area populations with human biomarkers in sewage. *Sci. Total Environ.* 414, 6–21. doi: 10.1016/j.scitotenv.2011.11.015

de Bar, M. W., Ullgren, J. E., Thunnell, R. C., Wakeham, S. G., Brummer, G.-J. A., Stuut, J.-B. W., et al. (2019). Long-chain diols in settling particles in tropical oceans: insights into sources, seasonality and proxies. *Biogeosciences* 16, 1705–1727. doi: 10.5194/bg-16-1705-2019

DeMenocal, P. B. (2001). Cultural responses to climate change during the late holocene. *Science* 292, 667–673. doi: 10.1126/science.1059827

Dong, G., Jia, X., An, C., Chen, F., Zhao, Y., Tao, S., et al. (2012). Mid-Holocene climate change and its effect on prehistoric cultural evolution in eastern Qinghai Province, China. *Quat. Res.* 77, 23–30. doi: 10.1016/j.yqres.2011.10.004

Dong, G., Yang, Y., Han, J., Wang, H., and Chen, F. (2017). Exploring the history of cultural exchange in prehistoric Eurasia from the perspectives of crop diffusion and consumption. *Sci. China Earth Sci.* 60, 1110–1123. doi: 10.1007/s11430-016-9037-x

Doumani, P., Frachetti, M., Beardmore, R., Schmaus, T., Spengler, R. N. III, and Mar'yashev, A. (2015). Burial ritual, agriculture, and craft production among Bronze age pastoralists at Tasbas (Kazakhstan). *Archaeol. Res. Asia* 1–2, 17–32. doi: 10.1016/j.ara.2015.01.001

Eglinton, G., and Hamilton, R. (1967). Leaf epicuticular waxes. *Science* 156, 1322–1335. doi: 10.1126/science.156.3780.1322

Engels, S., van Oostrom, R., Cherli, C., Dungait, J. A. J., Jansen, B., van Aken, J. M., et al. (2018). Natural and anthropogenic forcing of Holocene lake ecosystem development at lake Uddelermeer (The Netherlands). *J. Paleolimnol.* 59, 329–347. doi: 10.1007/s10933-017-0012-x

Evershed, R. P., and Bethell, P. H. (1996). Application of multimolecular biomarker techniques to the identification of fecal material in archaeological soils and sediments. *Archaeol. Chem.* 625, 157–172. doi: 10.1021/bk-1996-0625.ch013

Evershed, R. P., Bethell, P. H., Reynolds, P. J., and Walsh, N. J. (1997). 5β-stigmastanol and related 5β-stanols as biomarkers of manuring: analysis of modern experimental material and assessment of the archaeological potential. *J. Archaeol. Sci.* 24, 485–495. doi: 10.1006/jasc.1996.0132

Eyssen, H. J., Parmentier, G. G., Compernolle, F. C., De Pauw, G., and Piessens-Denef, M. M. (1973). Biohydrogenation of sterols by *Eubacterium* ATCC 21,408 — nova species. *Eur. J. Biochem.* 36, 411–421. doi: 10.1111/j.1432-1033.1973.tb02926.x

Farrington, J. D. (2005). De-development in Eastern Kyrgyzstan and persistence of semi-nomadic livestock herding. *Nomad. Peoples* 9, 171–197. doi: 10.3167/082279405781826191

Flohr, P., Fleitmann, D., Matthews, R., Matthews, W., and Black, S. (2016). Evidence of resilience to past climate change in Southwest Asia: early farming communities and the 9.2 and 8.2 ka events. *Quat. Sci. Rev.* 136, 23–39. doi: 10.1016/j.quascirev.2015.06.022

Foltz, R. (2010). *Religions of the Silk Road: Premodern Patterns of Globalization*. New York, NY: Palgrave Macmillan.

Frachetti, M. D. (2012). Multiregional emergence of mobile pastoralism and nonuniform institutional complexity across Eurasia. *Curr. Anthropol.* 53, 2–38. doi: 10.1086/663692

Frachetti, M. D., Smith, C. E., Traub, C. M., and Williams, T. (2017). Nomadic ecology shaped the highland geography of Asia's Silk Roads. *Nature* 543, 193–198. doi: 10.1038/nature21696

Frank, A. G., and Thompson, W. R. (2005). Afro-Eurasian bronze age economic expansion and contraction revisited. *J. World Hist.* 16, 115–172. doi: 10.1353/jwh.2005.0142

Gea, J., Sampedro, M. C., Vallejo, A., Polo-Diaz, A., Goicolea, M. A., Fernandez-Eraso, J., et al. (2017). Characterization of ancient lipids in prehistoric organic residues: chemical evidence of livestock-pens in rock-shelters since early neolithic to bronze age. *J. Sep. Sci.* 40, 4549–4562. doi: 10.1002/jssc.201700692

Grimalt, J. O., Fernandez, P., Bayona, J. M., and Albaiges, J. (1990). Assessment of fecal sterols and ketones as indicators of urban sewage inputs to coastal waters. *Environ. Sci. Technol.* 24, 357–363. doi: 10.1021/es00073a011

Hansen, V. (2012). *The Silk Road: A New History*. Oxford: Oxford University Press.

Hessl, A. E., Leland, C., Saladyga, T., and Byambasuren, O. (2017). "Hydraulic cities, colonial catastrophes, and nomadic empires: human-environment interactions in Asia," in *Dendroecology: Tree-Ring Analyses Applied to Ecological Studies*, eds M. M. Amoroso, L. D. Daniels, P. J. Baker, and J. J. Camarero, (Cham: Springer Internel Publishing), 345–363. doi: 10.1007/978-3-319-61669-8_15

Hou, J., Huang, Y., Zhao, J., Liu, Z., Colman, S., and An, Z. (2016). Large Holocene summer temperature oscillations and impact on the peopling of the northeastern Tibetan Plateau. *Geophys. Res. Lett.* 43, 1323–1330.

Huang, X., Oberhänsli, H., von Suchodoletz, H., Prasad, S., Sorrel, P., Plessen, B., et al. (2014). Hydrological changes in western Central Asia (Kyrgyzstan) during the Holocene as inferred from a palaeolimnological study in lake Son Kul. *Quat. Sci. Rev.* 103, 134–152. doi: 10.1016/j.quascirev.2014.09.012

Ilyasov, S., Zabenko, O., Gaydamak, N., Kirilenko, A., Myrsaliev, N., and Shevchenko, V. (2013). *Climate profile of the Kyrgyz Republic*. Vol. 99. Bishkek: The United Nations Development Programme.

Kinder, M., Tylmann, W., Bubak, I., Fiłoc, M., Gąsiorowski, M., Kupryjanowicz, M., et al. (2019). Holocene history of human impacts inferred from annually laminated sediments in Lake Szurpiły, northeast Poland. *J. Paleolimnol.* 61, 419–435. doi: 10.1007/s10933-019-00068-2

Koppes, M., Gillespie, A. R., Burke, R. M., Thompson, S. C., and Stone, J. (2008). Late quaternary glaciation in the Kyrgyz Tien Shan. *Quat. Sci. Rev.* 27, 846–866. doi: 10.1016/j.quascirev.2008.01.009

Konopka, T. (2019). *UMAP: Uniform Manifold Approximation and Projection*. R Package Version 0.2.3.1.

Kudo, A., Zheng, J., Koerner, R. M., Fisher, D. A., Santry, D. C., Mahara, Y., et al. (1998). Global transport rates of 137Cs and 239+240Pu originating from the Nagasaki A-bomb in 1945 as determined from analysis of Canadian Arctic ice cores. *J. Environ. Radioact.* 40, 289–298. doi: 10.1016/S0265-931X(97)00023-4

Lauterbach, S., Witt, R., Plessen, B., Dulski, P., Prasad, S., Mingram, J., et al. (2014). Climatic imprint of the mid-latitude Westerlies in the Central Tian Shan of Kyrgyzstan and teleconnections to North Atlantic climate variability during the last 6000 years. *Holocene* 24, 970–984. doi: 10.1177/0959683614534741

Leeming, R., Ball, A., Ashbolt, N., and Nichols, P. (1996). Using faecal sterols from humans and animals to distinguish faecal pollution in receiving waters. *Water Res.* 30, 2893–2900. doi: 10.1016/s0043-1354(96)00011-5

Leeming, R., and Nichols, P. (1996). Concentrations of coprostanol that correspond to existing bacterial indicator guideline limits. *Water Res.* 30, 2997–3006. doi: 10.1016/s0043-1354(96)00212-6

Ma, Y., Liu, K. -b, Feng, Z., Sang, Y., Wang, W., and Sun, A. (2008). A survey of modern pollen and vegetation along a south-north transect in Mongolia. *J. Biogeogr.* 35, 1512–1532. doi: 10.1111/j.1365-2699.2007.01871.x

Macdonald, I. A., Bokkenheuser, V. D., Winter, J., McLernon, A. M., and Mosbach, E. H. (1983). Degradation of steroids in the human gut. *J. Lipid Res.* 24, 675–700.

Madsen, D. B., Haizhou, M., Brantingham, P. J., Xing, G., Rhode, D., Haiying, Z., et al. (2006). The late upper paleolithic occupation of the northern Tibetan Plateau margin. *J. Archaeol. Sci.* 33, 1433–1444. doi: 10.1016/j.jas.2006.01.017

Marcott, S. A., Shakun, J. D., Clark, P. U., and Mix, A. C. (2013). A reconstruction of regional and global temperature for the past 11,300 years. *Science* 339, 1198–1201. doi: 10.1126/science.1228026

Martins, C. D. C., Fillmann, G., and Montone, R. C. (2007). Natural and anthropogenic sterols inputs in surface sediments of Patos Lagoon, Brazil. *J. Braz. Chem. Soc.* 18, 106–115. doi: 10.1590/s0103-50532007000100012

Mathis, M., Sorrel, P., Klotz, S., Huang, X., and Oberhänsli, H. (2014). Regional vegetation patterns at lake Son Kul reveal Holocene climatic variability in central Tien Shan (Kyrgyzstan, Central Asia). *Quat. Sci. Rev.* 89, 169–185. doi: 10.1016/j.quascirev.2014.01.023

McInnes, L., Healy, J., Saul, N., and Großberger, L. (2018). UMAP: uniform manifold approximation and projection. *J. Open Source Softw.* 3:861. doi: 10.21105/joss.00861

Mei, J. (2003). "Qijia and seima-turbino: the question of early contacts betweenNorthwest China and the Eurasian steppe", in *Bulletin of the Museum of FarEastern Antiquities*. Vol. 75, A. B. Damania, J. Valkoun, et al. (Stockholm: Museum of Far Eastern Antiquities), 31–54.

Meyer, M. C., Aldenderfer, M. S., Wang, Z., Hoffmann, D. L., Dahl, J. A., Degering, D., et al. (2017). Permanent human occupation of the central Tibetan Plateau in the early Holocene. *Science* 355, 64–67. doi: 10.1126/science.aag0357

Meyers, P. A. (2003). Applications of organic geochemistry to paleolimnological reconstructions: a summary of examples from the Laurentian Great Lakes. *Org. Geochem.* 34, 261–289. doi: 10.1016/s0146-6380(02)00168-7

Mischke, S., Rajabov, I., Mustaeva, N., Zhang, C., Herzschuh, U., Boomer, I., et al. (2010). Modern hydrology and late Holocene history of Lake Karakul, eastern Pamirs (Tajikistan): a reconnaissance study. *Palaeogeogr. Palaeoclimatol. Palaeoecol.* 289, 10–24. doi: 10.1016/j.palaeo.2010.02.004

Mosello, B. (2015). *The Syr Darya River Basin, How to Deal with Climate Change?* Bern: Springer International Publishing, 117–162. doi: 10.1007/978-3-319-15389-6_5

Motuzaite Matuzeviciute, G., Preece, R. C., Wang, S., Colominas, L., Ohnuma, K., Kume, S., et al. (2017). Ecology and subsistence at the Mesolithic and Bronze Age site of Aigyrzhal-2, Naryn valley, Kyrgyzstan. *Quat. Int.* 437, 35–49. doi: 10.1016/j.quaint.2015.06.065

Ortiz, J. E., Sánchez-Palencia, Y., Torres, T., Domingo, L., Mata, M. P., Vegas, J., et al. (2016). Lipid biomarkers in Lake Enol (Asturias, Northern Spain): coupled natural and human induced environmental history. *Org. Geochem.* 92, 70–83. doi: 10.1016/j.orggeochem.2015.12.005

Ossendorf, G., Groos, A. R., Bromm, T., Tekelemariam, M. G., Glaser, B., Lesur, J., et al. (2019). Middle stone age foragers resided in high elevations of the glaciated Bale Mountains, Ethiopia. *Science* 365, 583–587. doi: 10.1126/science.aaw8942

Panyushkina, I. P., Macklin, M. G., Toonen, W. H. J., and Meko, D. M. (2019). "Water Supply and Ancient Society in the Lake Balkhash Basin: Runoff Variability along the Historical Silk Road," in *Socio-Environmental Dynamics along the Historical Silk Road*, eds L. Yang, H.-R. Bork, X. Fang, and S. Mischke, (Cham: Springer), 379–410. doi: 10.1007/978-3-030-00728-7_18

Qin, F., Wang, Y.-F., Ferguson, D. K., Chen, W.-L., Li, Y.-M., Cai, Z., et al. (2015). Utility of surface pollen assemblages to delimit eastern Eurasian steppe types. *PLoS One* 10:e0119412. doi: 10.1371/journal.pone.0119412

R Core Team (2019). *R: A Language and Environment for Statistical Computing*. Vienna: R Foundation for Statistical Computing.

Rademaker, K., Hodgins, G., Moore, K. M., Zarrillo, S., Miller, C. E., Bromley, G. R. M., et al. (2014). Paleoindian settlement of the high-altitude Peruvian Andes. *Science* 346, 466–469. doi: 10.5061/dryad.96g44

Rahimon, R. M. (2012). "Evolution of land use in pastoral culture in Central Asia with special reference to Kyrgyzstan and Kazakhstan," in *Rangeland Stewardship in Central Asia*, ed. V. Squires, (Dordrecht: Springer), 51–67. doi: 10.1007/978-94-007-5367-9_3

Ranov, V. A. (1975). Pamir i problema zaseleniya vîsokogoriyi Azii chelovekom kamennogo veka. *Stranî i narodî Vostoka* 17, 136–157.

Ranov, V. A., and Kydyrov, S. A. (1969). Nakhodki kamennogo veka u ozera Chatyrkel. *Izvestiya Akad. Nauk Tadzhykskoi SSR* 1, 32–35.

Reille, M. (1995–1999). *Pollen et spores d'Europe et d'Afrique du Nord*. Marseille: Laboratoire de Botanique Historique et Palynologie.

Reimer, P. J., Bard, E., Bayliss, A., Beck, J. W., Blackwell, P. G., Ramsey, C. B., et al. (2013). IntCal13 and marine13 radiocarbon age calibration curves 0–50,000 years cal BP. *Radiocarbon* 55, 1869–1887. doi: 10.2458/azu_js_rc.55.16947

Richey, J. N., and Tierney, J. E. (2016). GDGT and alkenone flux in the northern Gulf of Mexico: implications for the TEX86 and UK'37 paleothermometers. *Paleoceanography* 31, 1547–1561. doi: 10.1002/2016pa003032

Ricketts, R. D., Johnson, T. C., Brown, E. T., Rasmussen, K. A., and Romanovsky, V. V. (2001). The Holocene paleolimnology of Lake Issyk-Kul, Kyrgyzstan: trace element and stable isotope composition of ostracodes. *Palaeogeogr. Palaeoclimatol. Palaeoecol.* 176, 207–227. doi: 10.1016/s0031-0182(01)00339-x

Rogge, W. F., Medeiros, P. M., and Simoneit, B. R. T. (2006). Organic marker compounds for surface soil and fugitive dust from open lot dairies and cattle feedlots. *Atmos. Environ.* 40, 27–49. doi: 10.1016/j.atmosenv.2005.07.076

Ryan, W. B .F., Carbotte, S. M., Coplan, J. O., O'Hara, S., Melkonian, A., Arko, R., et al. (2009). Global Multi-Resolution Topography synthesis. *Geochemistry, Geophysics, Geosystems* 10. doi: 10.1029/2008gc002332

Shnaider, S., Taylor, W. T., Abdykanova, A., Kolobova, K., and Krivoshapkin, A. (2018). Evidence for early human occupation at high altitudes in western Central Asia: the Alay site. *Antiquity* 92, 1–7. doi: 10.15184/aqy.2018.94

Shnaider, S. V., Kolobova, K. A., Filimonova, T. G., Taylor, W., and Krivoshapkin, I. (2018). New insights into the Epipaleolithic of western Central Asia: the Tutkaulian complex. *Quat. Int.* (in press). doi: 10.1016/j.quaint.2018.10.001

Shnitnikov, A. V., Livja, A. A., Berdovskaya, G. N., and Sevastianov, D. V. (1978). Paleolimnology of chatyrkel lake (Tien-shan). *Pol. Arch. Hydrobiol.* 25, 383–390.

Spengler, R., Frachetti, M., Doumani, P., Rouse, L., Cerasetti, B., Bullion, E., et al. (2014). Early agriculture and crop transmission among bronze age mobile pastoralists of Central Eurasia. *Proc. R. Soc. B Biol. Sci.* 281:20133382. doi: 10.1098/rspb.2013.3382

Spengler, R. N., and Willcox, G. (2013). Archaeobotanical results from Sarazm, Tajikistan, an early bronze age settlement on the edge: agriculture and exchange. *Environ. Archaeol.* 18, 211–221. doi: 10.1179/1749631413y.0000000008

Taft, J. B., Phillippe, L. R., Dietrich, C. H., and Robertson, K. R. (2011). Grassland composition, structure, and diversity patterns along major environmental gradients in the Central Tien Shan. *Plant Ecol.* 212, 1349–1361. doi: 10.1007/s11258-011-9911-5)

Taylor, W., Shnaider, S., Abdykanova, A., Fages, A., Welker, F., Irmer, F., et al. (2018). Early pastoral economies along the Ancient Silk Road: biomolecular evidence from the Alay Valley. Kyrgyzstan. *PLoS One* 13:e0205646. doi: 10.1371/journal.pone.0205646

Taylor, W. T. T., Shnaider, S., Spengler, R., Orlando, L., Abdykanova, A., and Krivoshapkin, A. (2019). Investigating ancient animal economies and exchange in Kyrgyzstan's Alay Valley. *Antiquity* 93, 1–5. doi: 10.15184/aqy.2019.4

Thienemann, M., Masi, A., Kusch, S., Sadori, L., John, S., Francke, A., et al. (2017). Organic geochemical and palynological evidence for Holocene natural

and anthropogenic environmental change at Lake Dojran (Macedonia/Greece). *Holocene* 27, 1103–1114. doi: 10.1177/0959683616683261

Thorpe, A., van Anrooy, R., Niyazov, B. N., Sarieva, M. K., Valbo-Jørgensen, J., and Millar, A. M. (2009). The collapse of the fisheries sector in Kyrgyzstan: an analysis of its roots and its prospects for revival. *Commu. Post Commun. Stud.* 42, 141–163. doi: 10.1016/j.postcomstud.2009.02.007

van der Maaten, L., and Hinton, G. (2008). Visualizing data using t-SNE. *J. Mach. Learn. Res.* 9, 2579–2605.

Wakeham, S. G. (1989). Reduction of stenols to stanols in particulate matter at oxic–anoxic boundaries in sea water. *Nature* 342, 787–790. doi: 10.1038/342787a0

Wang, C., Xu, J., Chen, Y., Bai, L., and Chen, Z. (2017). A hybrid model to assess the impact of climate variability on streamflow for an ungauged mountainous basin. *Clim. Dyn.* 50, 2829–2844. doi: 10.1007/s00382-017-3775-x

White, A. J., Stevens, L. R., Lorenzi, V., Munoz, S. E., Lipo, C. P., and Schroeder, S. (2018). An evaluation of fecal stanols as indicators of population change at Cahokia, Illinois. *J. Archaeol. Sci.* 93, 129–134. doi: 10.1016/j.jas.2018.03.009

Wickham, H. (2016). *ggplot2: Elegant Graphics for Data Analysis*. New York: Springer. ISBN: 978-3-319-24277-4

Wolff, C., Plessen, B., Dudashvilli, A. S., Breitenbach, S. F. M., Cheng, H., Edwards, L. R., et al. (2017). Precipitation evolution of Central Asia during the last 5000 years. *Holocene* 27, 142–154. doi: 10.1177/0959683616652711

Wright, S. M., Howard, B. J., Strand, P., Nylén, T., and Sickel, M. A. K. (1999). Prediction of 137Cs deposition from atmospheric nuclear weapons tests within the Arctic. *Environ. Pollut.* 104, 131–143. doi: 10.1016/S0269-7491(98)00140-7

Yang, L. E., Bork, H.-R., Fang, X., and Mischke, S. (2019a). *Socio-Environmental Dynamics along the Historical Silk Road*. Cham: Springer. ISBN: 978-3-030-00728-7.

Yang, L. E., Bork, H.-R., Fang, X., Mischke, S., Weinelt, M., and Wiesehöfer, J. (2019b). "On the paleo-climatic/environmental impacts and socio-cultural system resilience along the Historical Silk Road," in *Socio-Environmental Dynamics along the Historical Silk Road* eds L. Yang, H.-R. Bork, X. Fang, and S. Mischke, (Cham: Springer), 3–22. doi: 10.1007/978-3-030-00728-7_1

Zhang, X. L., Ha, B. B., Wang, S. J., Chen, Z. J., Ge, J. Y., Long, H., et al. (2018). The earliest human occupation of the high-altitude Tibetan Plateau 40 thousand to 30 thousand years ago. *Science* 326, 1049–1051. doi: 10.1126/science.aat8824

Zhao, J., An, C.-B., Huang, Y., Morrill, C., and Chen, F.-H. (2017). Contrasting early Holocene temperature variations between monsoonal East Asia and westerly dominated Central Asia. *Quat. Sci. Rev.* 178, 14–23. doi: 10.1016/j.quascirev.2017.10.036

Zhao, K., Li, X., Dodson, J., Atahan, P., Zhou, X., and Bertuch, F. (2012). Climatic variations over the last 4000 cal yr BP in the western margin of the Tarim Basin, Xinjiang, reconstructed from pollen data. *Palaeogeogr. Palaeoclimatol. Palaeoecol.* 32, 16–23. doi: 10.1016/j.palaeo.2012.01.012

**Conflict of Interest:** The authors declare that the research was conducted in the absence of any commercial or financial relationships that could be construed as a potential conflict of interest.

*Copyright © 2020 Schroeter, Lauterbach, Stebich, Kalanke, Mingram, Yildiz, Schouten and Gleixner. This is an open-access article distributed under the terms of the Creative Commons Attribution License (CC BY). The use, distribution or reproduction in other forums is permitted, provided the original author(s) and the copyright owner(s) are credited and that the original publication in this journal is cited, in accordance with accepted academic practice. No use, distribution or reproduction is permitted which does not comply with these terms.*

# *Supplementary Material*

## 1.1 Supplementary Figures

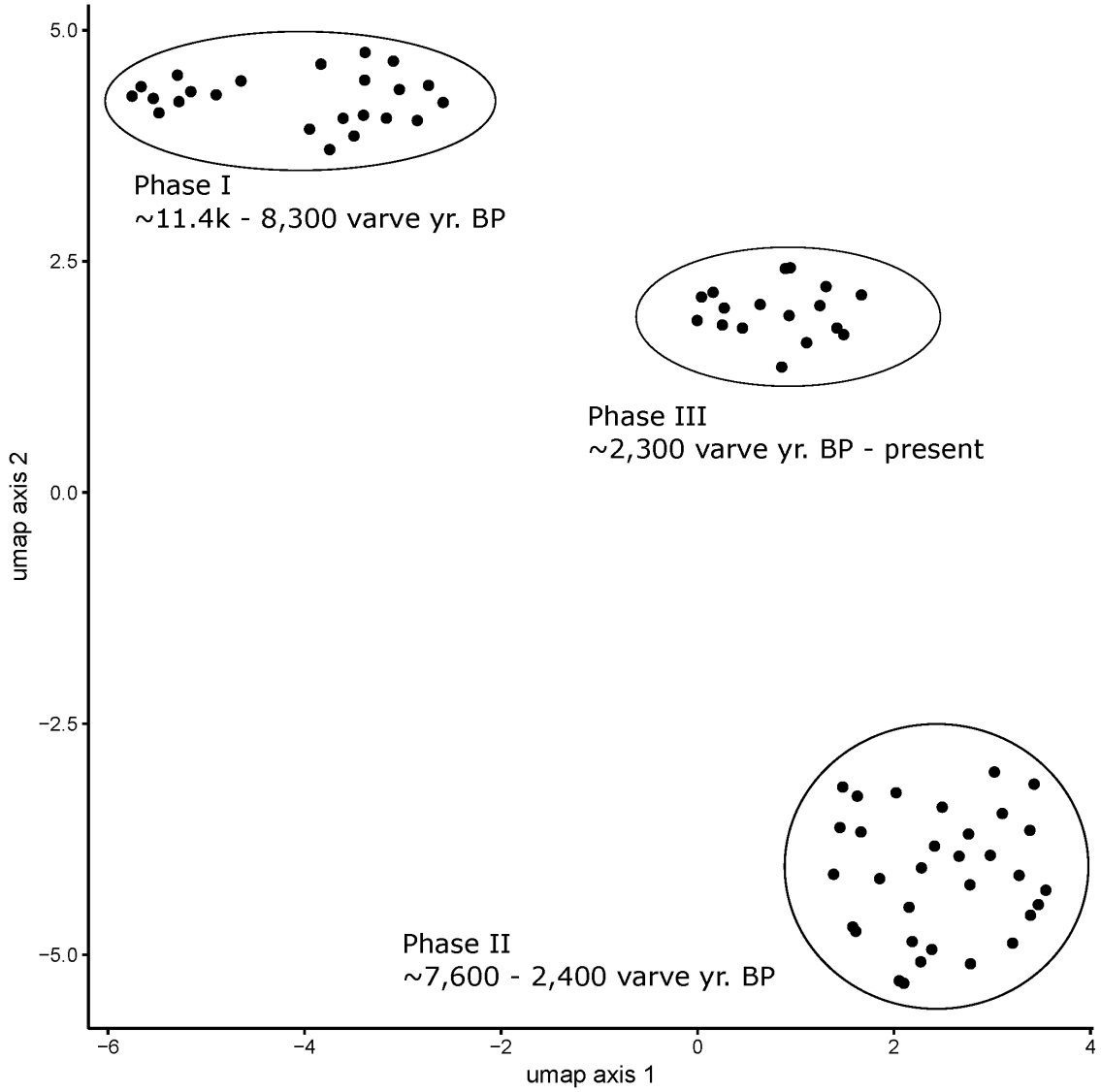


**Supplementary Figure S1.** Uniform Manifold Approximation and Projection (UMAP) graph for the analyzed Lake Chatyr Kol sediment samples, dividing the sediment core into 3 clusters.

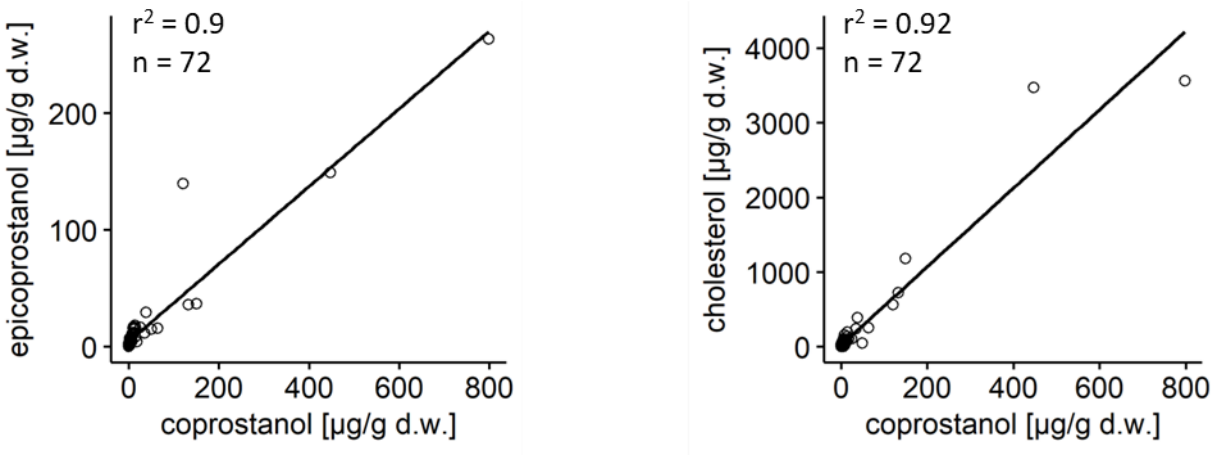


**Supplementary Figure S2.** Significant correlations between coprostanol and epicoprostanol and cholesterol and coprostanol suggest a common source for these fecal sterols.

## 1.2 Supplementary Tables

**Supplementary Table S1.** Pollen data analysis of Lake Chatyr Kol. Continued on following pages.

| Age varve a BP | Juniperus | Picea | Betula | Hippophaë | Ephedra total | Artemisia | Chenopodiaceae | Poaceae | Cyperaceae | AP (%) | NAP (%) |
|---|---|---|---|---|---|---|---|---|---|---|---|
| -57.55 | 1.7 | 0.4 | 0.0 | 0.2 | 0.2 | 55.2 | 14.7 | 15.0 | 2.1 | 3.0 | 97.0 |
| -18.25 | 0.4 | 0.0 | 0.2 | 0.0 | 0.2 | 54.2 | 20.0 | 11.9 | 2.7 | 1.3 | 98.7 |
| 20.47 | 0.3 | 0.8 | 0.0 | 0.0 | 0.0 | 61.3 | 20.0 | 9.5 | 1.5 | 2.4 | 97.6 |
| 58.93 | 0.0 | 0.2 | 0.0 | 0.3 | 0.3 | 50.2 | 22.7 | 13.8 | 2.0 | 0.8 | 99.2 |
| 84.73 | 0.4 | 0.1 | 0.0 | 0.0 | 0.0 | 45.4 | 28.1 | 15.8 | 2.2 | 1.2 | 98.8 |
| 111.20 | 0.6 | 0.2 | 0.0 | 0.0 | 0.0 | 47.7 | 28.9 | 13.9 | 1.3 | 1.6 | 98.4 |
| 147.67 | 0.4 | 0.1 | 0.1 | 0.3 | 0.4 | 51.2 | 23.0 | 14.9 | 0.5 | 1.7 | 98.3 |
| 170.80 | 0.2 | 0.0 | 0.0 | 0.0 | 0.0 | 48.6 | 24.4 | 14.1 | 1.2 | 1.2 | 98.8 |
| 183.40 | 0.2 | 0.0 | 0.0 | 0.0 | 0.0 | 48.0 | 27.4 | 16.1 | 0.9 | 1.2 | 98.8 |
| 208.60 | 1.1 | 0.1 | 0.0 | 0.0 | 0.0 | 47.0 | 27.5 | 15.4 | 0.8 | 2.2 | 97.8 |
| 233.44 | 0.2 | 0.2 | 0.0 | 0.0 | 0.0 | 46.2 | 28.4 | 13.8 | 1.5 | 0.7 | 99.3 |
| 274.31 | 1.2 | 0.1 | 0.0 | 0.4 | 0.4 | 48.1 | 27.9 | 13.0 | 0.8 | 2.4 | 97.6 |
| 312.06 | 0.3 | 0.0 | 0.2 | 0.0 | 0.2 | 54.6 | 25.9 | 10.4 | 0.8 | 0.7 | 99.3 |
| 336.60 | 2.4 | 0.3 | 0.1 | 0.0 | 0.1 | 52.3 | 23.0 | 12.3 | 1.4 | 3.1 | 96.9 |
| 355.44 | 0.5 | 0.3 | 0.0 | 0.0 | 0.0 | 50.2 | 25.3 | 14.5 | 1.4 | 2.2 | 97.8 |
| 365.62 | 0.4 | 0.0 | 0.0 | 0.0 | 0.0 | 49.4 | 22.1 | 14.1 | 1.0 | 1.7 | 98.3 |
| 389.66 | 0.2 | 0.1 | 0.1 | 0.1 | 0.2 | 53.8 | 26.7 | 10.7 | 1.0 | 1.7 | 98.3 |
| 426.31 | 0.0 | 0.0 | 0.0 | 0.0 | 0.0 | 52.5 | 25.6 | 12.9 | 1.8 | 0.4 | 99.6 |

| Age varve a BP | Juniperus | Picea | Betula | Hippophaë | Ephedra total | Artemisia | Chenopodiaceae | Poaceae | Cyperaceae | AP (%) | NAP (%) |
|---|---|---|---|---|---|---|---|---|---|---|---|
| 454.91 | 0.4 | 0.3 | 0.0 | 0.1 | 0.1 | 47.5 | 22.8 | 18.7 | 1.4 | 1.8 | 98.2 |
| 477.35 | 0.2 | 0.0 | 0.2 | 0.0 | 0.2 | 56.1 | 21.2 | 10.9 | 1.2 | 0.8 | 99.2 |
| 514.50 | 0.8 | 0.1 | 0.0 | 0.3 | 0.3 | 52.1 | 21.2 | 13.7 | 1.9 | 3.1 | 96.9 |
| 541.50 | 0.0 | 0.0 | 0.0 | 0.2 | 0.2 | 45.4 | 23.6 | 19.1 | 1.6 | 0.6 | 99.4 |
| 585.09 | 0.0 | 0.0 | 0.0 | 0.2 | 0.2 | 53.2 | 20.0 | 11.9 | 2.2 | 1.5 | 98.5 |
| 619.56 | 2.0 | 0.1 | 0.0 | 0.0 | 0.0 | 53.8 | 21.9 | 13.7 | 1.3 | 2.9 | 97.1 |
| 643.73 | 0.3 | 0.0 | 0.0 | 0.0 | 0.0 | 52.0 | 23.2 | 13.2 | 1.1 | 1.1 | 98.9 |
| 677.33 | 0.7 | 0.0 | 0.0 | 0.4 | 0.4 | 55.2 | 22.0 | 11.2 | 1.2 | 2.7 | 97.3 |
| 683.35 | 2.0 | 0.4 | 0.0 | 0.1 | 0.1 | 54.0 | 22.2 | 9.5 | 1.1 | 5.1 | 94.9 |
| 701.67 | 1.0 | 0.4 | 0.0 | 0.0 | 0.0 | 54.9 | 19.0 | 16.7 | 1.2 | 3.5 | 96.5 |
| 716.53 | 1.2 | 0.0 | 0.0 | 0.1 | 0.1 | 47.0 | 25.1 | 14.9 | 2.0 | 3.4 | 96.6 |
| 764.45 | 0.8 | 0.0 | 0.0 | 0.0 | 0.0 | 53.3 | 23.4 | 12.7 | 1.7 | 2.5 | 97.5 |
| 779.61 | 1.5 | 0.2 | 0.0 | 0.3 | 0.3 | 47.3 | 23.7 | 15.2 | 2.7 | 4.7 | 95.3 |
| 789.39 | 0.9 | 0.1 | 0.1 | 0.2 | 0.3 | 52.4 | 19.8 | 14.5 | 2.1 | 3.2 | 96.8 |
| 794.48 | 1.1 | 0.4 | 0.0 | 0.0 | 0.0 | 46.5 | 22.9 | 14.7 | 2.4 | 3.1 | 96.9 |
| 842.43 | 1.5 | 0.1 | 0.0 | 0.1 | 0.1 | 52.1 | 21.9 | 15.1 | 1.4 | 2.3 | 97.7 |
| 928.80 | 1.3 | 0.1 | 0.1 | 0.1 | 0.3 | 50.6 | 21.4 | 16.6 | 0.8 | 2.6 | 97.4 |
| 1017.67 | 0.5 | 0.2 | 0.3 | 0.0 | 0.3 | 48.5 | 23.6 | 14.2 | 1.9 | 2.4 | 97.6 |
| 1088.80 | 1.1 | 0.2 | 0.2 | 0.0 | 0.2 | 48.7 | 19.1 | 21.8 | 1.4 | 2.5 | 97.5 |
| 1176.25 | 0.8 | 0.0 | 0.0 | 0.2 | 0.2 | 49.1 | 22.8 | 15.1 | 1.6 | 2.4 | 97.6 |
| 1347.00 | 1.9 | 0.3 | 0.3 | 0.0 | 0.3 | 51.5 | 19.6 | 15.3 | 1.3 | 3.9 | 96.1 |
| 1489.40 | 0.5 | 0.2 | 0.0 | 0.0 | 0.0 | 49.5 | 19.7 | 15.6 | 2.2 | 1.9 | 98.1 |

| Age varve a BP | Juniperus | Picea | Betula | Hippophaë | Ephedra total | Artemisia | Chenopodiaceae | Poaceae | Cyperaceae | AP (%) | NAP (%) |
|---|---|---|---|---|---|---|---|---|---|---|---|
| 1613.00 | 0.8 | 0.0 | 0.0 | 0.0 | 0.0 | 51.9 | 19.0 | 17.7 | 1.1 | 2.2 | 97.8 |
| 1722.00 | 0.5 | 0.2 | 0.0 | 0.2 | 0.2 | 51.5 | 19.6 | 14.2 | 1.7 | 2.1 | 97.9 |
| 1882.00 | 1.3 | 0.2 | 0.1 | 0.0 | 0.1 | 43.7 | 22.7 | 18.7 | 1.9 | 3.3 | 96.7 |
| 1998.33 | 0.0 | 0.5 | 0.0 | 0.0 | 0.0 | 51.9 | 17.8 | 15.9 | 1.7 | 1.4 | 98.6 |
| 2163.20 | 1.8 | 0.0 | 0.0 | 0.1 | 0.1 | 48.8 | 23.2 | 12.1 | 2.0 | 3.4 | 96.6 |
| 2273.50 | 1.4 | 0.0 | 0.5 | 0.0 | 0.5 | 44.5 | 24.1 | 17.0 | 1.5 | 3.0 | 97.0 |
| 2352.00 | 1.8 | 0.1 | 0.0 | 0.1 | 0.1 | 49.1 | 18.4 | 18.8 | 0.7 | 4.6 | 95.4 |
| 2433.67 | 0.0 | 0.2 | 0.5 | 0.0 | 0.5 | 56.1 | 17.2 | 13.2 | 1.1 | 1.1 | 98.9 |
| 2555.67 | 1.3 | 0.2 | 0.0 | 0.0 | 0.0 | 54.7 | 15.4 | 12.2 | 2.4 | 3.7 | 96.3 |
| 2609.33 | 1.0 | 0.1 | 0.1 | 0.2 | 0.3 | 47.4 | 19.4 | 20.4 | 2.3 | 2.8 | 97.2 |
| 2692.83 | 0.5 | 0.3 | 0.2 | 0.0 | 0.2 | 52.1 | 16.6 | 14.7 | 2.9 | 2.3 | 97.7 |
| 2783.25 | 0.7 | 0.1 | 0.3 | 0.4 | 0.7 | 54.5 | 21.8 | 14.1 | 1.8 | 2.8 | 97.2 |
| 2879.60 | 0.2 | 0.0 | 0.0 | 0.2 | 0.2 | 47.1 | 24.2 | 14.6 | 1.8 | 1.6 | 98.4 |
| 3029.00 | 0.6 | 0.0 | 0.0 | 0.1 | 0.1 | 57.5 | 19.6 | 14.0 | 1.7 | 1.4 | 98.6 |
| 3177.33 | 0.2 | 0.2 | 0.2 | 0.2 | 0.3 | 47.7 | 23.2 | 14.8 | 1.5 | 1.5 | 98.5 |
| 3302.00 | 0.7 | 0.5 | 0.1 | 0.1 | 0.2 | 50.5 | 20.0 | 17.2 | 1.8 | 3.6 | 96.4 |
| 3428.33 | 1.1 | 0.2 | 0.2 | 0.1 | 0.3 | 59.4 | 16.2 | 14.1 | 1.2 | 2.2 | 97.8 |
| 3525.71 | 0.5 | 0.0 | 0.2 | 0.0 | 0.2 | 57.4 | 15.6 | 12.0 | 2.9 | 1.9 | 98.1 |
| 3559.25 | 0.9 | 0.2 | 0.2 | 0.1 | 0.4 | 55.9 | 15.4 | 16.7 | 1.0 | 2.9 | 97.1 |
| 3613.33 | 0.3 | 0.3 | 0.4 | 0.0 | 0.4 | 54.9 | 15.3 | 17.6 | 1.7 | 2.4 | 97.6 |
| 3664.33 | 1.0 | 0.7 | 0.0 | 0.0 | 0.0 | 42.1 | 20.3 | 19.9 | 3.4 | 4.6 | 95.4 |
| 3723.50 | 1.1 | 0.6 | 0.6 | 0.2 | 0.8 | 41.7 | 22.4 | 16.7 | 2.1 | 6.3 | 93.7 |

| Age varve a BP | Juniperus | Picea | Betula | Hippophaë | Ephedra total | Artemisia | Chenopodiaceae | Poaceae | Cyperaceae | AP (%) | NAP (%) |
|---|---|---|---|---|---|---|---|---|---|---|---|
| 3756.83 | 0.7 | 0.0 | 0.3 | 0.0 | 0.3 | 46.1 | 21.8 | 15.3 | 3.3 | 2.3 | 97.7 |
| 3794.00 | 0.4 | 0.3 | 0.7 | 0.0 | 0.7 | 47.3 | 17.9 | 18.3 | 1.7 | 3.3 | 96.7 |
| 3917.40 | 1.1 | 0.4 | 0.0 | 0.0 | 0.0 | 51.5 | 17.0 | 18.8 | 2.3 | 2.9 | 97.1 |
| 3972.33 | 1.9 | 0.5 | 1.4 | 0.1 | 1.5 | 43.9 | 24.9 | 15.6 | 1.7 | 6.1 | 93.9 |
| 4097.17 | 1.4 | 0.6 | 0.6 | 0.1 | 0.8 | 50.1 | 19.4 | 15.7 | 2.5 | 4.7 | 95.3 |
| 4180.50 | 2.7 | 0.6 | 0.3 | 0.0 | 0.3 | 45.7 | 17.4 | 19.1 | 3.0 | 6.1 | 93.9 |
| 4283.58 | 2.3 | 0.3 | 1.0 | 0.0 | 1.0 | 50.2 | 19.9 | 15.9 | 2.0 | 5.1 | 94.9 |
| 4303.33 | 1.4 | 0.2 | 0.9 | 0.3 | 1.2 | 39.8 | 20.1 | 21.6 | 2.6 | 4.7 | 95.3 |
| 4323.80 | 2.2 | 0.1 | 0.8 | 0.3 | 1.0 | 45.3 | 17.3 | 18.8 | 3.2 | 4.8 | 95.2 |
| 4403.25 | 2.3 | 0.4 | 0.6 | 0.0 | 0.6 | 42.4 | 21.2 | 18.5 | 2.6 | 6.0 | 94.0 |
| 4481.00 | 1.7 | 0.7 | 0.6 | 0.2 | 0.9 | 50.5 | 19.7 | 13.8 | 1.0 | 5.4 | 94.6 |
| 4540.50 | 0.8 | 0.1 | 0.3 | 0.3 | 0.6 | 49.0 | 16.4 | 18.1 | 2.2 | 4.3 | 95.7 |
| 4643.60 | 1.3 | 1.2 | 0.2 | 0.1 | 0.4 | 42.3 | 16.8 | 22.8 | 4.4 | 5.1 | 94.9 |
| 4701.67 | 1.1 | 0.1 | 1.3 | 0.1 | 1.5 | 43.4 | 19.1 | 23.6 | 0.8 | 5.2 | 94.8 |
| 4742.55 | 1.8 | 0.7 | 0.7 | 0.1 | 0.8 | 37.9 | 23.0 | 19.5 | 2.9 | 7.4 | 92.6 |
| 4822.80 | 3.0 | 0.5 | 0.5 | 0.1 | 0.7 | 43.8 | 19.3 | 18.0 | 1.3 | 7.2 | 92.8 |
| 4934.20 | 3.0 | 0.2 | 0.7 | 0.2 | 1.0 | 46.8 | 19.3 | 14.5 | 1.9 | 7.2 | 92.8 |
| 4972.17 | 1.6 | 0.3 | 0.7 | 0.3 | 0.9 | 47.7 | 18.9 | 17.2 | 1.2 | 5.5 | 94.5 |
| 5037.00 | 2.5 | 0.6 | 0.8 | 0.1 | 0.9 | 36.2 | 24.4 | 20.1 | 3.3 | 6.2 | 93.8 |
| 5137.00 | 1.1 | 0.2 | 0.8 | 0.1 | 0.9 | 47.4 | 25.6 | 15.7 | 1.1 | 4.3 | 95.7 |
| 5227.50 | 1.1 | 0.2 | 0.4 | 0.3 | 0.6 | 44.8 | 21.7 | 19.6 | 2.3 | 4.4 | 95.6 |
| 5263.75 | 1.8 | 0.1 | 0.9 | 0.0 | 0.9 | 38.8 | 19.5 | 20.2 | 3.9 | 6.4 | 93.6 |

| Age varve a BP | Juniperus | Picea | Betula | Hippophaë | Ephedra total | Artemisia | Chenopodiaceae | Poaceae | Cyperaceae | AP (%) | NAP (%) |
|---|---|---|---|---|---|---|---|---|---|---|---|
| 5324.00 | 2.4 | 0.1 | 0.4 | 0.0 | 0.4 | 42.9 | 23.1 | 17.4 | 2.5 | 5.5 | 94.5 |
| 5409.67 | 1.6 | 0.4 | 1.7 | 0.1 | 1.9 | 42.5 | 20.0 | 17.6 | 2.6 | 6.8 | 93.2 |
| 5447.80 | 0.5 | 0.0 | 0.6 | 0.2 | 0.8 | 38.4 | 22.3 | 21.1 | 3.6 | 2.9 | 97.1 |
| 5543.25 | 0.8 | 0.3 | 1.0 | 0.0 | 1.0 | 40.5 | 23.5 | 21.8 | 2.7 | 4.3 | 95.7 |
| 5608.00 | 3.4 | 1.7 | 0.8 | 0.1 | 0.9 | 38.5 | 19.9 | 17.8 | 4.0 | 10.1 | 89.9 |
| 5688.11 | 0.5 | 0.3 | 1.3 | 0.0 | 1.3 | 34.9 | 23.6 | 17.9 | 3.5 | 5.9 | 94.1 |
| 5705.00 | 2.4 | 0.3 | 1.7 | 0.3 | 1.9 | 40.8 | 20.0 | 18.9 | 3.1 | 7.9 | 92.1 |
| 5742.50 | 2.3 | 0.1 | 0.7 | 0.0 | 0.7 | 44.3 | 20.0 | 17.2 | 3.1 | 5.9 | 94.1 |
| 5863.00 | 2.3 | 0.7 | 2.4 | 0.1 | 2.5 | 35.9 | 20.8 | 21.2 | 2.8 | 9.5 | 90.5 |
| 5930.00 | 1.9 | 0.2 | 0.9 | 0.1 | 1.0 | 43.1 | 18.7 | 19.7 | 2.2 | 5.8 | 94.2 |
| 5975.00 | 1.2 | 0.0 | 0.7 | 0.2 | 0.8 | 39.3 | 21.3 | 19.5 | 2.6 | 4.8 | 95.2 |
| 5999.71 | 2.8 | 0.1 | 1.7 | 0.4 | 2.1 | 36.3 | 21.4 | 23.2 | 2.5 | 8.2 | 91.8 |
| 6059.67 | 2.6 | 0.5 | 2.2 | 0.1 | 2.3 | 37.1 | 20.0 | 20.0 | 2.2 | 8.7 | 91.3 |
| 6177.67 | 1.1 | 0.5 | 2.0 | 0.0 | 2.0 | 40.7 | 19.2 | 19.8 | 3.0 | 6.8 | 93.2 |
| 6274.00 | 1.8 | 0.4 | 1.6 | 0.0 | 1.6 | 39.2 | 19.4 | 19.2 | 3.0 | 6.9 | 93.1 |
| 6323.83 | 0.6 | 0.5 | 0.5 | 0.0 | 0.5 | 39.5 | 18.4 | 16.3 | 3.1 | 6.6 | 93.4 |
| 6367.80 | 1.8 | 0.5 | 1.2 | 0.2 | 1.4 | 42.8 | 17.4 | 20.3 | 3.7 | 7.4 | 92.6 |
| 6437.33 | 2.9 | 0.2 | 1.8 | 0.0 | 1.8 | 39.0 | 17.4 | 21.1 | 3.8 | 8.4 | 91.6 |
| 6487.60 | 0.3 | 0.3 | 1.1 | 0.0 | 1.1 | 46.8 | 16.9 | 18.2 | 2.3 | 3.6 | 96.4 |
| 6521.20 | 1.3 | 0.2 | 1.4 | 0.1 | 1.5 | 46.9 | 16.9 | 20.9 | 3.6 | 5.1 | 94.9 |
| 6586.11 | 3.1 | 0.3 | 0.9 | 0.0 | 0.9 | 41.7 | 17.0 | 16.7 | 3.6 | 7.9 | 92.1 |
| 6702.00 | 1.6 | 0.2 | 1.7 | 0.4 | 2.1 | 40.7 | 20.6 | 19.8 | 3.6 | 8.9 | 91.1 |

| Age varve a BP | Juniperus | Picea | Betula | Hippophaë | Ephedra total | Artemisia | Chenopodiaceae | Poaceae | Cyperaceae | AP (%) | NAP (%) |
|---|---|---|---|---|---|---|---|---|---|---|---|
| 6798.22 | 1.4 | 0.6 | 1.6 | 0.0 | 1.6 | 45.9 | 16.3 | 19.3 | 3.1 | 6.6 | 93.4 |
| 6898.00 | 3.2 | 0.5 | 2.9 | 0.0 | 2.9 | 37.5 | 20.6 | 16.1 | 3.4 | 11.2 | 88.8 |
| 6972.75 | 0.5 | 0.2 | 2.3 | 0.4 | 2.6 | 46.6 | 17.9 | 17.0 | 3.3 | 5.3 | 94.7 |
| 7042.20 | 0.4 | 0.0 | 1.2 | 0.1 | 1.3 | 42.9 | 18.6 | 15.3 | 2.4 | 5.9 | 94.1 |
| 7080.25 | 1.8 | 0.4 | 1.2 | 0.0 | 1.2 | 43.3 | 17.5 | 16.5 | 4.1 | 8.5 | 91.5 |
| 7161.83 | 2.6 | 0.4 | 1.5 | 0.1 | 1.6 | 44.5 | 17.4 | 16.3 | 2.9 | 8.2 | 91.8 |
| 7189.67 | 0.5 | 0.5 | 2.7 | 0.0 | 2.7 | 42.6 | 21.2 | 12.8 | 3.0 | 8.7 | 91.3 |
| 7285.00 | 1.3 | 0.2 | 1.1 | 0.1 | 1.2 | 43.4 | 18.3 | 17.6 | 2.5 | 6.9 | 93.1 |
| 7412.00 | 2.3 | 0.2 | 2.9 | 0.0 | 2.9 | 43.7 | 18.0 | 15.3 | 4.6 | 9.5 | 90.5 |
| 7466.29 | 1.7 | 0.5 | 2.5 | 0.0 | 2.5 | 43.7 | 19.6 | 13.4 | 2.8 | 9.9 | 90.1 |
| 7525.00 | 0.2 | 0.0 | 1.1 | 0.0 | 1.1 | 42.9 | 22.0 | 15.9 | 4.8 | 5.1 | 94.9 |
| 7668.00 | 2.6 | 0.6 | 1.5 | 0.0 | 1.5 | 41.8 | 18.2 | 19.4 | 2.2 | 8.3 | 91.7 |
| 7770.50 | 4.1 | 0.0 | 1.8 | 0.1 | 1.9 | 36.0 | 23.1 | 16.1 | 2.8 | 10.7 | 89.3 |
| 7979.00 | 1.6 | 0.0 | 1.7 | 0.3 | 2.1 | 37.8 | 20.5 | 17.5 | 4.4 | 7.8 | 92.2 |
| 8086.50 | 3.2 | 0.3 | 3.4 | 0.4 | 3.7 | 36.2 | 21.4 | 16.4 | 2.9 | 13.4 | 86.6 |
| 8226.50 | 1.1 | 0.3 | 1.8 | 0.0 | 1.8 | 39.2 | 20.2 | 15.0 | 3.8 | 7.7 | 92.3 |
| 8291.00 | 2.3 | 0.1 | 1.2 | 0.4 | 1.6 | 39.6 | 21.5 | 18.4 | 2.1 | 8.2 | 91.8 |
| 8395.33 | 1.2 | 0.4 | 2.6 | 0.1 | 2.8 | 43.7 | 18.3 | 16.3 | 3.9 | 9.9 | 90.1 |
| 8587.50 | 5.4 | 0.1 | 2.8 | 0.2 | 3.0 | 37.4 | 19.2 | 13.1 | 4.8 | 12.0 | 88.0 |
| 8737.00 | 1.9 | 0.1 | 2.8 | 0.3 | 3.1 | 42.8 | 19.1 | 16.5 | 3.3 | 9.2 | 90.8 |
| 8911.00 | 6.6 | 0.4 | 3.4 | 0.4 | 3.9 | 34.1 | 17.1 | 14.5 | 5.8 | 17.0 | 83.0 |
| 9048.50 | 0.6 | 0.0 | 2.7 | 0.3 | 3.0 | 50.1 | 18.1 | 16.9 | 0.3 | 6.7 | 93.3 |

| Age varve a BP | Juniperus | Picea | Betula | Hippophaë | Ephedra total | Artemisia | Chenopodiaceae | Poaceae | Cyperaceae | AP (%) | NAP (%) |
|---|---|---|---|---|---|---|---|---|---|---|---|
| 9271.67 | 3.2 | 0.1 | 2.7 | 0.0 | 2.7 | 37.8 | 18.9 | 15.2 | 6.9 | 9.1 | 90.9 |
| 9419.25 | 3.0 | 0.0 | 2.7 | 0.0 | 2.7 | 37.3 | 14.9 | 13.1 | 5.7 | 10.1 | 89.9 |
| 9617.67 | 2.2 | 0.0 | 1.3 | 0.3 | 1.6 | 40.5 | 19.4 | 15.4 | 5.4 | 8.4 | 91.6 |
| 9755.50 | 1.6 | 0.0 | 1.6 | 0.4 | 2.0 | 37.0 | 20.3 | 17.6 | 3.6 | 8.6 | 91.4 |
| 10003.33 | 3.5 | 0.0 | 1.6 | 0.2 | 1.9 | 39.6 | 20.3 | 15.6 | 4.7 | 9.8 | 90.2 |
| 10126.00 | 0.3 | 0.0 | 1.3 | 0.0 | 1.3 | 41.8 | 21.9 | 20.5 | 0.3 | 7.4 | 92.6 |
| 10266.67 | 2.7 | 0.0 | 1.8 | 0.4 | 2.2 | 39.1 | 20.8 | 10.7 | 3.7 | 11.3 | 88.7 |
| 10373.33 | 1.3 | 0.1 | 1.8 | 0.5 | 2.3 | 40.5 | 19.9 | 16.4 | 3.8 | 6.7 | 93.3 |
| 10537.00 | 1.4 | 0.0 | 0.5 | 0.5 | 1.1 | 34.6 | 21.5 | 13.7 | 5.2 | 9.1 | 90.9 |
| 10649.50 | 0.3 | 0.0 | 1.0 | 0.0 | 1.0 | 43.8 | 28.8 | 12.1 | 1.4 | 5.9 | 94.1 |
| 10757.40 | 1.4 | 0.0 | 0.3 | 0.0 | 0.3 | 36.6 | 26.3 | 13.2 | 1.7 | 6.0 | 94.0 |
| 10780.14 | 0.7 | 0.3 | 0.3 | 0.2 | 0.5 | 44.3 | 26.5 | 9.2 | 0.8 | 4.6 | 95.4 |
| 10798.00 | 1.4 | 0.0 | 0.4 | 0.3 | 0.8 | 41.8 | 21.5 | 13.3 | 2.6 | 6.2 | 93.8 |
| 10816.86 | 0.3 | 0.0 | 0.6 | 0.2 | 0.8 | 46.2 | 23.3 | 10.8 | 1.8 | 3.5 | 96.5 |
| 10831.69 | 1.2 | 0.0 | 0.1 | 0.7 | 0.8 | 47.8 | 25.2 | 12.0 | 0.9 | 5.2 | 94.8 |
| 10866.53 | 0.2 | 0.0 | 0.6 | 0.8 | 1.4 | 39.0 | 23.4 | 7.1 | 2.0 | 5.5 | 94.5 |
| 10921.92 | 0.8 | 0.1 | 0.2 | 1.0 | 1.2 | 49.2 | 23.7 | 12.2 | 1.5 | 4.5 | 95.5 |
| 11002.44 | 0.0 | 0.4 | 0.4 | 0.0 | 0.4 | 41.4 | 26.1 | 11.5 | 1.1 | 5.5 | 94.5 |
| 11092.00 | 0.8 | 0.1 | 0.2 | 1.9 | 2.1 | 44.6 | 24.4 | 13.0 | 1.7 | 5.9 | 94.1 |
| 11175.20 | 0.5 | 0.4 | 0.3 | 1.0 | 1.3 | 47.2 | 25.6 | 10.7 | 1.3 | 7.4 | 92.6 |
| 11314.17 | 0.0 | 0.0 | 0.3 | 1.1 | 1.3 | 51.2 | 25.7 | 10.1 | 0.7 | 3.5 | 96.5 |
| 11369.75 | 0.5 | 0.1 | 0.1 | 0.4 | 0.5 | 46.1 | 27.0 | 10.7 | 0.9 | 4.0 | 96.0 |

| Age varve a BP | Juniperus | Picea | Betula | Hippophaë | Ephedra total | Artemisia | Chenopodiaceae | Poaceae | Cyperaceae | AP (%) | NAP (%) |
|---|---|---|---|---|---|---|---|---|---|---|---|
| 11518.25 | 0.4 | 0.1 | 0.5 | 0.4 | 0.9 | 53.1 | 24.9 | 10.9 | 0.3 | 4.9 | 95.1 |
| 11614.42 | 0.5 | 0.2 | 0.6 | 1.4 | 2.0 | 47.1 | 26.8 | 8.8 | 0.2 | 6.3 | 93.7 |